Mode Control in Multimode Optical Fibre and its Applications

Andrew G Hallam

Doctor of Philosophy

ASTON UNIVERSITY

November 2007

ABSTRACT

MODE CONTROL IN MULTIMODE OPTICAL FIBRE AND ITS APPLICATIONS

Andrew G Hallam
Doctor of Philosophy
November 2007
ASTON UNIVERSITY

This thesis describes an investigation into methods for controlling the mode distribution in multimode optical fibres. The major contributions presented in this thesis are summarised below.

Emerging standards for Gigabit Ethernet transmission over multimode optical fibre have led to a resurgence of interest in the precise control, and specification, of modal launch conditions. In particular, commercial LED and OTDR test equipment does not, in general, comply with these standards. There is therefore a need for mode control devices, which can ensure compliance with the standards. A novel device consisting of a point-load mode-scrambler in tandem with a mode-filter is described in this thesis. The device, which has been patented, may be tuned to achieve a wide range of mode distributions and has been implemented in a ruggedised package for field use.

Various other techniques for mode control have been described in this work, including the use of Long Period Gratings and air-gap mode-filters. Some of the methods have been applied to other applications, such as speckle suppression and in sensor technology. A novel, self-referencing, sensor comprising two modal groups in the Mode Power Distribution has been designed and tested. The feasibility of a two-channel Mode Group Diversity Mutiplexed system has been demonstrated over 985m.

A test apparatus for measuring mode distribution has been designed and constructed. The apparatus consists of a purpose-built video microscope, and comprehensive control and analysis software written in Visual Basic. The system may be fitted with a Silicon camera or an InGaAs camera, for measurement in the 850nm and 1300nm transmission windows respectively. A limitation of the measurement method, when applied to well-filled fibres, has been identified and an improvement to the method has been proposed, based on modelled Laguerre Gauss field solutions.

Key words: mode-scrambler, mode-filter, long period grating, optical sensing, mode group mutiplexer.

ACKNOWLEDGEMENTS

I would like to acknowledge the support of my supervisor, Professor Ian Bennion, and members of the Photonics department, and my long-time friend, and business associate, Mr David Robinson of Arden Photonics Ltd. I would also like to thank Dr Nick Channon for his proof reading and helpful comments, and Dr Steve Hughes for his valuable encouragement.

I would especially like to thank my family who have showed me much understanding and support as I pursued this personal odyssey.

LIST OF CONTENTS

LIST OF FIGURES

LIST OF TABLES

CHAPTER 1

INTRODUCTION

1.1 Perspective

Following the manufacture of the first optical fibre with an attenuation of less than 20dB/km in 1970 [1], early optical communication systems were almost exclusively constructed with multimode fibre. The advantage of a higher bandwidth, offered by singlemode fibre, however, quickly led to a shift towards its widespread use. By the early 1980's, singlemode fibre was the medium of choice, where its higher bandwidth and lower losses could be readily exploited with newly developed laser sources operating at 1310nm and eventually at 1550nm.

The advent of the personal computer stimulated the demand for high speed Local Area Network (LAN) connection, typically over distances of less than a kilometre. To compete with entrenched copper-based systems, fibre needed to offer not just a bandwidth advantage but also be competitive in price. To achieve this, installers started switching back to multimode fibre, where component costs were less and field terminations were easier to make. Since the development of cheap, high speed, VCSEL laser sources in the 1990's there has been a steady resurgence of interest in multimode fibre for LAN applications. A raft of emerging Ethernet standards, offering, for example, 10Gbit/s over distances of 300m, have now made control of the launched mode distribution a critical element of high speed networks.

This thesis addresses the need to control the mode distribution in multimode fibres, for both operational and system test purposes in LAN applications. A novel device is described that may be tuned to achieve a wide range of mode distributions. The device has been patented and has been implemented in a ruggedised package for field use. Some of the techniques for mode control described in this work have also been applied to other applications of multimode fibre, such as in sensor technology.

1.2 Thesis Overview

The contents of this thesis may be grouped into four main parts:

(a) Chapter 2 gives a background review of the requirements for mode control in LAN applications,

(b) Chapters 3 and 4 present some multimode fibre theory, and describe a method for the measurement of mode distributions,

(c) Chapters 5 and 6 describe an investigation into methods for modifying the mode distribution, and presents some applications of the methods described,

(d) Chapter 7 presents a practical implementation of a mode control device for field use.

Specifically, Chapter 2 presents a comprehensive review of the use of multimode fibre in Local Area Networks, with particular emphasis on international standards. A description of the challenges to system performance is given, with reference to Differential Mode Delay and Differential Mode Attenuation (DMA). Measurements showing the effect of DMA on the mode distribution on a 200m fibre length are reported. The need for tight control of the launched mode distribution is demonstrated by loss measurements carried out on a link of concatenated fibres.

Chapter 3 lays out aspects of optical fibre theory that are relevant to the understanding of the mode control techniques described in this work. Mode-field equations are derived for step-index and graded-index fibre types. Use of the Mode Overlap Integral is presented, for computing coupling efficiencies between different mode distributions. For graded-index fibres, an analysis of leaky modes is given. The presence of leaky modes can lead to errors in the measurement of mode distributions.

An essential part of this thesis was to develop test apparatus to measure the mode distribution. Chapter 4 describes the theory of the measurement, and its practical implementation. The apparatus constructed consists of a purpose-built video microscope and comprehensive analysis software. The measurement technique employed has already been described in the literature but the opportunity was taken to author a standard test method for the International Electrotechnical Commission (IEC). This chapter also discusses limitations of the method, and an improvement to the method using modelled mode functions is proposed. A novel reconstruction method is also presented, for estimating the accuracy of computed mode distributions.

Chapter 5 contains the bulk of the work on techniques for modifying the mode distribution. These include mode-scramblers, such as Long Period Gratings and a novel point-load method, and mode-filters, including mandrel wrapping, an air gap filter, an offset launch and fused biconic-tapers.

Examples of the mode control techniques described in Chapter 5 are presented in Chapter 6, where applications include, compliance with LAN standards, speckle suppression, multimode sensors and a novel mode division multiplexier. The control of leaky modes is discussed and the sensitivity of some of the techniques to wavelength and spectral width is investigated.

A practical implementation of a device for field use is described in Chapter 7. The device has been designed to be rugged, reliable and relatively low-cost. Issues regarding reliability are described, such as coating delamination and temperature cycling, and suggestions are given to improve the device.

Finally, Chapter 8 presents some conclusions and an analysis of the thesis. Some areas for future work are suggested. A list of references is given in Chapter 9.

Results of a patent search on existent technology for mode control are presented in Appendix A and notes from a market survey on commercial devices is given in Appendix B. A tabulation of the mode set for a typical 50um fibre is given in Appendix C, this is a useful aid to understanding mode theory and selective mode excitation. Appendix D gives publications to date, arising from the thesis, and Appendix E details the main software programs developed in the course of the work. These include MathCad software for computing mode fields and mode overlap integrals, and Visual Basic software for instrument control. Appendix F gives a glossary of some of the terms used in this work.

CHAPTER 2

REVIEW OF MODAL REQUIREMENTS IN LOCAL AREA NETWORKS

This chapter introduces the use of multimode fibre in Local Area Networks and describes how, in order to compete with copper technology, operating bandwidths are continually being pushed upwards. Standards are now becoming available to support 10Gbit/s performance on multimode fibre in both the 850nm and 1300nm transmission windows.

Specification, and control, of the launched mode distribution have become quintessential requirements for the operation of these systems.

2.1 Introduction to Local Area Networks

A Local Area Network (LAN) is a system for communication between computer terminals and related equipment within the same general area. A network might encompass a commercial building complex, or a small residential area, where link lengths between terminals are generally up to a few hundred metres.

A typical network consists of a main *backbone* cable, which could be fibre or copper based, entering a building complex in the basement area and terminated at a main *cross-connect* enclosure. The enclosure has the function of providing switching to internal *riser* cables, which pass up through the building in special cabling ducts. These are terminated at smaller cross-connect enclosures on each floor of the building, from where *horizontal* cabling connects them to wall-mounted outlet points in the various work areas of each floor of the building. In a large complex, the riser cables are described as *vertical* backbones. The work areas contain equipment such as personal computers (PCs), shared printers, scanners and telephones, which are fitted with Network Interface Cards (NICs) for connection to the outlet points, via short cable runs of a few metres or so.

Traditional copper-based networks offering 10Mbit/s data-rates are becoming unable to cope with the growing demands on bandwidth resulting from the ever increasing power of PCs and the demand for network connection. Ethernet standards for higher bandwidths, such as for 100Mbit/s and 1000Mbit/s, have been developed and are now becoming widely used, but even these are not sufficient for the main network backbones where many operators are shifting to the new 10Gbit/s standards being offered by optical fibre.

Since the 1980s the trend has been to install single-mode fibre for *telecommunication* systems, connecting main exchanges, and switching centres, where gigabit bandwidths are required over long distances, and to employ multimode fibre for LAN backbones and main riser cables. Horizontal connection, however, from the risers to the workstation areas continues to be copper twisted-pair due to the higher cost of fibre connectors and devices, and it is unlikely that *Fibre to the Desk* (FTTD) will become widespread for some time, except for specific applications requiring extremely high data-rates. As speed requirements increase, and the price of optical fibre components continues to fall, then FTTD may start to become a reality.

2.2 Multimode Fibre in the Local Area Network

The growing use of fibre in the LAN backbone is due to the advantage of the *bandwidth-times-distance* product of fibre over copper, enabling higher data-rates over longer link lengths. For example, the new Category 6/Class E copper cabling standard supports 10Gbit/s transmission, known as 10GBASE-T, but is limited to distances of up to 55m, whereas fibre is able to achieve tens times this reach at the same data-rate. This length benefit manifests itself in the need for less repeaters than copper and the ability to operate star-type topologies where each user group may be connected directly to a centralised hub. This topology has the advantage of requiring less cross-connect enclosures, which are expensive, and is considerably easier to operate and maintain than ring-based networks.

There are also other advantages of fibre over copper, such as its immunity to electrical noise, lighter weight, increased data security, low spark risk hazard and upgradeability to higher bandwidths.

The main industry standard for Ethernet LAN systems is IEEE802.3 [2], which covers 1, 10, 100 and 1000Mbit/s systems. For each of these categories, the use of both copper and fibre is specified. Regarding 1000Mbit/s, the specifications for fibre are known as 1000BASE-SX and 1000BASE-LX, for 850nm and 1300nm respectively. For the former, both 50um and 62.5um core diameter fibres are specified, with respective bandwidth-distance products of 500MHz.km and 200MHz.km at 850nm and maximum operating distances of 550m and 275m respectively. For 1000BASE-LX, 50um and 62.5um fibres are again specified, both with 500MHz.km bandwidth at 1300nm and a maximum operating distance of 550m.

In order to achieve 1000Mbit/s over the maximum operating distance, IEEE802.3 specifies a range of transmitter and receiver characteristics, such as launched optical power level, return loss, detector sensitivity and eye closure. Of particular interest to this thesis is the interplay of the optical characteristics of the transmitter with the fibre link itself in terms of its bandwidth and loss performance. Regarding bandwidth, 1000BASE-SX specifies the launch characteristics of the 850nm laser source in terms of the *mode distribution* it launches into the fibre, using a parameter known as *Coupled Power Ratio* (CPR). The CPR is required to be above a certain value to ensure that the bandwidth performance of the fibre is not dominated by a few individual modes. A draft addendum to the standard, IEEE802.3z, specifies the modal distribution of the source in terms of an *Encircled Flux* distribution [3]. The purpose of this is to ensure that neither the lowest order, nor the highest order, modes dominate.

For 1000BASE-LX, where 1300nm laser sources are specifically designed for use with singlemode fibre, the standard stipulates the use of a *mode-conditioning patchcord* to ensure the launch of mid and higher order modes. The mode-conditioning patchcord comprises an offset joint between the singlemode laser pigtail and the multimode output fibre.

Further addenda, IEEE802.3ae and IEEE802.3aq, provide specifications for 10Gbit/s operation at 850nm and 1310nm, called 10GBASE-SR and 10GBASE-LRM, respectively. These standards also specify the mode distribution in terms of Encircled Flux templates.

The launched mode distribution directly affects the system bandwidth, and the system reach, through the respective effects of *differential mode dispersion* and *channel loss.* These processes will now be described.

2.3 Differential Mode Dispersion

Measurement of fibre bandwidth has traditionally been carried out with an *Over-filled Launch* (OFL) [4], as this type of launch has been found to give reproducible results with different types of test equipment. The development of the 850nm VCSEL laser source in the 1990's, however, found immediate application in LAN systems due to its high power, low threshold current, high modulation speed and circular optical symmetry. Installers soon found that they could achieve system bandwidths far in excess of the values associated with an OFL and so it was clear that some other performance standard was required that would be a better predictor of system performance.

The Telecommunications Industries Association (TIA) responded with a two-pronged approach. Firstly, the fibre bandwidth would be measured using a *Restricted Mode Launch* (RML) and, secondly, the output from the source VCSEL would have to satisfy some sort of modal template. For the RML, the TIA chose to use a launch fibre with a core diameter of 23.5 μm and a numerical aperture of 0.208 [5]. For the VCSEL, its output when measured via a patchcord would have to satisfy an Encircled Flux template. So, if the fibre bandwidth with the RML launch exceeded 385MHz.km and the VCSEL source passed the template then the fibre link should operate at 1Gbit/s over distances up to 500m [6].

For 10Gbit/s the situation was a little more complex, as the requirement on fibre bandwidth was 2000MHz.km and it was found that the RML launch was not adequate to guarantee this performance. The TIA preferred a direct measurement of Differential Mode Delay. The technique [7] consists of scanning a singlemode launch fibre across the input end of the fibre under test and measuring the relative time delay of pulses launched into the fibre as a function of radial position. The overall DMD of the fibre is then given as the time delay between the leading edge of the pulse with the least delay through the fibre and the trailing edge of the slowest pulse. In order to meet the bandwidth requirements for 10Gbit/s, a series of six alternative DMD templates were introduced [8]. As an example, the measured DMD must be less than 0.25ps/m in the radial range 5um to 10um and less than 5ps/m in the range from zero to 23um.

In tandem with the DMD template, which characterises the fibre itself, there is also the Encircled Flux template that the transmitter source must also satisfy. So, if both fibre and source meet their respective specifications then the fibre link should operate at 10Gbit/s over distances up to 300m [9].

In contrast to systems operating at 850nm, long wavelength systems generally use 1300nm singlemode lasers, although this situation may change as 1300nm VCSELs will soon become available. Coupling a singlemode fibre to a multimode system clearly only excites a few low-order modes and it might be expected that the DMD envelope would be much narrower. This is generally the case but it has been reported [10] that modal dispersion for a laser launch on the axis can be much worse than launching a full range of modes from a larger source. This is due to imperfections around the centre of the index profile of the fibre, such as ripples or a dip. It was found that by introducing a small lateral offset between the singlemode and multimode fibres, the bandwidth could be maximised. This is due to the offset causing a range of mid-order modes to be launched [11] where the index profile is more uniform, thus avoiding the central dip.

This type of launch has been included in the IEEE802.3 standard for 1Gbit/s and 10Gbit/s systems, where the specified offset is 20um for 62.5um fibre and 13um for 50um fibre. The actual modal distribution resulting from this type of launch has hitherto not been specified in the literature due to lack of mode profiling test equipment at 1300nm.

2.4 Channel Loss

Channel loss is the total optical loss between the transmitter and the receiver including the fibre and any connectors and splices. The short-wave 1Gbit/s standard, 1000BASE-SX, specifies a maximum channel loss of 3.56dB for 50um fibre and 2.60dB for 62.5um fibre. At 1300nm, 1000BASE-LX specifies 2.35dB for both fibre types. For 10GBASE-S the maximum channel insertion loss is 2.6dB.

The measured channel loss is known to be dependent on the launched mode distribution, particularly if slight offsets between connector interfaces are present, due to *differential mode attenuation* (DMA).

In order to ensure the required channel loss performance is met, it is important to verify this parameter prior to commissioning the system. The measurement of channel loss is normally carried out using an Optical Time Domain Reflectometer (OTDR), or a Light Source and Power Meter (LSPM). It has been found, however, that loss measurements made with OTDRs are usually more optimistic than those made with the LSPM method, due to the difference in mode distribution launched by the laser source in an OTDR compared to that launched by a typical LED source in the LSPM method. In fact, there would seem to be some merit in testing an installed system using a source that is modally similar to the actual transmitter source to be fitted to the system. There is, therefore, a clear need for standards to define the mode distribution for testing such that reproducible results may be obtained with differing types of test equipment. A link-testing standard published in 2006, ISO/IEC14763-3 [12], has now addressed this issue by specification of a mode distribution template to verify the conformance of test equipment.

2.4.1 Differential Mode Attenuation

Generally speaking, higher-order modes are attenuated more than lower-order modes. There are several mechanisms causing DMA, including variations in fibre diameter [13], refractive index inhomogeneities, and macrobending and microbending [14], [15].

The effect of DMA in a fibre is to preferentially filter out higher-order modes, leading to spatial transients. These might extend over a few cm, to several km, depending on the type and severity of the filtering mechanism. The effect on the measurement of fibre loss is usually to give a pessimistic value when measurements are normalised to dB/km. It is common practice, therefore, to deliberately filter out the highest-order modes within the first 1m, or so, of the fibre using, for example, a mandrel-wrap mode-filter.

Whilst some care may be taken to avoid unduly stressing and bending the fibre, the process of encapsulating it into a protective cable may cause microbending [16]. As an example, Figure 2.1 shows the mode power distribution for four different launch distributions after propagation through a 202m length of cabled 62.5um graded-index fibre compared to the launched distribution after 1m. It can be seen that the MPD of the well-filled launches, in blue and magenta, are preferentially attenuated for higher-order mode groups, and their peak positions after 202m are shifted to the left, compared to the positions after 1m. The mid-launch, in green, also suffers losses at the higher end but to a much lesser degree and the peak position is only shifted very slightly to the left. The extreme under-fill launch, in red, does not show DMA, but rather that the peak moves to the right slightly due to *mode-coupling*.

A situation can be envisaged where a combination of mode-coupling and DMA causes power to be continuously transferred to higher-order modes and these modes being preferentially attenuated, leading to an *equilibrium mode distribution* (EMD). In fact, in Figure 2.1 there is a tendency of the launched mode distributions to move towards the mid-launch curve (green). This distribution is largely unaffected by propagation through the fibre and represents a approximation to the EMD of the fibre. Several efforts have been made in the literature to simulate an EMD launch, such as (a) restricting both the launch spot-size and the NA to 70% of the values of the test fibre, (b) employing a long fibre length situated between the source and the fibre under test, and (c) inducing a large amount of mode-coupling using controlled microbending in tandem or a mandrel-wrap mode filter. Some of these methods will be reviewed in more detail in CHAPTER 5.

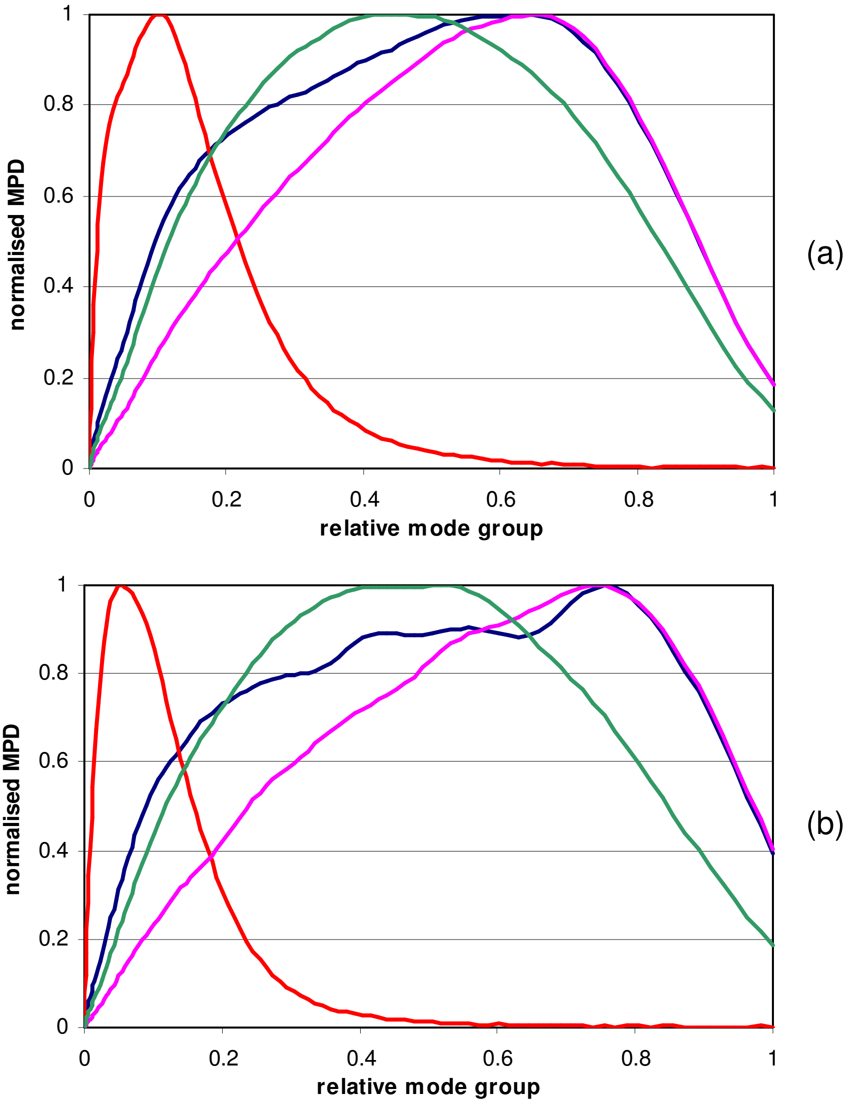

Figure 2.1. Plots of normalised MPD in a length of 62.5um tight-buffered fibre cable after (a) 202m, and (b) 1m

It is now useful to clarify the difference between the terms Equilibrium Mode Distribution and *Steady-State Distribution* (SSD), which are often used interchangeably. They have, however, very distinct definitions. An EMD has the property that irrespective of the launch distribution, the output is consistently the same and is a characteristic of the fibre, or device. In an SSD, the output distribution is the same as the input distribution. Thus, there may be many different SSD distributions for a particular fibre or device. For example, in the absence of mode coupling, an underfilled-mode distribution will remain largely unaffected by transmission through a long fibre and so could be regarded as an SSD. An EMD launch is clearly a special case of an SSD launch.

Furthermore, the EMD of a mode control device may have a different characteristic from the EMD of a fibre or device to which it is coupled, and loss measurements may display length-dependent transients. The advantage, however, of using a mode control device, with a given EMD, is that loss measurements will be completely independent of the type of test source used, enabling reproducible measurements to be obtained.

Another source of DMA may arise at connectors and splices. If a small amount of transverse offset is present between the two mating fibres, which could be due to a concentricity error in either the connector ferrule or in the fibre itself, then light travelling near to the core/cladding boundary will be preferentially attenuated. In particular, higher-order modes will be most affected. In order to demonstrate this, an experiment was carried out, consisting of measuring the insertion loss of 10 concatenated patchcords. Each patchcord was 3m long and of 50um graded-index fibre, and the connector types used were a combination of FC, SC and ST. The insertion loss was measured using a variety of light sources having different modal distributions. The loss results, shown in Figure 2.2, range from 0.5dB, for an axial singlemode launch, to 5.9dB for an offset singlemode launch, where only high-order modes were excited. Some light sources were commercial test sets and other were empirical. Measurements of the mode distributions of several of these launches will be presented in CHAPTER 6.

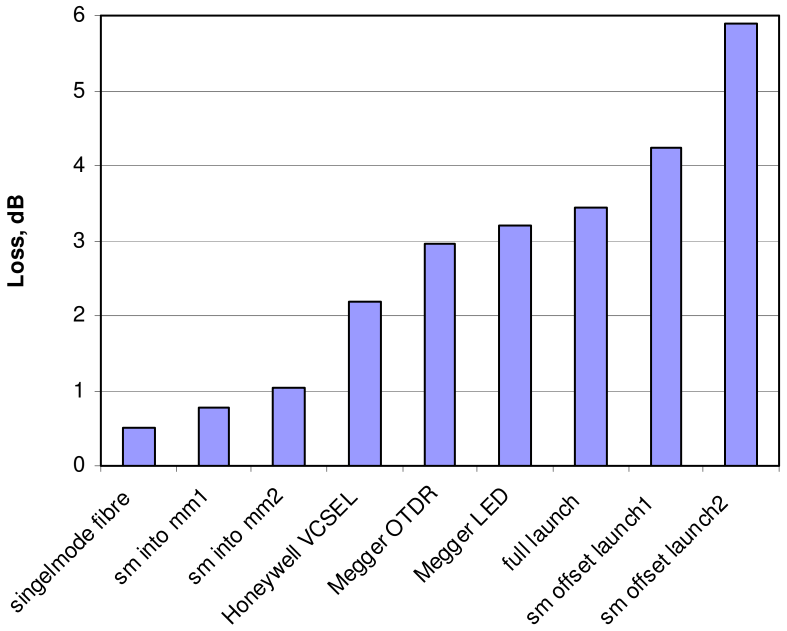

Figure 2.2. Insertion loss of 10 concatenated 50um patchcords for different launch conditions.

2.5 Mode Control

It is clear, therefore, from both bandwidth and channel loss requirements, that a practical means of controlling the modal distribution would be advantageous to the industry. Such a device should be able to reproduce the same output mode distribution that was independent of the launched distribution so that measurements of channel loss would be the same regardless of what type of test source was used. The device would ideally also be adjustable during manufacture so that its output could be tuned to reflect particular requirements, or changes in the evolving standards.

2.6 Literature Survey

In the literature, most mode control devices may be catergorised by whether they are mode-scramblers or mode-filters. A mode-scrambler redistributes light across the mode spectrum to give a more or less uniform distribution whilst a mode-filter selectively attenuates certain mode groups. Some devices are designed to carry out both functions to produce a given output distribution that is independent of the input distribution.

2.6.1 Patent Search

A patent search was carried out to establish existent technology for mode control. A total of 33 patents were found, for a variety of devices, using techniques such as mechanical distortion, fibre winding, fibre etching, planar waveguides, tapered fibres and multi-segment fibres. Most devices were claimed to be mode scramblers, but some were claimed to produce an EMD distribution. It was found that the devices could be broadly categorised according to whether they were generally intended as Mode Scramblers (22), Mode Conditioners and Filters (7), or EMD generators (4).

A review of the patent search is given in Appendix A. Of particular interest is US4998792 which features an air gap mode-filter followed by a mandrel-wrap mode-scrambler. This device is claimed to produce an EMD. Experiments in this thesis have shown that a mandrel-wrap does not perform very effectively as a mode-scrambler for an under-filled distribution. Also, this device potentially has a high insertion loss, if the input fibre is well-filled, as a high degree of filtering occurs prior to the mode-scrambler. An alternative, novel, device has been described in this thesis, consisting of a point-load mode-scrambler followed by an air-gap mode-filter. This device should have a lower insertion loss, and also be more easily adjusted than the existent technology. A patent was subsequently filed on this device [70].

2.6.2 Commercial Mode Control Devices

A market survey was also carried out, to review commercially available devices for modifying the mode distribution.

It was found that there are four main types of mode control devices on the market, these are: Mode Conditioning Patchcords, used for Gigabit Ethernet systems, Mode Scramblers, which are generally used for testing purposes, Mode Filters, also used for testing, and Deadzone Eliminators, which are used with OTDRs.

The effectiveness of one particular mode-scrambler, the FM-1 from Newport Corp., was tested in this study and the results are presented in CHAPTER 5.

A review of the commercial devices is given in Appendix B.

2.7 Chapter Summary

To summarise, this chapter has introduced the requirement for controlling the mode distribution in modern multimode fibre systems. Reproducible measurements, which are representative of the system operating parameters, can only be achieved by precise control of the mode distribution of test equipment. A description of Differential Mode Attenuation (DMA) and Differential Mode Dispersion (DMD) has been given and the results of an experiment, to demonstrate the effect of DMA on connector losses, have been presented. A patent survey on mode control techniques and commercial devices has been carried out.

CHAPTER 3

OPTICAL FIBRE MODE THEORY

This chapter presents a derivation of the field solutions for multimode fibres, enabling any given modal distribution, and corresponding near-field intensity profile, to be computed. The categorisation of LP modes into mode groups is described. The problem of avoiding the launch of leaky modes in graded-index fibres is highlighted and use of the mode overlap integral for computing coupling efficiency between fibres is demonstrated.

3.1 Step Index Fibre

Electromagnetic phenomena are governed by Maxwell's equations. These may be used to derive the *Wave Equation*, which describes the propagation of the electric field vector E in space and time [17], as follows:

$$\nabla^2 \overline{E} - \frac{\varepsilon_r}{c^2} \frac{\partial^2 \overline{E}}{\partial t^2} = 0 \qquad \textbf{(3.1)}$$

where ∇^2 is the Laplacian operator, which in polar co-ordinates, is given by

$$\nabla^2 = \frac{\partial^2}{\partial r^2} + \frac{1}{r}\frac{\partial}{\partial r} + \frac{1}{r^2}\frac{\partial^2}{\partial \phi^2} + \frac{\partial^2}{\partial z^2} \qquad \textbf{(3.2)}$$

ε_r is relative permittivity and c is the velocity of light in a vacuum.

Fibre modes are solutions to the wave equation that satisfy certain boundary conditions and have a spatial distribution that does not change as it propagates. For simplicity it will be assumed that the fibre cladding extends to infinity. This assumption is valid because the power in the highest-order modes in both step-index and graded-index fibres, with 50um core diameter, falls to a negligible value of less than 10^{-22} of its peak value at a radial distance of 62.5um, which is the typical cladding radius of the fibres used in this work.

Assuming separability, solutions for E, in polar co-ordinates, are of the form:

$$E(r,\phi,z,t) = F(r)e^{j(\eta\phi)}e^{j(\beta z-\omega t)} \tag{3.3}$$

where: F(r) is a radial field function,

$e^{j(\eta\phi)}$ is a periodic function,

η is the azimuthal mode number and takes integer values,

ϕ is the azimuthal angle,

$e^{j(\beta z-\omega t)}$ is a periodic function of distance and time,

β is the propagation constant and ω is the angular frequency of the optical wave.

Substituting eqns. (3.3) and (3.2) into eqn. (3.1) gives

$$\frac{\partial^2 F}{\partial r^2} + \frac{1}{r}\frac{\partial F}{\partial r} - \frac{\eta^2}{r^2}F - \beta^2 F + \frac{\omega^2}{v^2}F = 0 \tag{3.4}$$

Rearranging gives

$$r^2\frac{\partial^2 F}{\partial r^2} + r\frac{\partial F}{\partial r} + \left[r^2\left(n_{core}{}^2 k_o{}^2 - \beta^2\right) - \eta^2\right]F = 0 \tag{3.5}$$

which is *Bessel's Equation*, where k_o is the free-space wave number ($2\pi/\lambda$) and n_{core} is the refractive index of the fibre core.

For a bound mode the propagation constant, β, takes values in the range

$$k_o n_{clad} \leq \beta \leq k_o n_{core} \tag{3.6}$$

Thus, in the core the inner bracket in eqn. (3.5) is positive giving a solution of the form

$$F(r) = J_\eta\left(r\left(n_{core}^2 k_o{}^2 - \beta^2\right)^{1/2} \right) \tag{3.7}$$

where J_η is a Bessel function of order η. F(r) is thus aperiodic with core radius.

Similarly, in the cladding the inner term is negative and the solution is of the form

$$F(r) = K_\eta\left(r\left(\beta^2 - n_{clad}^2 k_o{}^2\right)^{1/2} \right) \tag{3.8}$$

where K_η is a modified Bessel function of order η. F(r) is thus exponentially decaying in the cladding

Ignoring t and z in eqn. (3.3) the solution for the transverse component of the TE and TM fibre mode fields is

$$E(r,\phi) = J_\eta\left(r\left(n_{core}^2 k_o{}^2 - \beta^2\right)^{1/2} \right) \cdot e^{j(\eta\phi)} \tag{3.9}$$

in the core, and

$$E(r,\phi) = K_\eta\left(r\left(\beta^2 - n_{clad}^2 k_o{}^2\right)^{1/2} \right) \cdot e^{j(\eta\phi)} \tag{3.10}$$

in the cladding.

There is, however, a small field component in the forward, or z, direction which must be considered when calculating exact field solutions. This component leads to two further types of modes designated as EH and HE, depending on whether the electric or magnetic field is dominant in the z-direction. In a typical communications fibre, however, the index difference between the core and the cladding is very small, leading to only glancing angles at the core/cladding interface. The transverse, TE and TM, components thus dominate and certain groupings of TE, TM, HE and EH modes have almost identical propagation constants enabling them to be combined into *Linearly Polarised*, or LP, modes [18]. The LP approximation thus enables the fibre modes to be fully described by eqns. (3.9) and (3.10).

In order to calculate the mode fields it is necessary to determine the values of β. This may be achieved by matching the tangential field components at the core/cladding interface, resulting in the following expression:

$$U\frac{J_{\eta\pm1}(U)}{J_{\eta}(U)} = \pm W\frac{K_{\eta\pm1}(W)}{K_{\eta}(W)} \qquad \textbf{(3.11)}$$

where:

$$U = a\left(n_{core}^{2}k_{o}^{2} - \beta^{2}\right)^{1/2} \qquad \textbf{(3.12)}$$

and

$$W = a\left(\beta^{2} - n_{clad}^{2}k_{o}^{2}\right)^{1/2} \qquad \textbf{(3.13)}$$

As an example, a plot of the terms in eqn. (3.11), for a 50um core diameter fibre with 0.21NA at 850nm, is shown in Figure 3.1, where a value of η=4 has been used. The required values of β correspond to the crossing points of the two sets of curves, for the left and right sides of eqn. (3.11). In this example, there are 11 modes for this particular azimuthal mode number.

Each discrete mode, with the same η value, is designated by its radial mode number, μ, where μ=1 corresponds to the mode at the right end of the plot with the highest value of β and μ=11 corresponds to the mode nearest cut-off.

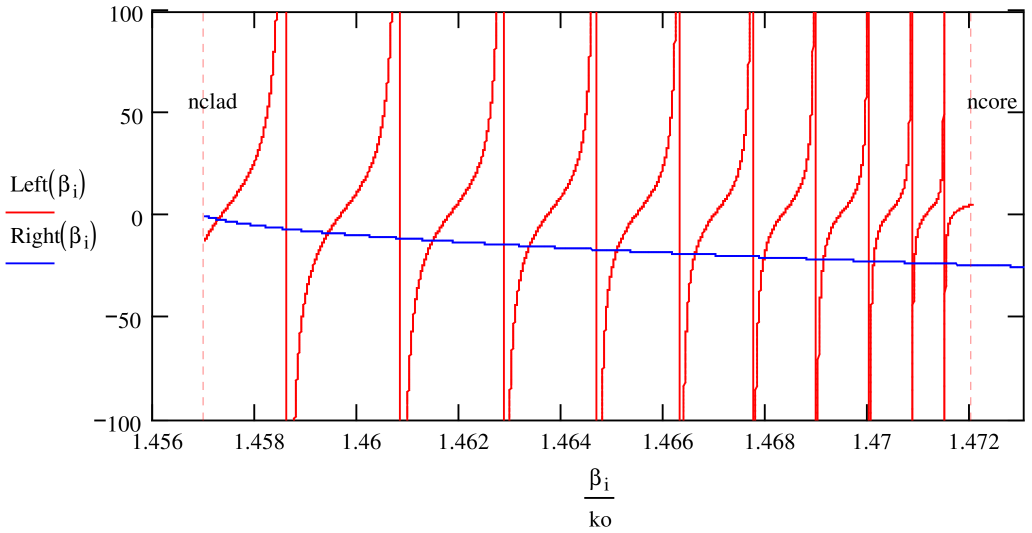

Figure 3.1. Matching tangential fields at core/cladding interface to determine propagation constants in a step-index fibre.

Mathcad software [19] was then used to compute the mode fields and some examples for η=4 are given in Figure 3.2, where red is positive and blue is negative field values.

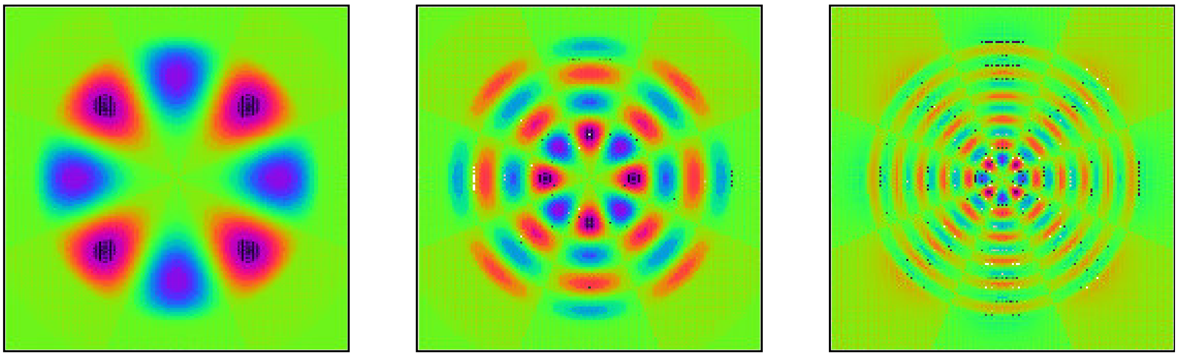

μ=1 μ=4 μ=11

Figure 3.2. Examples of field distributions for modes in step-index fibre having azimuthal mode number η=4 and different radial mode numbers, μ.

The mode pattern that would be observable with, for example, a camera, is given by the square of the field. The corresponding power plots for the modes above are shown in Figure 3.3.

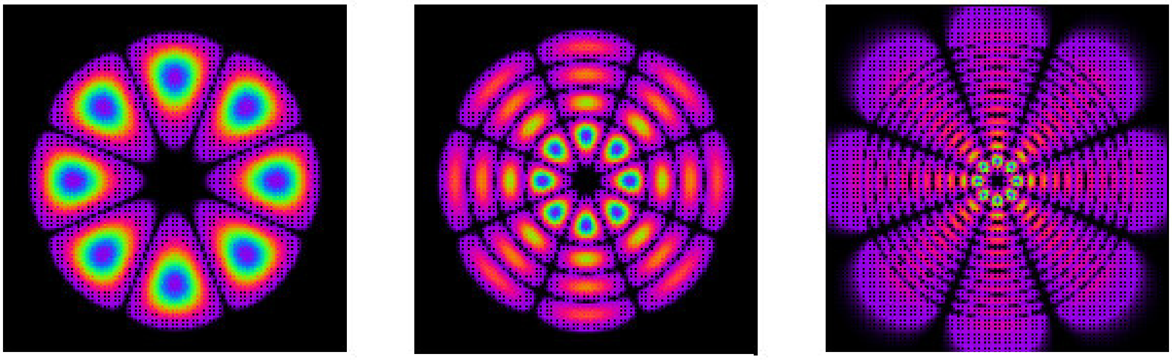

$\mu=1$ $\mu=4$ $\mu=11$

Figure 3.3. Examples of power distributions for modes in step-index fibre having azimuthal mode number $\eta=4$ and different radial mode numbers, μ.

The standard designation for the LP modes shown here is LP$_{\eta,\mu}$. It can be seen that μ gives the number of intensity maxima in the radial direction and 2η gives the number of intensity maxima in the azimuthal direction.

It can be seen from the exponential terms in eqns. (3.9) and (3.10) that the azimuthal dependence can be either $\cos(\eta\phi)$ or $\sin(\eta\phi)$, subject to arbitrary phase. The effect of this is give two degenerate modes for each β value, which are rotated slightly with respect to each other. An example in shown in Figure 3.4, below, for the two degenerate LP$_{3,2}$ modes.

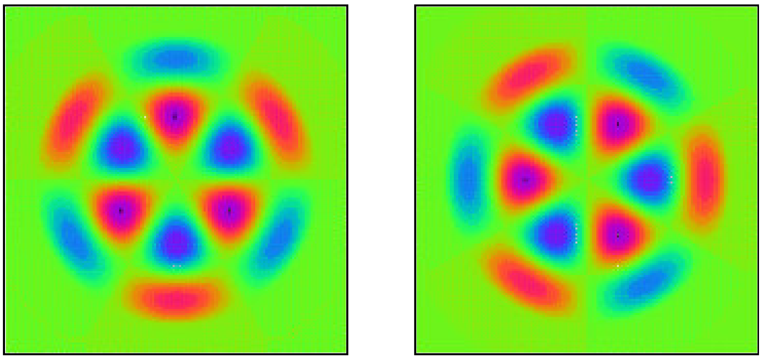

$\mu=2$, $\eta=3$

Figure 3.4. Field plots of two degenerate forms of LP$_{3,2}$ mode in step-index fibre.

3.1.1 Modal Excitation of Step-Index Fibre

The number of modes, N, in a step-index fibre is given approximately by [18]

$$N = \frac{V^2}{2} \quad \textbf{(3.14)}$$

where V is the *normalised frequency*, given by:

$$V = ak_o NA \quad \textbf{(3.15)}$$

and a is the core radius, NA is the fibre numerical aperture, given by,

$$NA = n_{core}\sqrt{2\Delta} \quad \textbf{(3.16)}$$

and Δ is the relative index difference of the fibre, given by,

$$\Delta = \frac{n_{core}^2 - n_{clad}^2}{2n_{core}^2} \quad \textbf{(3.17)}$$

For example, for a 50um step-index fibre, 0.21NA at 850nm there are 753 modes. This number is made up from the fact that each LP mode, where $\eta \neq 0$ has two orientations and, in addition, all modes have two polarisation states.

To simulate a fully-filled fibre, the intensity distributions of the entire mode set were computed and linearly combined. The normalised intensity distribution, and a profile through its centre, are shown in Figure 3.5. It can be seen that the intensity profile is a similar same shape to the step-index profile, as expected.

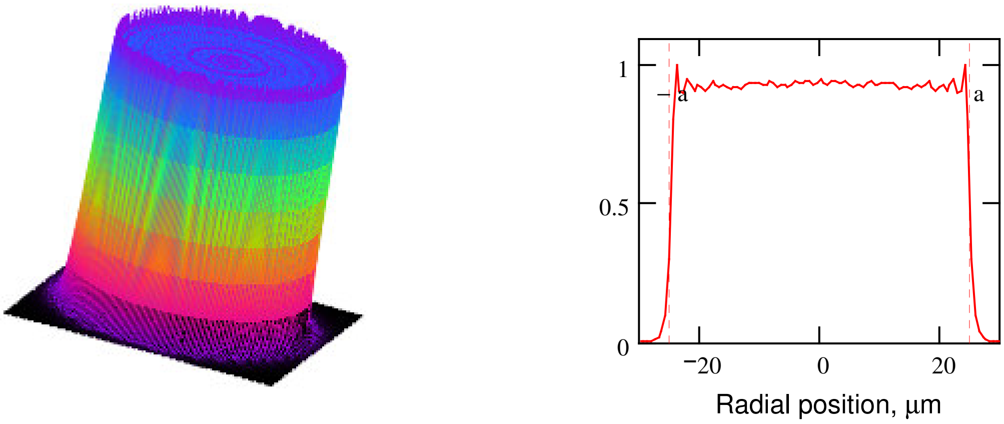

(a) (b)

Figure 3.5. Power distribution of all guided modes, equally weighted, in 50um core diameter step-index fibre, (a) 3-D model, (b) intensity profile.

3.2 Graded-Index Fibre

Consider a power-law index profile, n(r), given by,

$$n(r) = n_{core}\left[1 - 2\Delta\left(\frac{r}{a}\right)^{\alpha}\right]^{0.5} \qquad \left(\frac{r}{a}\right) \leq 1 \tag{3.18}$$

where α is the profile factor.

Substituting eqn. (3.18) into eqn. (3.5) gives,

$$r^2\frac{\partial^2 F}{\partial\ r^2} + r\frac{\partial F}{\partial r} + \left[r^2\left(n(r)^2 k_o{}^2 - \beta^2\right) - \eta^2\right]F = 0 \tag{3.19}$$

This is the *Helmholtz equation* and, for a parabolic index profile where α=2, has solutions in the form of *Laguerre-Gauss* modes [20], as follows

$$E_{\eta,\mu}(\rho,\phi,z) = \rho^{\eta} e^{\frac{-\rho^2}{2}} L_{\mu-1}^{\eta}(\rho^2)\sin(\eta\phi + \theta_o)e^{-j(\beta z)} \tag{3.20}$$

where the radial variable is given by

$$\rho = \frac{r}{a}\sqrt{V} \tag{3.21}$$

and

$$L_{\mu'}^{\eta}(\rho^2) = \sum_{s=0}^{\mu'} \frac{(\mu'+\eta)!(-1)^s \rho^{2s}}{(\eta+s)!(\mu'-s)!s!} \tag{3.22}$$

is the generalised Laguerre polynomial, where, for convenience, the substitution $\mu'=\mu-1$ has been made. $\theta_o = 0$ or $\pi/2$, represents pairs of degenerate modes when $\eta \neq 0$.

Some typical field plots for a 50um, 0.21NA fibre at 850nm are shown in Figure 3.6 and the corresponding intensity distributions are shown in Figure 3.7.

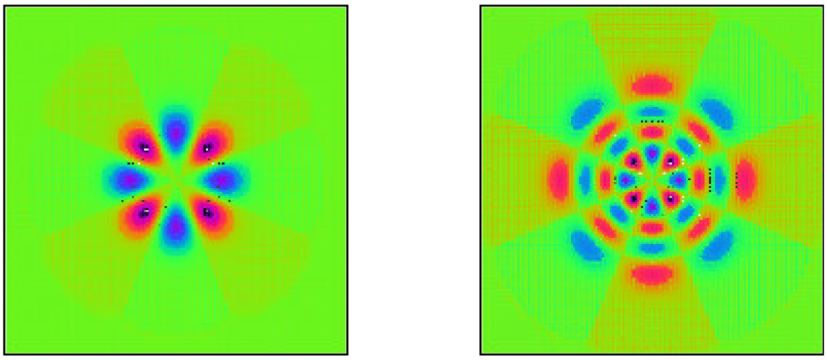

$\mu=1$, $\eta=4$ $\mu=4$, $\eta=4$

Figure 3.6. Examples of field distributions for modes in parabolic-index fibre having azimuthal mode number $\eta=4$ and different radial mode numbers, μ.

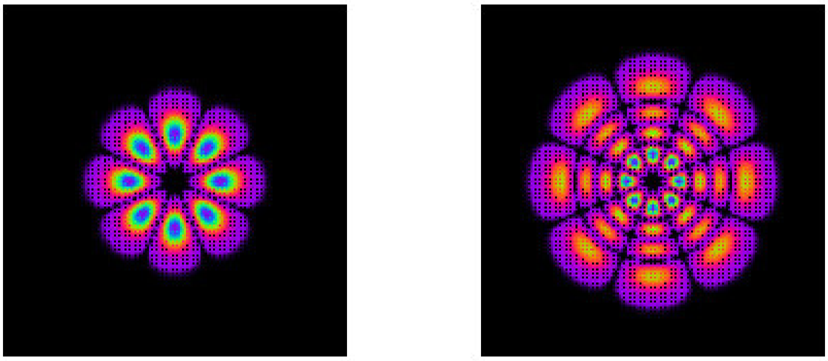

$\mu=1,\ \eta=4$ $\mu=4,\ \eta=4$

Figure 3.7. Examples of power distributions for modes in parabolic-index fibre having azimuthal mode number $\eta=4$ and different radial mode numbers, μ.

Comparing Figure 3.7 with Figure 3.3 it can be seen that, for the same radial mode number, the physical size is smaller in the graded fibre than for the step fibre. The reason for this may be described in terms of geometrical ray optics, where a meridional ray undergoes a constant change in angle as it travels radially out from the centre. Now for a particular ray the propagation constant, β, defined as

$$\beta = k_o n(r)\cos(\theta) \tag{3.23}$$

is invariant. Thus, as a ray enters a region of lower refractive index, towards the cladding boundary, from eqn. (3.23), θ decreases accordingly and eventually turns back towards the core centre. The higher-order mode, therefore, occupies a physically greater proportion of the core diameter than a lower-order mode.

3.2.1 Modal Excitation of Graded-Index Fibre

The number of modes, N, in a graded-index fibre is given approximately by

$$N = V^2\left[\frac{\alpha}{2(\alpha+2)}\right] \tag{3.24}$$

As an example, in a 50µm graded-index fibre, 0.21NA at 850nm there are about 276 modes.

Figure 3.8 shows a linear combination of the entire mode set for a parabolic index fibre. The intensity profile is a similar shape to the parabolic index profile.

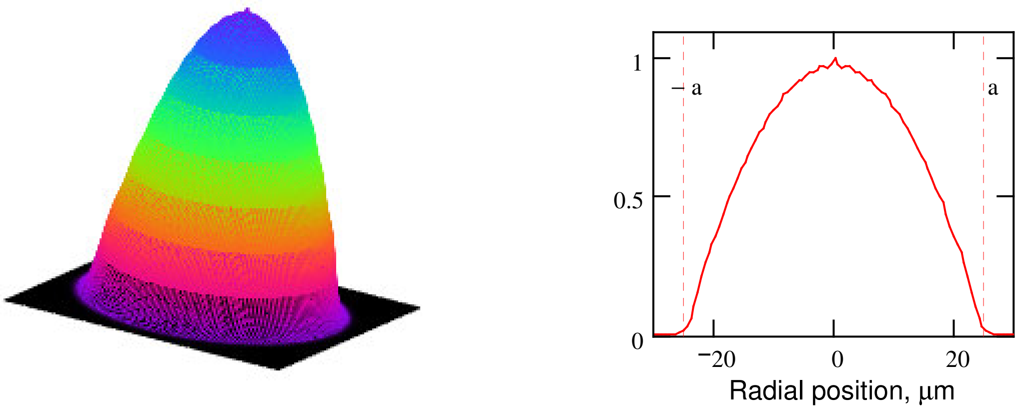

(a)

(b)

Figure 3.8. Power distribution of all possible guided modes, equally weighted, in 50um core diameter parabolic index fibre, (a) 3-D model, (b) intensity profile.

3.2.2 Mode Groups

Using the *WKB approximation* [21] the propagation constant of a mode in a graded-index is given by [22]

$$\beta = k_o n_{core}\left(1-2\Delta\left(\frac{m}{M}\right)^{2\alpha/(2+\alpha)}\right)^{1/2} \tag{3.25}$$

where m is the *Principal Mode Number*, defined as

$$m = 2\mu + \eta - 1 \tag{3.26}$$

and M is the maximum principal mode number, given by

$$M = \sqrt{\frac{\alpha}{\alpha + 2}} k_o n_{core} a \sqrt{\Delta} \tag{3.27}$$

From eqn. (3.26) there are several combinations of (η,μ) that have the same principal mode number and are therefore degenerate. For example, in a parabolic index fibre with 50um core diameter and 0.21 NA, there are, from eqn. (3.27) 19 mode groups at 850nm.

It should be noted, however, that *Finite Element* methods [23] show that propagation constant of modes within in the same mode group typically differ from each other by about 0.0007%. This is much smaller than the difference in propagation constant between adjacent mode groups, typically 0.055%, and so is negligible for most purposes.

The number of individual modes in each mode group is equal to twice the mode group number. For example, in mode group m=5 the possible combinations of (η,μ) are $LP_{4,1}$, $LP_{2,2}$ and $LP_{0,3}$. Now, as described in section 3.1.1, there are two field orientations for modes when $\eta \neq 0$, and two polarisation states for each mode, making a total of ten modes in this group.

The $LP_{\eta,\mu}$ modes of the first 16 mode groups in a 50um core diameter graded-index fibre, at 850nm, are shown in Figure 3.9. The complete mode set for this fibre is given in Appendix C.

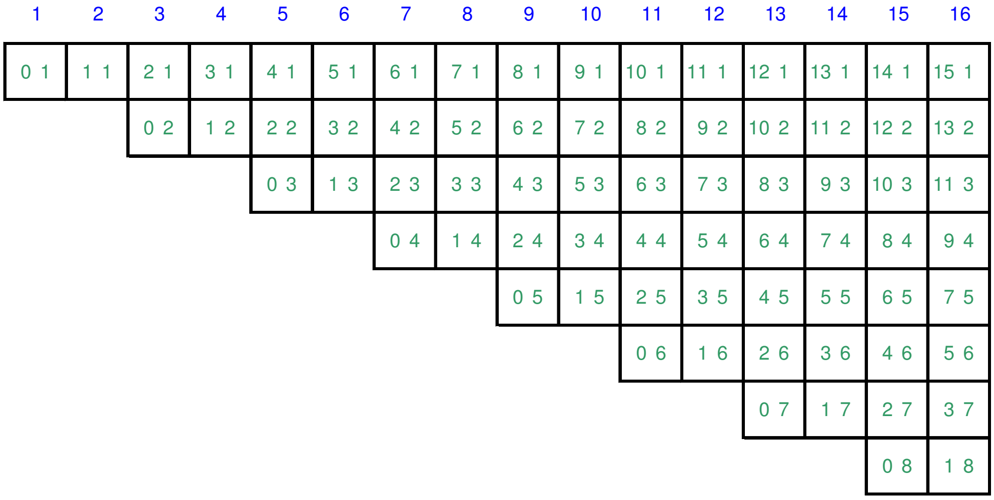

1	2	3	4	5	6	7	8	9	10	11	12	13	14	15	16
0 1	1 1	2 1	3 1	4 1	5 1	6 1	7 1	8 1	9 1	10 1	11 1	12 1	13 1	14 1	15 1
		0 2	1 2	2 2	3 2	4 2	5 2	6 2	7 2	8 2	9 2	10 2	11 2	12 2	13 2
				0 3	1 3	2 3	3 3	4 3	5 3	6 3	7 3	8 3	9 3	10 3	11 3
						0 4	1 4	2 4	3 4	4 4	5 4	6 4	7 4	8 4	9 4
								0 5	1 5	2 5	3 5	4 5	5 5	6 5	7 5
										0 6	1 6	2 6	3 6	4 6	5 6
												0 7	1 7	2 7	3 7
														0 8	1 8

Figure 3.9. Tabulation of the first 16 mode groups in a 50um graded-index fibre at 850nm. Mode group numbers in blue and LP$_{\eta,\mu}$ designation in green.

Assuming all modes are equally excited, the near-field intensity distribution P$_g$ of each mode group m is given by

$$P_g(m) = \sum_{\mu=1}^{\mathrm{int}[(m+1)/2]} \left[\left(E_{\eta,\mu}\right)^2_{\theta_o=0} + \left(E_{\eta,\mu}\right)^2_{\theta_o=\pi/2} \right] \qquad \textbf{(3.28)}$$

where, from eqn. (3.26), $\eta = m+1-2\mu$.

The total near-field distribution P$_{tot}$ is given by

$$P_{tot} = \sum_{m=1}^{M} \left[P_g(m) \cdot \mathrm{MTF}(m) \right] \qquad \textbf{(3.29)}$$

where, for a fully-filled fiber, MTF(m)=1 for all mode numbers.

Examples of near-field profiles for mode group numbers 4 and 14 are shown in Figure 3.10 where it can be seen that the power distributions consist of circularly symmetric rings where the number of rings corresponds to half the mode group number.

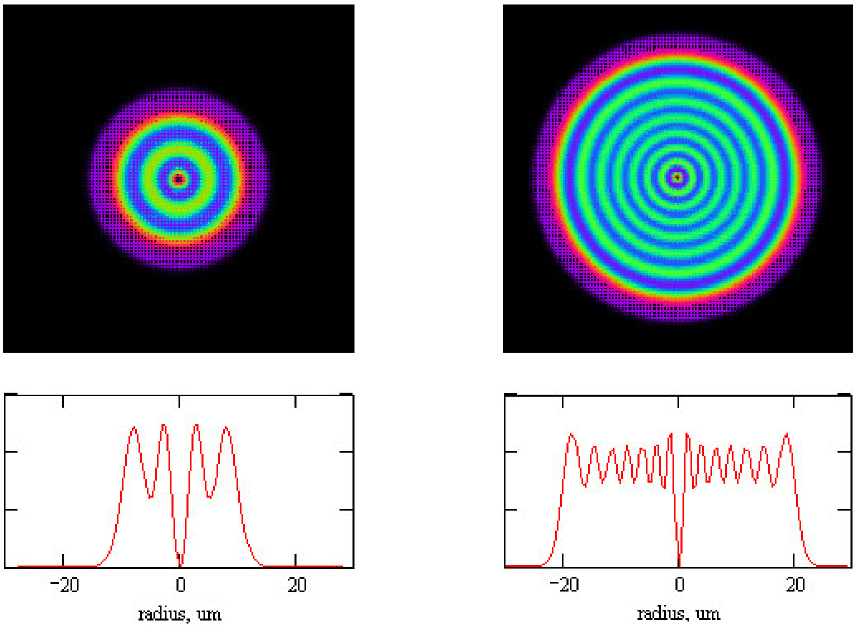

mode group 4

mode group 14

Figure 3.10. Intensity distributions of mode group numbers 4 and 10 in a 50um graded-index fibre.

3.2.3 Leaky modes

In the guided mode regime where

$$k_o n_{clad} \le \beta \le k_o n_{core} \tag{3.30}$$

modes exist within two caustics, defined by positive values of the coefficient of F(r) in the Helmholtz equation, eqn. (3.19), as follows,

$$\left(n(r)^2 k_o{}^2 - \beta^2\right) - \left(\frac{\eta^2}{r^2}\right) \ge 0 \tag{3.31}$$

There exists, however, a region where the mode is beyond cut-off, but satisfies the following inequality [24]:

$$k_o^2 n_{clad}^2 - \frac{\eta^2}{a^2} \le \beta^2 < k_o^2 n_{clad}^2 \qquad \textbf{(3.32)}$$

This situation is represented in Figure 3.11, where the LP$_{16,3}$ mode, for example, is bound in the region 11um to 24um and is radiative beyond 32um. From a quantum-mechanical point of view, the guided light can be described as *tunnelling* through part of the cladding, via the evanescent tail, and then coupling to a radiation mode. Some leaky modes are rapidly attenuated after a few cm whereas other may propagate for a km or more [25].

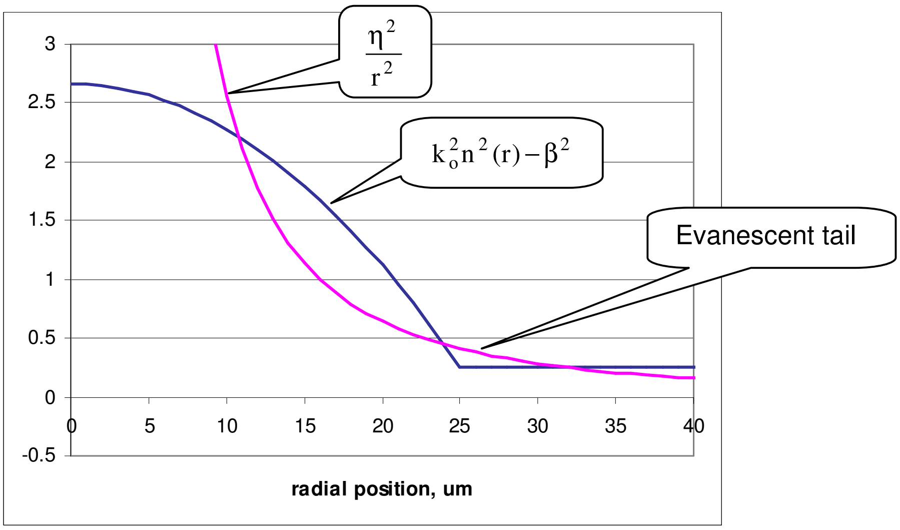

Figure 3.11. Plot of terms in eqn.(3.31) showing a leaky mode, LP$_{16,3}$

In a graded-index fibre the total number of leaky modes is given by,

$$N_{leaky} = \frac{V^2}{12} \qquad \textbf{(3.33)}$$

where :

$$V = k_o aNA \qquad \textbf{(3.34)}$$

Comparison with eqn. (3.24) indicates that leaky modes can carry up to 25% of the total power in a graded-index fibre.

The field distributions of leaky modes can also be calculated using eqn. (3.20), where the (η,μ) values of leaky modes must satisfy the following inequality [25],

$$M \leq 2\mu + \eta - 1 \leq M + \frac{\eta^2}{4M} \qquad \textbf{(3.35)}$$

where M is the number of guided mode groups, given by eqn. (3.27)

As an example, in a 50um fibre at 850nm there are 120 leaky modes, including both polarisations and azimuthal orientations, making a total of 30 discrete (η,μ) combinations. A tabulation of the complete set of guided and leaky modes for a 50um fibre at 850nm is given in Appendix C.

The effect of leaky modes is to distort the near-field intensity distribution. This can be seen in Figure 3.12 where the complete leaky mode spectrum has been added to the guided mode spectrum, shown in blue. The intensity profile is much squarer than the quasi-parabolic shape of the guided modes alone.

The presence of leaky modes has long been a source of difficulty for refractive index profiling methods that are based on the principle that the shape of the index profile is approximately proportional to the intensity profile if all the guided modes are equally excited. The presence of leaky modes seriously perturbs the accuracy of these methods and several efforts have been made to compensate for them [26].

Leaky modes are difficult to avoid as they lie entirely within the meridional NA of a fibre. The impact of leaky modes in mode control devices will be discussed in CHAPTER 6.

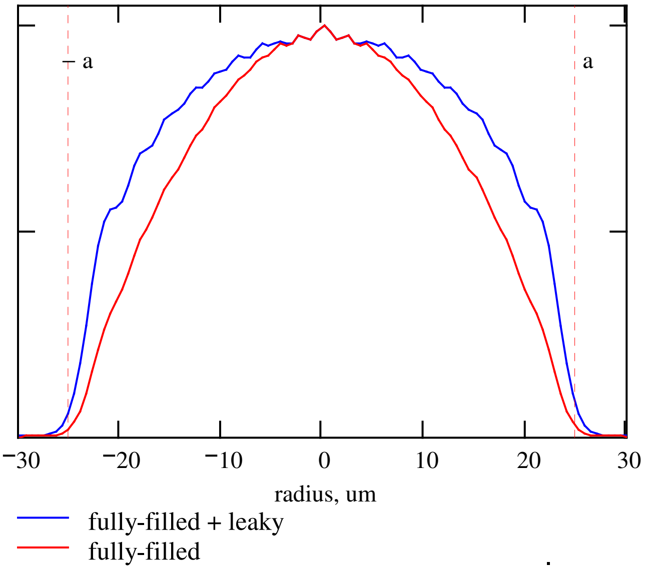

Figure 3.12. Computed near-field intensity profile of 50um graded-index fibre showing guided modes (red) and effect of adding leaky modes to guided modes (blue).

3.3 Mode Overlap Integral

To determine the mode distribution coupled into a target fibre from a source fibre it is necessary to compute the mode overlap factor ε of each source mode E_S with each target mode E_T. The overlap integral required to do this is as follows,

$$\varepsilon = \frac{\int\int E_S(x,y)E_T(x,y)dxdy}{\sqrt{\int\int E_S(x,y)E_S(x,y)dxdy}\sqrt{\int\int E_T(x,y)E_T(x,y)dxdy}} \quad \textbf{(3.36)}$$

The mode overlap factor can take values from zero, in the case of no overlap, for example belonging to the same waveguide, to unity, for complete overlap.

The overlap integral has to be evaluated numerically for each mode combination and is therefore computationally intensive. It was found, however, that for Bessel and Laguerre-Gauss (LG) modes ε was negligibly small for coupling between modes of a different azimuthal mode number η. Thus, it was only necessary to compute ε for modes having the same value of η.

As an example, Table 3.1 shows $|\varepsilon|$ values for coupling between the $LP_{2,1}$ Bessel mode and the $LP_{2,\mu}$ LG modes. Note that the sum of the squares of the coefficients in the Table is close to unity, indicating that power coupled into modes with a different azimuthal mode number is very small.

$LP_{2,1}$	$LP_{2,2}$	$LP_{2,3}$	$LP_{2,4}$	$LP_{2,5}$	$LP_{2,6}$	$LP_{2,7}$	$LP_{2,8}$	$LP_{2,9}$
0.305	0.414	0.451	0.437	0.389	0.319	0.238	0.154	0.077

Table 3.1. Overlap coefficients between $LP_{2,1}$ Bessel mode and $LP_{2,\mu}$ Laguerre-Gaussian modes.

To compute the near-field power distribution coupled into the graded fibre for the $LP_{2,1}$ mode in the example above, the power distributions of the modes shown in Table 3.1 were added in proportion to the square of the value of their respective overlap coefficients. Figure 3.13 shows the power distribution of the $LP_{2,1}$ Bessel mode and the resultant power distribution coupled into a graded-index fibre. It can be seen that the latter has the same four-lobed shape as the $LP_{2,1}$ Bessel mode but that power is distributed over a range of radial mode numbers μ.

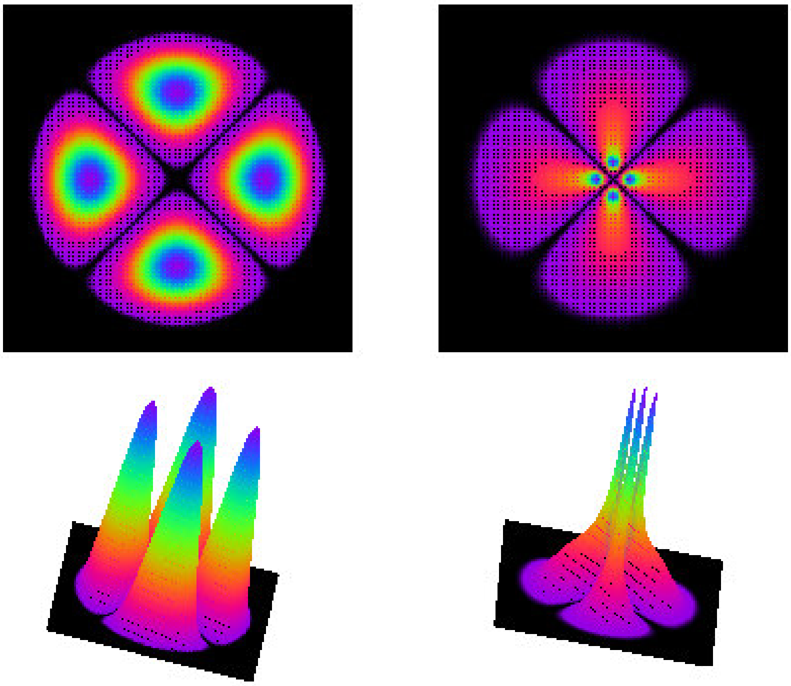

$LP_{2,1}$ Bessel mode

Laguerre-Gauss modes

Figure 3.13. Mode power distributions for the $LP_{2,1}$ Bessel mode in a step-index fibre and for the power distribution coupled into a graded-index fibre.

3.4 Chapter Summary

This chapter has described how to compute the mode power distribution in step-index and parabolic-index fibres for any mode combination. It was shown that the entire leaky mode set of a graded-index fibre falls within the meridional numerical aperture for a graded-index fibre, and that leaky modes may cause distortion of the intensity profile. The use of the mode overlap integral to compute mode coupling between dissimilar fibres has been demonstrated and it was found that coupling efficiency between the modes in step and graded-index fibres of differing azimuthal mode number, was negligible.

CHAPTER 4

MEASUREMENT OF MODE DISTRIBUTION

This chapter describes the design and construction of an apparatus for measuring the mode distribution in multimode fibres. The method is based on original work by Daido et al. [27], which was further developed by Leminger et al. [28]. The mode distribution is computed from a measurement of the near-field intensity distribution in the fibre and the method is well suited to real-time study of modal effects in fibres and devices.

4.1 Measurement Theory

For a fibre with a power-law index profile n(r), eqn. (3.18), the near-field intensity profile in the fibre I(r) may be determined from an integration of the Mode Transfer Function, MTF(δ), which represents the relative amount of power in the fibre modes. Ignoring constants, MTF(δ) is given by:

$$I(r) = \int_{\Delta\left(r/a\right)^{\alpha}}^{\Delta} MTF(\delta).d\delta \qquad \textbf{(4.1)}$$

where: δ is the normalised propagation constant, given by

$$\delta = \frac{1}{2}\left(1 - \frac{\beta^2}{n_{core}^2 k_o^2}\right) \qquad \textbf{(4.2)}$$

Differentiating both sides of eqn. (4.1), ignoring constants, gives

$$\mathrm{MTF}(\delta)=\left[\frac{dI(r)}{dr}\cdot\frac{1}{r^{\alpha-1}}\right]_{\delta=\Delta\left(r/a\right)^{\alpha}} \tag{4.3}$$

The MTF is usually plotted as in terms of the ratio of the principal mode number m and the maximum principal mode number M. For a power-law fibre, this ratio is determined by substituting eqn. (4.2) into eqn. (3.25), giving

$$\frac{m}{M}=\left[\frac{\delta}{\Delta}\right]^{(2+\alpha)/2\alpha} \tag{4.4}$$

Also, for a power law fibre,

$$\frac{\delta}{\Delta}=\left[\frac{r}{a}\right]^{\alpha} \tag{4.5}$$

thus from eqns. (4.4) and (4.5)

$$\frac{m}{M}=\left[\frac{r}{a}\right]^{(2+\alpha)/2} \tag{4.6}$$

The term (m/M) is usually referred to as the relative mode number, or the normalised mode number. The maximum principal mode number M is given by eqn. (3.27).

Thus, from a measurement of the near-field intensity profile at the end of the fibre, and knowledge of the fibre radius and the index profile shape factor, the MTF can be determined. The MTF is a measure of the relative power in the modes in the fibre and for a fully-filled fibre the MTF assumes a unity value for all mode numbers. If certain mode groups are less well filled than others then the MTF will show this by the presence of peaks and troughs.

It was stated in section 3.2.2 that the number of modes in a mode group is equal to the mode group number. Thus, higher-order mode groups contain more discrete modes and therefore carry more power. A useful measure of mode-filling in a fibre is the *Mode Power Distribution* (MPD), which is equal to the MTF multiplied by the mode group number:

$$\mathrm{MPD}(m') = \mathrm{MTF}(m')m' \tag{4.7}$$

where the substitution m' = m/M has been made.

Figure 4.1 shows an example of an MTF and its corresponding MPD. Also shown is the *normalised MPD,* which is sometimes used as a performance metric in international standards.

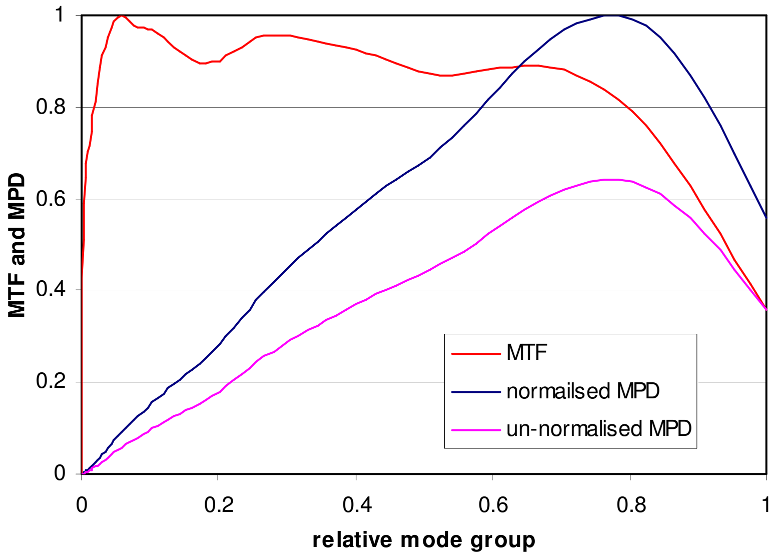

Figure 4.1. Example of an MTF and its corresponding MPD.

4.1.1 Constraints and Assumptions

The MTF measurement method described here is only valid under certain conditions, which are as follows:

4.1.1.1 There are no leaky modes present.

The presence of leaky modes results in a distortion of the near-field intensity profile. As the leaky modes in a graded-index fibre all occur within the meridional NA of the fibre, they cannot be distinguished from guided modes by the MTF measurement method and can lead to a distortion in the computed MTF. Some care is therefore required in interpreting MTF curves when it is thought leaky modes may be present. This issue will be considered in more detail in section 6.3.1.

4.1.1.2 The near-field profile is azimuthally symmetric.

This requirement is met if

(a) the index profile is circularly symmetric, and
(b) modes within a mode group carry the same power, and
(c) there are random phases between the propagating modes.

Generally, (a) can be assumed for fibres under the current study. Constraint (b) will normally occur due to mode-coupling between degenerate modes [27]. Regarding constraint (c), if the relative time delay between modes is less than the coherence time of the source then interference between different modes can occur leading to speckle.

It has been found [29] that both conditions, (b) and (c), can be simultaneously met if the line-width $\Delta\lambda$ of the source is sufficiently broad, leading to *the Mode-Continuum Approximation*, given by

$$\frac{\Delta\lambda}{\lambda} \geq \frac{\sqrt{2\Delta}}{a \cdot k_o \cdot N} \qquad \textbf{(4.8)}$$

where N is the group index, given by:

$$N = n_{core} - \lambda \cdot \frac{dn_{core}}{d\lambda} \qquad \textbf{(4.9)}$$

Typically, for a 50μm core diameter fibre, with 0.21 numerical aperture, then $\Delta\lambda$>0.5nm at 850nm and $\Delta\lambda$>1.0nm at 1300nm both satisfy this condition.

If the source line-width does not meet this criterion then the method can, however, still be applied by gently agitating the fibre so as to cause a temporal averaging of the speckle pattern. In this case, it is important to ensure the near-field is azimuthally symmetric. This can be achieved by checking that the MTFs measured at 45-degree intervals are sufficiently similar.

4.1.1.3 A large Number of Modes are Excited

There is an assumption in eqn. (4.1) that the near-field intensity distribution is equal to a summation of the power distributions of individual mode groups. Daido et al. [27] have shown that at least three mode groups must be present to satisfy this requirement, and also that there should be no abrupt changes in power between mode groups.

4.1.1.4 The Intensity Profile is the same as the Index profile

The assumption is also made in eqn. (4.1) that the intensity profile of a fully-filled fibre is the same shape as the square of the index profile. While this is generally true for a good proportion of the fibre radius, it can lead to errors towards the core/cladding boundary. The limitation of this constraint will be discussed further in section 4.4.

4.2 Instrumentation

The MTF measurement technique consists of measuring the near-field intensity distribution in the fibre under test, using a video microscope, and then inserting the derivative of the measured intensity profile into eqn. (4.3).

MTF test equipment was designed and built by this author, in collaboration with Arden Photonics Ltd [30]. A detailed knowledge of the system has enabled it to be modified to suit the requirements of this thesis. Figure 4.2 shows a plan view of the apparatus.

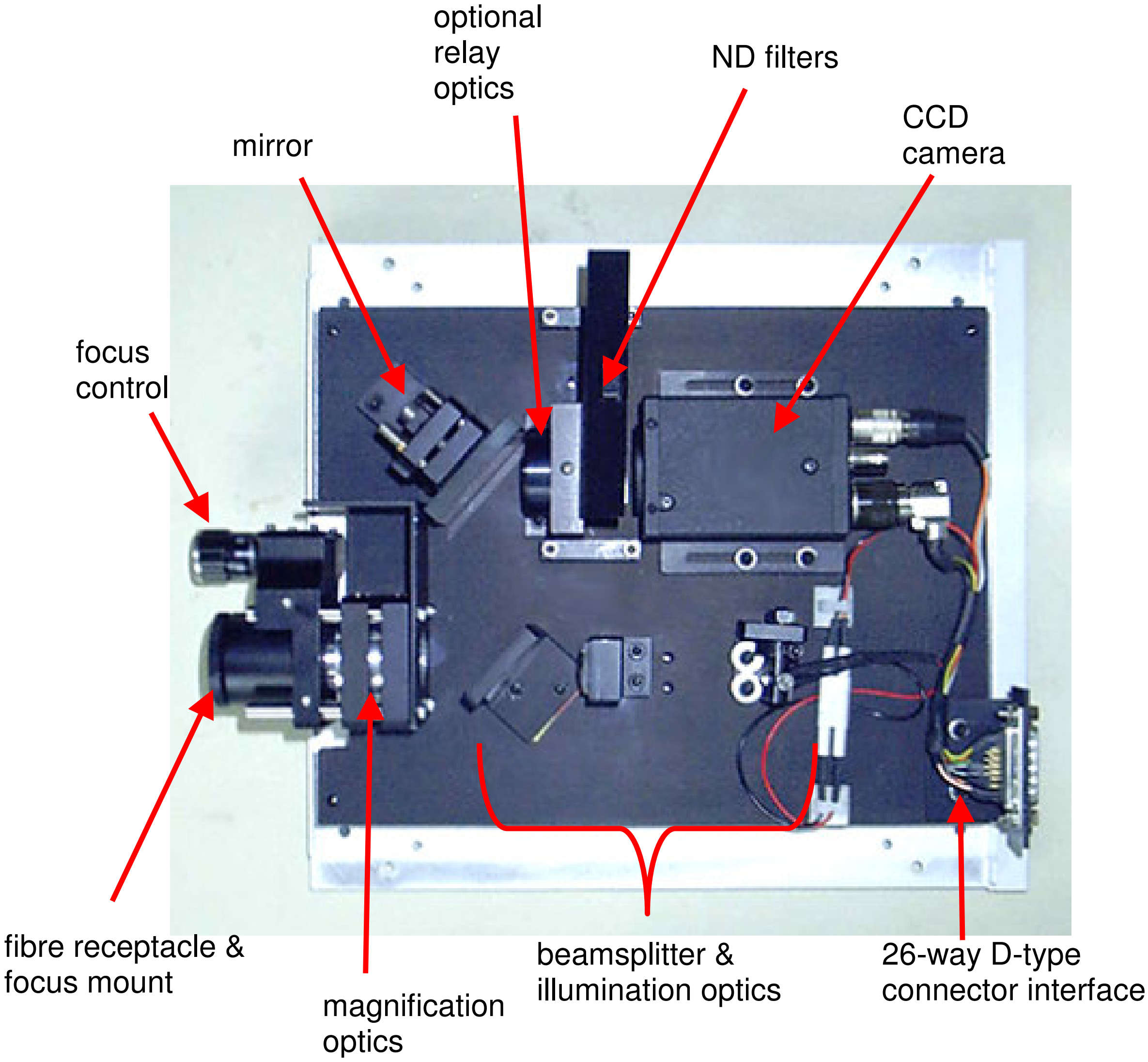

Figure 4.2. Apparatus for measuring mode power distributions.

The optical system consists of a receptacle to position the fibre end, some magnifying optics and a camera. Additional illumination optics and a beamsplitter are provided so that an end-view image of the fibre end can be formed for checking the cleanliness of the fibre end and for focussing.

The receptacle is, for example, a standard 2.5mm diameter adaptor, which can accommodate fibres terminated with SC, FC or ST connector types. Alignment of the fibre to the optical axis is by dead reckoning, although a tip/tilt gimbal mount on the mirror can effect some lateral adjustment. A microscope objective focusses the image onto a CCD camera via a beamsplitter, a mirror and optional neutral density (ND) filters. For measurement of fibre diameters up to 1mm, some additional relay optics may be fitted in front of the camera to increase the field of view of the system.

A schematic of the electronic and software interfaces is shown in Figure 4.3. The camera settings, such as gain and electronic shutter, are controlled via an RS232 computer interface and the video signal is captured by an 8-bit framegrabber. The software, which was written in Visual Basic, makes use of some commercial ActiveX control tools, *Common Vision Blox*, for controlling the camera settings and for data acquisition by the framegrabber.

A real-time display of MTF and MPD is then computed, together with Coupled Power Ratio (CPR) and Encircled Flux (EF), which are also used in international standards [3], [31].

Data analysis, which was also coded in Visual Basic, consisted of the following operations:

1. Acquire a bitmap image and convert to XY data array.
2. Average several frames for noise and speckle reduction.
3. Subtract background level to improve linearity.
4. Locate the centroid and extract intensity profile passing through it.
5. Differentiate intensity profile using a Savitsky-Golay filter [32].
6. Locate centre of differentiated profile using a weighted symmetry algorithm.
7. Compute MTF using eqn. (4.3).
8. Compute and MPD, EF and CPR
9. Display plots of the results

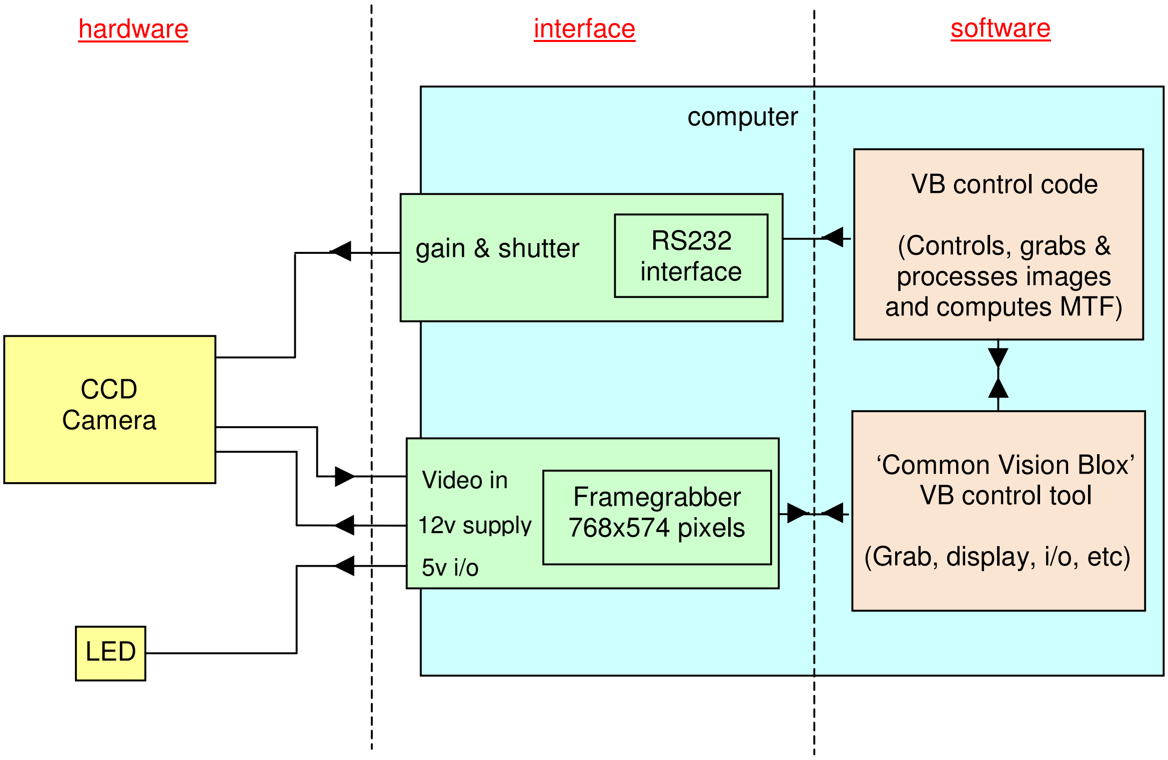

Figure 4.3. Schematic of control system of the measurement apparatus.

Initially, the system employed a silicon CCD camera (JAI CV-A60) for measurement at 850nm. A further part of the project was to fit an InGaAs camera to enable modal measurements to be made in the 1300nm window. The InGaAs camera (Xenics XEVA-USB) had only 320x256 pixels and was somewhat inferior to the silicon CCD camera in terms of the number of dead pixels and some fixed pattern noise. It was necessary, therefore, to develop and implement correction algorithms to improve the quality of the image. This is discussed further in the next section. For the InGaAs camera, linear interpolation was used to increase the apparent resolution to 640x512 pixels.

4.2.1 Accuracy and Calibration

The accuracy of the near-field measurement is determined by: (a) spatial uniformity of the camera array, (b) pixel response uniformity, (c) intensity linearity, (d) calibration of the optical magnification, and (e) numerical computation, [33].

(a) Spatial Uniformity

The spatial uniformity of the cameras was not checked, but it is understood that the spatial uniformity of modern silicon CCD cameras is extremely good. One method of checking the spatial uniformity, however, is to determine the position of, for example, the centre of the near-field distribution from a singlemode fibre as it is moved around the field-of-view using a calibrated micrometer. A second method is to make use of a calibrated chrome-on-glass artifact consisting of a regular array of dots, or cross-hairs. The spatial uniformity of the InGaAs camera is unlikely to be as good as the silicon CCD and measurements of this type would be advantageous.

(b) Pixel Uniformity

Several InGaAs cameras were tested and were all found to have a number of *dead pixels*. These are pixels that are permanently dark, or light, or show a highly non-linear response. For example, Figure 4.4 shows a 10 x 7 pixel portion of the image of a uniformly grey field, where a number of dead pixels are located. In this example the dead pixels form into two clusters, each containing white pixels, black pixels and also some with intermediate values, which are slightly darker than the background. In order to isolate dead pixels, the image of a uniformly grey field was scanned numerically for pixels that deviate from the mean intensity of the whole field by a certain amount, typically 30 ADC counts for an 8 bit image. The dead pixels were then replaced with values interpolated from nearest neighbours, although some care was required where clusters of dead pixels occurred, as in the figure. In this case, the immediate neighbours were avoided. The fraction of dead pixels was typically about 1.2%, corresponding to about 1000 pixels, although it was found that the first column and the last two columns were consistently faulty in this model of camera, amounting to 768 of the dead pixels.

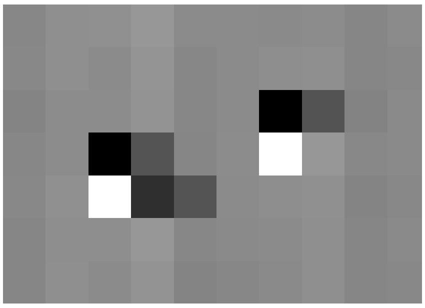

Figure 4.4. Example of faulty pixels in InGaAs camera.

A second uniformity effect present in all of the InGaAs cameras tested was that *of fixed pattern* noise. This was manifested as vertical striations in the image, whose amplitude was independent of the optical signal level.

Figure 4.5 shows a comparison of the pixel values across a sample of 50 columns for (a) a dark field, and (b) a grey field. In each case, the pixel values were the average of the 256 pixels in each column. It can be seen that the variation between columns is almost identical for both fields, although the mean values for the dark and grey fields were 14.2 counts and 123.7 counts, respectively. It was found to be possible to compensate for fixed pattern noise by acquiring a dark image and then subtracting this from all subsequent measurements. Note that the camera had been configured with a positive dark level offset of about 14 counts so that frame averaging would give a net improvement in the signal to noise ratio. This offset, as well as the fixed pattern noise, is removed by subtracting the background image.

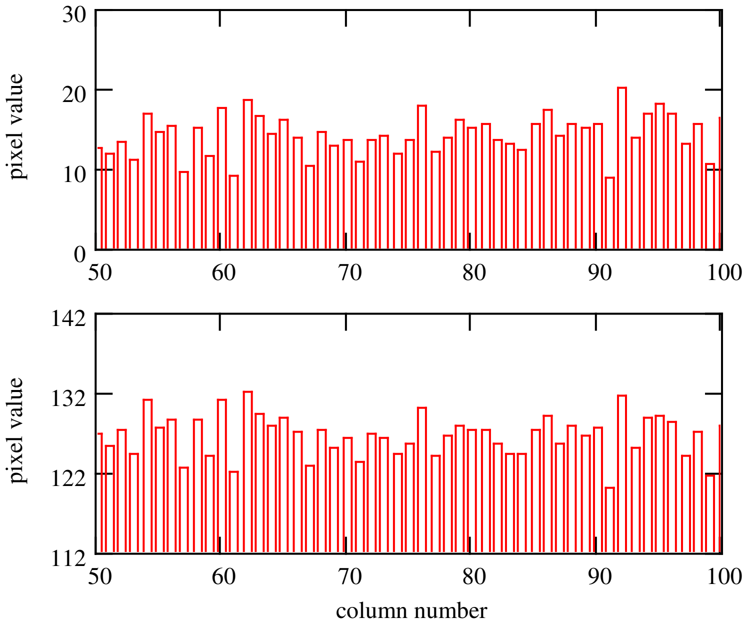

Figure 4.5. Example of fixed pattern noise in InGaAs camera, (a) dark field, and (b) grey field.

(c) Intensity Linearity

The intensity linearity of the system was verified in two ways, (i) by comparing measurements made at a given light level, with a range of different camera shutter settings, and (ii) by comparing measurements made at a fixed shutter setting, with different light levels. Firstly, the near-field of a well-filled 50um fibre was measured and pixel correction and background subtraction applied, for a range of shutter settings, over an order of magnitude. The chosen metric was Encircled Flux as this measurement consists of radial integration and is therefore very susceptible to dark-field offset, and to intensity linearity.

Figure 4.6 shows the results, where the encircled flux values have been plotted as a deviation from the mean value, at each radial position. The peak deviation is about ±0.002 occurring in the radial region 20um to 25um. Note that encircled flux is defined as a normalised function and so this level of deviation corresponds to ±0.2%.

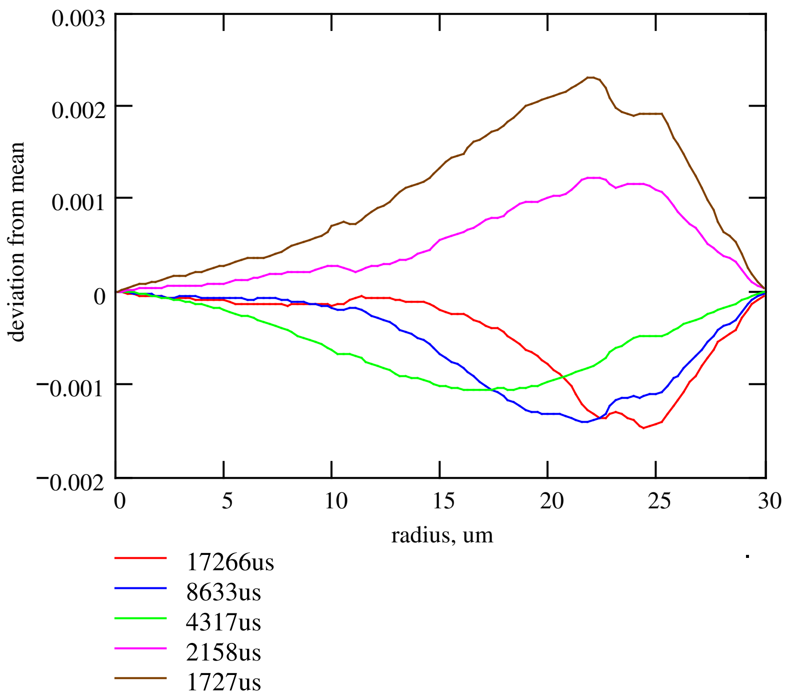

Figure 4.6. Deviation of measured encircled flux from the mean value on an InGaAs camera, with a range of exposure settings.

The other test consisted of using a fixed shutter setting and comparing measurements with and without a 10dB neutral density filter in front of the camera. It was found that the peak offset between the curves was 0.0022, occurring between 15um and 25um.

The tolerance range for encircled flux at 1300nm, given in draft IEC specification, 61280-4-1 34 is shown in Table 4.1. The measured results are well within the required tolerance ranges for all radial positions except for the value at 22um where it is only just inside. It was concluded that the InGaAs camera was sufficiently linear for accurate measurements of encircled flux and MPD, although some further work on characterising the intensity uniformity of individual pixels would be of merit using, for example, the method described by Fatadin et al. [33] with a calibrated attenuator.

Radial position, um	EF tolerance range
5	0.0387
10	0.1128
15	0.1080
20	0.0157
22	0.0051

Table 4.1. Summary of tolerance ranges for encircled flux at 1300nm in draft standard, IEC61280-4-1.

(d) Magnification

The system magnification was initially calibrated by measuring the size of a fibre of known diameter, using incident illumination. The calibration factor was typically 0.28um/pixel for the silicon camera and 0.26um/pixel for the InGaAs camera, with pixel interpolation in the latter. A disadvantage with this method is that some decision on the intensity threshold corresponding to the true fibre edge position is required. Baines et al [35] showed that the true edge of a fibre occurs at between 25% and 40% intensity levels, depending on the coherence of the illuminating source. Furthermore, they showed that the 50% level was the least sensitive to defocus. They described the use of a calibration annulus, where the average of the inner and outer edge positions was found to be insensitive both to the intensity level chosen, and to defocus. A 125um chrome-on-glass annulus, with 20um line-width, was therefore obtained for this work. The annulus was illuminated with incident light and brought into focus, then the edge points for the inner and outer edges of the chrome were located, using the 50% intensity threshold. Circle fits were then applied to both sets of edge points and the average of the two fits was computed. Finally, the magnification was calculated from the known diameter of the annulus.

(e) Numerical Methods

MTF and MPD are derived parameters requiring differentiation of the near-field image. To do this a Savitsky-Golay filter [36] was used, comprising a sliding polynomial fit over a number of adjacent datapoints, followed by analytical differentiation of the fit function. The number of points used in the fit determines the amount of smoothing that occurs and there is therefore a trade-off between spatial resolution and noise. Figure 4.7 shows the computed MPD for a measurement on a well-filled 62.5um fibre as a function of the number of datapoints used in the fit. It can be seen that as the number of datapoints is increased, the noise on the curves is reduced, but the ripple on the rising edge, which is structure due to individual mode groups, is also smoothed out. Further, the peak position of the MPD curve moves slightly to the left and the falling edge is less steep. So, clearly, some care is required to select the optimum number of points. In the example shown, 13 datapoints is probably a good compromise. In this particular experiment, the magnification was 0.22um/pixel and so 13 datapoints corresponded to a fit width of 2.6um.

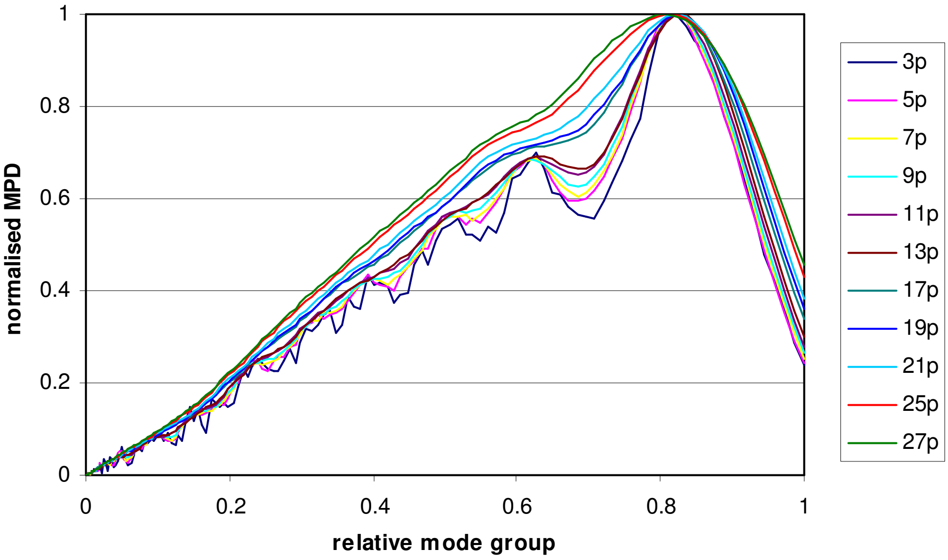

Figure 4.7. Normalised MPD as a function of the number of fitted datapoints for measurements on 62.5um fibre.

A further aspect of measurement accuracy is that in eqn. (4.6) a knowledge of the profile shape and core diameter is required. The effect of these parameters on MPD, for the 62.5um fibre with 13 datapoints, in the above example, is shown in Figure 4.8 and Figure 4.9. The effect of assuming too high a value of alpha is to shift the peak MPD to the left, but with reducing effect on the falling edge towards higher mode-groups. For comparison, assuming too high a value of core diameter also shifts the peak MPD to the left, but, in this case, the falling edge is also shifted towards the left.

Some care must be exercised, therefore, when selecting values for core diameter and alpha. As an example of a typical manufacturing specification, the core diameter tolerance of high bandwidth fibre from Corning, Inc. or OFS, Inc. is specified as ±2.5um. An uncertainty of this magnitude would clearly have a very large effect on the measured MPD. The core diameter of a particular fibre sample can, however, routinely be measured to an accuracy of better than 0.5um using commercial apparatus, where core diameter is defined as the diameter at the 2.5% intensity level of the near-field of the fibre under fully-filled conditions [37].

In the case of alpha, fibre manufacturers do not report this value as it is generally part of the proprietary design of the fibre, although typical values are in the range 1.9 to 2.0. Also, many fibres do not have a perfect power-law profile but may have a dip, or some ripple structure around the core centre, in which case a knowledge of the exact index profile would be advantageous and could be used in eqn. (4.3). Finally, there is an assumption in eqn. (4.1) that the intensity profile of a fully-filled fibre is the same shape as the square of the index profile. This assumption, however, is not strictly true and can lead to measurement errors, particularly for well-filled fibres. This aspect is considered in detail in section 4.4.

As well as accuracy, another important performance metric is the measurement reproducibility. To test this, a series of ten measurements was carried out on a 62.5um patchcord where, between each measurement, the fibre connector was removed from the measurement system and then re-inserted and the image re-focussed. The results, shown in Figure 4.10, indicate that the positions of the peak MPD and the ripples on the rising edge were quite static, but the amplitudes of the latter were variable. The effect of this on the falling edge is quite marked with a peak to peak variation of 0.1 at unity mode group number. The number of datapoints used in the fit was 13.

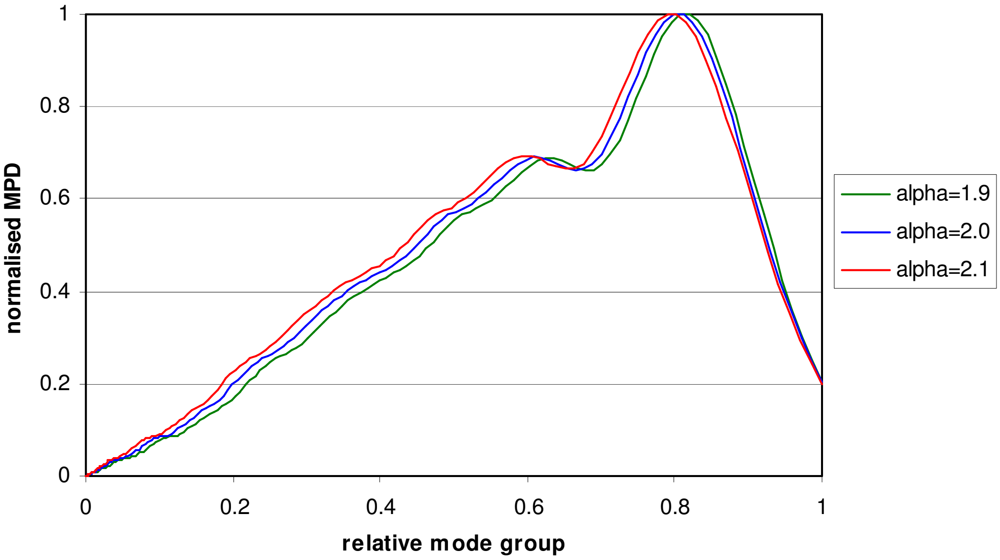

Figure 4.8. Effect on computed MPD for 62.5um fibre as function of assumed alpha value.

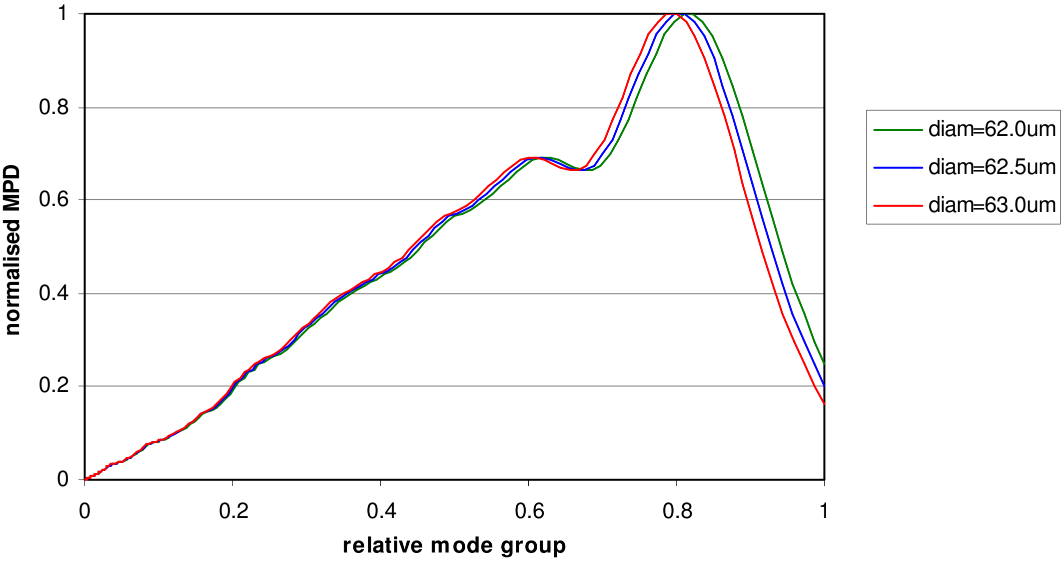

Figure 4.9. Effect on computed MPD for 62.5um fibre as function of assumed core diameter.

It was postulated that this was due to the normalisation process, in that variations in the peak MPD in the un-normalised data translated into variations in the MPD on the falling edge in the normalised data. In an effort to improve reproducibility, the data was reprocessed using 21 datapoints in the fit. In this case, the variation in magnitude between the curves was less and the subsequent range in MPD at unity mode group number was reduced to 0.05, as shown in Figure 4.11.

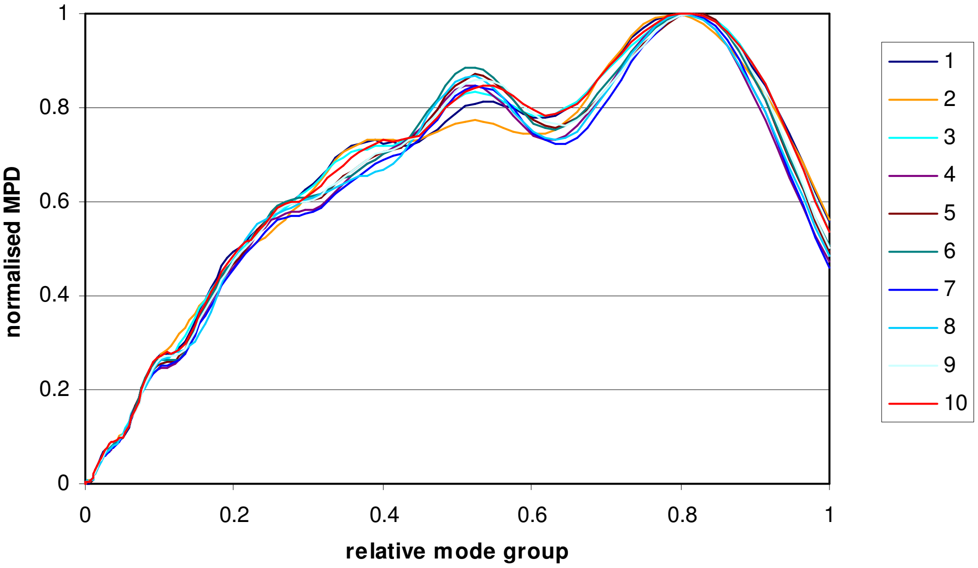

Figure 4.10. Measured MPDs on 62.5um fibre, using 13 datapoints in fit, to evaluate reproducibility.

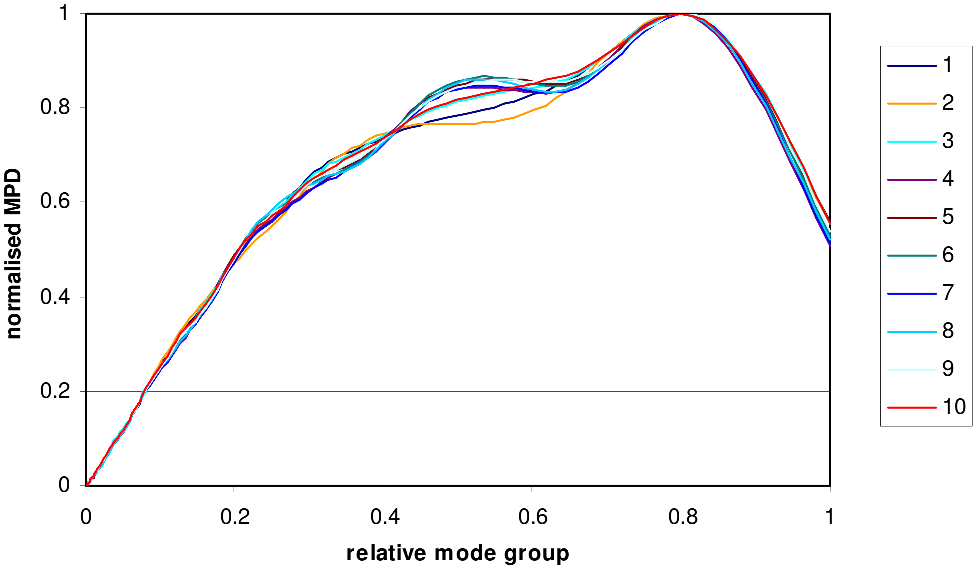

Figure 4.11. Measured MPDs on 62.5um fibre, using 21 datapoints in fit, to evaluate reproducibility.

Thus, the measurement reproducibility may be improved by increasing the number of datapoints in the fit, but there is, of course, a trade-off against resolution. In order to preserve detail, such as the ripple structure in the rising edge, it is an advantage to use a smaller number of fit points, but to take the average of a large number of measurements.

4.3 Far-Field Measurement Technique for MTF

Although a near-field measurement method was employed in this project, it is also possible to make MTF measurements in the far-field. Comparative measurements made by Rittich [38] showed that measurements made in the two domains agreed well with each other. The advantage of the far-field method is that imaging optics are not required, but, conversely, the data processing is more complicated.

4.3.1 Far-Field Scans

In order to obtain a better understanding of the relationship between the near-field and far-field, some far-field measurements were carried out. The apparatus used to do this and the results obtained are now described.

4.3.1.1 Apparatus

The apparatus, shown in Figure 4.12, comprised an angular rotation mount and a power meter (Megger MPM2000). The fibre under test was mounted on the rotation stage such that its end was accurately positioned on the axis of the stage, using micro-translators. A 1mm diameter pinhole was positioned in front of the detector and the distance between the fibre end and the pinhole was 42mm. This corresponded to an angular resolution at the detector of approximately 1.4°

4.3.1.2 Measurements

Figure 4.13 shows near-field measurements on several different mode distributions in a 50um fibre and Figure 4.14 shows the corresponding far-field scan data.

It can be seen that the near-field and far-field distributions are very similar in shape to each other for all of the launch distributions tested. This indicates that the field shapes of modes in a graded-index fibre are unchanged by propagation through free space.

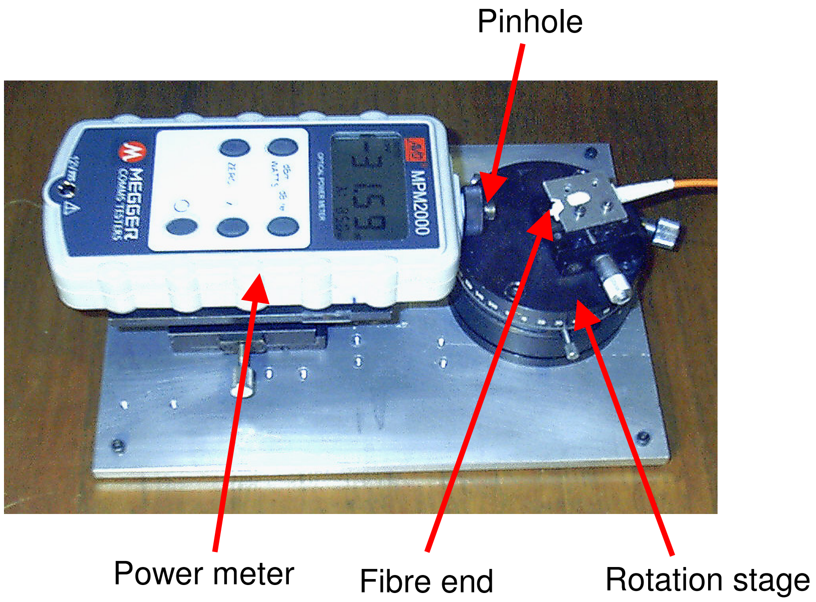

Figure 4.12. Apparatus for measuring the far-field distribution of an optical fibre.

To investigate this observation, the far-field distribution was modelled by computing the diffraction field of individual modes, as follows:

4.3.1.3 Far-Field Modelling

The far-field distribution F(u,v) of an individual mode is given be by the Fourier Transform (FT) of the near-field distribution P(x,y) as follows,

$$F(u,v) = \int\int P(x,y) e^{jk_o(ux+vy)} dxdy \qquad \textbf{(4.10)}$$

where (x,y) are Cartesian co-ordinates in the fibre plane and (u,v) are far-field diffraction angles. Note that P(x,y) and F(u,v) are both field distributions rather than intensity distributions.

Assuming incoherence between the fibre modes, the FTs of each mode may be linearly combined in the same proportion as they occur in the near-field.

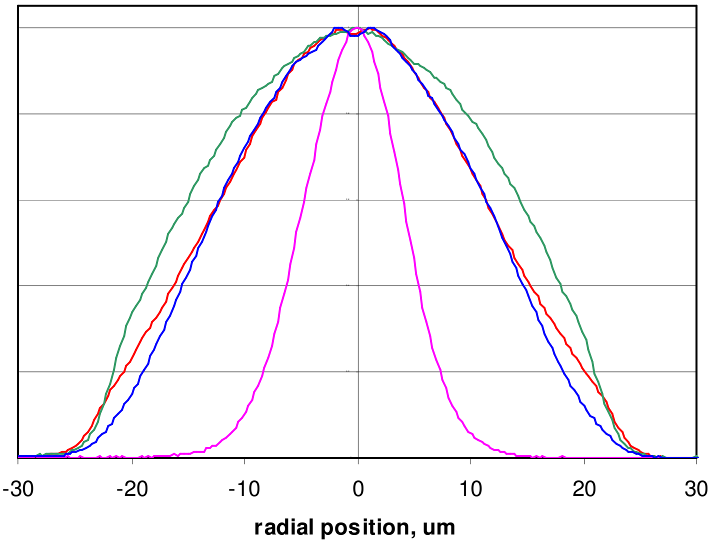

Figure 4.13. Measured near-field intensity profiles in 50um graded-index fibre.

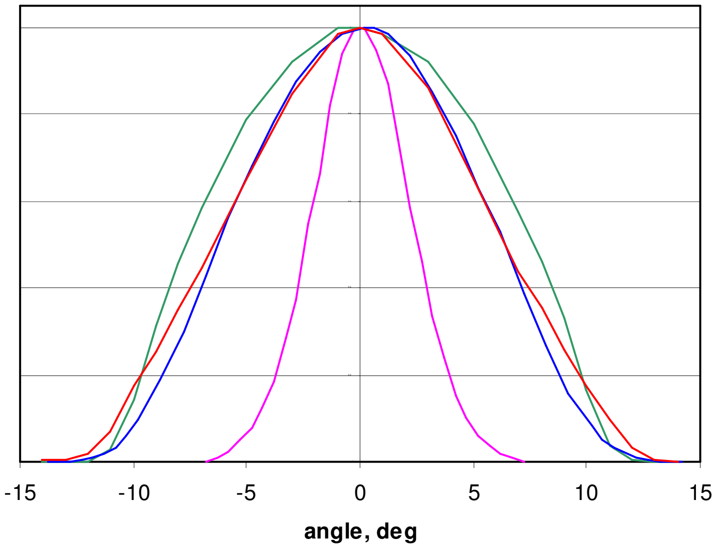

Figure 4.14. Measured far-field intensity profiles in 50um graded-index fibre.

It can be seen in eqn. (4.10) that every point in the far-field consists of a summation of the magnitude and phase of every point in the near-field. The near-field modes were computed on a square matrix of 100x100 points and thus for a far-field grid of the same resolution, a total of 10^8 summations is required to calculate the FT of each mode. Clearly, this operation is computationally intensive, and it was found that the Mathcad program developed for this work took about 12 hours to compute the FT of the mode set in a 50um graded-index fibre.

As an example, Figure 4.15(a) shows the computed near-field and far-field intensity distributions for the $LP_{1,1}$ mode for a graded-index fibre and Figure 4.15(b) shows the intensity distributions for the $LP_{4,5}$ mode. It can be seen in both cases that the shapes of the near-field and far-field distributions are the same. Note that the near-field is plotted over ±30um and the far-field is plotted over ±0.25NA. The fibre radius for the computation was 25um and the NA was 0.21.

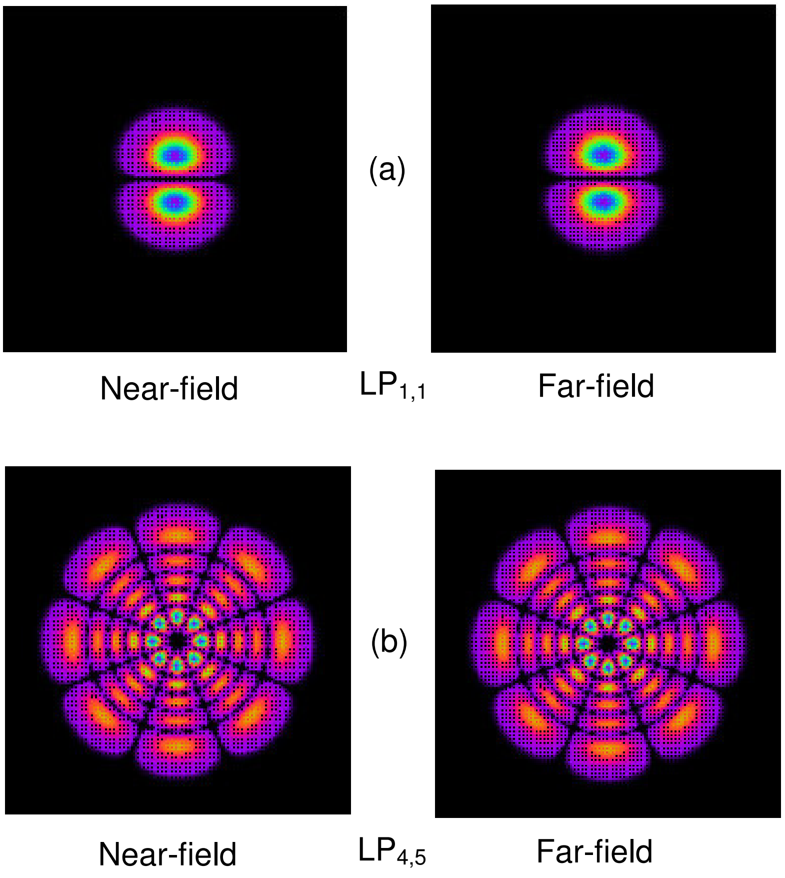

Figure 4.15. Computed near-field and far-field intensity distributions of (a) $LP_{1,1}$, and (b) $LP_{4,5}$ modes in a graded-index fibre.

For comparison, the same modes in a step-index fibre were computed in both domains, shown in Figure 4.16. In this case, the spatial extent of the far-field distribution is inversely proportional to the near-field. This is similar to normal diffraction behaviour associated with plane waves incident on an aperture.

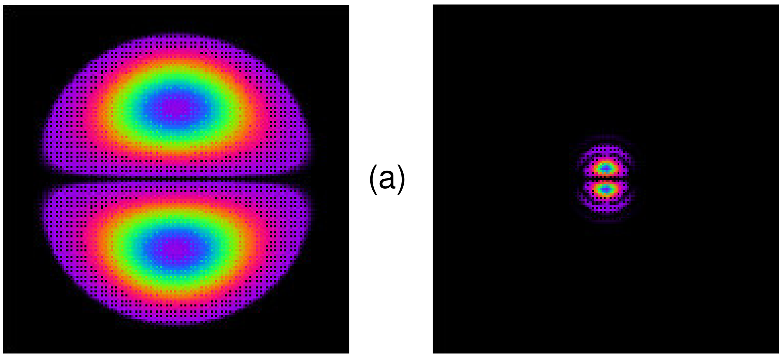

Near-field $LP_{1,1}$ Far-field

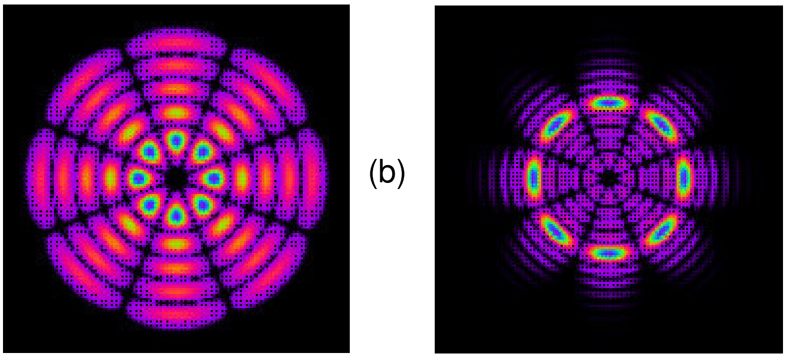

Near-field $LP_{4,5}$ Far-field

Figure 4.16. Computed near-field and far-field intensity distributions of (a) $LP_{1,1}$, and (b) $LP_{4,5}$ modes in step-index fibre.

4.3.1.4 Comparison of Far-Field and Near-Field Measurements

To directly compare measurements made in the far-field with those made in the near-field, the far-field was reconstructed from the near-field as follows:

(i) Measure the near-field distribution and calculate the MPD.

(ii) Compute the relative power of each individual mode by dividing the MPD of each mode group by the number of modes in that mode group and assign this weighting to each mode in that mode group.

(iii) Compute the FT of the entire mode set.

(iv) Combine the FT of each mode in the proportions determined in Step(ii).

A comparison of the measured far-fields from Figure 4.14 with the computed far-fields is shown in Figure 4.17. The agreement is good, indicating that the measurement of MPD by the near-field method described above is an accurate measure of mode-filling.

The similarity of the near-field and far-field mode patterns shows that the MPD can still be measured even if the fibre end is slightly out of focus, as long as a geometrical correction factor is applied to the fibre dimension. This may be useful when the NA of the imaging objective is limited, as it allows the fibre to be moved towards the lens to effectively increase the NA of the optical system.

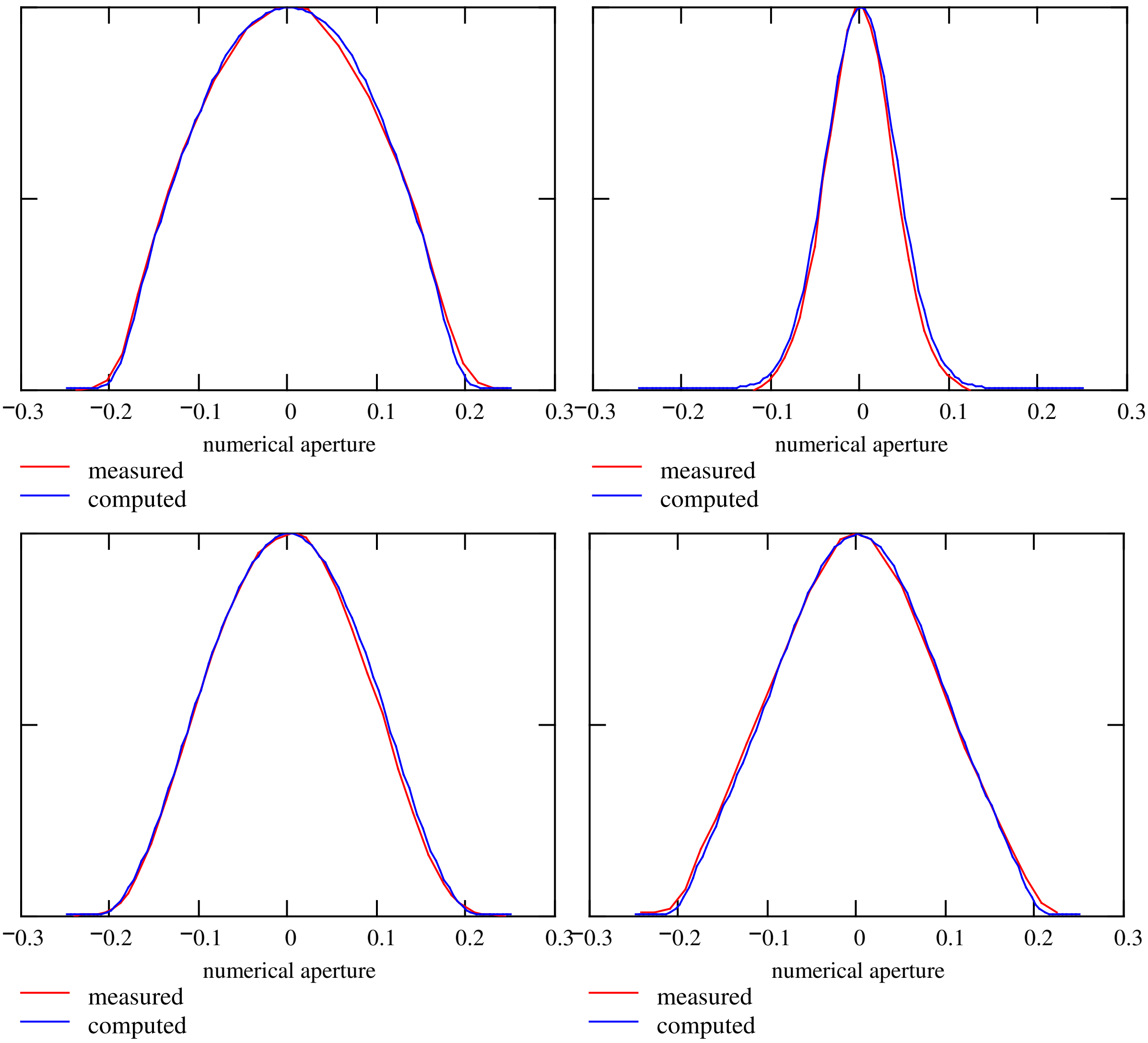

Figure 4.17. Comparison of measured far-field distributions (red) with those computated from near-field measurements (blue).

4.4 Measurement Theory Revisited

In section 4.1.1.4 it was stated that there is an assumption in the measurement method that the intensity profile, $I(r/a)$, of a fully-filled fibre is proportional to the square of the index profile [22], [39]. So, from eqn. (3.18),

$$I(r/a) \propto (r/a)^{\alpha} \tag{4.11}$$

In order to test this assumption, the near-field distribution of a fully-filled 50um graded-index fibre was computed by summing the entire set of Laguerre-Gauss functions. Figure 4.18 shows the computed near-field distribution superimposed on a parabolic profile for comparison and Figure 4.19 shows detail at the core/cladding boundary. Two features can be seen at the boundary: (a) the Laguerre profile oscillates about the parabola with approximately 4um period, and (b) there is an exponential tail extending at least 2um into the cladding.

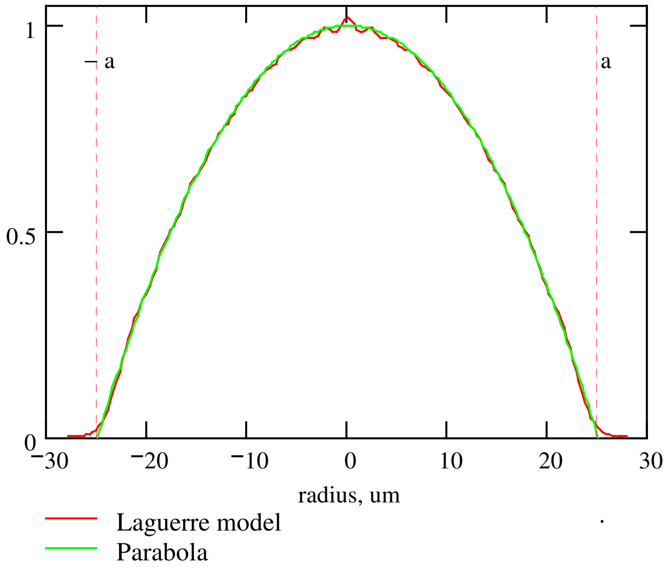

Figure 4.18. Computed near-field intensity profile of 50um graded-index fibre (red) and a parabola for comparison (green).

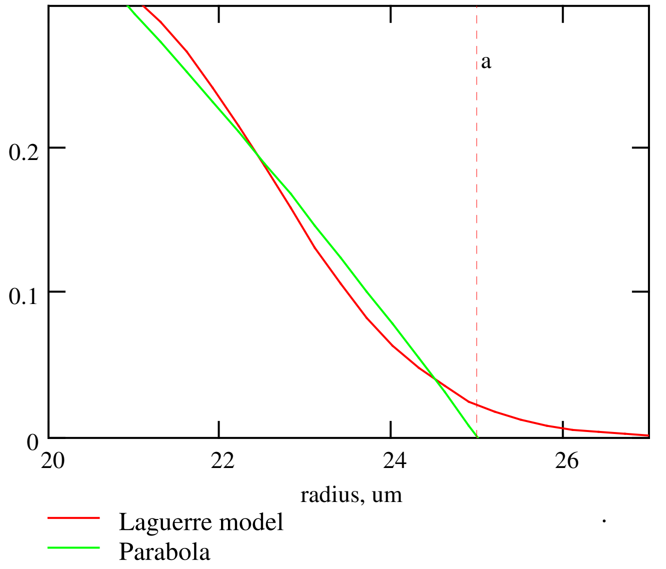

Figure 4.19. Magnified view of core/cladding boundary in Figure 4.18

To demonstrate the effect of this difference, the MTF of the Laguerre model was computed using a parabolic reference profile and the result, shown in Figure 4.20, exhibits, (a) a growing oscillation for higher mode group numbers, and (b) a roll-off towards the core boundary. For reference, the blue line shows the MTF for a parabolic intensity profile, which is simply unity value for all mode groups.

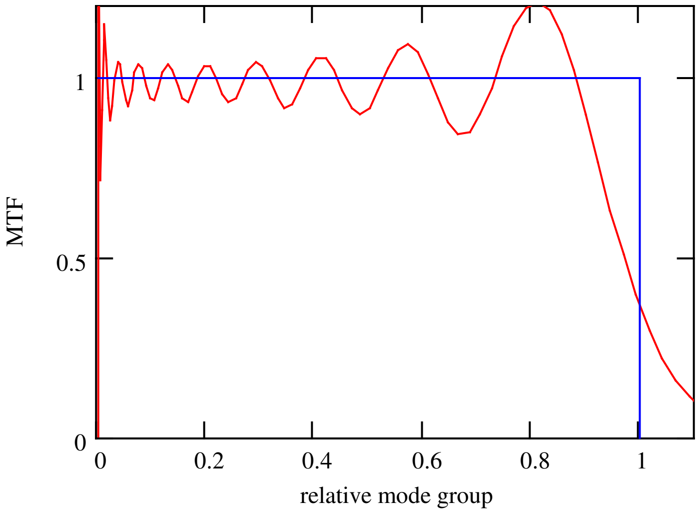

Figure 4.20. Computation of MTF for Laguerre intensity profile (red) and parabolic intensity profile (blue), using a parabolic reference. Filter width is 2.7um.

Here, the filter width is 2.7um. For comparison, the MTF with a 5.7um filter is shown in Figure 4.21, where the MTF, though much smoother, starts to roll-off sooner.

It is clear from these results that the use of a parabolic reference causes the higher-order modes in a fully-filled fibre to appear to be progressively less well-filled. This distortion is not easy to spot in practice due to the higher attenuation of higher-order modes which often lead to depletion in this region.

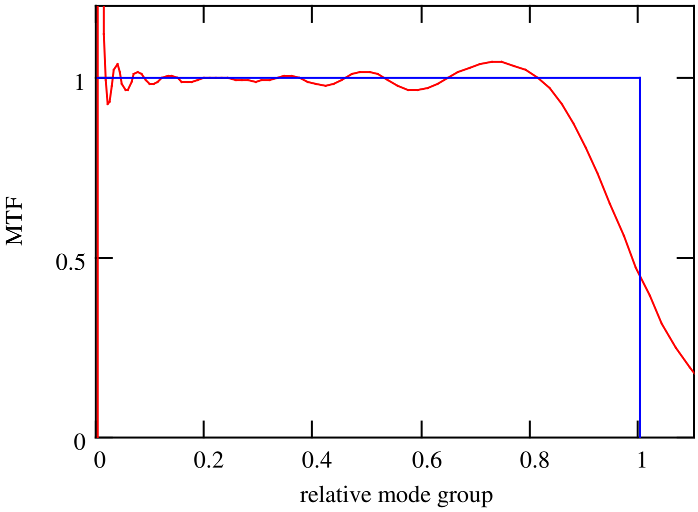

Figure 4.21. Computation of MTF for Laguerre intensity profile (red) and parabolic intensity profile (blue) using a parabolic reference. Filter width is 5.7um.

4.4.1 A Practical Example

To investigate the accuracy of the computed Laguerre profile for a fully-filled fibre, a mode scrambler was built, consisting of a short length of 100um step-index fibre followed by a 62.5um graded-index fibre. This was then spliced onto a 50um graded-index test fibre. The idea being that the near-field of the step-index fibre would spatially overfill the 62.5um graded fibre, leading to fairly high angular excitation in the latter which would then overfill the 50um output fibre both spatially and angularly.

A comparison of the measured near-field profile with the computed Laguerre profile is shown in Figure 4.22. The agreement is good, indicating that the fibre is well-filled. Figure 4.23 shows a magnified view of the core/cladding boundary.

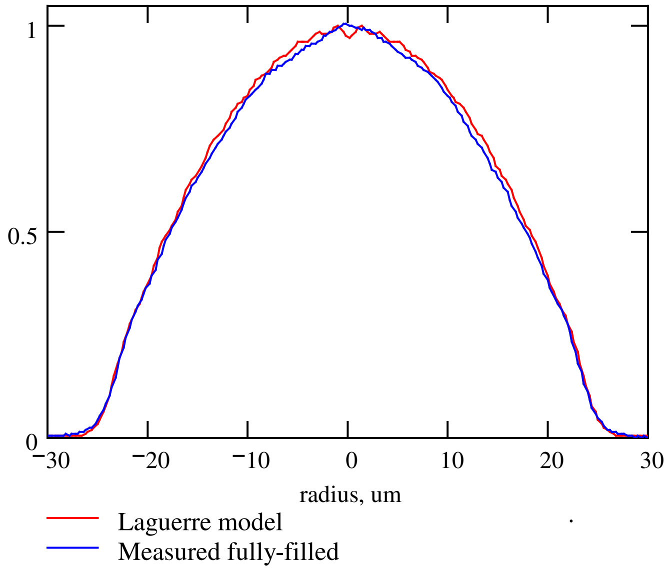

Figure 4.22. Computed near-field intensity profile of 50um graded-index fibre (red) and measured profile of fully-filled fibre (blue).

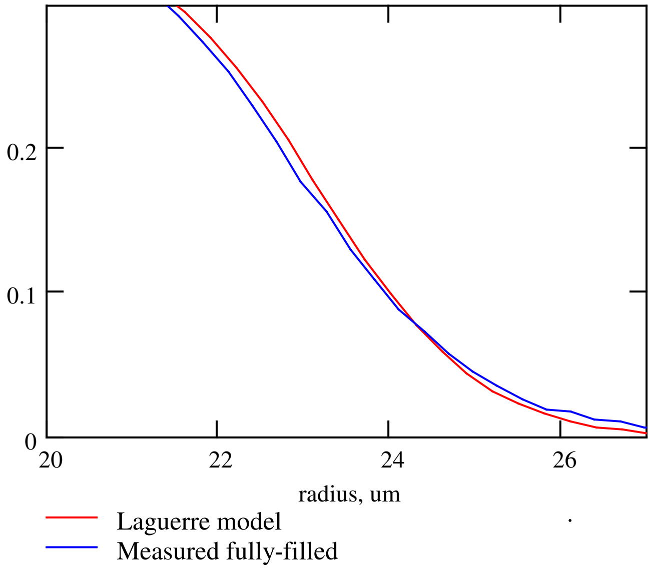

Figure 4.23. Magnified view of the core/cladding boundary in Figure 4.22.

It was postulated, therefore, that the accuracy of an MTF measurement could be improved by using the derivative of the fully-filled Laguerre profile as the denominator in eqn. (4.3) rather than the derivative of a power-law index profile, as this would better approximate actual intensity profiles. The resulting expression is, then

$$\mathrm{MTF}(\delta)=\left[\frac{\mathrm{dI(r)}}{\mathrm{dr}}\cdot\frac{1}{\mathrm{dI_{LG}(r)/dr}}\right]_{\delta=\Delta\left(r/a\right)^{2}} \tag{4.12}$$

To validate the accuracy of this method, the MPD of the near-field data in Figure 4.22 was computed from eqn. (4.12), and the near-field profile was reconstructed by combining Laguerre mode groups in proportion to the calculated MPD. In this way, comparison with the measured near-field profile is a direct check of the validity of the MPD. Figure 4.24(a) shows the computed MPDs and the reconstructed near-field profiles at the core/cladding boundary, for a parabolic reference and the Laguerre reference, for a filter width of 2.7um. Figure 4.24)b) shows corresponding results for a filter width of 7.5um.

The MPD for the parabolic reference clearly rolls off at approximately 0.8 mode group number in (a), whereas the Laguerre reference follows the green line which represents an idealised fully-filled fibre. The near-field profile reconstructions for the Laguerre reference, for both filter widths, agree well with the measured data, but the reconstructions for the parabolic reference deviate from the measured data towards the core/cladding boundary, especially for the 7.5um filter width. This indicates a dearth of the higher-order modes in the reconstruction, as expected from the roll-off in the MPD, for the parabolic reference.

A further example of profile reconstruction is shown Figure 4.25, which is a slightly less well-filled fibre. The reconstruction using the Laguerre reference agrees well with the measured data, but the reconstruction using the parabolic reference deviates from the measured data at around 20um radius. The central dip in the measured data is due to a dip in the index profile of the fibre. This dip does not occur in the reconstructed near-field profiles as the computed MPDs are based on monotonic reference profiles.

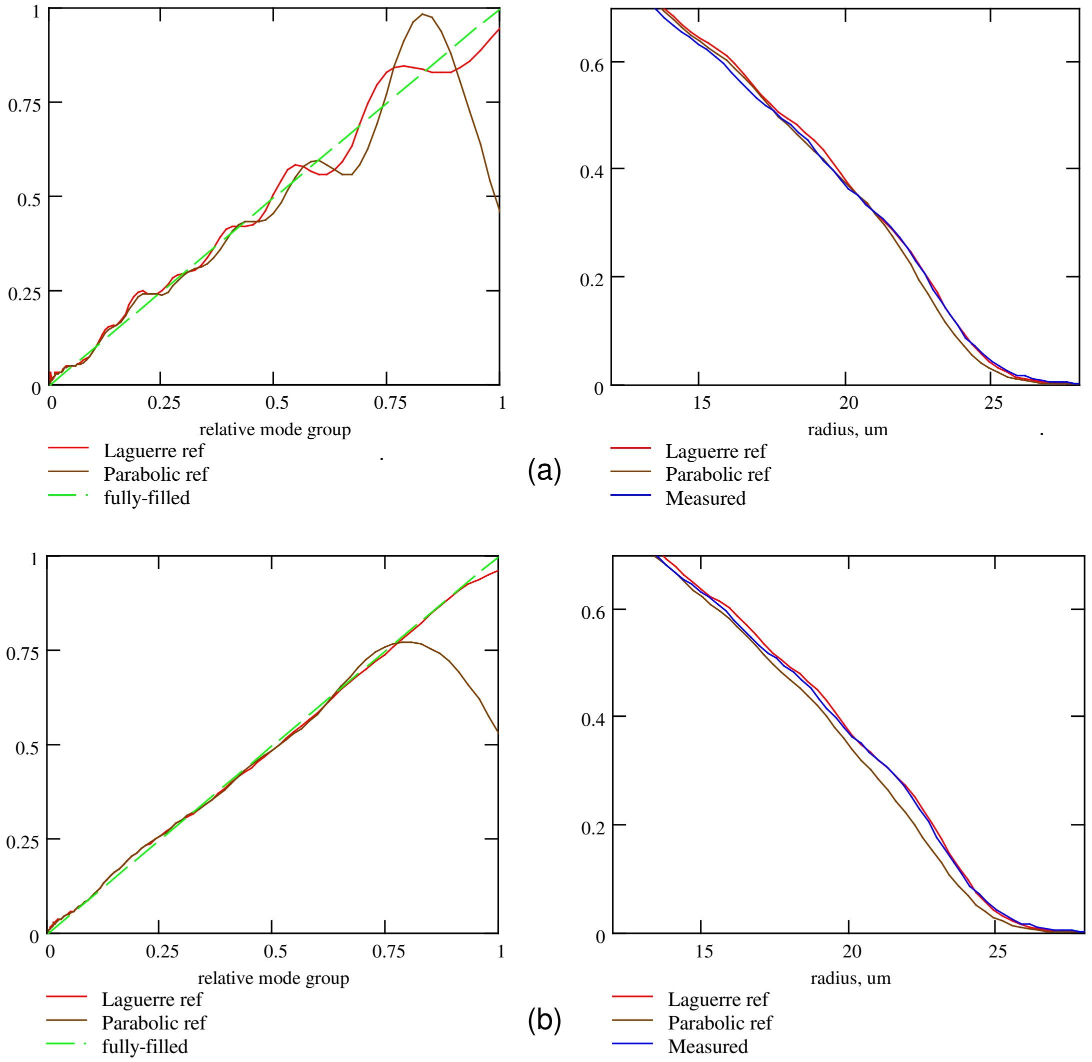

Figure 4.24. MPD of fully-filled fibre computed with Laguerre and parabolic reference profiles (left) and reconstructed near-field profiles (right) for filter widths (a) 2.7um and (b) 7.5um.

The corresponding MPDs and near-field reconstructions, with a 2.7um filter width are shown left in Figure 4.26. In this example, the peak of the MPD for the parabolic reference is at about 0.79 mode group number.

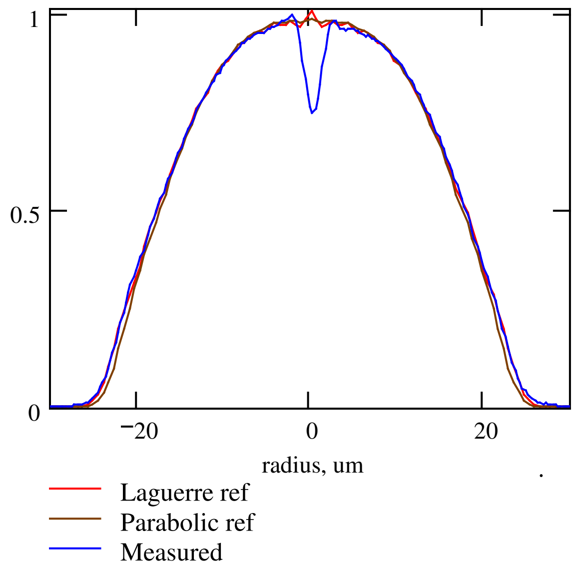

Figure 4.25. Computed near-field intensity profiles of 50um graded-index fibre using Laguerre reference (red) and parabolic reference (brown). The measured profile is shown in blue.

It can be concluded, therefore, that for fibres that are well-filled, the Laguerre reference gives a more accurate measure of mode-filling, resulting in a more accurate profile reconstruction, but for fibres that are less well-filled the parabolic reference is equally good, particularly if a narrow filter width is used, typically 3um. As a guide, if the peak MPD using a parabolic reference occurs at a relative mode group value of less than 0.7 at 850nm, or less than 0.6 at 1300nm, then there is no benefit to be gained from using a Laguerre reference. Unless otherwise stated, a parabolic reference is used in the measurements presented in this thesis.

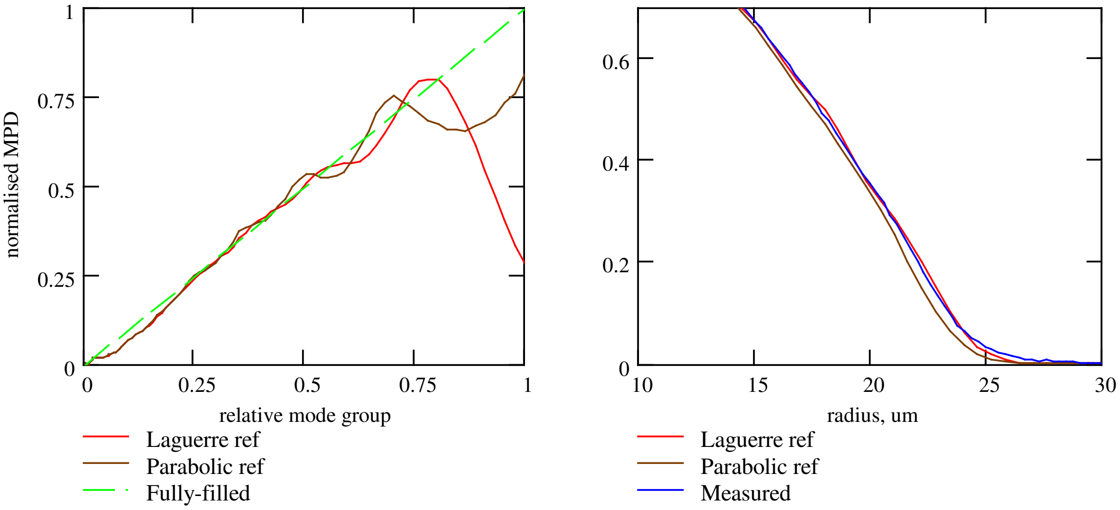

Figure 4.26. MPD of 50um graded-index fibre computed with Laguerre and parabolic reference profiles (left) and reconstructed near-field profiles (right), for 2.7um filter width.

4.4.2 Generalised Index Profile

For a generalised refractive index profile, given by

$$n(r) = n_{\text{core}}\left[1 - 2\Delta f(r/a)\right]^{0.5} \tag{4.13}$$

where f(r/a) is the profile function, eqn. (4.3) may be written in an alternative form, given by

$$\mathrm{MTF}(\delta) = \left[\frac{dI(r)}{dr}\cdot\frac{1}{f'(r/a)}\right]_{\delta=\Delta f(r/a)} \tag{4.14}$$

Thus, if the index profile is known then eqn. (4.14) should be used instead of eqn. (4.3). To show this, the index profile of a typical 50um graded fibre was measured using the *Refracted Near-Field* method at 633nm. The core radius determined from the profile, which is shown in Figure 4.27, was 24.7um at the 2.5% level, and the Numerical Aperture was 0.21. The Laguerre-Gauss profile at 850nm was computed with these parameters and detail of this profile, and the normalised index profile f(r/a), at the core boundary, is shown in Figure 4.28. Also shown is the corresponding parabolic profile for the same fibre parameters. It can be seen that the Laguerre model corresponds well with the measured index profile, and displays a similar evanescent tail in the cladding. Both profiles begin to diverge from the parabola beyond a radius of about 24.3um.

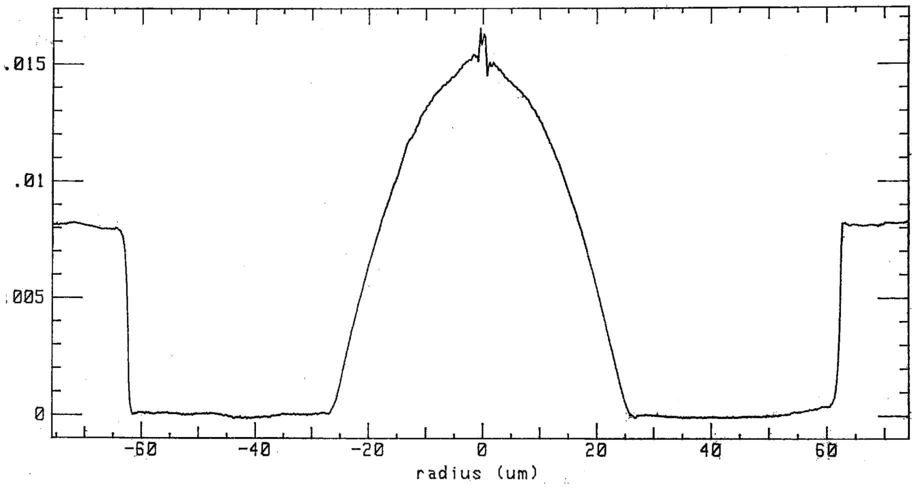

Figure 4.27. Refractive index profile of 50um graded index fibre.

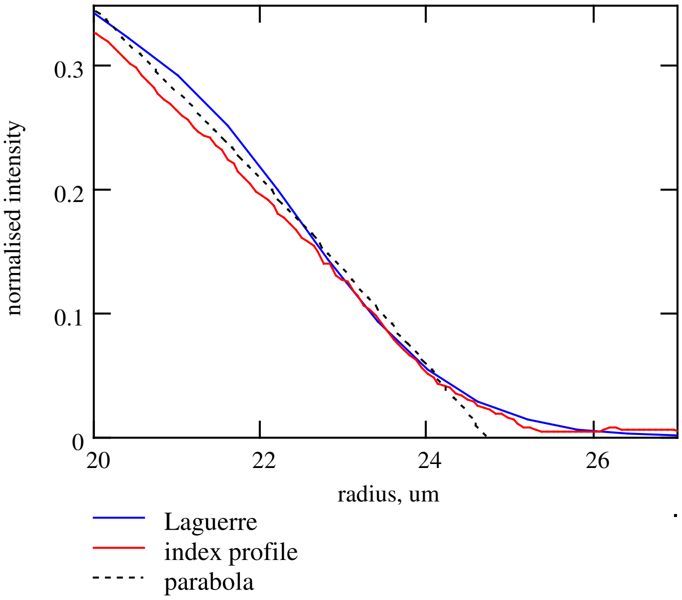

Figure 4.28. Comparison of near-field Laguerre model (blue), with the measured index profile (red), and a parabolic profile (black).

The fibre was then excited with a mode-scrambler launch at 850nm, and the MPD was measured with both the Laguerre profile and the RIP as the reference. The near-fields were then reconstructed, as described in the previous section, and compared to the measured near-field. The resulting profiles, over the radial range 15um to 27um, are shown in Figure 4.29, where a logarithmic scale has been used for the ordinate. Both methods agree well with the measured data indicating that the Laguerre method is satisfactory if the RIP is unavailable.

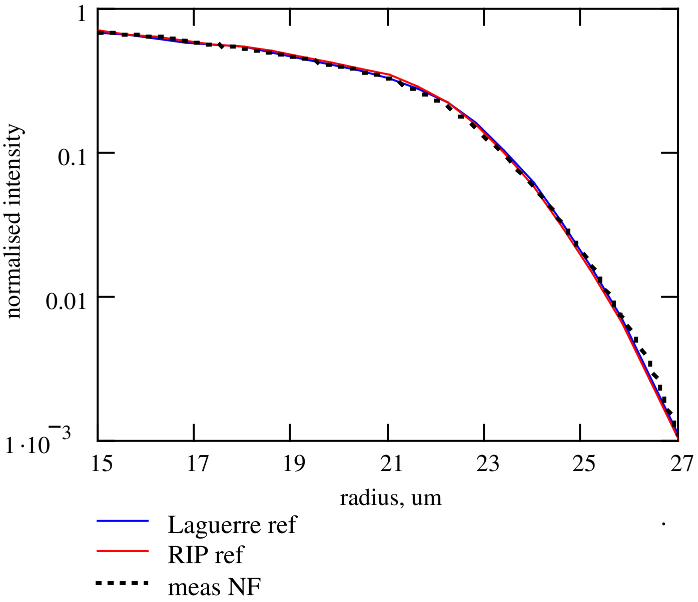

Figure 4.29. Near-field reconstructions using Laguerre reference (blue) and RIP reference (red). The measured near-field profile is shown black dashed. Note that a logarithmic scale has been used.

4.5 Chapter Summary

In this chapter, an experimental apparatus for measuring mode profile has been presented, and aspects of accuracy and measurement reproducibility have been described. The sensitivity of the measured mode profile to core diameter and profile shape factor was presented and it was highlighted that some care is required when interpreting the degree of mode-filling, due to sensitivity of the mode profile to these parameters.

It has been shown that there is a direct correspondence between the shape of the intensity profile in the far-field domain with that in the near-field. Experimental far-field measurements were shown to agree well with the far-field computed from MPD measurements made in the near-field.

A method for validating mode profile measurements was described, using near-field reconstruction with modelled Laguerre-Gauss field profiles. The limitations of the near-field method were discussed and a new method using a modelled Laguerre-Gauss reference profile was proposed.

CHAPTER 5

MODE CONTROL INVESTIGATION

This chapter describes an investigation into methods and devices for modifying the mode distribution in multimode fibres. These are divided into two categories: *mode-scramblers,* that generate a fully-filled distribution irrespective of the launch distribution, and *mode-filters,* that selectively attenuate certain mode-groups. By using a combination of these devices, it is possible to tune the distribution for a variety of applications.

5.1 Mode Scramblers

A review of patented mode-scramblers is given in Appendix A. The scrambling methods described include extrinsic fibre perturbation mechanisms, intrinsic modification of the fibre waveguide properties, the use of scattering surfaces and geometrical launch conditioning. In this section, two types of mode-scrambler are investigated, these are *Long Period Gratings* and a *Point-Load* method.

5.1.1 Mode coupling

An ideal mode-scrambler would re-distribute the light, from any given launched mode, throughout the entire mode spectrum, so that all modes of the fibre were equally excited. As the modes in a multimode fibre are orthogonal, power is not readily exchanged between them, so some perturbation is therefore required to generate non-zero overlap coefficients and facilitate power transfer between modes.

Gross scattering mechanisms, such as diffusing surfaces, completely destroy the phase-front of a mode, leading to overlap with large numbers of other modes. This type of mode-scrambler works well but incurs large losses, as a proportion of light is scattered outside of the numerical aperture of the fibre. Using a geometrical imaging system to precisely replicate the fully filled distribution is an effective method, but it is also difficult to achieve an efficient launch. In contrast, extrinsic perturbations to the fibre, such as microbending, or intrinsic perturbations, such as refractive index variation, are very efficient methods for coupling between modes. Some mechanisms cause a rapid re-distribution of light, such as a sharp bend, whereas other mechanisms, such as refractive index perturbations, may require a long interaction length, as power transfer is progressive.

It was shown in section 3.2.2 that the modes in graded-index fibres fall into groups of approximately equal propagation constant. Modes within these groups are thus phase-matched, enabling even tiny amounts of scattered light caused by, for example, microscopic fibre inhomogeneities, to couple efficiently between them. It is generally assumed, therefore, that light coupled into one particular mode will quickly become equally distributed between all of the modes in that group.

The difference in propagation constant $\Delta\beta$ between adjacent mode groups in a graded-index fibre may be calculated from eqn.(3.25). For a 50um parabolic fibre at 850nm, it is found that $\Delta\beta$ between adjacent mode groups varies by less than 0.5% of the mean value for the 19 possible mode groups. In a step-index fibre, however, the situation is very different, as mode grouping does not occur, and $\Delta\beta$ between adjacent modes may vary by several orders of magnitude.

5.1.2 Long Period Gratings

In order to increase the coupling efficiency of weak coupling mechanisms, a periodic sequence of perturbations may be used. In this case, the period is chosen such that it equals the *beat-length*. The small amounts of power coupled at each perturbation add in-phase leading to a gradual transfer of power. The optimum beat length Λ is given by

$$\Lambda = \frac{2\pi}{\Delta\beta} \qquad \textbf{(5.1)}$$

where $\Delta\beta$ is the difference in propagation constant between the coupled modes.

As an example, for the parabolic-index fibre mentioned above, the required period for coupling between adjacent mode groups varies from 1077um for mode groups 1 & 2, to 1067um for mode groups 18 & 19. It is likely, therefore that an average grating period of around 1072um should be sufficient for coupling between all pairs of adjacent mode groups.

Periodic perturbations of this sort are called Long Period Gratings (LPGs), to distinguish them from *Fibre Bragg Gratings* (FBGs) which typically have much shorter periods and work by a different mechanism. LPGs have been widely used in singlemode fibres as band-rejection filters [40] and sensors [41] [42], where coupling from the fundamental mode to radiative cladding modes is utilised, and in multimode fibres as microbend sensors [43]. The use of multimode LPGs for mode-scramblers is now described, where three types of LPG are considered: microbend gratings, taper gratings and refractive index gratings.

5.1.2.1 Microbend Gratings

A microbend grating typically consists of a series of cylindrical pins against which the fibre is pressed. A simple grating was made comprising seven steel pins, each 1.0mm diameter, attached to a rigid base and laid side-by-side in contact with each other. A primary-coated graded-index fibre was positioned at right angles to the pins and covered with a former of high density cardboard attached to another rigid base. A schematic of the grating is shown in Figure 5.1.

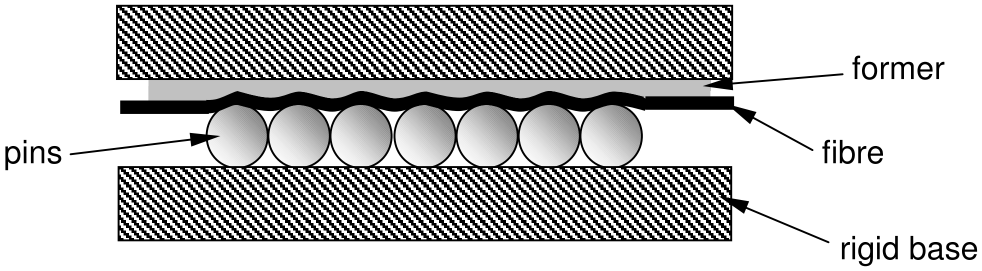

Figure 5.1. Schematic of microbend grating

A compressive force was then applied to the structure and the near-field intensity profiles were measured, shown in Figure 5.2. In this case the fibre core diameter was 50um and was excited at 850nm with a singlemode fibre positioned on the fibre axis. The force was then increased from zero, shown as ‘ref’ in the figure, up to a maximum of 10N for curve 9.

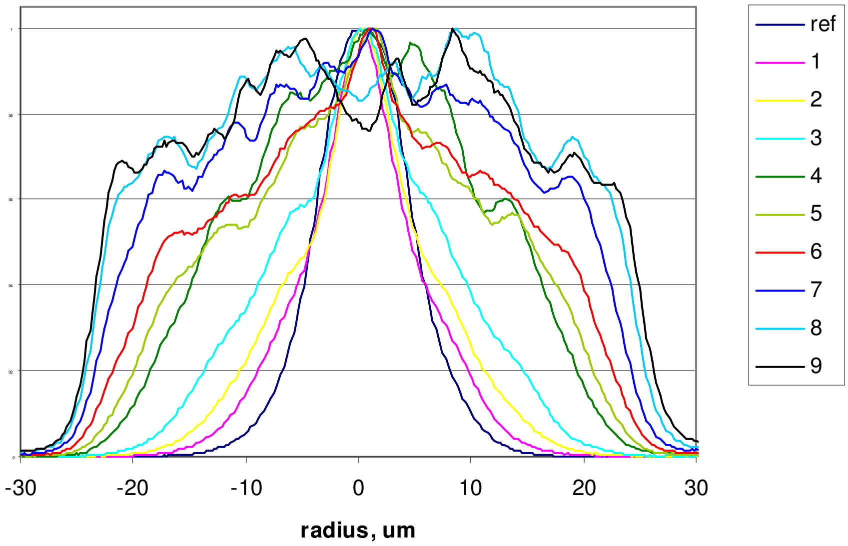

Figure 5.2. Near-field profiles of a 50um graded-index fibre in a microbend grating vs load number.

As the load was increased, the profiles broadened at the base, for curves 1 to 3, and then developed *shoulders* for curves 4 to 6. Comparison of the profiles for the higher loads, curves 7 to 9, with the theoretical leaky mode distribution, indicated that they probably correspond to leaky modes.

A plot of insertion loss of the fibre is given in Figure 5.3, where it can be seen that the loss is quite low up to measurement 7, and then rapidly increases as light is progressively coupled to leaky modes and subsequently to cladding modes.

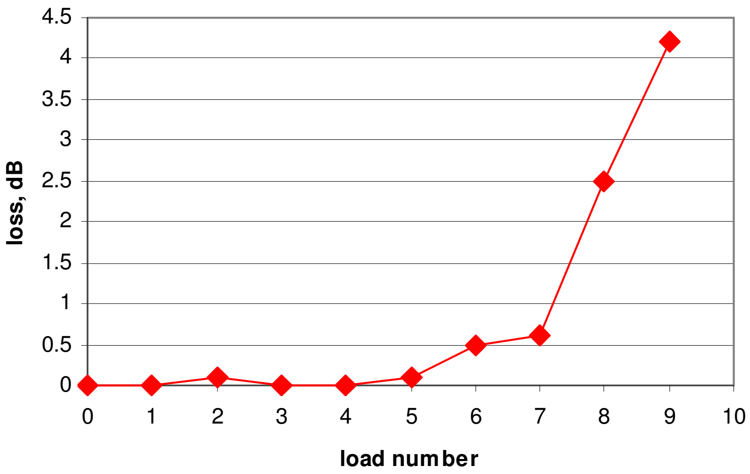

Figure 5.3. Insertion loss of a 50um graded-index fibre in a microbend grating as the load is increased.

It was expected that light would be progressively coupled from the fundamental mode through all the mode groups until the fibre was uniformly filled, but this is clearly not the case. Plots of the MPDs for these intensity profiles show that, for the greater loads, there is distinct bias towards higher-order modes at the expense of the lower-order modes, which are almost absent.

Recent work by Su et al. [44] appears to explain these observations. Su has shown that a microbend structure causes light to be preferentially coupled from the fundamental mode, LP_{01}, into *Hermite-Gauss* modes, HG_{p0}, where p is an integer. The particular HG modes excited depend on both the amplitude of the grating and the number of periods. In fact, for a given amount of coupling, Su states that these two parameters are inversely proportional. Coupling to the HG modes, which are non-circularly symmetric, rather than to the Laguerre-Gauss (LP) modes, occurs because the microbending is in only one plane. For the measurements shown in Figure 5.2, however, the near-field distributions were observed to be circularly symmetric, indicating that coupling from the HG modes to the LP modes of the fibre must have occurred. In contrast, a similar experiment with a 62.5um fibre clearly displayed excitation of the HG modes, as shown in Figure 5.4. Here, by adjusting the load on the grating it was possible excite several HG$_{p,0}$ modes, where p=0 to 3.

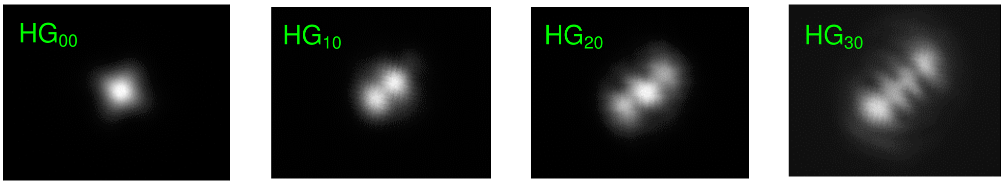

Figure 5.4. Launching Hermite-Gauss modes with microbend grating on 62.5um fibre.

The reason that HG modes were not observed with the 50um fibre was probably due to intrinsic perturbations in the fibre, causing a high degree of mode coupling between HG and LP modes. Refractive index profiles of the two fibres, Figure 5.5, reveal that the 50um fibre had a sharp, asymmetric, spike near to the centre of the fibre, whereas the profile of the 62.5um fibre was symmetric in this region, in spite of a small dip. It was likely, therefore, that the asymmetry in the 50um fibre encouraged rapid coupling between the HG and LP modes.

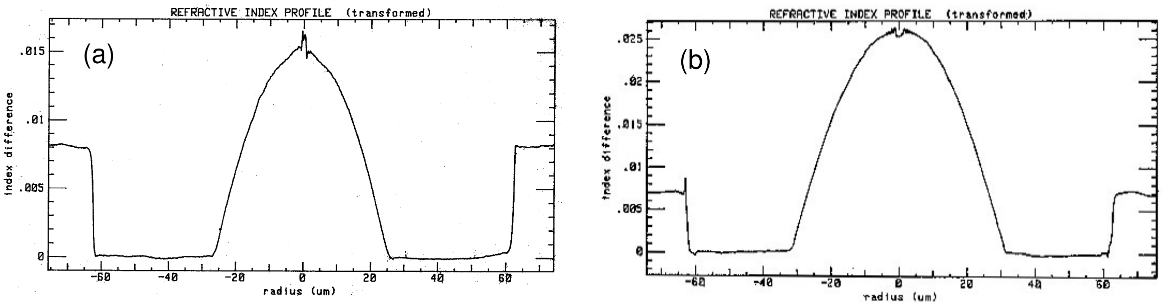

Figure 5.5. Refractive index profiles for (a) 50um and, (b) 62.5um fibres used in microbend experiment.

The overlap coefficients of HG and LP modes in a parabolic profile fibre were computed, using eqn. (3.36), and it was found that a given HG$_{p0}$ mode has a finite overlap with each of the LP$_{\eta\mu}$ modes in a particular LP mode-group, and would be expected to be readily re-distributed between the LP modes of that group. As an illustration, the relative overlap of the HG$_{60}$ mode with the LP modes in mode group 7 is given in Table 5.1.

LP mode	Relative overlap with HG_{60}
LP_{61}	0.031
LP_{42}	0.188
LP_{23}	0.469
LP_{04}	0.312

Table 5.1. Relative overlap of HG_{60} mode with LP modes in mode group 7

Following Su, the MPDs for a 7-pin microbend grating were computed, as a function of grating amplitude, shown in Figure 5.6. The grating amplitudes in the computation were chosen to aid comparison with the measured MPD curves, which are shown in Figure 5.7. Note that each point in Figure 5.6 corresponds to a discrete mode-group, whereas the measured MPDs in Figure 5.7 are computed as continuous functions. It is clear from these sets of curves that power is progressively shifted across the mode spectrum as the load, and therefore amplitude, is increased. Use of the microbend grating as a mode-scrambler appears, therefore, to be limited, recalling that the MPD of a fully filled fibre is a straight line of unity gradient. There is, however, a commercial microbend device available, from Newport, Inc. that is promoted as a device for generating a stable mode distribution that is independent of launch conditions. The device, called the *FM-1 Mode Scrambler*, consists of interlocking corrugated jaws with a period of 1.1mm. The fibre is placed between the jaws and these are progressively brought together by a precision translation stage, such that a total of three microbend periods are imposed on the fibre.

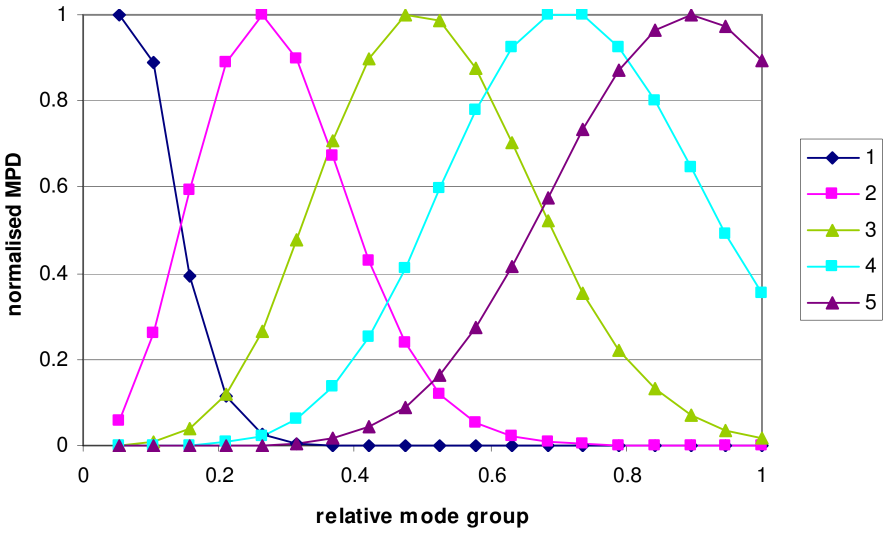

Figure 5.6. Computed MPDs for 7 pin microbend grating for grating amplitudes from 1.1um (curve 1) to 4.8um (curve 5).

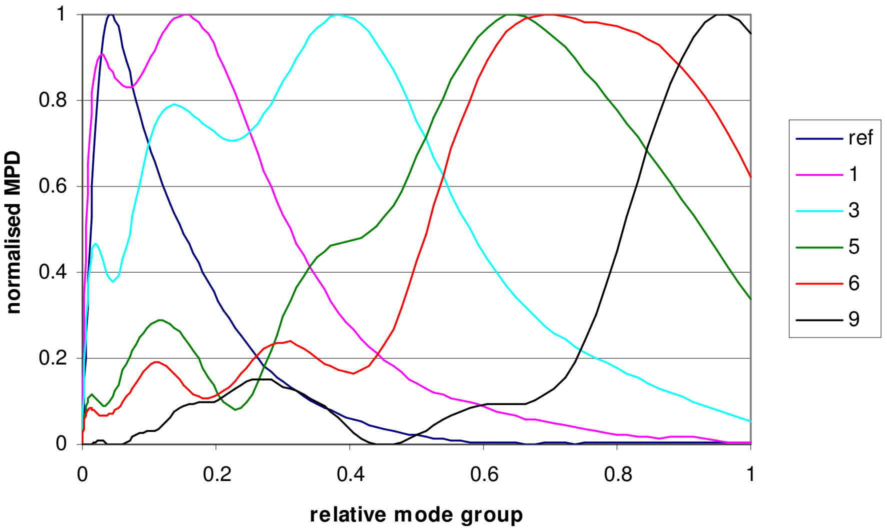

Figure 5.7. Measured MPDs for 7-pin microbend grating with applied loads from zero to 1kg.

A series of measurements were made on the FM-1 with the same type of fibre used in the 7-pin grating. The results, shown in Figure 5.8 for range of jaw positions, indicate a similar behaviour to the 7-pin grating. In the FM-1, however, there appears to be a significant amount of light in the lowest order modes as well as in the highest order modes. The reason for this difference between the gratings is not clear but it may be related to the presence of the cardboard former in the 7-pin grating.

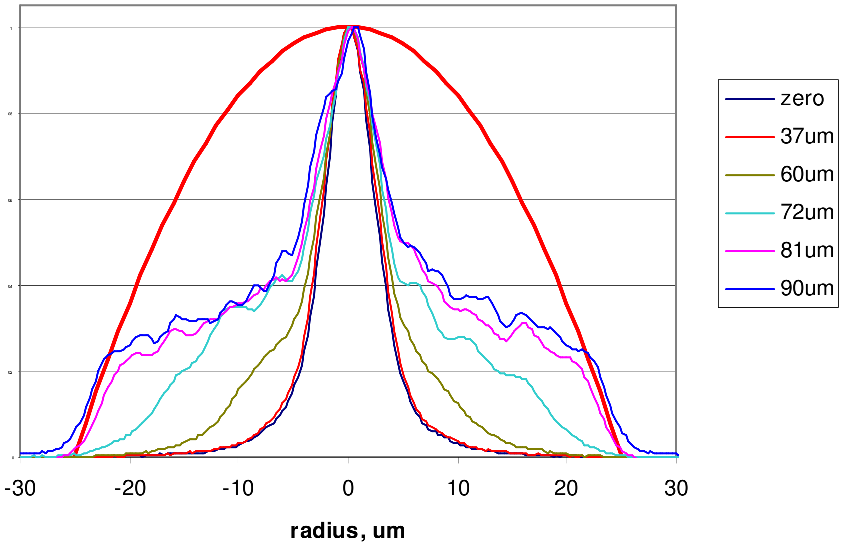

Figure 5.8. Near-field profiles of a 50um graded-index fibre in Newport FM-1 device vs position of jaws. The red parabolic curve represents a fully-filled distribution.

In any event, neither grating tends towards a fully-filled distribution, or even an Equilibrium Mode Distribution, which is characterised by an almost triangular profile. Both gratings were also tested with a fully filled launch and it was found that neither produced a profile that was independent of the launch conditions.

5.1.2.2 Taper Gratings

Another form of LPG is that of the periodic taper. Here, the fibre is locally heated under tension so that it *necks down*, forming a periodic ripple in the fibre diameter. Gratings of this kind for sensor applications have been successfully written in multimode fibre using a focussed CO_2 laser [45] and in single-mode fibre for wavelength-filtering using a fusion splicing apparatus [46]. Their use as mode scramblers has, however, not been fully investigated. An advantage of the fusion splicer method over laser manufacturing methods is that it requires less sophisticated equipment, and would therefore be much cheaper.

A schematic of the experimental set-up for forming a grating is shown in Figure 5.9. The fusion splicer was *Type-35SE* from Sumitomo Electric Industries. The arc current was adjustable from 0001 to 0016 manufacturer's units, which is equivalent to a range of 12mA to 15mA. The arc duration was controlled in hundredths of a second up to 20s. A short section of fibre was stripped and lightly held in the V-grooves in the splicer with small weights. One end of the fibre was attached to a translation stage, the other was passed over a smooth radius and a weight attached to control the tension in the fibre. When the fibre was softened by the arc the tensioning weight caused the fibre to neck down by an amount dependent on the arc power, the arc duration and the mass of the tensioning weight.

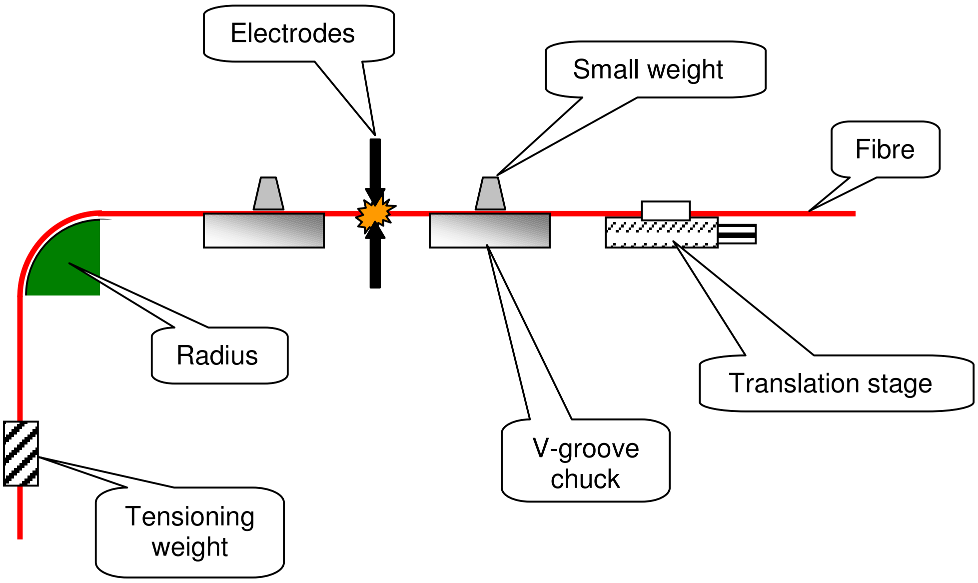

Figure 5.9. Schematic of apparatus for making taper LPG using fusion splicer

An example of a short section of grating is shown in Figure 5.10, where, in this case, the arc power was set to 0002 units, the arc duration was 1.0s, the tensioning weight was 0.5g and the period was 1.1mm. The diameter at the centre of the taper was approximately 100um and the taper angle was approximately 3.5°. By using a step-and-repeat process, gratings typically up to 25mm could be readily made. It was found, however, that occasionally the degree of necking varied, from almost none to about twice the amount shown in the figure. The cause of this inconsistency was unclear but may be due to fluctuations in the dynamics of the arc, possibly due to electrode contamination, or the fibre sticking slightly in the V-grooves.

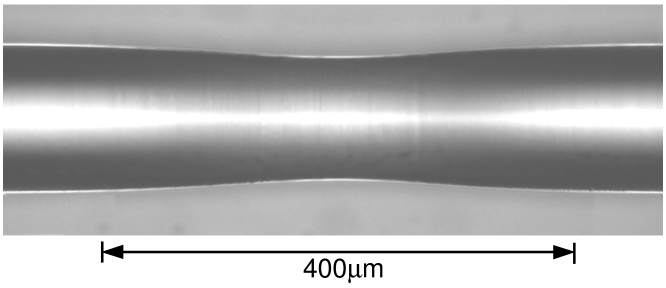

Figure 5.10. Photograph of section of taper grating made with fusion splicer.

The near-field profiles of a typical taper grating are shown in Figure 5.11 as a function of the number of shots. Note that the number of periods is equal to one less than the number of shots. In this particular grating, the degree of necking was reasonably constant along the grating. For the first few shots the profiles gradually broadened and then shoulders developed after approximately 10 shots. The shoulders continued to broaden until shots 12 and 14, which fall just outside the parabolic reference curve. Next, the shoulders became narrower and then for shots 20-24 the profiles became slightly more triangular.

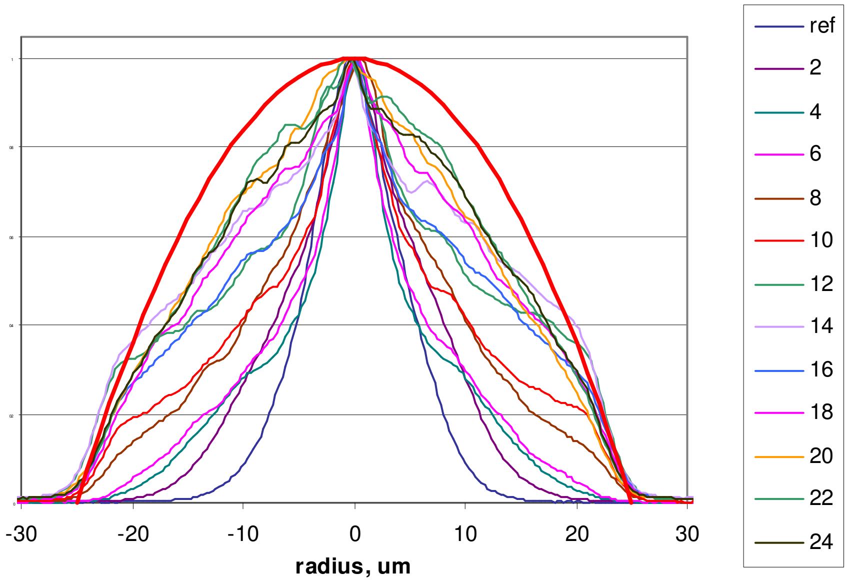

Figure 5.11. Near-field profiles of a 50um graded-index fibre with taper grating vs number of shots. The red parabolic curve represents a fully filled distribution.

Comparison with the near-field profiles for the microbend grating, shown in Figure 5.2, indicates a similar sort of behaviour at first, with the formation of shoulders due to coupling to high-order modes. The taper grating, however, does not appear to progressively couple to leaky modes, but rather tends towards a more triangular distribution, as the number of periods is increased.

The insertion loss of the taper grating, shown in Figure 5.12, was negligible up 6 periods and then rose sharply to about 8dB for shots 7 to 13, as coupling to leaky and radiation modes occurred, and continued to rise gradually up to 9dB over the final 11 shots.

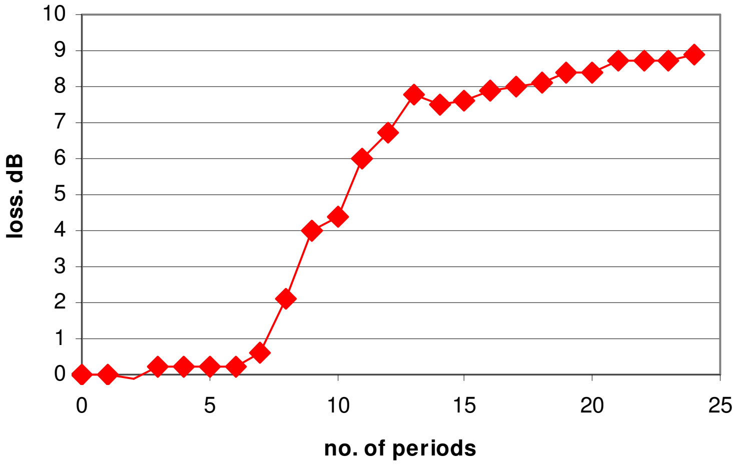

Figure 5.12. Insertion loss of a 50um graded-index fibre taper grating vs number of shots, with 850nm singlemode source.

The taper grating was therefore not very effective at generating a fully filled mode distribution, but it did distribute light more evenly that the microbend grating. In order to investigate its sensitivity to launch, a similar experiment was carried out with both a fully-filled launch and a singlemode launch. The results showed that there was some tendency for the corresponding profiles to converge, but this only occurred when the singlemode insertion losses were around 8 to 9dB. Thus the device does not appear to be suitable as either a mode-scrambler or an EMD generator.

5.1.2.3 Refractive Index Gratings

A third form of LPG was investigated, consisting of a periodic variation in the refractive index. The experimental method consisted of exposing the fibre in a step-and-repeat process with a UV laser. The fibre was a conventional 50um graded-index with silica cladding and doped silica core. To increase its photosensitivity the fibre was exposed to a hydrogen-rich atmosphere for several days. An Argon-ion laser, with frequency doubling to 244nm, was focussed to a spot approximately 15um in height by a cylindrical lens. The laser power was typically 95mW.

A grating with 20 periods, of 1070um pitch and 50% duty cycle, was written, using an exposure rate, initially, of 0.6mm/s. The fibre was excited with an 850nm LED source launched from a singlemode fibre butt-coupled to it. The near-field distribution at the output of the grating fibre was measured after each exposure, up to a total of 18 exposures. The exposure was increased progressively over the first 5 exposures to 0.1mm/s and then to 0.05mm/s after 12 exposures. It can be seen from the results in Figure 5.13 that, after 5 exposures, the profiles became wider at their base and then after 6 to 8 exposures developed shoulders. Finally, the profiles then became more rectangular in shape, having steeper sides and a flat top with a local ripple structure on it.

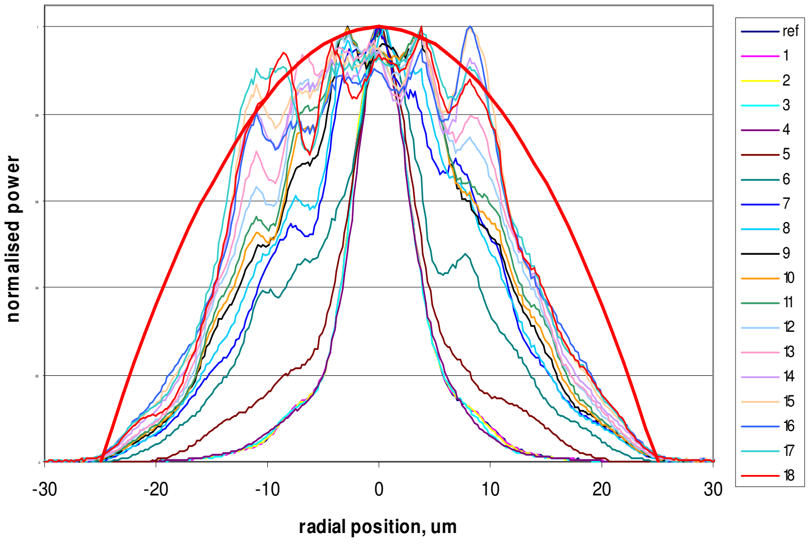

Figure 5.13. Near-field profiles of a 50um graded-index fibre with refractive-index grating vs number of exposures. The red curve represents a fully-filled distribution.

There appears to be no tendency towards the fully filled, parabolic, shape or that of an Equilibrium Mode Distribution. The insertion loss for the singlemode launch, shown in Figure 5.14, was very low up to exposure 6 and then increased approximately linearly to 2.5dB for exposure 16, after which it dropped by about 0.5dB over the remaining two exposures.

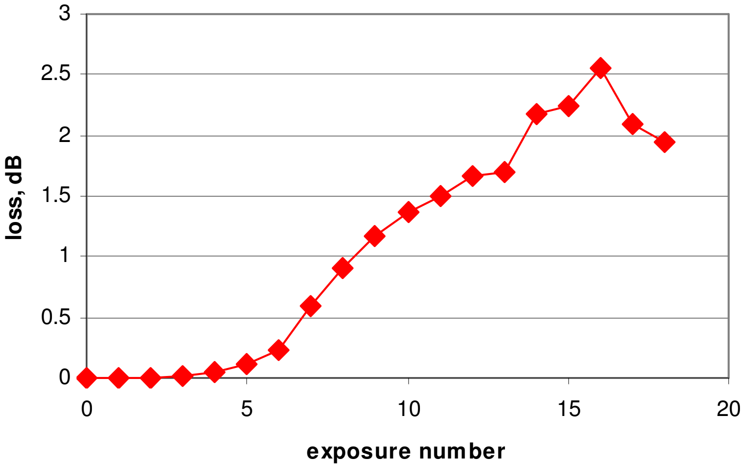

Figure 5.14. Insertion loss of a 50um refractive-index fibre taper grating vs number of exposures, with 850nm singlemode source.

5.1.3 Discussion of Long Period Gratings

The behaviour of three types of LPG were found to be somewhat different, although none of them performed well as a mode-scrambler. The 7-pin microbend grating progressively transferred power to higher-order modes, and eventually leaky modes, resulting in a broad, squarish, profile. The insertion loss increased rapidly from 0.5dB to 4dB once leaky modes were excited. The Newport microbending device also generated high-order modes, but, in contrast, it retained a sharp central peak corresponding to the singlemode launch. The 7-pin gating did not show this feature, possibly due to the asymmetrical nature of the latter, having a deformable material on one side.

The taper grating readily coupled light to higher-order modes, resulting in clear shoulders after 8 shots. Increasing the number of shots further did tend to create a fairly well filled profile, but the loss increased rapidly up to 8dB after 13 shots and then to 9dB after 24 shots. It was found to be difficult to reproduce the performance of a taper grating reliably, and the occasional occurrence of a more severe necking changed the characteristic of the whole grating.

The refractive index grating tended to produce a squarish profile with steep sides, as the number of exposures was increased. This type of behaviour also occurred in the 7-pin microbend grating, except that the profile of the index grating was much narrower, and, unlike the microbend grating, it did not appear to excite leaky modes. A possible cause of this was that the height of the laser writing spot was somewhat less than the diameter of the fibre core and so the grating would not physically extend into the region of the core supporting the highest-order modes, near to the core/cladding boundary. This type of grating could, however, find application in providing restricted launch conditions, such as those specified for certain multimode bandwidth measurements [47].

5.1.4 Point-Load Mode-Scrambler

In contrast to Long Period Gratings, the Point-Load mode-scrambler consists of inducing a point perturbation to the fibre. A novel implementation of this method was developed in this study and comprises bending a fibre round in a loop such that it crosses back over itself, and applying a load to the crossover point. In this manner, each fibre section acts as a source of point loading for the other. The resultant distortion to the fibre leads to a wide spectrum of spatial frequencies, in contrast to the LPG, which has a single modulation frequency. This is an advantage for mode coupling in step-index fibres, where adjacent modes are not evenly spaced. For example, in a typical 50um step-index fibre at 850nm, $\Delta\beta$ varies from $1.5\text{x}10^{-6}\text{um}^{-1}$ to $2.5\text{x}10^{-3}\text{um}^{-1}$. Therefore, the point-load mode-scrambler is well suited for encouraging mode scrambling in this type of fibre.

A schematic of the crossover region of the fibre loop is shown in Figure 5.15, where Fibre A and Fibre B are two parts of a continuous length of fibre looped back on itself. The crossover point is sandwiched between two slabs of elastic material, such that application of a compressive force to the structure causes each fibre to be pressed into the elastic material. A particular feature of this device is that it can be tuned by adjusting the applied force. A further advantage is that point loading is applied equally to the fibre at two longitudinal positions, one loop apart, potentially leading to a more complete mode scrambling in the fibre.

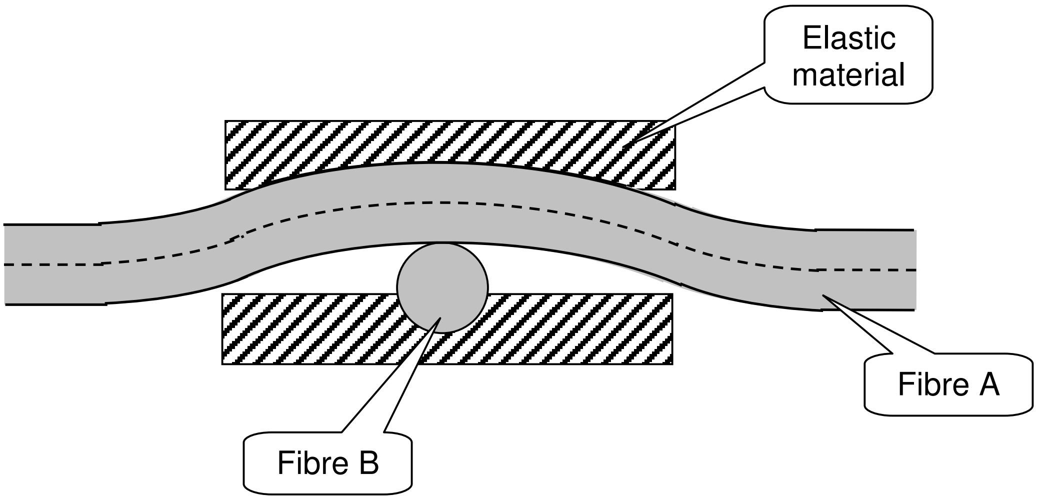

Figure 5.15. Schematic of crossover point in single loop mode-scrambler with silica fibre and elastic compression jaws.

In order to calculate the distortion of the fibre, bending beam theory was used. According to *Roark* [48], the displacement y(z) of a concentrated load applied to an infinite beam on an elastic foundation, as a function of axial distance z, is given by

$$y(z) = -\frac{W}{8EI\beta^3} e^{-\beta z} (\cos\beta z + \sin\beta z) \qquad \textbf{(5.2)}$$

where:

$$\beta = \left(\frac{b_o k_o}{4EI}\right)^{1/4} \qquad \textbf{(5.3)}$$

and

W is the applied load,

E is Young's modulus of the beam,

I is the moment of inertia of the beam,

b_o is the beam width,

k_o is the foundation modulus (unit stress per unit deflection).

According to Olshansky [49], the linear force constant g for a fibre pressed against an elastic material by a small bump is approximately equal to the Young's modulus of the elastic material E_e, where $g=b_o k_o$ in eqn. (5.3). Thus, from eqns. (5.2) and (5.3) the displacement at z=0 is given by

$$y(0) = \frac{W}{8EI}\left(\frac{4EI}{E_e}\right)^{3/4} \quad \textbf{(5.4)}$$

where the moment of inertia for a cylinder, of radius a, is given by

$$I = \frac{\pi}{4}a^4 \quad \textbf{(5.5)}$$

In the situation shown in Figure 5.15, however, the displacement of each individual fibre is equal to one-half of the displacement calculated from eqn.(5.4), as both jaws are compressed equally.

As an example, consider two silica fibres of 125um diameter, and Young's modulus $7.2\text{x}10^{10}$ Pa, between two elastic surfaces, each of Young's modulus $1.0\text{x}10^{8}$ Pa. For a load of 5N the compressive displacement of each fibre, from eqn. (5.4), is equal to 29um.

The local curvature of the fibre c(z) is given by, [50]

$$c(z) = \frac{y''(z)}{\left(1 + y'(z)^2\right)^{3/2}} \quad \textbf{(5.6)}$$

It is known [51] that the coupling strength between modes is proportional to the curvature power spectrum in the fibre. Figure 5.16 shows the curvature spectrum for this example, computed as the Fourier Transform of c(z). It can be seen that the spectrum has a peak at 3.3mm^{-1}. Also shown in the figure is a histogram of the values of $\Delta\beta$ between *adjacent* modes in a step-index fibre (green), and in a graded index fibre (red). There is thus some overlap of the curvature spectrum with both fibre types.

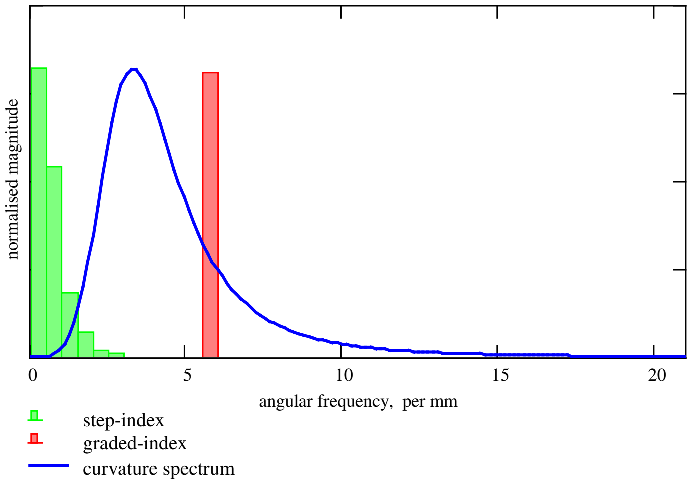

Figure 5.16. Plot of curvature spectrum of point-load mode-scrambler and angular frequency, Δβ, for adjacent modes in 125um step-index and graded-index fibres.

Now if all possible mode combinations are considered, the spectrum for step-index fibre is much wider, as shown in Figure 5.17.

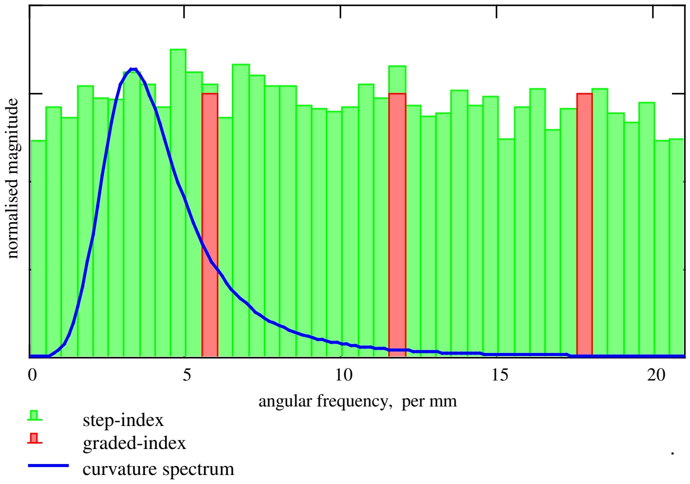

Figure 5.17. Plot of curvature spectrum of point-load mode-scrambler and angular frequency, Δβ, spectrum for all mode combinations in 125um step-index and graded-index fibres.

The curvature spectrum overlaps a wide range of Δβ values in the step-index fibre, indicating that that mode coupling over a large range of modes should occur. In contrast, for the graded-index fibre, the spectrum only significantly overlaps Δβ for adjacent modes, indicating that coupling in this type of fibre would be progressive between adjacent mode groups, similar to that found in the LPGs studied.

5.1.4.1 Choice of Materials

For a given fibre, the shape of the curvature spectrum depends on the Young's modulus of the jaw material and its amplitude depends on the applied load. Thus correct selection of the jaw material, and adjustment of the applied load, can be used to achieve some degree of tuning.

Removing the protective primary coating before inserting the fibre into the point-load device was found to compromise its strength and it was easily broken. It was found, therefore, advantageous to retain the primary coating in this device. Fibres generally have two coating layers, a soft inner coating to minimise the incidence of microbending, and a tougher outer coating to provide protection against the environment. In this case, compression will occur at the point of contact of the fibres as well as at the jaws. In order to compute the curvature spectrum, an average value for Young's modulus of the fibre materials is taken. Values of Young's modulus for silica fibre and typical polymeric coatings on a double-coated fibre [52] are given in Table 5.2. Taking an area-weighted mean of the three values gives an average Young's modulus of 1.8×10^{10} Pa.

Material	Radius	Young's modulus
Silica	62.5 um	7.2×10^{10} Pa
Inner coating	100 um	1.0×10^{7} Pa
Outer coating	125 um	1.3×10^{9} Pa

Table 5.2. Typical values for the radius and Young's modulus of fibre materials.

The dependence of the curvature spectrum on Young's modulus of the jaw material is demonstrated in Figure 5.18, where Young's modulus for the fibre was taken as 1.8×10^{10} Pa and the applied load was 5N. As Young's modulus of the jaw is reduced, the spectrum becomes much narrower, its peak moves to lower frequencies and the relative magnitude increases markedly.

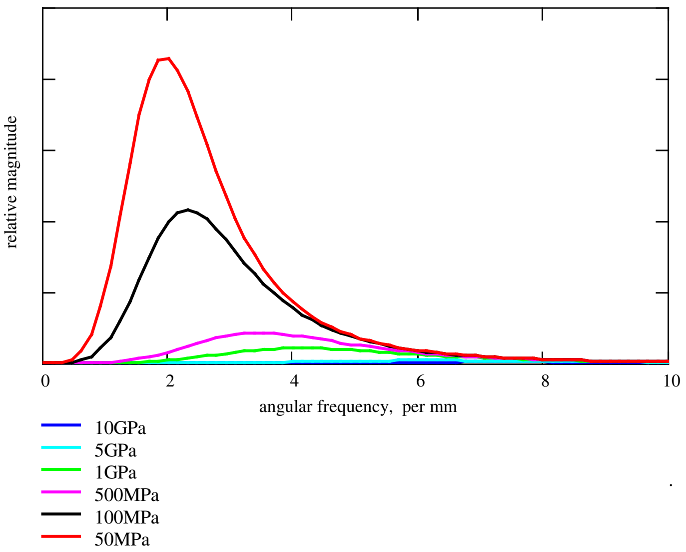

Figure 5.18. Plot of curvature spectrum of point-load mode-scrambler with dual-coated fibre, for a range of Young's modulus of the jaw.

Comparison with Figure 5.16 indicates that a smaller Young's modulus (E) for the jaw material would give a better overlap with the spectrum of adjacent modes for a step-index fibre. Conversely, the corresponding reduction in the width of the spectrum would reduce the overlap with the spectrum for non-adjacent modes. In order to determine the optimum jaw material, a variety of jaw materials were tested, including aluminium, polypropylene, polyethylene, ABS (arylonitrile-butadiene-styrene), rubber, neoprene (polychloroprene), nylon (polyamide) and a rubber ferrite material. Each material was tested in a point-load mode-scrambler with an underfilled step-index fibre. The required force to give a flat near-field profile, from the step-index fibre, was measured. The results, shown in Figure 5.19 indicate that the softer materials, such as the low density polyethylenes required slightly less force than the harder materials. Young's modulus of low density polyethylenes is typically in the range 200MPa to 500Mpa, while for nylon and ABS Young's modulus is in the range 1GPa to 2.5Gpa.

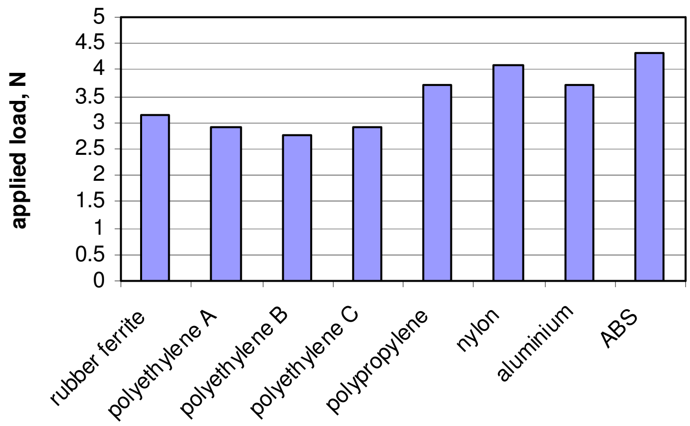

Figure 5.19. Load required in point-load mode-scrambler to give flat near-field in step-index fibre for different jaw materials.

The results for rubber and neoprene have not been included as it was found that a flat near-field profile could not be obtained, even with much greater loads. The reason for this was that the fibre became completely compressed into the jaws which then made contact with other, preventing further bending of the fibre. Young's modulus for rubber is typically around 2MPa which, for a 5N load, the jaw compression is 383um, which is greater than the fibre diameter.

Apart from rubber, the difference in applied load between the various materials is not significant and the choice of jaw material is determined by other parameters, such as ease of use, surface quality and availability.

5.1.4.2 Graded-Index Fibre Tests

In a particular implementation of the device, the jaws were made of aluminium with a 400um thick sheet of polypropylene attached to them. Young’s modulus of polypropylene is approximately 1.5GPa.

Figure 5.20(a) shows the near-field profiles of a 50um core diameter graded-index dual-coated fibre, with a singlemode launch, as the load on the jaws is increased. At first the profile widens with and then becomes constant for loads 5 and 6. Figure 5.20(b) shows the results for a multimode launch, where the profile at first becomes narrower and then appears to broaden slightly. A detailed inspection of the two sets of curves shows that for load 4, corresponding to approximately 6.5N, the multimode and singlemode launches had very similar shapes. This suggests that the device is producing a stable distribution that is independent of the launch for this load. The red curves in the figures correspond to a theoretical equilibrium mode distribution proposed by Yamashita 53.

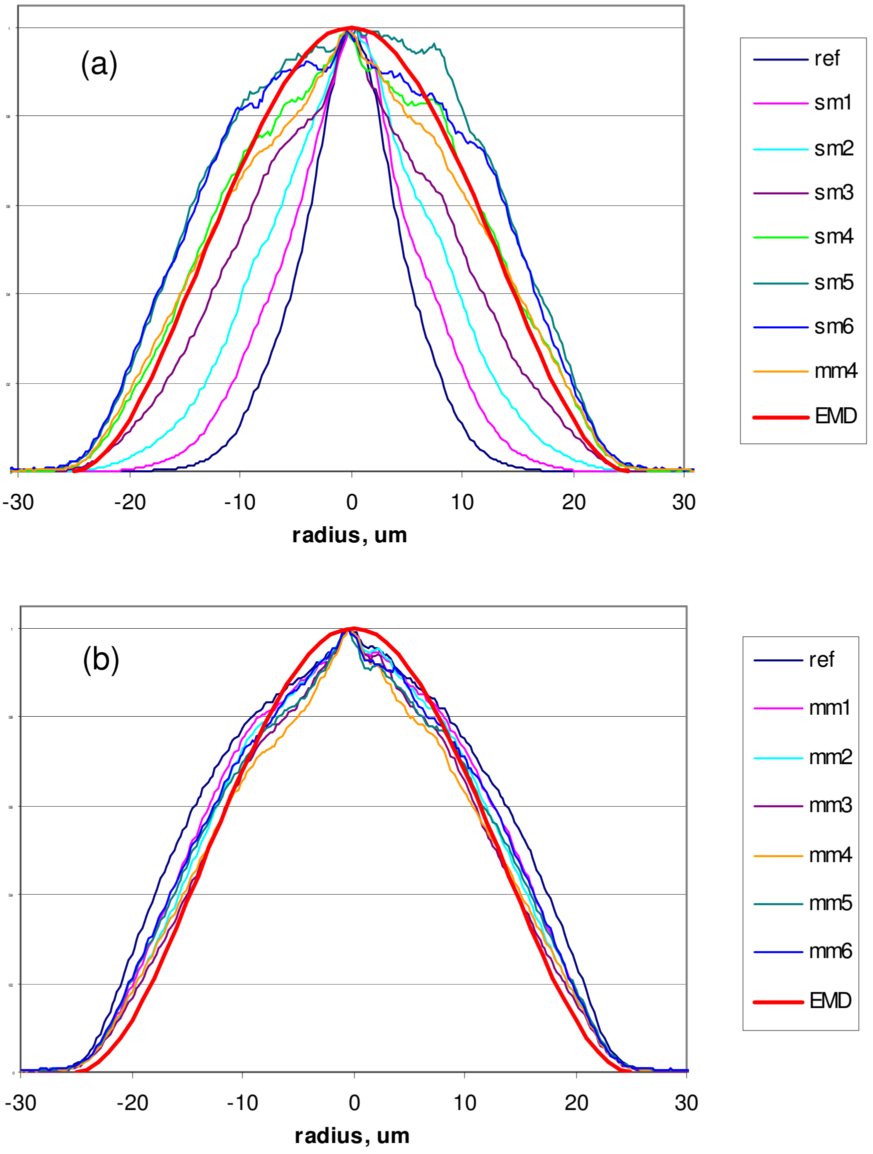

Figure 5.20. Near-field profiles of a 50um graded-index fibre with point-load mode-scrambler vs load number for (a) singlemode launch, and (b) multimode launch. The red curve represents an Equilibrium Mode Distribution.

The insertion loss of the device is shown in Figure 5.21, where it can be seen that the loss for the singlemode launch is very low at first and starts to increase as light is coupled to radiative modes. In contrast, the loss for the multimode launch increases almost linearly, as light is continuously coupled to radiative modes.

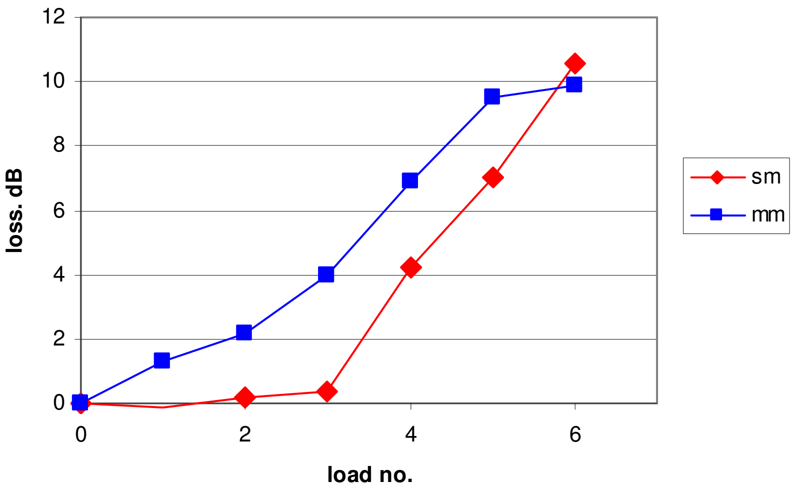

Figure 5.21. Insertion loss of a 50um graded-index fibre with point-load mode scrambler vs load number. Red is singlemode launch and blue is multimode launch.

5.1.4.3 Step-Index Fibre Tests

A point-load mode-scrambler was then applied to a 50um step-index fibre. For the singlemode launch, shown in Figure 5.22(a) the near-field profile had a reasonably flat top, for zero loading, but is not very steep at the edges. A fully-filled profile, see Figure 3.5, would be expected to have very steep edges as well as a flat top. Increasing the load to 4N steepens the edges as well a producing an even flatter top. Note that the profiles have been displaced vertically to aid clarity. Increasing the loading further causes the top of the profile to become concave, as more power is launched into higher-order and leaky modes. In contrast, for the multimode launch, Figure 5.22(b), the near-field is slightly convex for zero loading, but it also becomes quite flat at 4N and then concave for greater values of load. Thus a load of 4N produces uniform filling for both singlemode and multimode launch conditions.

The step-index fibre was then fused to a 50um graded-index fibre and the experiment repeated. It can be seen in Figure 5.23 that the near-field distribution for a load of around 6N, approximates that of a fully filled distribution for both singlemode and multimode launches. The corresponding MPDs for zero load and 6N load, for both launches, are shown in Figure 5.24. The MPDs for 6N load agree with each other extremely well, indicating that device is functioning properly, as a launch-independent mode-scrambler. It should be noted that the graded fibre is, in fact, fully filled and the reason the MPD peaks at 0.85 mode group is due to the use of a parabolic reference, as discussed in section 4.4.

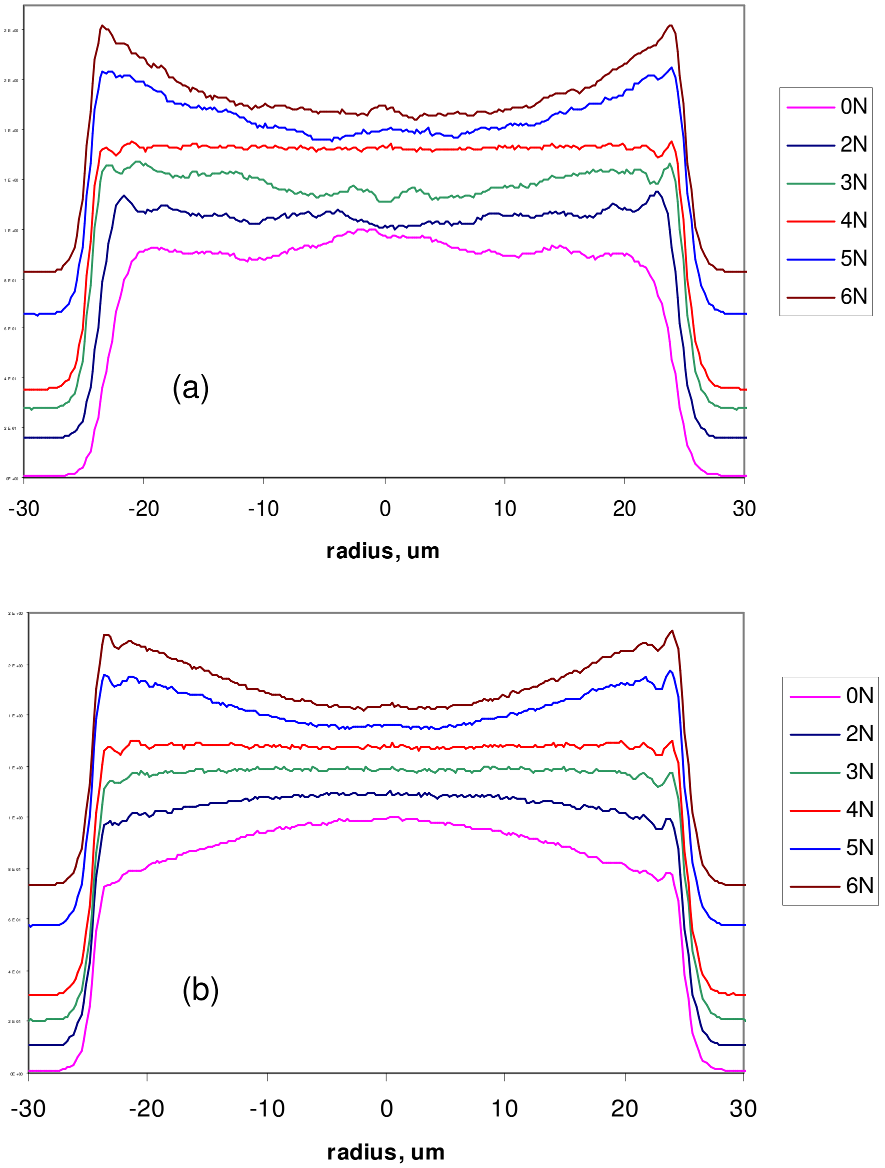

Figure 5.22. Near-field profiles of a 50um step-index fibre with point-load mode-scrambler vs load for (a) singlemode launch, and (b) multimode launch.

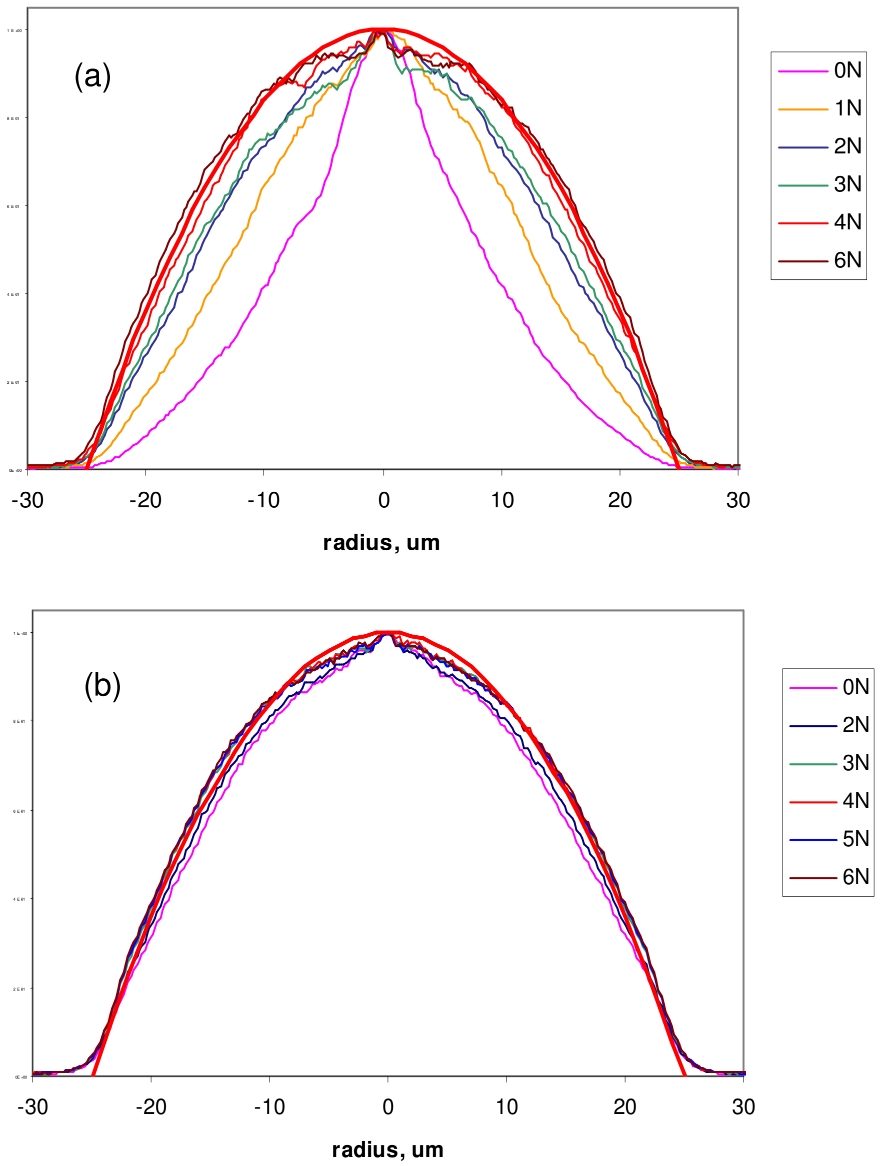

Figure 5.23. Near-field profiles of a 50um graded-index fibre connected to step-index point-load mode-scrambler vs load for (a) singlemode launch, and (b) multimode launch. The red parabolic curve approximates a fully filled distribution.

The insertion loss of the device with 6N load was typically 1.4dB for the singlemode launch and 2.4dB for the multimode launch.

The step-index point-load device shows great potential as a means of producing a fully-filled distribution in a graded-index fibre. The device was found to be insensitive to the launch distribution, it could be tuned in real-time and the loss should be satisfactory for most practical applications. In order to produce an arbitrary mode distribution, though, some means of modifying the fully-filled mode distribution is required. The next section will explore various techniques to achieve this through the use of mode-filtering.

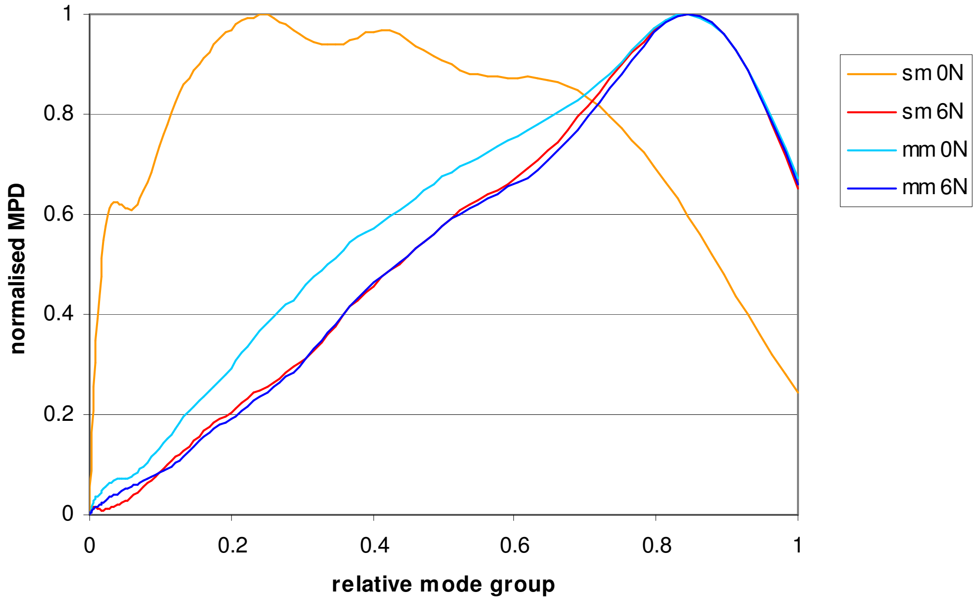

Figure 5.24. Measured MPDs of graded-index fibre connected to point-load step-index mode scrambler, for singlemode and multimode launches.

5.2 Mode filters

A variety of mode-filtering mechanisms was investigated including: a longitudinal air-gap, mandrel-wrapping, concatenated fibres, long fibre lengths, an offset launch and fused taper filters.

5.2.1 Air-Gap Mode-Filter

The air-gap mode-filter consisted of a small longitudinal gap between two sections of step-index fibre. The principle, in a geometrical sense, is that the angle subtended at the target fibre by the source fibre, decreases as the width of the gap is increased, effectively limiting the numerical aperture of the target fibre. Rays travelling at greater angles would simply miss the core of the target fibre and be lost. From a modal point of view, the overlap of the higher order-modes from the source fibre with the modes in the target fibre is reduced as the gap is increased.

To investigate the use of the mode-filter with step-index fibres, a 50um step-index fibre was passed through a point-load mode-scrambler and then aligned with a second fibre using a precision xyz manipulator. The output fibre was spliced to a 50um graded-index fibre and the MTF/MPD from this fibre was measured. The results for gap widths between zero and 1mm are shown in Figure 5.25.

As the gap increased, the MTF spectrum was selectively attenuated, approximately proportional to the mode group number. Also, for the largest gap values the MTF appeared to have a ‘plateau’ region around mode group 0.5, this resulted in the double peak seen in the MPD curves for these gap values.

In order to investigate these observations further, the step-index fibre was cleaved just prior to the splice with the graded-index fibre, and the near-field measured, for each gap value. The profiles, shown in Figure 5.26, indicate that for zero gap the near-field was slightly concave, denoting a slight bias towards higher-order modes. As the gap increased to 300um, the near-field became rounded, as higher angle rays failed to impinge on the core of the target fibre. Beyond this distance, however, side lobes appeared giving the appearance of a bright central spot surrounded by an outer ring. For example, Figure 5.27 shows a photograph of the near-field intensity pattern for 1000um gap, where the outer ring is clearly visible.

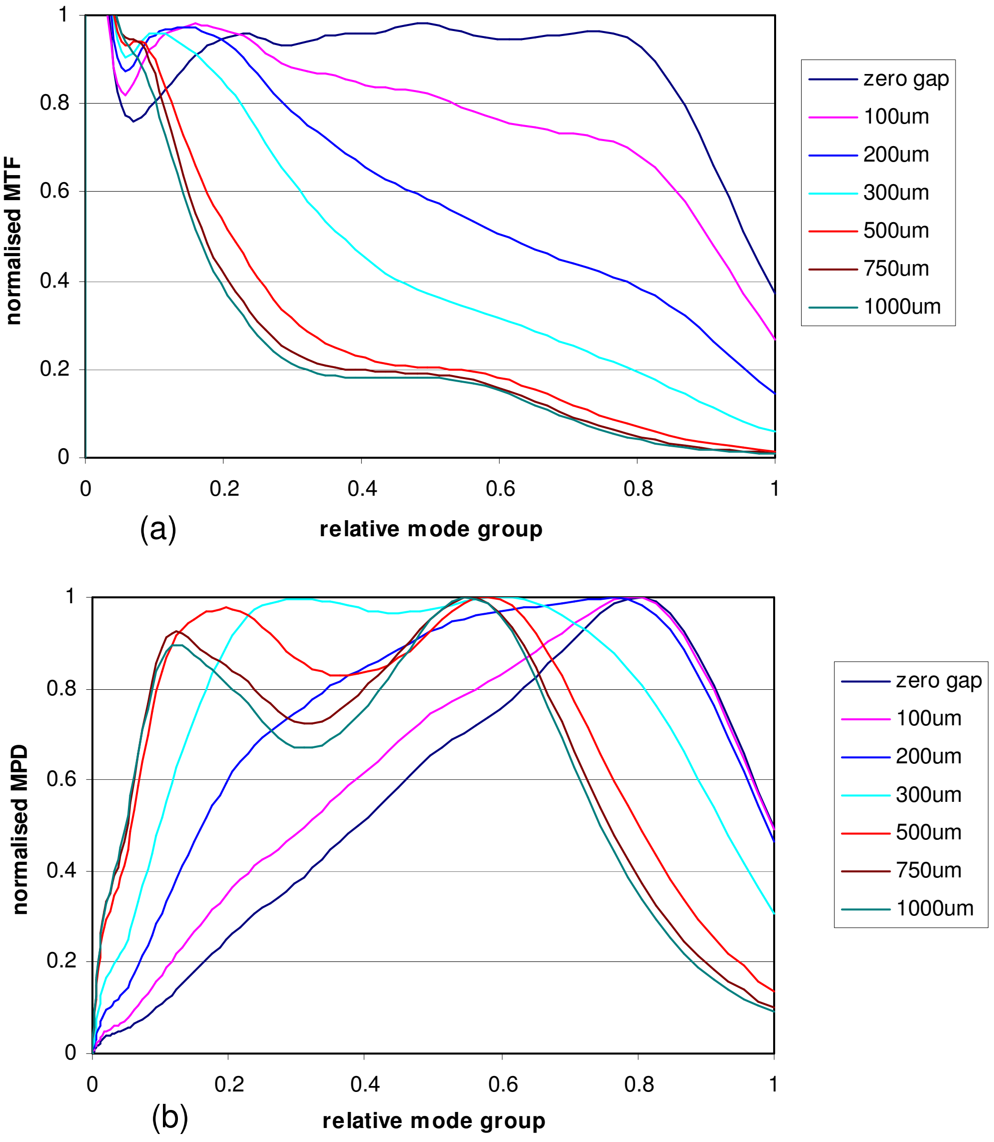

Figure 5.25. Measurement of a 50um graded fibre spliced to a step-index fibre with an air gap vs gap width, (a) MTF, (b) MPD.

The near-field profiles of the output graded-index fibre, Figure 5.28, show that for zero gap the profile was approximately parabolic as expected for a fully-filled fibre. As the gap increased the profile became triangular in shape and eventually slightly concave.

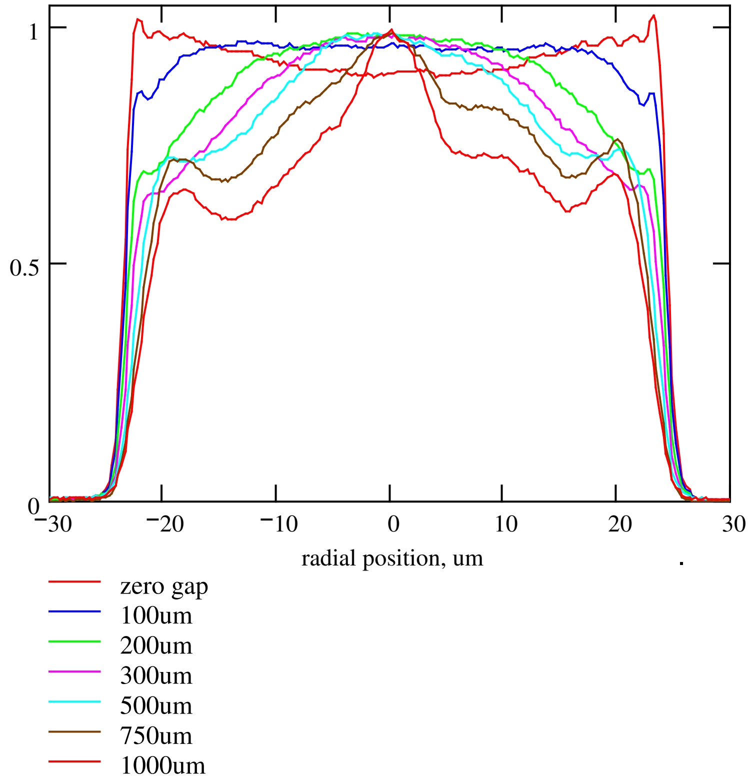

Figure 5.26. Measured near-field profiles of step-index fibre with air gap mode-filter vs gap width.

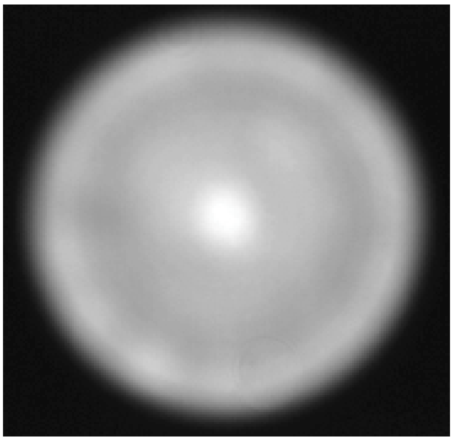

Figure 5.27. Near-field image of step index fibre with air gap mode-filter for 1000um gap width.

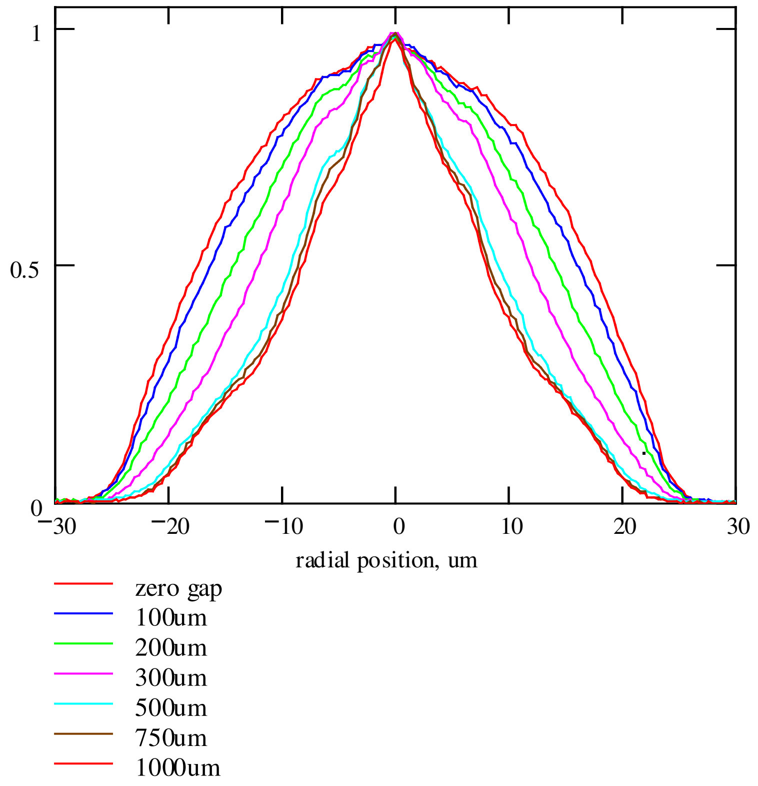

Figure 5.28. Measured near-field profiles of graded-index fibre vs air gap in the mode-filter.

This is caused by the side lobes in the step-index intensity profiles and also leads to the plateau in the MTF curves and the double peak in the MPD plots.

In order to understand this behaviour more fully, the air-gap mode-filter was modelled. Firstly, the field propagation across the gap was computed using diffraction theory and then the overlap with the target fibre of each mode was computed. This process, and the results obtained, are now described.

5.2.1.1 Model of the Gap Filter

To model the gap filter, several mathematical operations are required, as follows:

a) Compute the Bessel modes in the launch step-index fibre just prior to the gap,

b) Compute the diffraction field of each Bessel mode after it has traversed the gap,

c) Compute the overlap between each and every diffracted Bessel mode with each and every Bessel mode in the second step-index fibre,

d) Compute the overlap of each and every Bessel mode in the second step-index fibre with each and every Laguerre-Gauss mode in the graded-index fibre.

This process is shown schematically in Figure 5.29, where, for example, the $LP_{3,1}$ Bessel mode in the input fibre is being considered. The diffracted field across the gap couples into several Bessel modes in the target fibre. The excited Bessel modes in the target fibre then couple to the Laguerre-Gauss modes of the graded-index fibre to give the resultant output distribution. The whole process has to be performed for each Bessel mode in the source fibre and then the resultant intensity distributions summed to give the overall intensity distribution in the graded-index fibre.

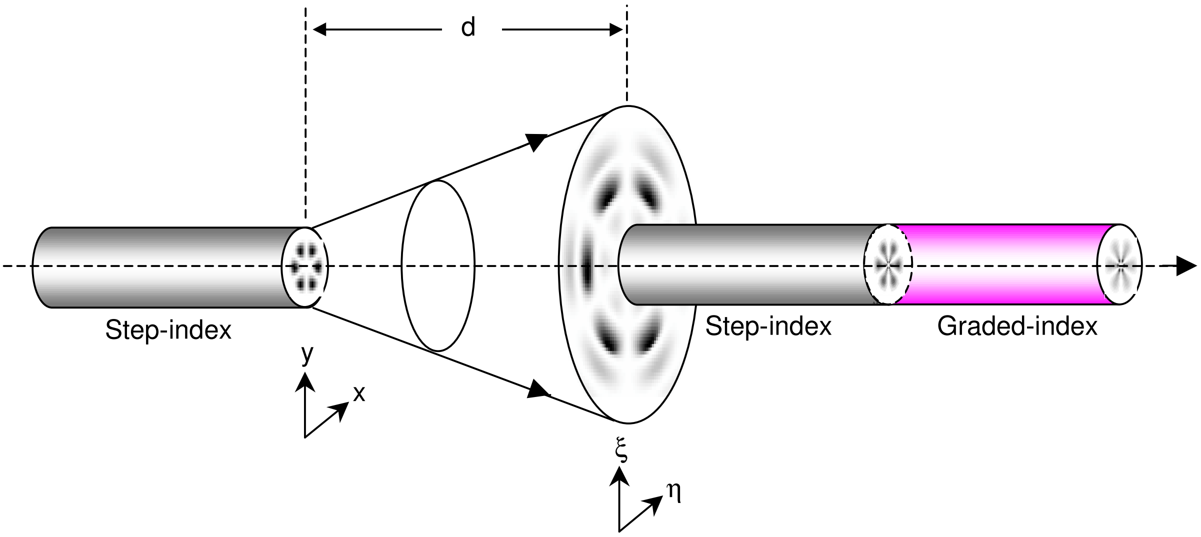

Figure 5.29. Schematic of air-gap mode-filter.

It was shown in section 4.3.1.3 that the far-field distribution of a fibre mode may be calculated from the near-field distribution using a two-dimension Fourier Transform. The far-field, or Fraunhofer, domain is normally defined as the region where

$$d >> \frac{a^2}{\lambda} \tag{5.7}$$

Therefore, for a fibre radius of 25um and a wavelength of 850nm, the right-hand side is equal to 735um. Clearly, for the gap widths employed here, this condition is not satisfied and so it is necessary to use the Kirchhoff diffraction integral [54].

Ignoring constants, the Kirchhoff diffraction integral is given by,

$$E_F(\xi,\eta) = \int\int \frac{E_N(x,y)}{R} e^{-ikR} dxdy \tag{5.8}$$

where: $E_N(x,y)$ is a Bessel mode in plane (x,y) just prior to the gap,

$E_F(\xi,\eta)$ is the diffracted mode in plane (ξ,η) after the gap

and

$$R = \zeta\left\{1 - \frac{2(\xi x + \eta y)}{\zeta^2} + \frac{x^2 + y^2}{\zeta^2} + \frac{\xi^2 + \eta^2}{\zeta^2}\right\}^{0.5} \tag{5.9}$$

Next, the overlap of each diffracted mode with each Bessel mode in the target fibre is calculated using an overlap integral of the form given in eqn. (3.36). Then, the overlap coefficients are summed for each particular Bessel mode in the target fibre.

Computed profiles, for the same conditions used in the experiment, are shown in Figure 5.30. Agreement with the measured results in Figure 5.26 is very good and the presence of side lobes for the larger gaps is clearly seen.

The final step was to compute the overlap between each Bessel mode in the step-index target fibre with each Laguerre mode in the graded-index fibre, using the overlap integral. The results are shown in Figure 5.31. There is again good agreement with the measured profiles shown in Figure 5.28. The gap filter may therefore be accurately modelled using the diffraction approach described above.

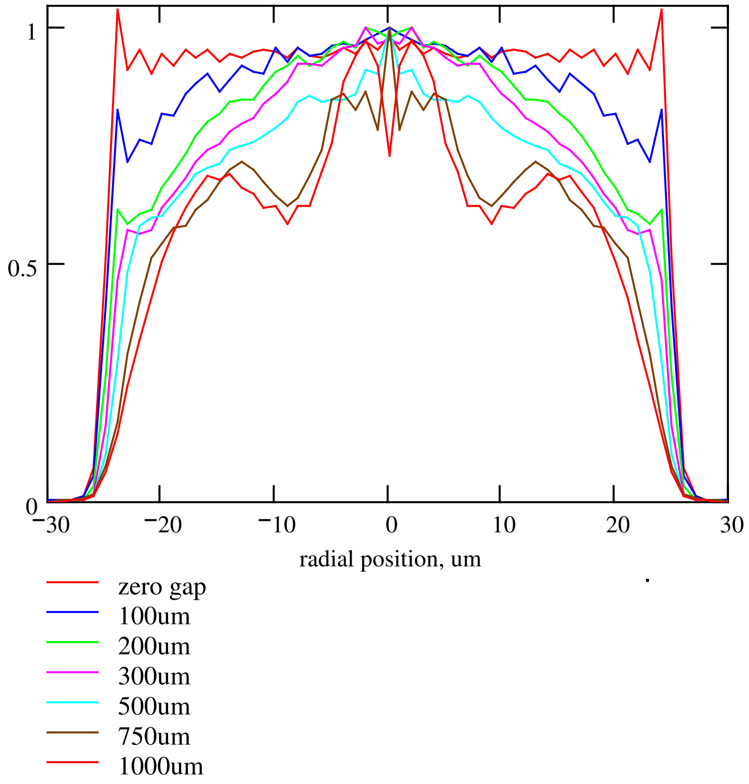

Figure 5.30. Model near-field profiles of step-index fibre with air gap mode-filter vs gap width.

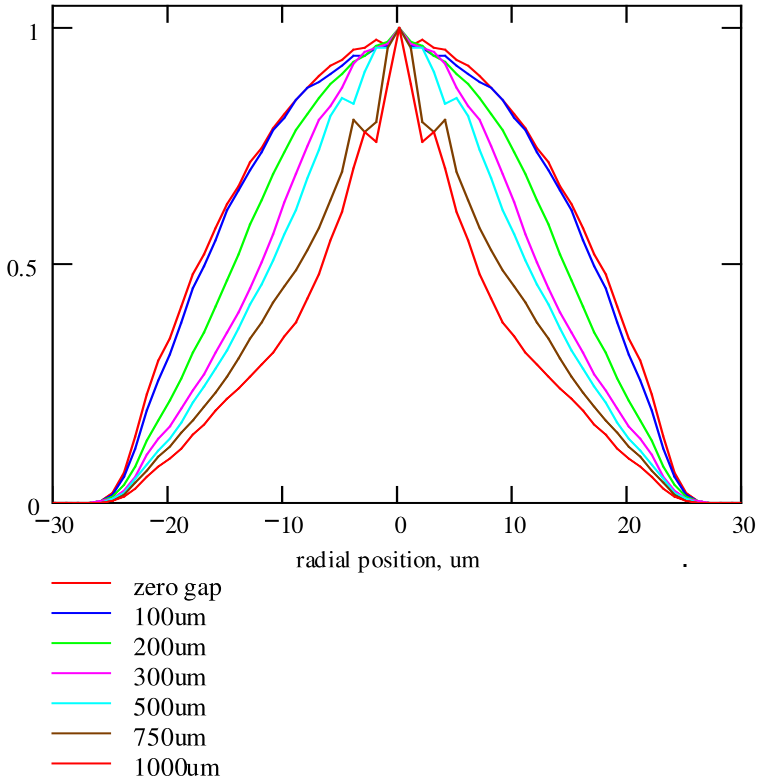

Figure 5.31. Model of near-field profiles of graded-index fibre vs air-gap in the mode-filter

It should be mentioned, however, that an extra computational step of equalising the powers between modes within the same mode group in the graded-index fibre was necessary to achieve this level of agreement with experimental data. This indicated that mode coupling between the degenerate modes in the fibre was occurring as expected. As described in section 4.1.1.2, equal power distribution between the degenerate modes in a mode group is a requirement of the MTF measurement method.

The MTFs of the modelled data are shown in Figure 5.32. Comparison with the MTFs of the measured data in Figure 5.25(a) shows excellent qualitative agreement.

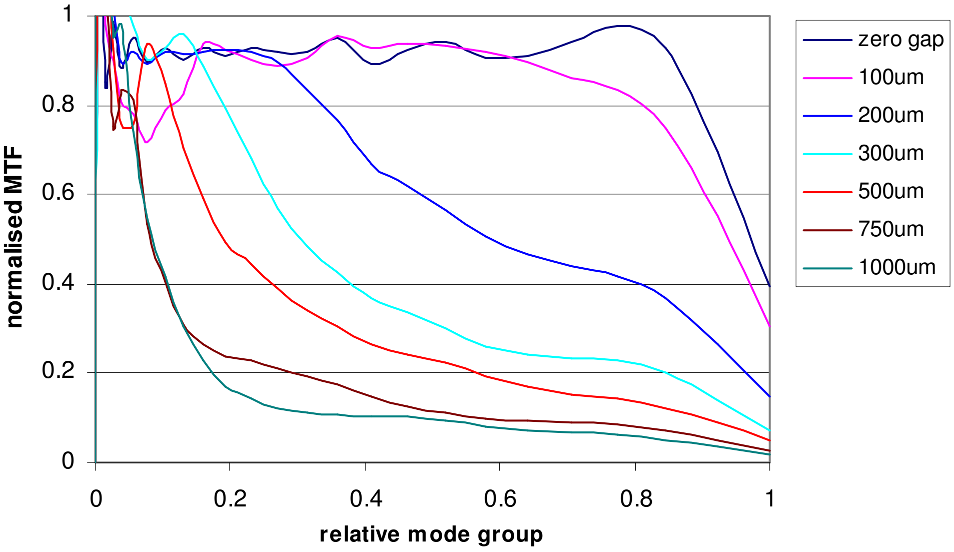

Figure 5.32. Model MTF of a 50um graded fibre spliced to a step-index fibre with an air gap vs gap width.

The modelling technique described here could, in fact, be used to investigate the incidence of intra-group mode coupling in graded-index fibres. This could be achieved by comparing measured MPDs following the mode-filter with those calculated with differing amount of mode equalisation.

5.2.2 Mandrel Wrap Filter

It is well known that introducing a bend in a multimode fibre causes preferential attenuation to higher-order modes [14] and the method has, in fact, been widely used in the industry for creating pseudo steady-state modal conditions from an overfilled launch. Bending is normally applied in the form of several turns around a mandrel of a particular size. For example, IEC standard 61300-3-4 [55] specifies the use of five turns around an 18mm diameter mandrel for 50um fibre and five turns around a 20mm diameter mandrel for 62.5um. While this type of filter is satisfactory for overfilled fibres, it is not able to produce an EMD from an under-filled source, as it does not induce a significant amount of mode coupling.

To investigate the mandrel-wrap filter, a fibre was bent with a single turn around a series of different diameter mandrels and the mode profile was measured. The fibre used for the experiment was a 50um graded-index fibre and was excited by a point-load mode-scrambler.

The MTF and MPD measurements are shown in Figure 5.33 and Figure 5.34, respectively. It can be seen that the MTF curves remained fairly flat up to a certain ‘knee’ position, after which the higher-order modes became increasingly attenuated. The position of the knee moved to the left as the mandrel diameter was reduced. Similarly, the peak position in the MPD curves moved steadily to the left, from a peak at mode group number 0.8, in this case, for the largest mandrels to a peak at 0.3 for the 5mm mandrel.

The corresponding near-field intensity profiles are shown in Figure 5.35. As the bend became tighter, the profiles became progressively narrower, but still retained a pseudo-parabolic shape. This may be expected by noting from eqn. (4.3) that as long as $I(r)$ is parabolic, MTF(δ) will have unity-value up to the radial extent of the near-field, whatever its width. This is the general form of the MTF curves in Figure 5.33.

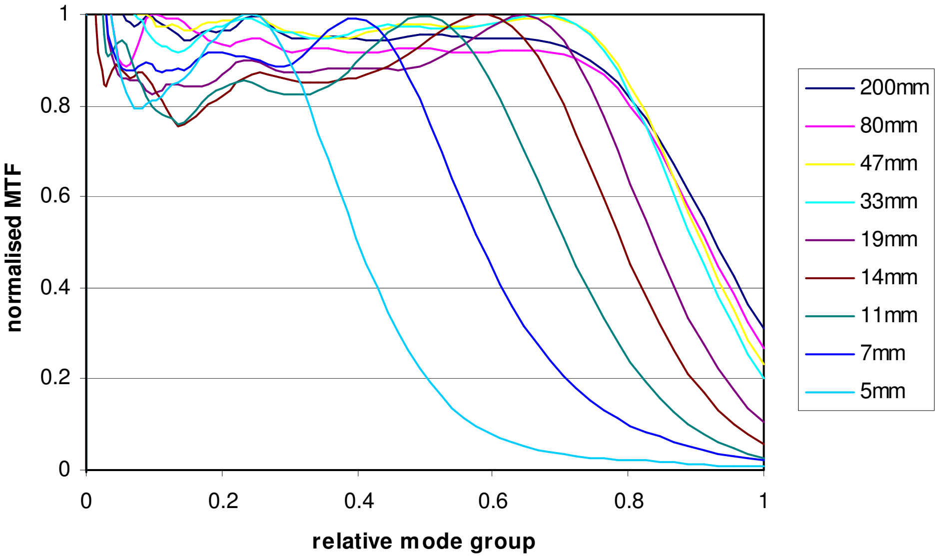

Figure 5.33. MTF of 50um graded-index fibre vs bend diameter of single-turn mandrel-wrap mode-filter.

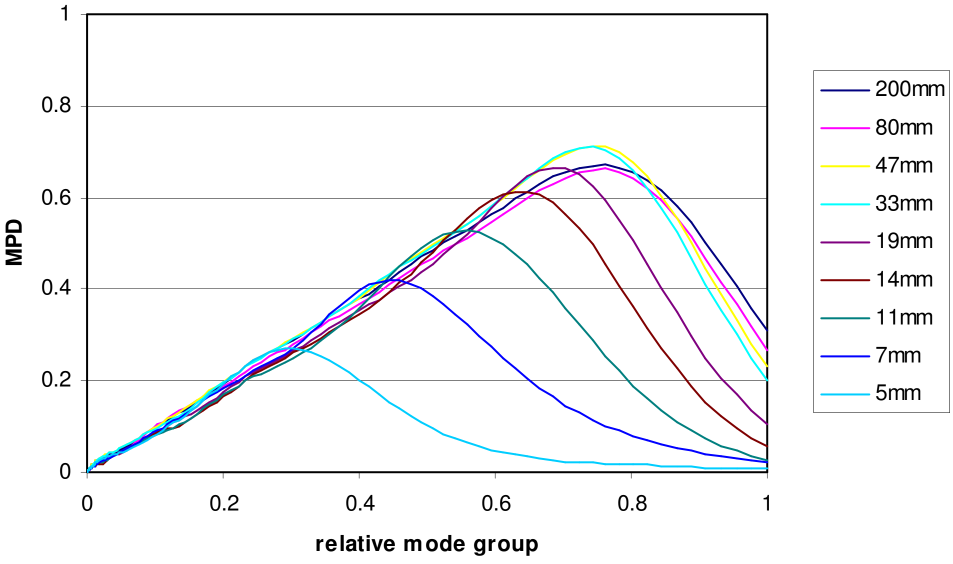

Figure 5.34. Un-normalised MPD of 50um graded-index fibre vs bend diameter of single-turn mandrel-wrap mode-filter.

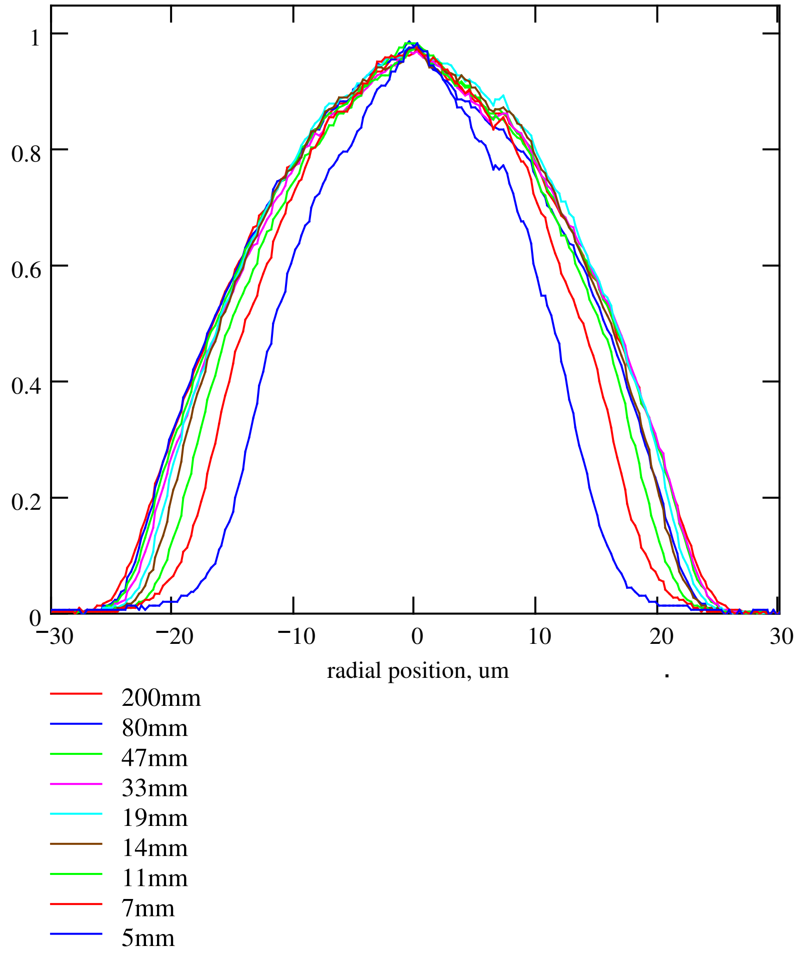

Figure 5.35. Near-field profiles of 50um graded-index fibre vs bend diameter of single-turn mandrel-wrap mode-filter.

These profiles may be contrasted with the intensity profiles for the air-gap mode-filter, which are shown in Figure 5.28. The main difference is that for the mandrel-wrap filter the intensity profiles remained reasonably parabolic in shape as the bend was tightened, whereas, for the gap filter, the profiles maintained the same approximate width but became more triangular, and even concave, in shape as the gap was increased. The two types of mode-filter are, therefore, complementary and may be used to achieve different forms of mode distribution.

5.2.3 Concatenated Fibres

In a fibre LAN channel, there are usually at least two connectors, the loss of which must be kept to a minimum to achieve required system power budgets. High precision, PC (*Physical Contact*) reference connectors may have an insertion loss of better than 0.05dB when used with fibres with very low core-to-cladding eccentricity error. In an installed system, however, cheaper, lower quality, connectors are normally employed leading to misalignment of the core centres. Also, the geometry of the fibre may not be consistent though the channel, as the fibre cables are likely to have been obtained from different suppliers.

Resulting mis-matches in core diameter and core alignment at connector interfaces create additional loss, particularly if the modal volumes of the fibres are well filled. Furthermore, the effect of mode filtering by connectors upstream can lead to lower losses of subsequent connectors.

To demonstrate the mode filtering effect, an experiment was carried out to measure the insertion loss of a series of nine concatenated 50um patchcords. The patchcords were each 3m long and had a variety of FC, SC and ST connectors. A well-filled launch was provided by an 850nm LED source. Figure 5.36 shows the measured MPD at the output of each patchcord as the link was progressively dissembled. The MPD after a single length peaked at about 0.85 mode group number and then the curves moved progressively to the left as higher-order modes were filtered out by subsequent connectors. It is interesting that the MPDs after eight and nine sections are very similar, indicating the convergence to a stable mode distribution.

The corresponding insertion losses of the eight connector pairs are shown in Figure 5.37. The average loss per connector is 0.34dB. The loss of the last connector, however, is less than the others, as might be expected from the observed convergence of the MPDs.

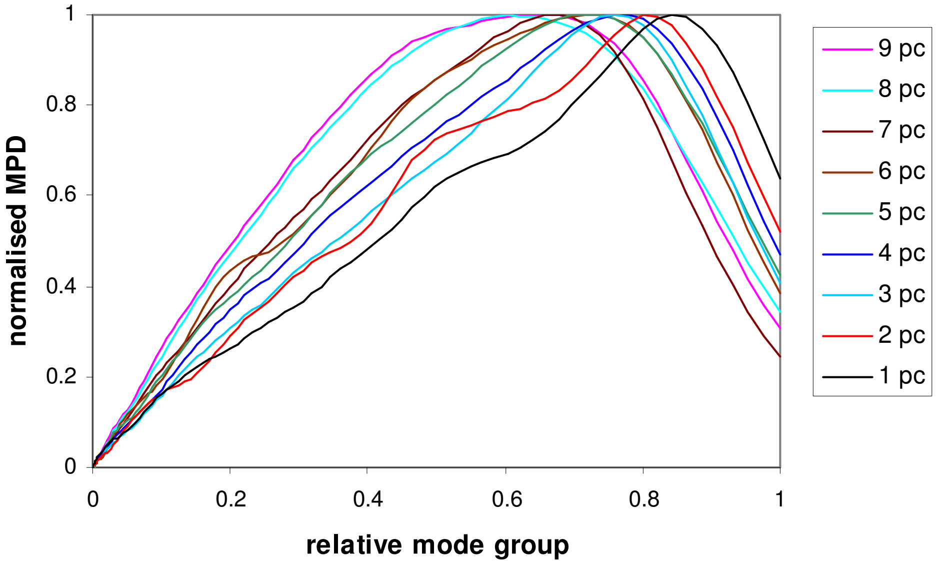

Figure 5.36. Measured MPDs for each length in concatenation of nine patchcords.

It appears, therefore, that a series of concatenated patchcords acts as a mode-filter, which tends towards a stable mode distribution. This arrangement may find application in enabling reproducible loss measurements to be made on individual connectors, with an MPD that is representative of LAN-based applications. It should be noted, however, that the performance of this method of mode-filtering depends on the particular patchcords used in the concatenation, their quality and the cleanliness of the connectors.

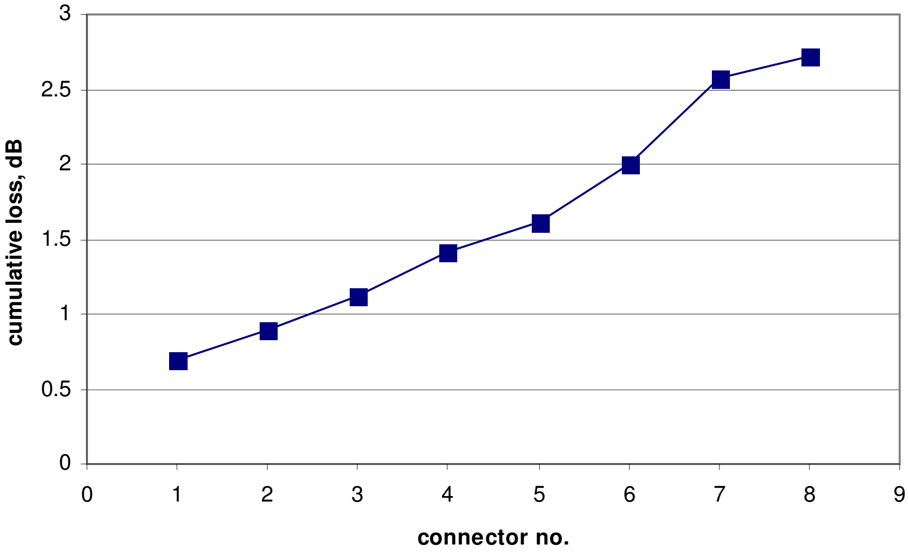

Figure 5.37. Measured insertion losses of concatenated patchcords

5.2.4 Long Length Equalisation

It was shown in section 2.4.1 that there is some tendency in long fibre lengths for the modal distribution to tend towards an equilibrium distribution. To investigate this further, a series of different fibre types were tested, including tight buffered, gel-filled, and uncabled fibres, and lengths ranging from 100m to 2.7km. Each length was excited with three modal distributions, under-filled, medium-filling, fully-filled. The MPDs after transmission through each fibre were measured and then the fibres were, in turn, cut back to one metre length to measure the launched MPD. In each case it was found that, while higher-order modes suffered greater attenuation, in much the same way as the mandrel-wrap filter in section 5.2.2, the low-order modes did not undergo appreciable mode conversion. Long fibres therefore have some merit as mode-filters but are not really suitable as mode-scramblers, or a means of producing an EMD, unless some other mechanism is applied to them, such as microbending.

5.2.5 Offset Fibre Launch

It was mentioned in section 2.2 that in order to minimise pulse dispersion due to DMD in high bandwidth LAN systems, laser sources must not launch exclusively low-order modes. One way of equalising the mode distribution from a single-mode laser source is to introduce a small offset between the laser pigtail and the multimode system fibre [56].

As an example, Figure 5.38 shows the output of a 50um graded-index fibre as a function of the offset of a single-mode fibre launch, measured at 850nm. The mode field diameter of the launch fibre was approximately 5.4um. The corresponding encircled flux of for each launch position was measured and it was found that the encircled flux for a launch offset of 11.1um passed through the centre of the IEEE template for 10Gb/s Ethernet [2].

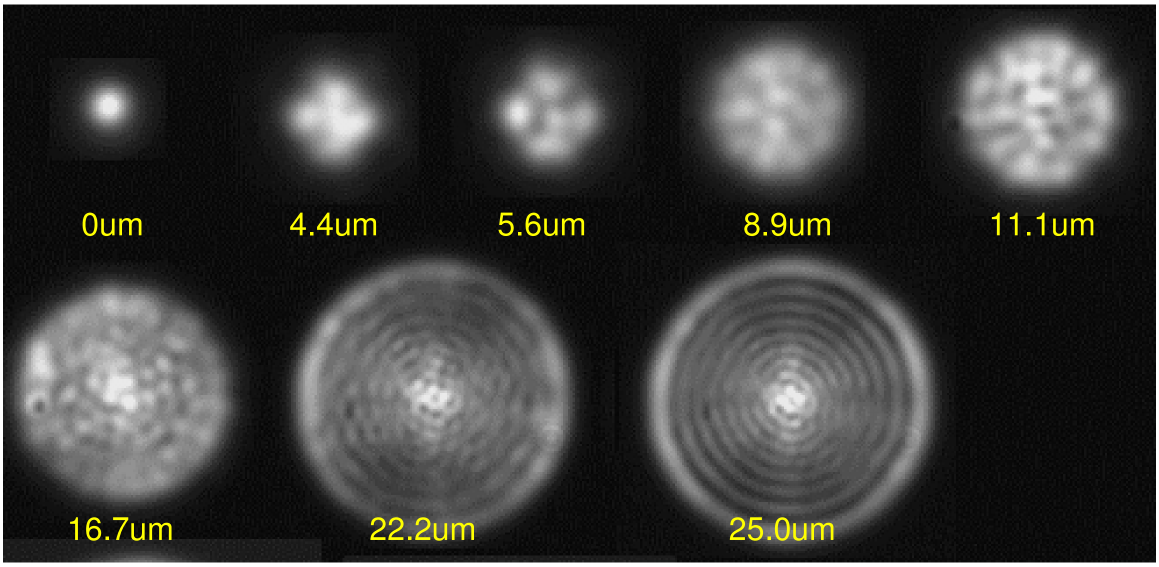

Figure 5.38. Near-field images of 50um graded-index fibre with offset single-mode launch. Offsets given in yellow.

It may also be seen that there is a lobular structure in some of these distributions, particularly for the smaller offsets. It will be recalled from section 4.1.1.2 that azimuthal symmetry is requirement for the measurement of MTF and MPD and so some care is required when making measurements of these distributions. In contrast, encircled flux is a radial integration method and is therefore more appropriate for this type of mode distribution and is likely to give better reproducibility.

5.2.6 Fused Biconic Tapered Coupler

A typical fused biconic-tapered coupler is a four-port device used for splitting, or combining, optical signals in fibres. Typical applications are in simplex fibre communication systems, dual-wavelength test equipment and in OTDRs. A fused biconic-tapered coupler is made by twisting two fibres together and then heating under tension, such that the two cores come into close proximity. Light incident in one of the two launch ports is split between the two output ports in a ratio that is dependent on the length and width of the taper. Tests on a typical commercial splitter showed that the split ratio varied from 50/50 for a nearly well-filled launch to 57/43 for an underfilled launch. The reason for this sensitivity to launch is that predominantly high-order modes are coupled into the *cross-channel* of the coupler, leaving lower-order modes in the *through-channel*. So, for an underfilled launch, the through-channel will retain a greater proportion of the launched distribution than is coupled into the cross-channel, thus acting as a mode-filter. To investigate this further, the near-field distributions at the output ports of a 95/5 coupler were measured when a fully-filled distribution was launched into one of the input ports.

The normalised near-field profiles, shown in Figure 5.39, show that the output of the 95% port, which is the through-channel, is slightly narrower than the launch distribution. This is because some of the high-order modes have been coupled into the cross-channel, 5%, port. The profile of the latter is almost rectangular, indicating a predominance of high-order modes. This is demonstrated in the corresponding plots of the MPDs, shown in Figure 5.40. The MPD of the 95% port has moved slightly to the left of the launched MPD, whereas the MPD of the 5% port shows a complete dearth of low-order modes.

This device is clearly an effective method of generating a high-order mode spectrum and could find application as a source for sensors, such as those which utilise microbending to couple light to radiation modes.

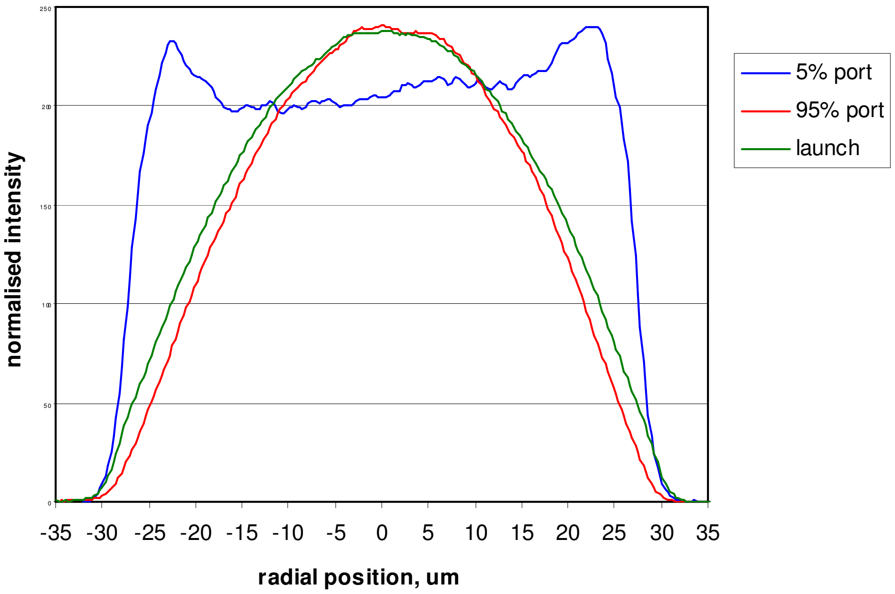

Figure 5.39. Near-field intensity profiles of 95/5% coupler showing the launched distribution and the output of the two output ports.

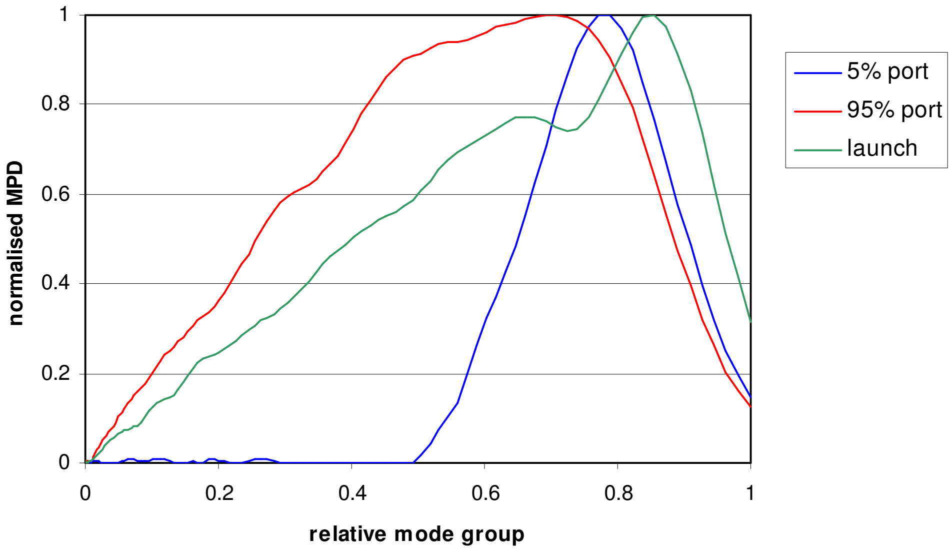

Figure 5.40. Normalised MPDs of 95/5% coupler showing the launched MPD and the MPDs of the two output ports.

5.3 Chapter Summary

This chapter has investigated ways of modifying the mode distribution in multimode fibres. These have been broadly divided into two categories: those that scramble, or re-distribute, light between guided modes, and those that selectively attenuate, or filter out, certain modes.

For mode-scramblers, this study has concentrated on two particular techniques; these are Long Period Gratings, which are widely employed in both multimode and singlemode fibres for sensor applications, and a novel point-load device. It was found that the behaviour of three types of LPG were somewhat different, these were microbend gratings, taper gratings and refractive index gratings. Although none of them performed well as a mode-scrambler, they all were able all to transfer power from a singlemode launch into higher-order modes. The main drawback was that they tended to transfer power in a progressive manner, eventually exciting very high-order and leaky modes at the expense of the lower-order modes. The microbend grating produced a broad, squarish, profile with an insertion loss that increased rapidly from 0.5dB to 4dB once leaky modes were excited. The taper grating was easy to manufacture using a step-and-repeat method with a commercial fusion splicer and it did produce a reasonably well-filled distribution but the insertion loss was very high at around 8dB. Also, the uniformity of the grating was difficult to maintain as the amount of taper, or necking, was somewhat unpredictable. The refractive index grating tended to produce a squarish profile with steep sides, similar to he microbend grating except that the near-field profile of the index grating was much narrower, and, unlike the microbend grating, it did not appear to excite leaky modes. A possible cause of this was due to the small size of the focussed laser beam using for writing. The insertion loss of this grating was, however, only about 2dB.

The point-load mode-scrambler was found an effective means of generating mode-coupling in a graded-index fibre. A near-field distribution could be produced that was similar to a theoretical EMD, for both a singlemode and multimode launch. The insertion loss, however, was around 4dB and it was found that the point-load device was more effectively applied to a step-index fibre where a fully-filled distribution could be easily produced for both singlemode and multimode launches. Coupling the output of this device to a similar-sized graded-index fibre produced a stable, fully-filled, distribution which could then be modified, as required, by appropriate mode filtering.

Several mode filters have been investigated, including an air gap between two step-index fibre sections, a mandrel-wrap filter, concatenated fibres, long length equalisation, an offset launch and a fused tapered coupler. It was found that the air gap filter, when coupled to a graded-index fibre, attenuated modes in a manner roughly proportional to the mode group number, leading to an approximation to an EMD. The mandrel-wrap filter tended to selectively attenuate only the highest order modes, depending on the bend radius used. A series of concatenated fibres caused a well-filled distribution to converge to a stable mode power distribution after 8 or 9 connectors. An offset fibre launch, as specified by the IEEE, coupled light directly to mid-order modes, producing a squarish profile, which was compliant with an IEEE encircled flux template. A fused tapered coupler was found to selectively filter out high-order modes into the crossover port, particularly for high coupling ratios, and might find application in sensors as a means of selectively launching high-order modes.

In summary, the point-load mode-scrambler, with a step-index fibre, was found to be a very effective mode-scrambler, which when used with an appropriate mode-filter, should enable a wide range of modal distributions to be obtained.

CHAPTER 6

APPLICATIONS OF MODE CONTROL

Using a combination of a mode-scrambler and mode-filters, it is possible to produce a variety of Mode Power Distributions. Several examples of mode control are described in this chapter, to satisfy launch requirements for fibre characterisation. These are an Equilibrium Mode Distribution, a Limited Phase Space launch, and compliance with Mode Power Distribution and Encircled Flux templates. Further examples of mode control are also given, for speckle suppression, multimode sensing applications and mode division multiplexing.

6.1 Equilibrium Mode Distribution

According to Yamashita [53] the Mode Transfer Function MTF(m) of a theoretical Equilibrium Mode Distribution (EMD) is given by:

$$\mathrm{MTF(m)} = 1 - \mathrm{m}^{0.75} \tag{6.1}$$

where m is the relative mode group number.

The MTF, from eqn.(6.1), and the corresponding Mode Power Distribution (MPD) are shown Figure 6.1. The MTF is an approximately linear decreasing function and the MPD displays a peak around 0.5 mode group number.

The MTF is similar in shape to that obtained using the gap mode-filter, shown in Figure 5.25(a), with a gap of 200-300um. This suggests that an EMD could be generated by a combination of a step-index point-load mode-scrambler and an air gap mode-filter. Such a device was constructed using a 50um step-index fibre spliced to a 62.5um graded-index fibre. The MTF results are shown in Figure 6.2, where the green line represents the output with zero gap, indicating that the graded-index fibre is, as expected, not fully-filled by the smaller step-index fibre. Introducing a gap of 130um gives the MTF shown by the red line. The addition of a mandrel-wrap filter, comprising one quarter turn around a 12mm diameter mandrel, caused the MTF curve, shown in blue, to converge to zero at maximum mode group number, resulting in quite good agreement with the theoretical EMD curve.

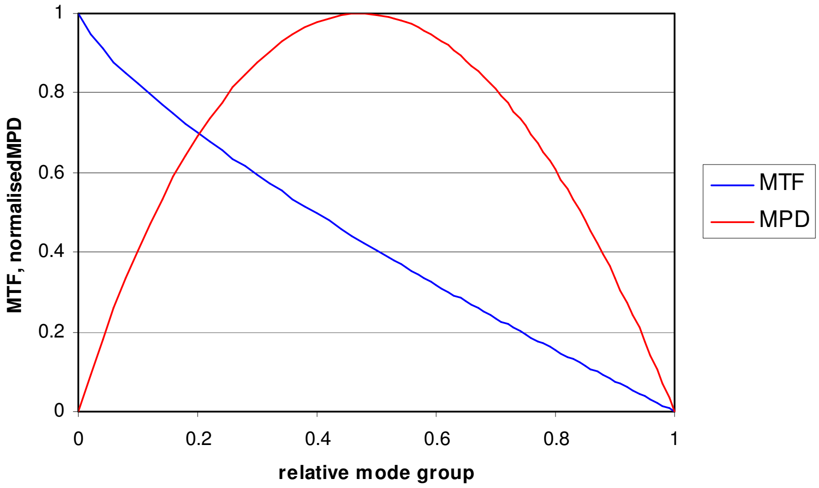

Figure 6.1. Theoretical Equilibrium Mode Distribution (after Yamashita)

Inspection of the corresponding MPD curve for this result, given by the blue line in Figure 6.3, shows that the measured MPD is slightly asymmetrical compared to the model, but the peak also occurs around 0.5 relative mode group number. Thus, the combination of the mode-scrambler and the air-gap and mandrel-wrap filters enables a reasonable approximation to the EMD to be achieved.

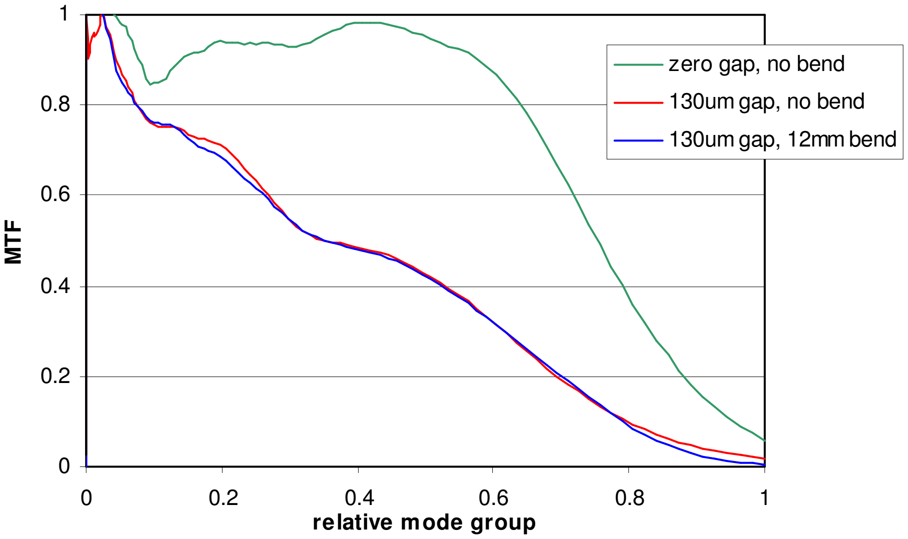

Figure 6.2. MTF measurements on EMD mode control device

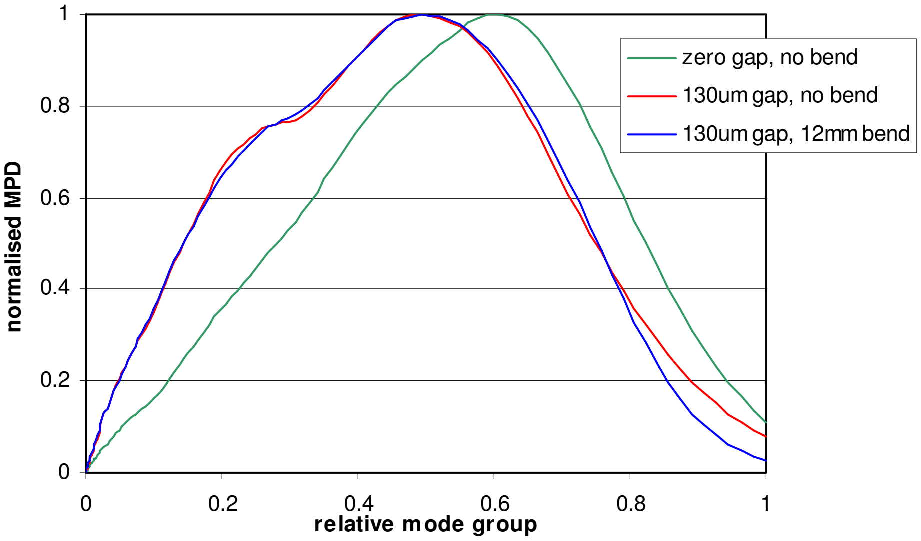

Figure 6.3. MPD measurements on EMD mode controller

6.2 Limited Phase Space Launch

A limited Phase Space (LPS) launch is a geometrical launch where the spot-size and NA of the launch are restricted to a given fraction of the core diameter, and NA, of the target fibre. A launch of 70% is generally accepted by the standards community to be the maximum theoretical launch that does not put power into leaky modes [57], thereby minimising the incidence of transients in loss measurements.

The reason behind this choice is demonstrated in Figure 6.4, where several LPS launches are shown superimposed on the local NA of a graded-index fibre. The NA at the radial extent of the 70% LPS launch is equal to the local NA of the graded-index fibre. By contrast, a 50% LPS launch lies entirely within the local NA, while an 85% launch, which is often specified in avionics standards, exceeds the local NA in the region 13um to 21.25um. To simulate the 70% launch, the overlap coefficients between the modes in a step-index fibre and a graded-index fibre were computed, where the step-index fibre was 70% of the diameter and NA of the graded fibre. It was found that highest-order azimuthal mode number in the step-in fibre was 15 and, of this, 95% was coupled into the $LP_{15,1}$ and $LP_{15,2}$ guided modes of the graded fibre and only 5% into the leaky $LP_{15,3}$ and $LP_{15,4}$ modes. In total, for the whole mode set, the fraction of light coupled from the step fibre into leaky modes was only 0.23%. This compares to 24% for a 100% launch.

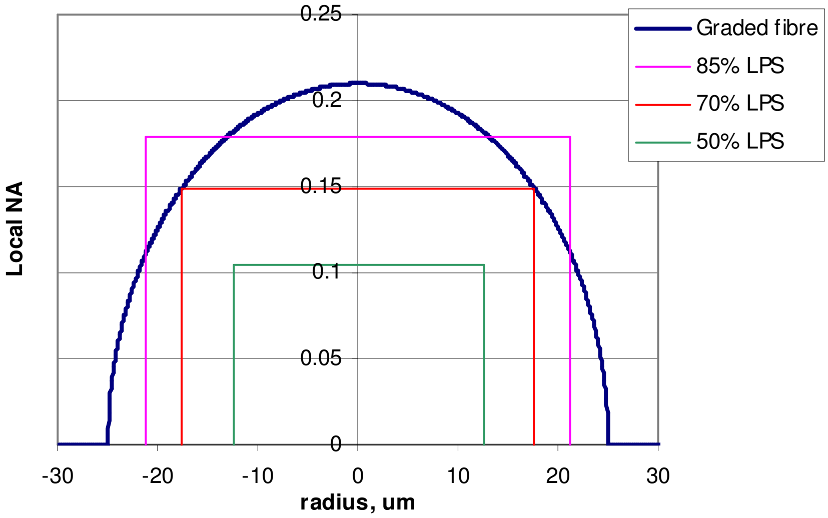

Figure 6.4. Local NA of graded-index fibre and several LPS launches. The diameter and NA of the graded fibre were 50um and 0.21, respectively.

The near-field profile for the 70% LPS launch is shown in Figure 6.5, where power was equalised between modes in the same mode group. Also shown, for reference, is the fully-filled distribution. The corresponding MPDs are shown in

Figure 6.6, where it can be seen that the peak MPD for the 70% launch occurs near to 0.5 mode group number.

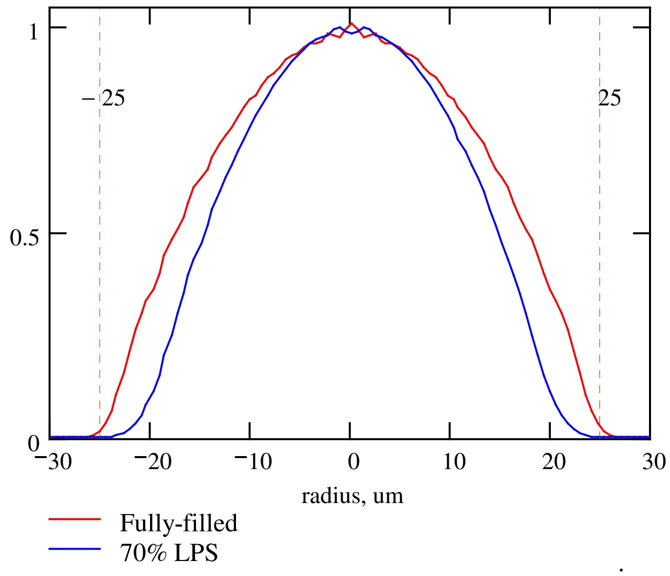

Figure 6.5. Simulated near-field profile of 50um graded fibre for a 70% LPS launch (blue), and a full set of guided modes (red).

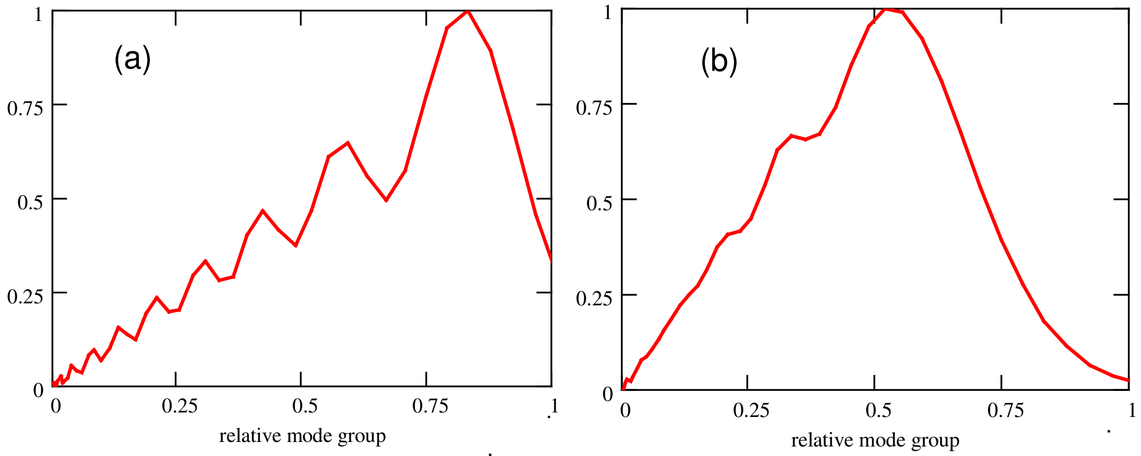

Figure 6.6. Simulated MPD in 50um graded fibre for (a) a full launch (excluding leaky modes), and (b) a 70% LPS launch.

Experimentally, it was found that an approximation to a 70% LPS launch could be achieved by passing a fully-filled 50um fibre once around an 8mm diameter mandrel. The resulting MPD, shown in Figure 6.7, which may be compared with Figure 6.6(b), has a peak MPD at 0.5 mode group number and a similar overall shape. This device is useful as a means of producing an LPS launch as it is independent of the launch conditions, and is therefore easier to implement that a geometrical launch.

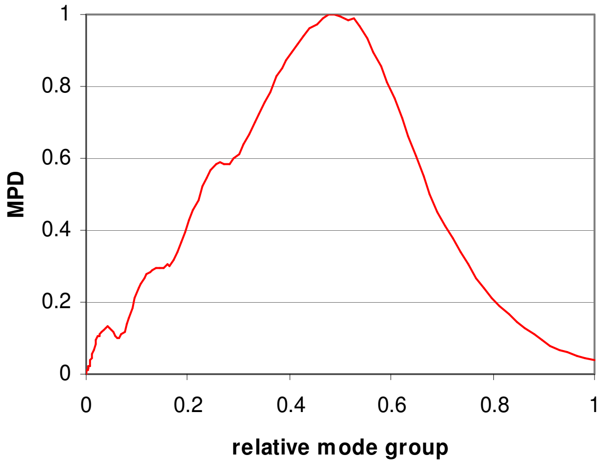

Figure 6.7. Experimental simulation of 70% LPS launch by inserting one turn around 8mm diameter mandrel on a fully-filled 50um fibre.

The peak for the EMD launch, shown in Figure 6.1, was also at 0.5 mode group, indicating a roll-off of higher-order modes. The shape of the MPD for the EMD launch is, however, more convex than for the LPS launch, thus the EMD and LPS launch criteria are not identical, as is sometimes assumed in the industry.

6.3 MPD Standard for Link Testing

An update in 2006 in the ISO/IEC link testing standard [12] introduced the use of an MPD pass/fail template for sources used for testing the insertion loss of installed links. The template ensures a fairly well-filled mode distribution, but without the highest-order modes, to avoid transient losses.

It was found that a mode control device consisting of a point-load mode-scrambler followed by a mandrel-wrap mode-filter was able to pass the MPD template, shown in Figure 6.8, where the three delineated regions represent failure areas. It can be seen that the device comfortably passes the template. The diameter of both the step-index and graded-index fibres was 50um and a mandrel-wrap consisting of one half-turn of 30mm diameter was inserted in the graded fibre, immediately after the splice to the step-index fibre.

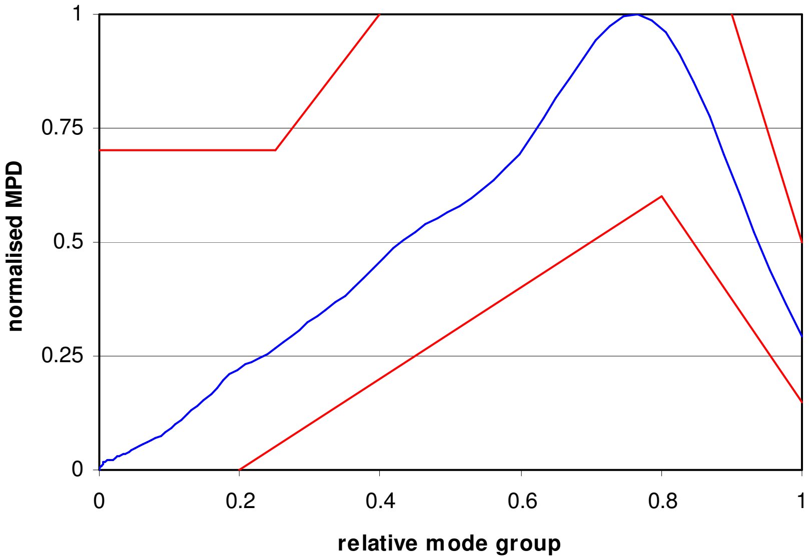

Figure 6.8. Measured MPD of mode control device designed to comply with ISO/IEC template.

As an example of the performance of this device, a concatenated link of eleven 50um patchcords was assembled, consisting of 3m fibre lengths and a mixture of ST, SC and FC connectors. The insertion loss of the link was measured using a variety of launch conditions, including a singlemode launch, a commercial LAN tester, a mode-scrambler and a singlemode offset launch. The loss values, shown in Figure 6.9, range from 0.5dB for the singlemode launch to 5.1dB for the offset launch. The experiment was then repeated with the mode control device positioned between the launch patchcord and the link under test. The peak to peak range of losses was reduced to 0.2dB, compared to 4.6dB without the device. The mean loss with the mode control device was 2.98dB.

The MPDs of each of the launches were measured and are shown in Figure 6.10(a). The effect of adding the mode controller is shown in Figure 6.10(b), where it can be seen that the MPDs are almost identical, particularly for the higher-order mode groups, where sensitivity to connector loss mechanisms, such as eccentricity, is more pronounced. This device should find immediate use in field test applications, for improving measurement reproducibility between different test sets.

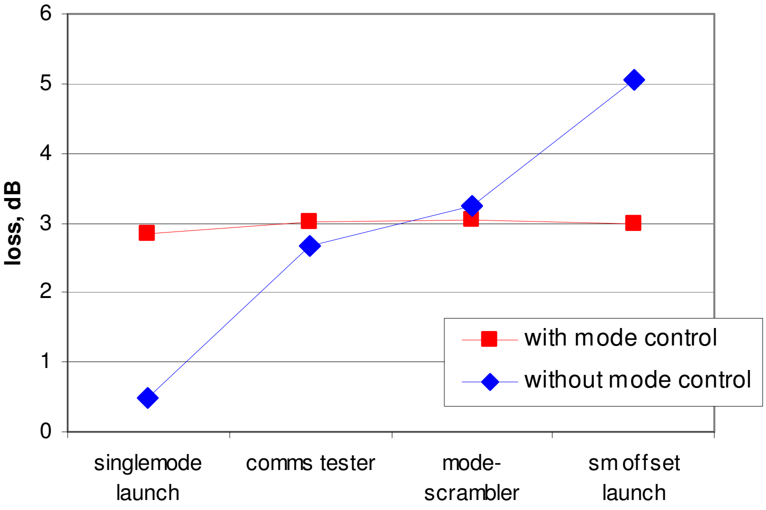

Figure 6.9. Measured insertion loss of 11 concatenated patchcords for four different launch distributions.

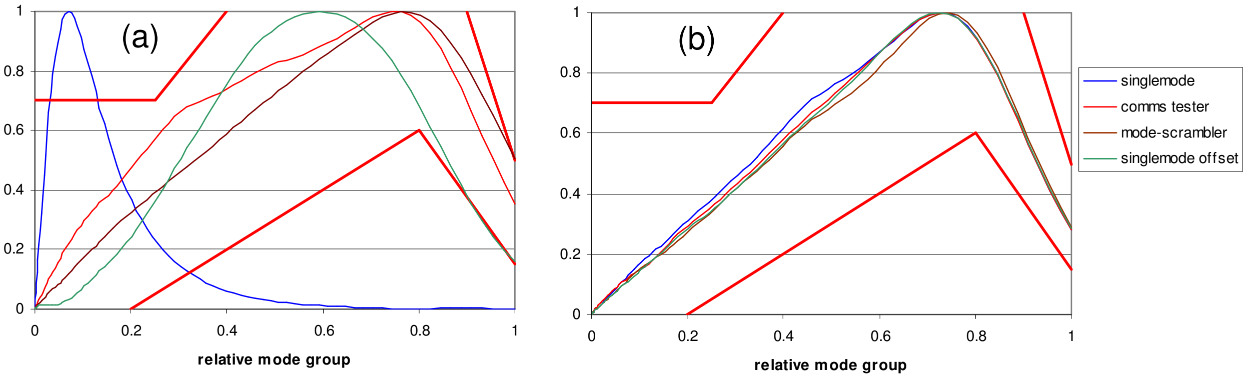

Figure 6.10. Measured MPDs, (a) direct from launch, and (b) after mode controller.

6.3.1 Leaky Mode Control

It was shown in section 3.2.3 that the presence of leaky modes causes the near-field intensity distribution to deviate significantly from the guided mode profile. As leaky modes fall entirely within the meridional NA for a graded-index fibre, it is not possible to quantify them by the measurement technique discussed in CHAPTER 4, as they effectively correspond to a relative mode group number greater than one. It is important, however, to take steps to minimise their presence in a mode controller so that accurate predications of system performance can be made.

Figure 3.12 shows the effect on the near-field profile of adding the entire leaky mode spectrum to a fully-filled 50um graded-index fibre. The computed MPDs for these profiles are plotted in Figure 6.11, where the red, fully-filled, curve approximately follows a straight line, and the blue curve, which includes the presence of leaky modes, causes the MPD to be concave on its rising edge and peak at a slightly higher mode group number.

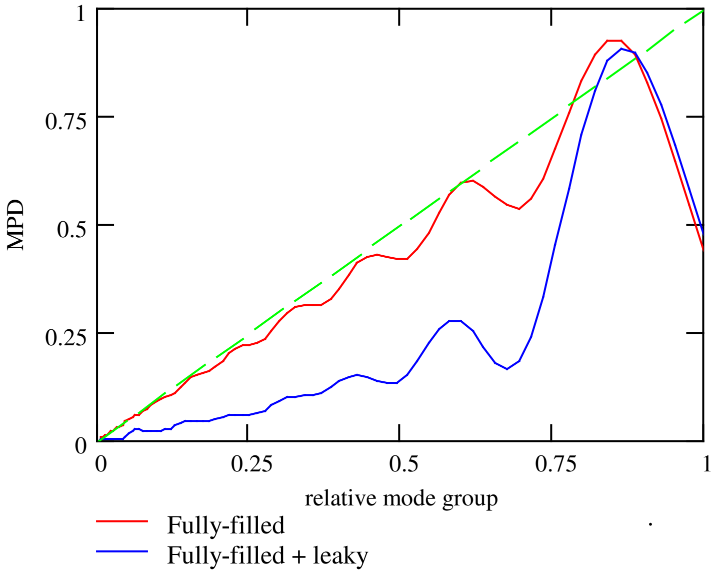

Figure 6.11. Modelled un-normalised MPD of graded-index fibre with fully-filled launch (red), and fully-filled launch plus leaky modes (blue).

The concave rising edge of the MPD appears to be a good indicator of the presence of leaky modes and has been found to be useful when interpreting MPD curves and tuning mode control devices.

To demonstrate the onset of leaky modes, a point-load mode-scrambler with a 40um step-index was spliced to a 50um graded-index output fibre. The load was then progressively increased to see if leaky modes could be generated even though the diameter of the step-index fibre was smaller than the graded-index fibre. The resultant near-fields, plotted in Figure 6.12, showed that as the load was increased the near-field profile developed shoulders, becoming similar in shape to the modelled leaky mode profile, shown in red. This was particularly so up to about 20um radius, which is consistent with the fact that the launch fibre was 40um in diameter.

The resulting MPDs are shown in Figure 6.13 where the occurrence of a concave rising edge, as the load is increased, is quite marked.

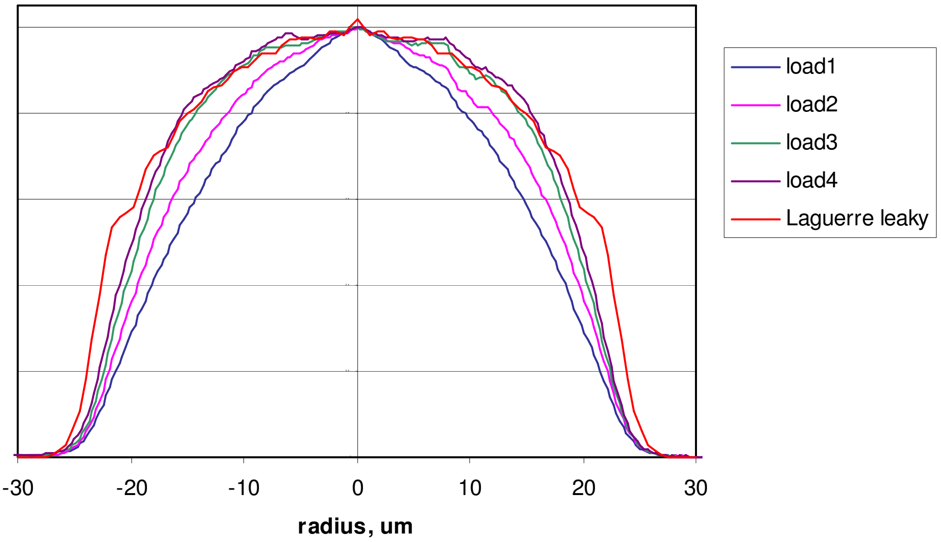

Figure 6.12. Effect on near-field profiles of graded-index fibre of increasing the load on 40um point-load mode-scrambler. Also shown is the simulated fully-filled fibre plus leaky modes (Laguerre leaky).

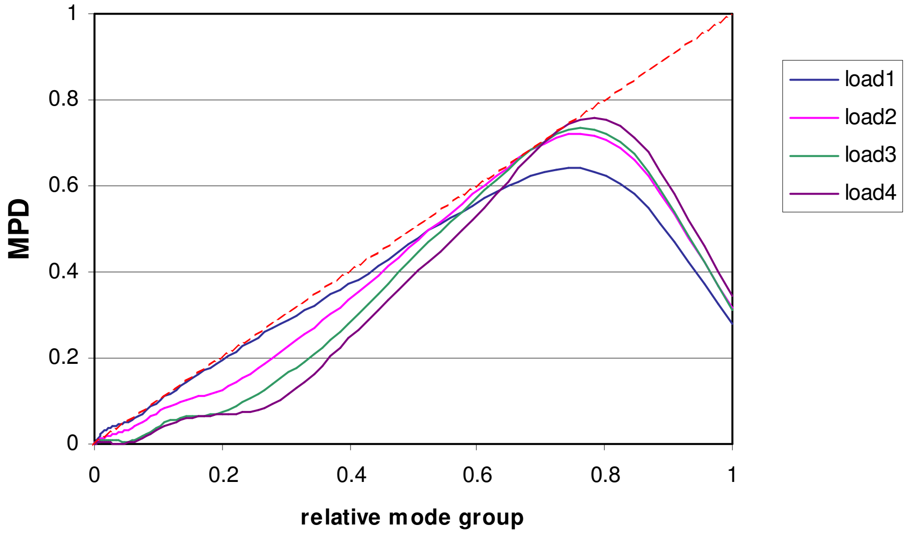

Figure 6.13. Effect on MPD of graded-index fibre of increasing the load on 40um point-load mode-scrambler.

It is clear from these results, therefore, that care must be taken to avoid leaky modes even when the step-index fibre is smaller in diameter than the graded-index output fibre. Thus, there is a trade-off between applying enough load to ensure insensitivity to the input distribution, and preventing leaky modes from being launched.

6.3.2 Wavelength Sensitivity

The Laguerre-Gauss solution for the modes of a parabolic index fibre, eqn. (3.20), has a dependency on optical wavelength through the normalised frequency, V, eqn. (3.15). To demonstrate this, Figure 6.14 shows the radius of a modelled near-field distribution, at the 2.5% threshold level, as a function of wavelength. The saw-tooth shape of the curve is due to the successive cut-off of higher-order mode groups with increasing wavelength. For example, there are 19 mode-groups in the region 825nm to 868nm, where the radius increases at the rate of 0.015um per nm. At 869nm the 19th mode-group is cut-off, and the radius drops by 0.61um.

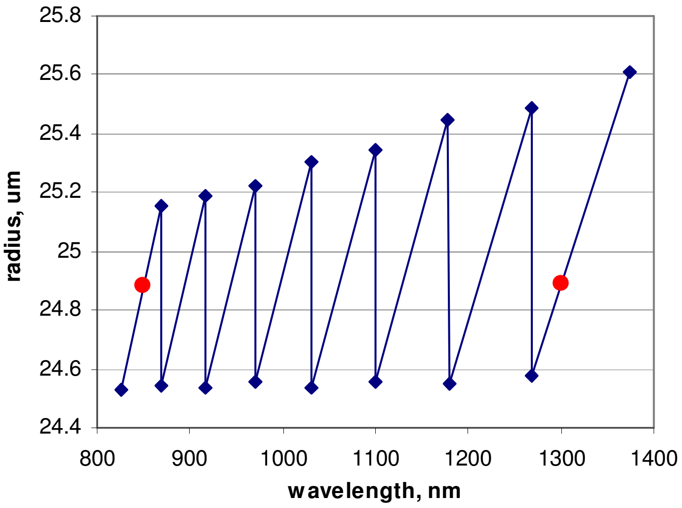

Figure 6.14. Radius of theoretical near-field in parabolic index fibre at the 2.5% intensity level as a function of wavelength.

The red dots in the figure correspond to 850nm and 1300nm, where it can be seen that the radius is very similar at these two wavelengths. The actual near-field profiles are, however, not the same as can be seen from Figure 6.15, where the two curves cross over at the 2.5% level, but the profile at 850nm is steeper than at

1300nm. The effect of this on the respective MPDs, computed using a parabolic reference profile is shown in Figure 6.16, where the MPD at 850nm peaks just to the right of that at 1300nm.

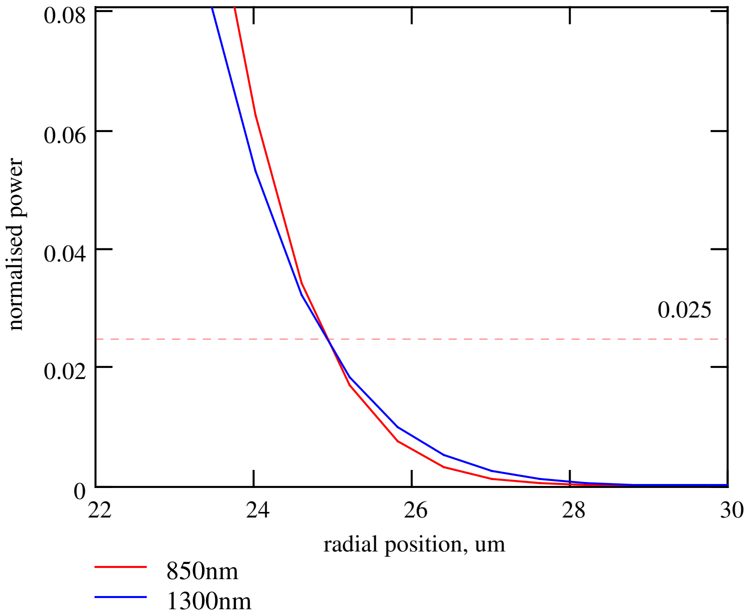

Figure 6.15. Theoretical near-field of parabolic index fibre near the core boundary at 850nm and 1300nm.

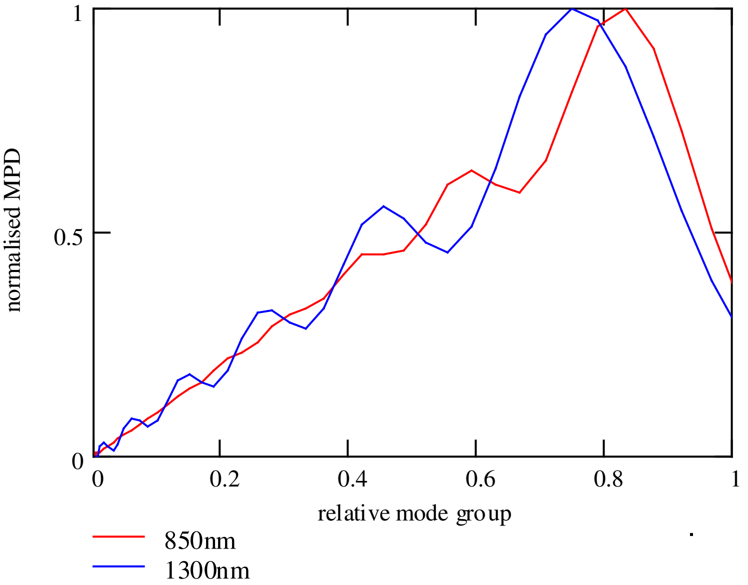

Figure 6.16. Normalised MPD of theoretical near-field of parabolic index fibre at 850nm and 1300nm, using parabolic reference.

To demonstrate this, a 50um graded-index fibre was fully-filled, using a point-load mode-scrambler, and the MPDs were measured at 850nm and 1300nm, shown in Figure 6.17. The MPD at 850nm peaks slightly to the right of 1300nm, as expected.

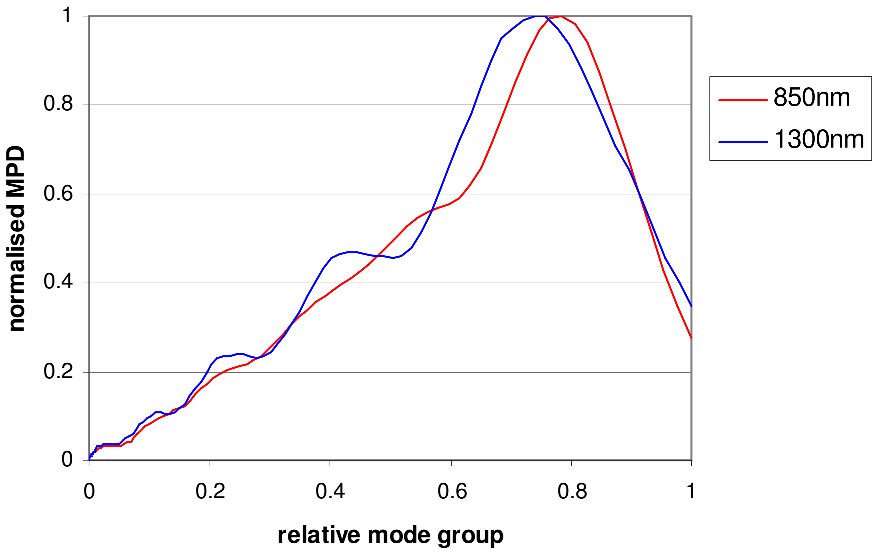

Figure 6.17. Measured MPD of fully-filled 50um graded-index fibre at 850nm and 1300nm, using parabolic reference.

The observed wavelength dependence of MPD is, however, within the tolerance given by the link-testing template, shown in Figure 6.8, and so a given mode control device should be able to comply with the template at both wavelengths.

Another aspect is the wavelength sensitivity to the spectral width of the source where, for example, a spectral width of ±25nm at 850nm will excite 19 mode groups at 825nm and 18 mode groups at 875nm. Thus the resultant near-field will be a combination of these distributions. Figure 6.18 shows the comparative MPDs for zero spectral width and for 50nm spectral width (FWHM), where the magnitudes of the components at 825nm and 875nm were taken as 50% of that at 850nm, to simulate a triangular spectral distribution. The effect is to shift the MPD peak slightly to the left. Thus, some care is required when specifying modal distribution as it depends on both the wavelength of operation and also the spectral width.

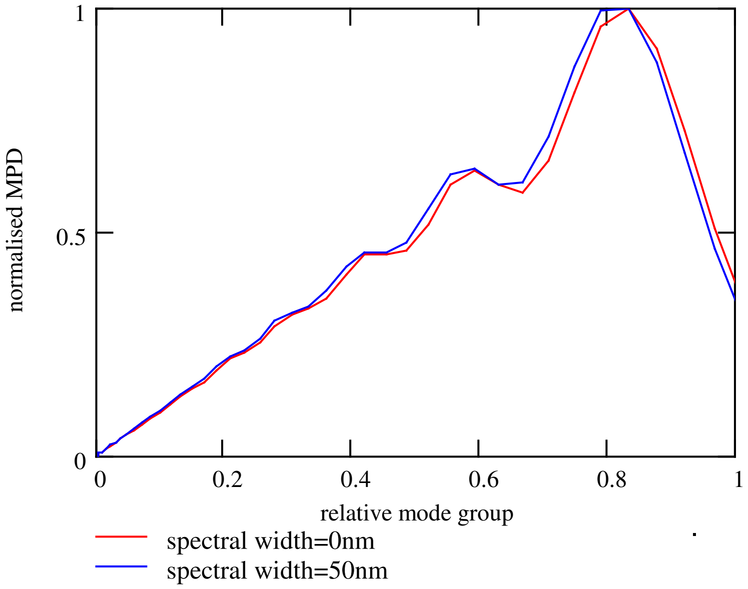

Figure 6.18. Normalised MPD of theoretical near-field of parabolic index fibre at 850nm as a function of spectral width.

It is important at this point to recall the work presented in section 4.4, regarding the efficacy of using a parabolic reference for the MPD computation. It was shown there that the deviation of the actual near-field profile from a parabola caused the MPD to peak at a mode group of less than unity. This effect is particularly significant in fibres that are fully-filled, which is the case for the fibres in this section. The measured data in Figure 6.17 was then recomputed using the corresponding Laguerre-Gauss reference profiles, as the reference, and the results, shown in Figure 6.19, reveal that the fibre was, in fact, fully-filled, particularly at 1300nm. In these plots, the un-normalised MPD has been plotted so that the difference between using the two types of reference can be clearly seen.

Thus, some care is required in checking compliance of a source with the MPD template as it depends on the reference profile used. For encircled flux, however, which is described in the next section, this shortcoming does not apply, as no assumptions about core radius or profile shape are required in the calculations.

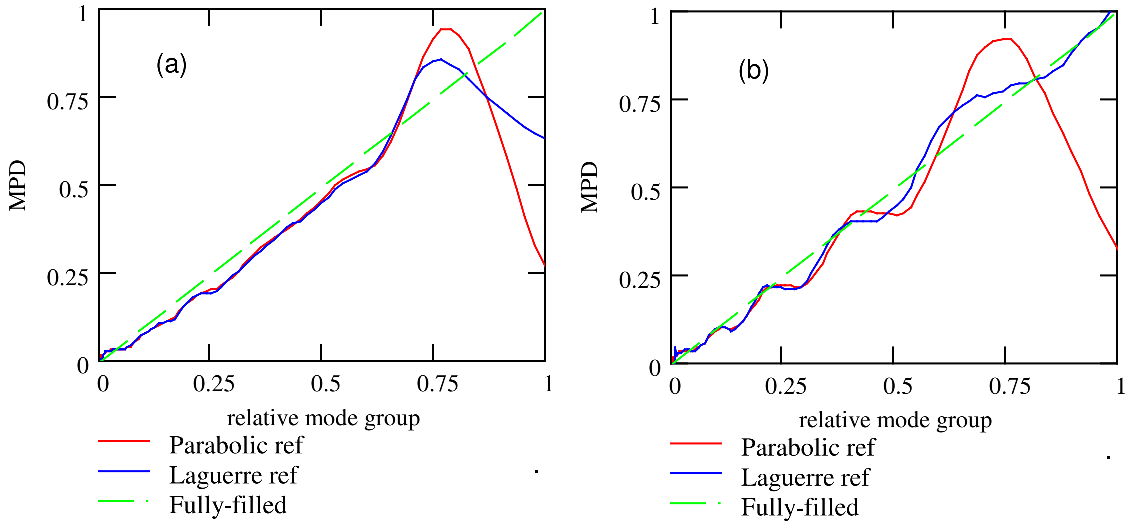

Figure 6.19. Recomputed data from Figure 6.17 using Laguerre-Gauss reference profiles, (a) 850nm and, (b) 1300nm.

6.4 Encircled Flux Template for Link testing

In order to improve the reproducibility of link loss testing, the IEC has, in 2007, introduced an Encircled Flux template [58] as an alternative to the MPD template described in the previous section. Encircled flux E(r) is computed by integrating the near-field outwards from the fibre centre, defined as,

$$EF(r) = \frac{\int_0^r r'I(r')dr'}{\int_0^a r'I(r')dr'} \qquad \textbf{(6.2)}$$

where r is a radial variable, a is the fibre radius and I(r') is the near-field intensity profile as a function of radial position.

The IEC encircled flux template is, however, considerably tighter than the MPD template and will provide a challenge to manufacturers of optical test equipment. The template, shown in Figure 6.20, is defined by maximum and minimum values of encircled flux at five radial positions. It was found that a 50um step-index point-load mode-scrambler connected to a 50um graded output fibre, with an 15mm diameter mandrel-wrap filter, was able to meet the requirements of the template for both a singlemode launch and a fully-filled launch. Very careful real-time tuning was, however, required to achieve this due to the sensitivity to applied load and mandrel radius, particularly at the larger radial positions.

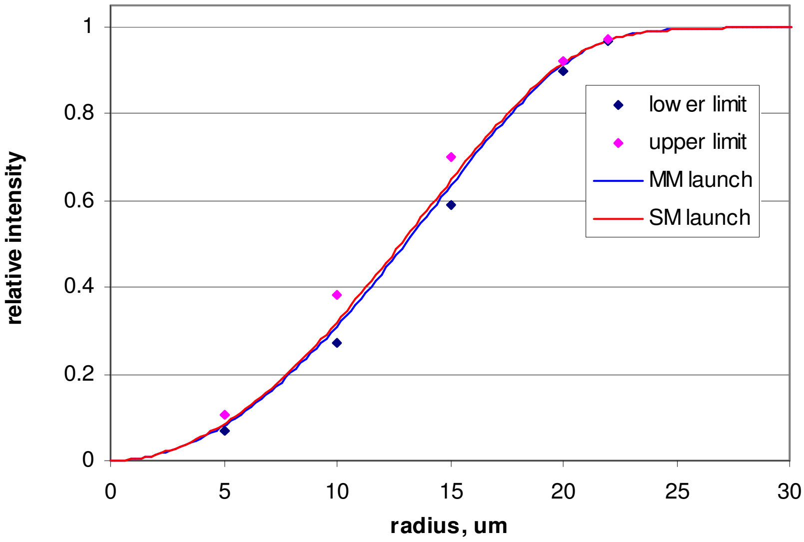

Figure 6.20. IEC Encircled Flux template for link loss testing and results of 50um mode control device with singlemode (red) and multimode (blue) launches.

At the 22um radial location the tolerance band on encircled flux, specified by the IEC, is ±0.0029, which is clearly very tight. To improve tuning sensitivity, a finer pitch screw thread would be an advantage, and also a controlled means of adjusting the bend fibre radius would be useful.

The point-load mode-scrambler appears to be well-suited to this application, enabling both singlemode and full launches to produce almost exactly the same encircled flux results. This device should find application as a means of ensuring test equipment complies with the recent addition of an Encircled Flux template to the IEC standard.

6.5 Speckle Suppression

The near-field intensity pattern at the output of a multimode fibre, illuminated by a laser source, usually exhibits a granular nature, known as *speckle.* This is caused by coherent interference between the various propagating modes. The size, and number, of speckles is related to the number of modes present, such that in a few-moded fibre the speckles are fewer in number, but are of greater size, than in a well-filled fibre. In a particular application, the occurrence of speckle was blamed for repeated failures in a commercial 2x2 microelectromechanical (MEMs) fibre switch, consisting of a moving mirror mechanism. In this case, the switch was an integral part of Distributed Temperature Sensor (DTS) system. The DTS utilised a multimode fibre medium, to maximise the generation of Raman frequencies, and was excited with a singlemode fibre laser at 1064nm. It was suspected that the large, high intensity, speckle were causing thermal damage to the mirror coating. The use of a mode-scrambler was suggested as a means of widening the modal spectrum to reduce the speckle size, thus eliminating *hotspots* in the beam profile at the mirror.

Figure 6.21(a) shows the output from a multimode fibre excited with a VCSEL source, where a few hotspots can be seen, in contrast with the more uniform distribution from the mode-scrambler, shown in Figure 6.21(b). In both these figures the maximum intensity has been normalised, so, in absolute terms, the peak in (b) is much less than that in (a) as the power is distributed over a larger area of smaller sized speckles.

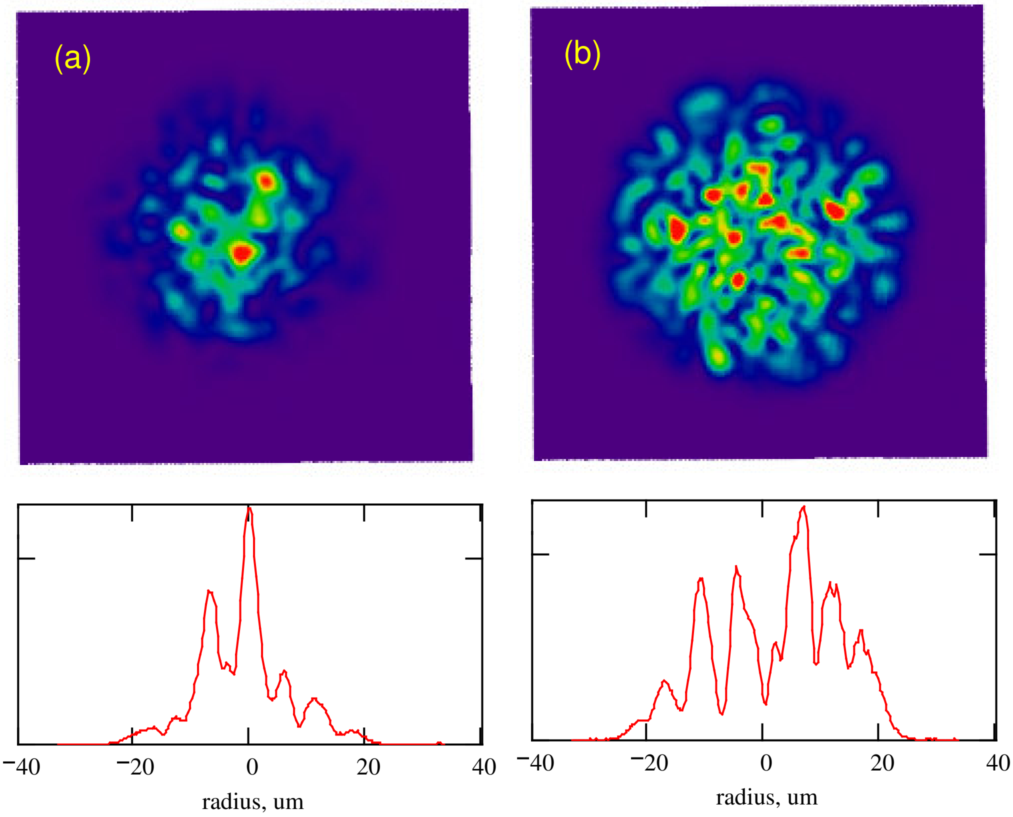

Figure 6.21. Near-field image of 50um fibre with (a) VCSEL source, and (b) VCSEL source with mode scrambler.

6.6 Multimode Sensor

The majority of sensors employing multimode fibre operate on the principle of measuring a change in the fibre transmission in response to its environment. Examples are pressure sensors, utilising loss induced by microbending [43], strain sensors, using long period gratings [45], and chemical sensors, using tapered fibres [59]. A major drawback of these types of sensor is that they are sensitive to changes in optical power level caused by, for example, source instability. A new type of sensor is proposed here that utilises a change in the modal distribution, rather than the intensity, as the measurand. A schematic of the device is shown in Figure 6.22.

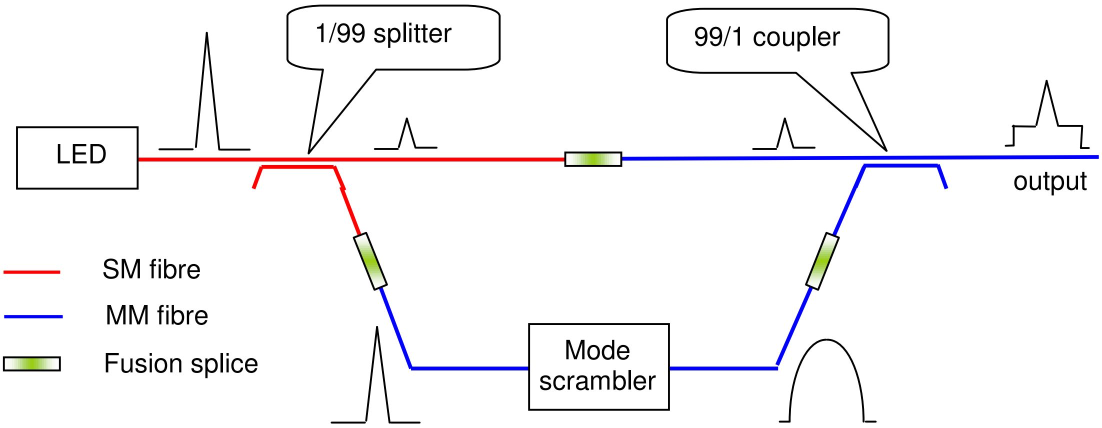

Figure 6.22. Schematic of novel, self-referencing, multimode fibre sensor.

Light from an LED, or laser, source is launched into a singlemode fibre splitter with a split ratio of 99:1. The high power channel is fused onto a multimode point-load mode-scrambler, of the type described in 5.1.4, and the output coupled to the cross-channel of a fused biconic-tapered multimode fibre coupler, with a 99:1 coupling ratio. As mentioned in 5.2.6, the fused-biconic coupler acts as a very effective high-order mode filter, producing a rectangular intensity distribution in the output fibre. This is combined with the low-power singlemode channel to produce a near-field intensity profile consisting of a narrow, singlemode, peak superimposed on a wide, high-order, pedestal. A typical profile is shown in Figure 6.23(a). The corresponding MPD consists of two peaks, a narrow peak at 0.02 mode group number, and a broader peak centred at 0.85 mode group, shown in Figure 6.24(a).

The principle of the sensor is that the greater sensitivity of the higher-order modes, to the environment, results in preferential loss to these modes, whilst the low-order modes are unaffected. Now, by normalising the MPD to the low-order mode peak, a change in the height of the high-order peak may be used as a measure of modal attenuation. The advantage, therefore, of this device is that it is self-referencing, being independent of the light level launched into it.

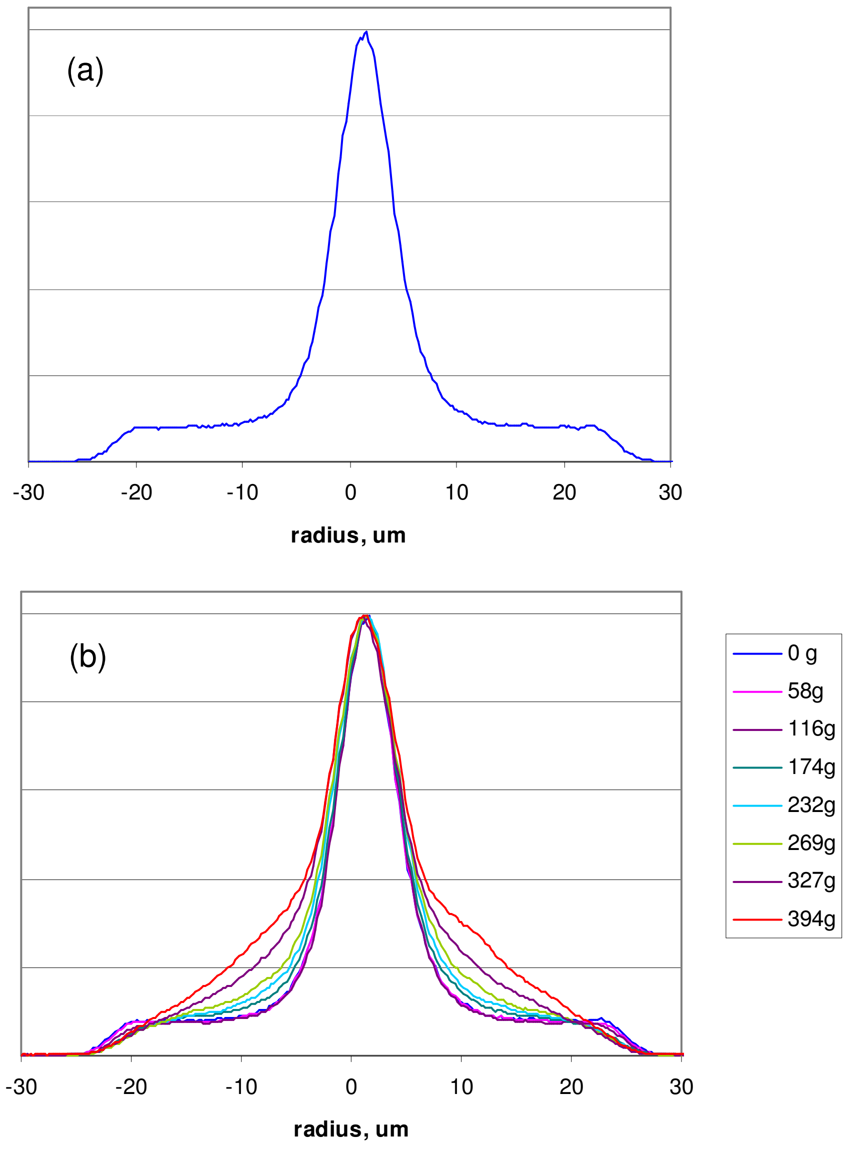

Figure 6.23. Near-field intensity profiles of self-referencing multimode fibre sensor, (a) with zero load, and (b) as a function of applied grating load.

As an example of its use, a microbend grating, of the type described in 5.1.2.1, was applied to the output fibre of the sensor. Figure 6.23(b) shows the evolution of the near-field profile as the load was progressively increased. The effect on the corresponding MPDs, shown in Figure 6.24(b) is to reduce the height of the high-order peak and move it to the left slightly, for loads up to 116g. As the load was increased further, power was coupled from low-order to mid-order modes causing the high-order peak to be less distinct and for loads greater than 232g the high-order peak actually increased in magnitude. This transfer of power from the fundamental, or very lowest, order modes to mid-order modes has, in fact, been exploited for sensor applications [60], where a singlemode probe fibre was used to measure the decrease in power in the central region of a multimode fibre as a function of microbending.

A plot of the results of this sensor is shown in Figure 6.25, where the MPD at the mode group number corresponding to the peak position at 0g is plotted as a function of the applied load. There is a clear correlation between MPD value and applied loads up to about 230g, indicating the potential of the device as a pressure sensor in this region.

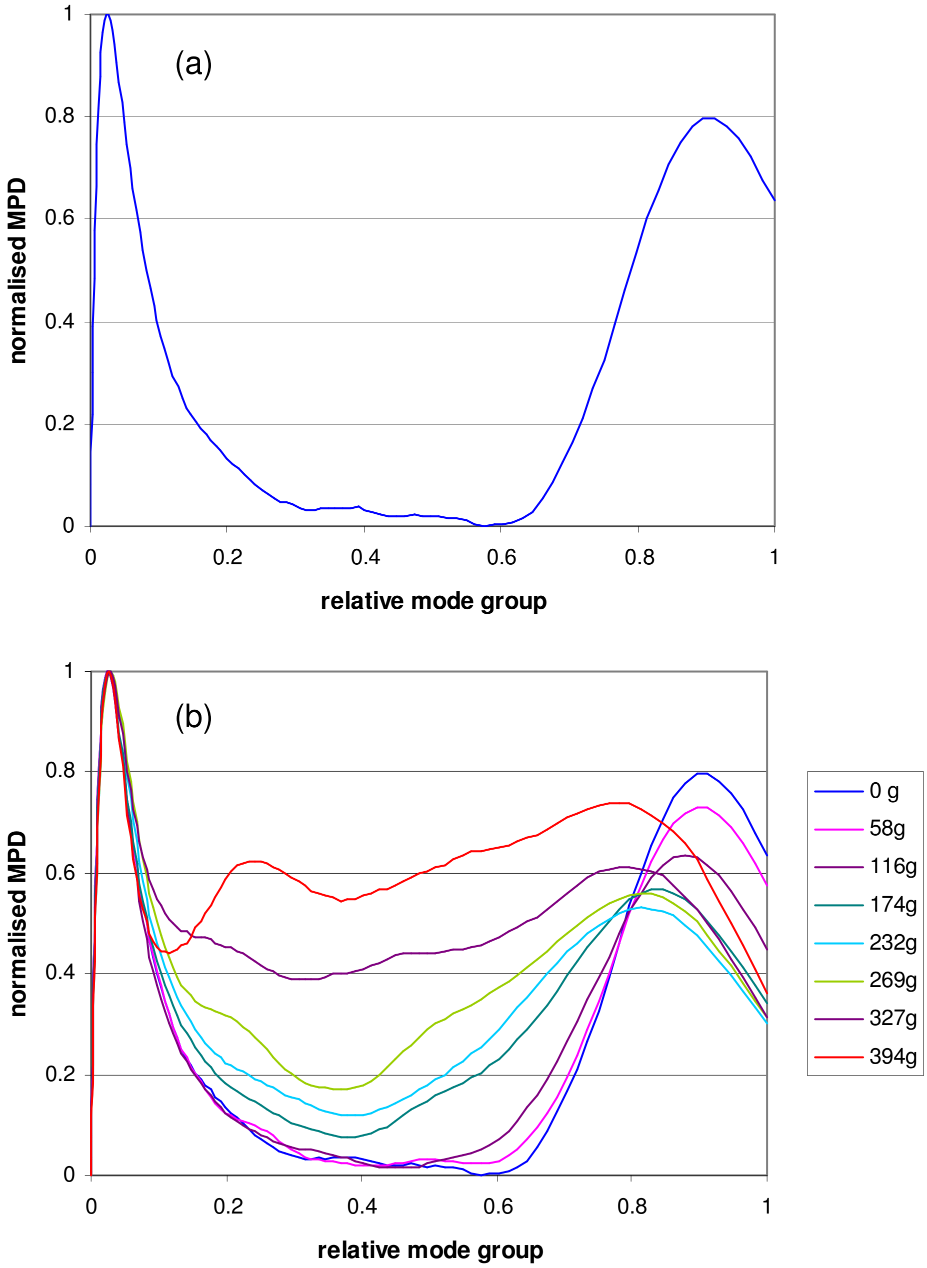

Figure 6.24. MPDs of self-referencing multimode fibre sensor, (a) with zero load, and (b) as a function of applied grating load.

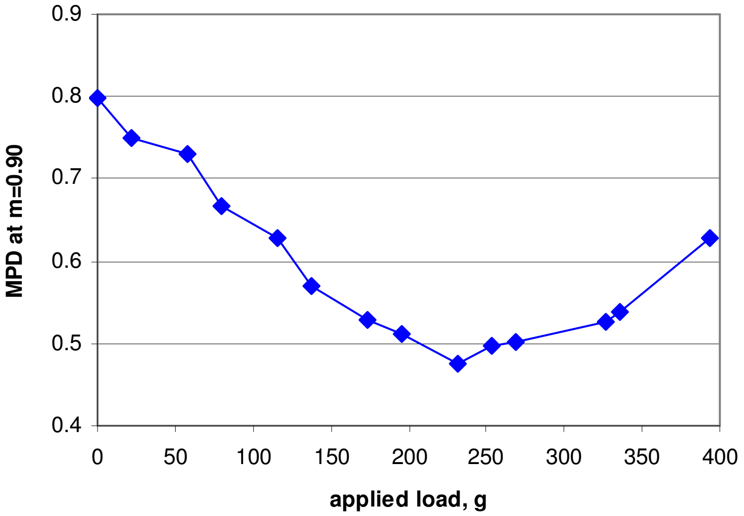

Figure 6.25. Measured MPD value at m=0.86 vs applied grating load for self-referencing multimode sensor.

As a second example of the device, the output fibre of the sensor was formed into a loop, by bending it round passing the end back through the loop. In this way, a stable loop could be formed and by applying longitudinal force to the fibre, the diameter of the loop could be modulated. This induced preferential loss to the high-order modes and a consequent change in the measured MPD value. The MPD, with a parabolic reference, was measured at 0.89 mode group number, corresponding to the peak position for a bend radius of 51mm, against longitudinal displacement of the fibre. The results are shown in Figure 6.26. Also shown is the corresponding MPD with a Laguerre reference profile, measured at 1.0 mode group number. For convenience, this has been normalised to the value of the parabolic reference at zero displacement. The corresponding plots of MPD against fibre curvature are given in Figure 6.27. As the displacement was increased, the MPD decreased slowly at first and then more steeply at about 160mm displacement for the parabolic reference, corresponding to a loop radius of about 26mm. The Laguerre reference was similar but slightly less steep. For very large displacements both curves flattened out, corresponding to about 3mm radius. The reason for this is that most of the high-order power has been lost and the MPD curves converge towards zero. This can be seen from the near-field intensity profiles in Figure 6.28, where the high-order mode power is progressively attenuated.

The corresponding MPD plots for these profiles, with a parabolic reference, are shown in Figure 6.29. The high-order mode peak decreases in magnitude, and moves to the left slightly, as the displacement is increased.

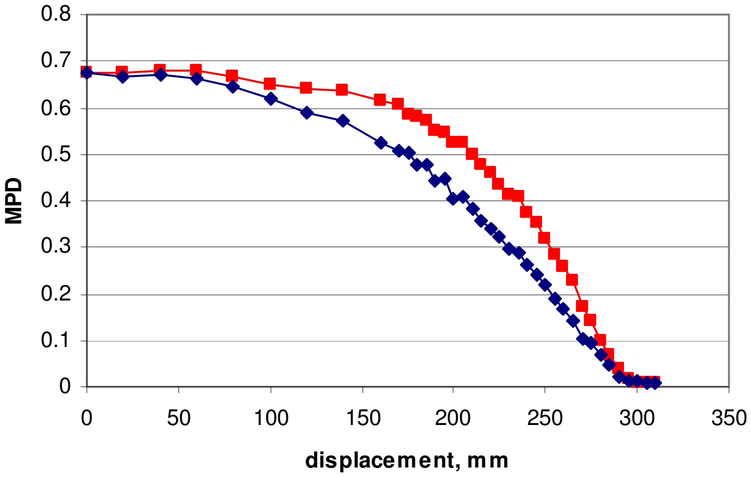

Figure 6.26. Measured MPD vs longitudinal fibre displacement for self-referencing multimode sensor with parabolic reference at m=0.89 (red), and with Laguerre reference at m=1 (blue). Note that curves are normalised to the same value at zero displacement.

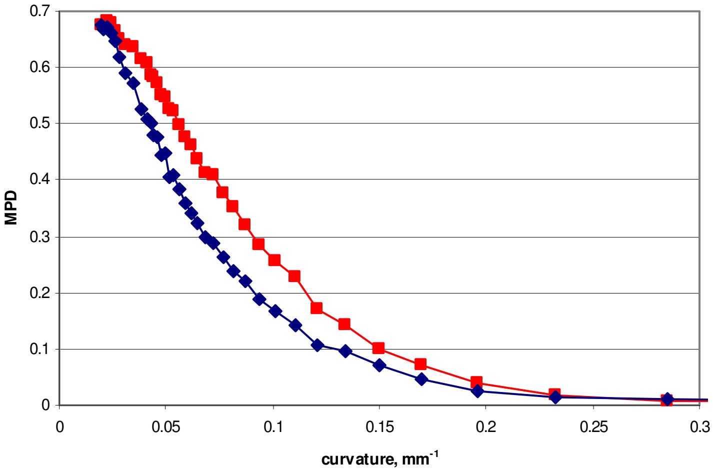

Figure 6.27. Measured MPD at m=0.89 vs fibre curvature for self-referencing multimode sensor with parabolic reference at m=0.89 (red), and with Laguerre reference at m=1 (blue). Note that curves are normalised to the same value at zero displacement.

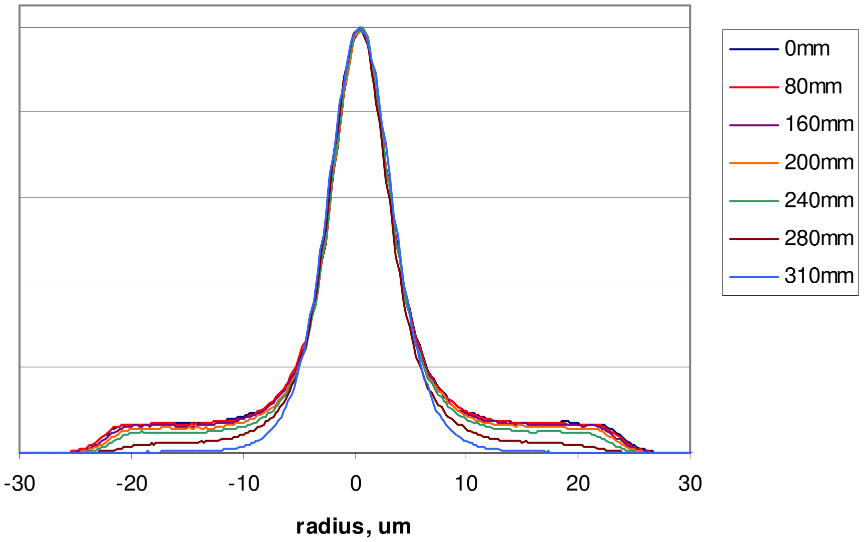

Figure 6.28. Near-field intensity profiles of self-referencing multimode fibre sensor as a function of longitudinal fibre displacement.

It is interesting to compare the behaviour of the pressure and displacement sensors. In the former, Figure 6.24 indicates there is a transfer of power from the lowest-order to the mid-order modes as the pressure on the sensor is increased, as well as attenuation of the highest-order modes. This is to be expected, however, as the induced LPG causes coupling between all adjacent mode-groups, as discussed in 5.1.2. In contrast, Figure 6.29 shows that the displacement sensor preferentially attenuates the high-order modes whilst not affecting the low-order modes.

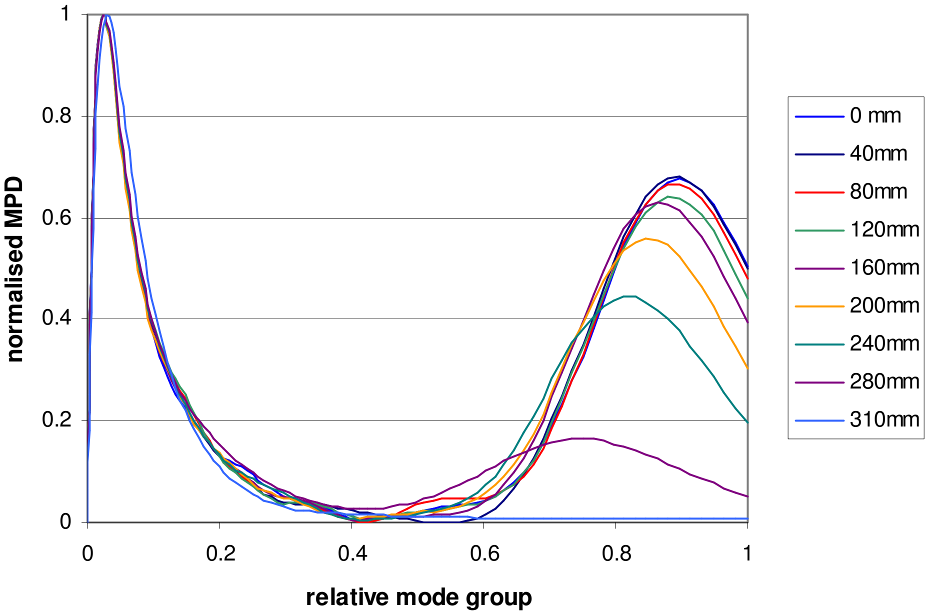

Figure 6.29. MPDs of self-referencing multimode fibre sensor as a function of longitudinal fibre displacement, for a parabolic reference.

The particular advantage of these sensors is their self-referencing nature, being independent of launched power levels. A shortcoming of all multimode sensors is that they are sensitive to modal loss induced by other factors, such as fibre deployment, temperature and vibration. Furthermore, the presence of connector interfaces between the device itself and the sensing fibre may cause a degree of mode-filtering and therefore affect the calibration of the sensors. Another drawback with this type of sensor is its non-linear response, but it could, however, work well as a threshold detector.

6.7 Mode Division Multiplexing

To increase the bandwidth of a multimode fibre link, Wavelength-Division Multiplexing (WDM) is sometimes employed. This is where information is coded on to several parallel channels of different wavelengths, which are transmitted simultaneously. Another, little used, scheme is that of Mode Division Multiplexing (MDM). This is where information is simultaneously carried by different modes in the fibre. In one such scheme [20], non-overlapping tubular modes $LP_{2,1}$ and $LP_{12,1}$ were launched using spatial filters. The integrity of these modes persisted over a length of 10m, after which they could be discriminated using a second set of spatial filters. Other methods for launching individual modes include, a geometric launch from an off-axis spot, whose size and direction angle can be independently adjusted [61], holographic filters [62], [63] and by side excitation via a prism [64].

The main drawback with MDM is degradation in the purity of the launched modes caused by mode coupling, which might be induced by intrinsic defects in the fibre or by extrinsic perturbations, such as microbending. A more promising scheme is that of Mode Group Diversity Multiplexing (MGDM), where small groups of modes are employed rather than individual modes. The number of channels is less than MDM by this scheme, but it is likely to offer better discrimination over longer distances. Recent work by Tsekrekos [65] showed that MGDM with three mode groupings is possible over a distance of 1km. In this case, the launch was provided by a singlemode fibre, positioned in turn, at radial distances of 0um, 13um and 26um. With this system, small groups of modes rather than individual modes are launched. Examples of profiles for a singlemode offset launch are shown in Figure 5.38. Here it can be seen that the mode patterns are, in fact, circular in spite of the launch being asymmetric. The diameter of the mode patterns is directly proportional to the value of the fibre offset.

A practical implementation of a two-channel offset launch mechanism, using an integrated optic device, has been described by Asawa [66]. In this case, however, the device was intended for intrusion detection of a secure communications channel.

It was shown in section 6.6 that a high-ratio fused biconic-tapered coupler can be used to launch high-order modes for sensor applications. A similar implementation is proposed here for MGDM applications. The launch system used to investigate this is shown in Figure 6.30.

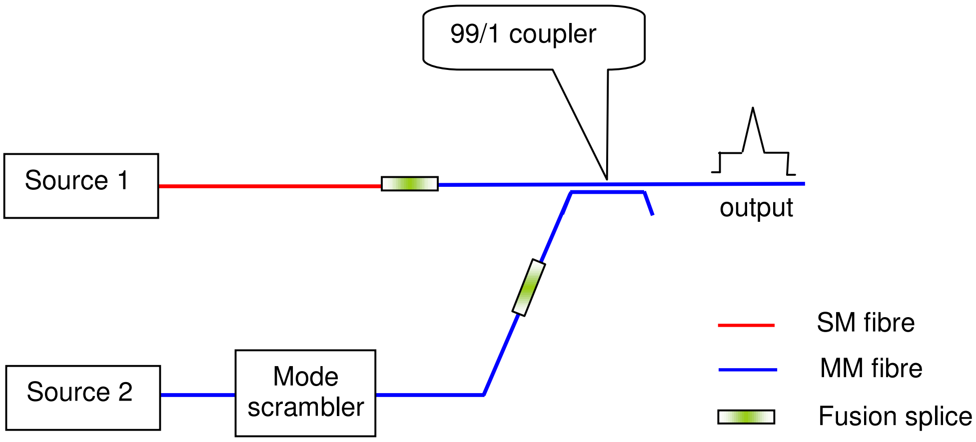

Figure 6.30. Schematic of launch for novel MGDM system

The output from Source 1 is coupled through a singlemode fibre to a high ratio multimode coupler, where it is combined with light from Source 2. The resulting near-field intensity profile in the fibre consists of a narrow low-order peak superimposed on a much wider, high-order, pedestal.

As mentioned above, the performance of an MGDM system is very dependent on the amount of mode-coupling occurring, as this leads directly to crosstalk between channels. To investigate this, an experiment was set up with a 985m length of 62.5um '*High-Performance Laser-Optimized*' graded-index fibre, from OFS, Inc. The fibre was wound on a standard 15cm diameter shipping spool. In order to avoid launching the very highest modes, which were likely to suffer from higher attenuation, the output of the launch system was coupled to the test fibre via a 1m length of 50um graded-index fibre.

Figure 6.31 shows the near-field intensity profiles in the test fibre after distances of 1m and 985m, where the plots have been normalised to their peak values. On first inspection, the broadening of the central peak suggests that a small degree of mode-coupling is occurring. To investigate this further, the intensity profiles of the two channels were each measured in the absence of the other. Figure 6.32 shows the comparative profiles in the test fibre after 1m and 985m for the low-order and high-order channels. Note that the 985m profiles have been scaled by a factor of x2, to compensate for fibre attenuation, by increasing the camera exposure.

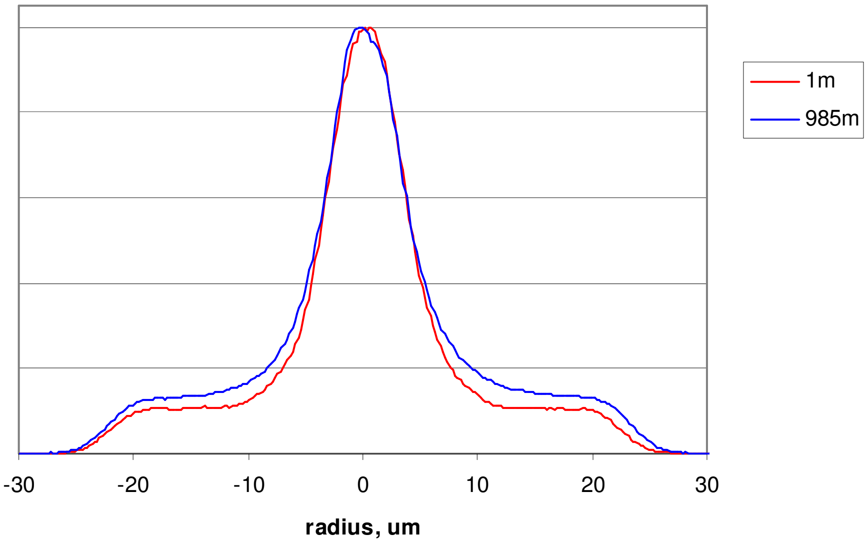

Figure 6.31. Near-field profiles of MGDM after 1m and 985m in 62.5um graded-index fibre.

It can be seen that the profile in channel 1 appears to have suffered greater attenuation than for channel 2, over the length of the fibre. The insertion loss was measured to be 3.00dB for channel 1 and 2.69dB for channel 2. The reason for this unexpected behaviour may be due to the occurrence of a high concentration of OH$^-$ ions near to the core centre [67] leading to greater attenuation in this region. The effect of this differential attenuation on the normalised intensity profiles, in Figure 6.31, is to cause the level of channel 2 to be increased relative to the peak at the core centre. This explains the apparent broadening of the central peak, where, in fact, the profiles in Figure 6.32 show that very little mode-coupling is occurring in either of the channels. In this experiment, therefore, the modal groups chosen are well-suited to this particular fibre, for MDGM purposes.

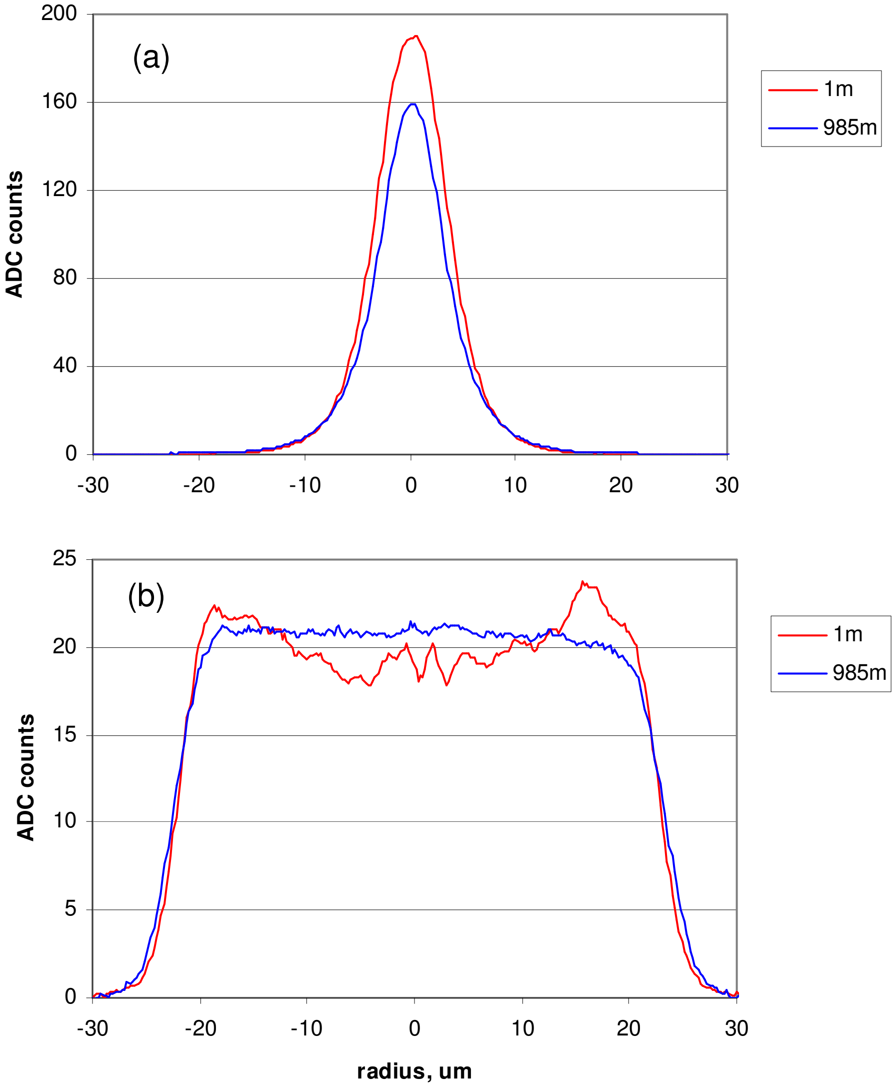

Figure 6.32. Comparison of near-field intensity profiles after 1m and 985m in 62.5um multimode fibre, (a) channel 1, and (b) channel 2. Note that the profiles at 985m have been multiplied by x2.

The MGDM detection scheme envisaged here consists of two annular regions, where the inner region extends from zero to a variable R and the outer extends from R to, for example, 30um. In order to determine the optimum value for R to minimise crosstalk between channels, a plot of encircled flux at the 1m position, in the two regions was computed, shown in Figure 6.33.

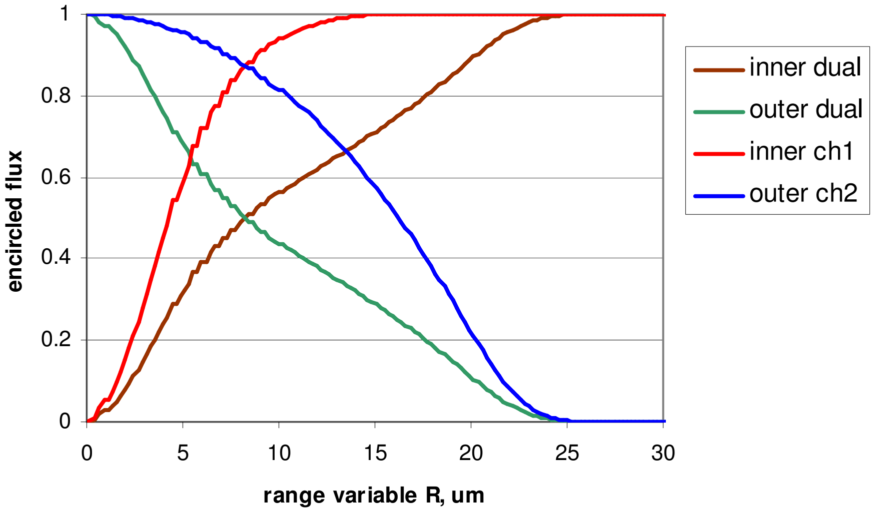

Figure 6.33. Plot of encircled flux for inner and outer regions of dual channels, and separately for ch1 (sm) and ch2 (mm), vs range variable R, for MGDM system.

The brown and green curves show the encircled flux in the inner and outer regions, respectively, as a function of R. The two curves cross at 8.2um where the power in each region is the same. To determine the signal isolation of each channel, the integrated power in the inner region for channel 1, and in the outer region for channel 2 were computed separately, shown as the red and blue curves, respectively. These curves also cross at 8.2um, where the value of encircled flux is 0.88, corresponding to a crosstalk value of about -8.6dB in each channel. In this analysis, equal power is assumed in both channels whereas, in the experiment above, the power in channel 1 was approximately half that in channel 2. A similar analysis could, however, be carried out for a range of relative power levels.

Near-field imaging allows R to be actively adjusted, if required, to suit variations in fibre loss and in the degree of mode-coupling. A radially segmented photodiode for MGDM applications has been described [68], where, in this case, varying the distance between the fibre end and the photodiode would enable R to be optimised.

The MGDM methods described here could also find application as a means of ensuring a secure communication channel [69]. The data signal would be encoded onto the singlemode channel of the device and a reference signal launched into the high-order mode channel. Any change in power in the latter would indicate that the fibre had been tampered with, such as by the use of a tapping device.

6.8 Chapter Summary

In this chapter, several of the techniques described in CHAPTER 5, for modifying the modal distribution in multimode fibres, have been employed in practical situations.

It was found that an approximation to a theoretical Equilibrium Mode Distribution (EMD) could be achieved by using an air-gap mode-filter in series with a mode-scrambler. The addition of a small mandrel-wrap mode-filter ensured that the MPD dropped to zero for the highest-order mode groups, to comply with the model. As an alternative to the EMD launch, a Limited Phase Space (LPS) launch is often employed, this takes the form of a top-hat distribution. In order to compare this with an EMD launch, the mode overlap was computed for coupling from a step-index fibre to a graded index fibre where the NA and radius of the former were 70% of that of the latter. It was found that the MPD peaked at 0.53, compared to 0.47 for the EMD. The MTF for the EMD was, however, approximately a linear decreasing function where the MTF for the LPS was nearly flat up to 0.5 mode group, where it then rolled-off. It was found, empirically, that a good approximation to the LPS launch could be achieved by fitting an 8mm diameter mandrel to a fully-filled fibre.

An update in 2006 of the ISO/IEC link testing standard specified modal-filling conditions for loss testing in terms of an MPD template. Experimentation showed that a mode controller comprising a 30mm diameter mandrel in series with a point-load mode-scrambler was able to satisfy this requirement at both 850nm and 1300nm wavelengths, independent of the launch conditions. A remarkable improvement in the measured insertion loss, on a link consisting of 11 concatenated patchcords, was demonstrated using this device. It was also highlighted how some care is required in setting up this type of device, in order to minimise the occurrence of leaky modes whilst maintaining insensitivity to launch conditions. This device clearly has potential as a commercial device for ensuring standards compliance. A typical insertion loss of this device is about 2.5dB.

A draft (2007) IEC Encircled Flux template has also been described, that is much tighter than the MPD template and, while it was found to be possible to satisfy the template for both singlemode and multimode launch conditions, it is likely to be difficult to achieve this at both 850nm and 1300nm simultaneously. The template has, however, not yet ratified by the IEC and is currently under discussion. Improvements to the tuning sensitivity of the mode control device were proposed, such as a finer pitch screw in the pinch plate and also a more controlled means of adjusting the bend fibre radius.

A slightly different application of the point-load mode-scrambler was in scrambling the output from a singlemode laser source, so as to reduce the incidence of hotspots in the speckle pattern formed at the output of the fibre. By increasing the mode volume of the fibre the granularity of the speckle pattern was reduced and the optical power was more evenly distributed over the core of the fibre.

A multimode sensor was demonstrated, comprising a high-ratio singlemode fibre splitter, a point-load mode-scrambler, and a high-ratio multimode coupler. The near-field output of the device comprised a narrow singlemode peak on top of a much wider, high-order mode, pedestal. The MPD was measured and by normalising to the singlemode peak, it was found that the height of the high-order mode peak was sensitive to both microbending, and bend diameter. The advantage of this device is that the measurand is the ratio of the two modal peaks, making it independent of the launched light intensity. It shares, however, a disadvantage with other multimode sensors in that the modal distribution is sensitive to other environmental factors such as temperature and vibration.

Finally, a Mode Group Diversity Multiplexing system was proposed using a fused biconic-tapered coupler. It was found that, for the two-channel system tested, a maximum isolation of 8.6dB was achievable. The degree of mode-coupling on the 985m length of fibre tested was almost negligible for the mode groups chosen for the experiment.

CHAPTER 7

A RUGGEDISED MODE CONTROL DEVICE

In CHAPTER 6 various mode control devices were described, but, for practical use, these devices require a means of packaging for protection against the environment. For example, a mode control device to satisfy the requirements of the IEC MPD template for link loss testing was described in section 6.3 and comprised a point-load mode-scrambler in series with a controlled bend. This device has immediate applicability to the fibre industry as a means of ensuring LAN testing is carried out according to the standard, independent of the test source used. This chapter, therefore, describes, therefore, the design and manufacture of ruggedised packaging for this particular device, so that it might be supplied to the industry on a commercial basis. In order to protect the principle of the device, a patent has been filed on the use of a point-load mode-scrambler and air-gap filter for the purposes of mode control [70].

7.1 Requirements for a practical device

In order to gain widespread acceptance by the industry, a packaged version of the mode control device must satisfy certain requirements. These are, for example, standards compliance, reliability, stability, ease of use, size and cost. In addition, the device should be secure against reverse engineering and be easy to manufacture.

7.1.1 Description of Mechanical design

The approach taken was to mount the fibres on a rigid aluminium baseplate, and then fit this inside an outer protective box. In this way, protection for the fibres is provided and also a means of strain relief for the cables.

A photograph of the assembly is shown in Figure 7.1, where the step-index input fibre is shown in blue and the graded-index output fibre in red. The step-index fibre enters the box from the right-hand side and then passes round a 20mm diameter mandrel and under a pinch plate, which provides the point-loading. The fibre is spliced to the graded-index fibre and the splice protector is mounted in a slot in the baseplate, shown at the top in the figure. The graded fibre then loops back on itself with a half-turn of approximately 30mm diameter and exits the box on the left-hand side.

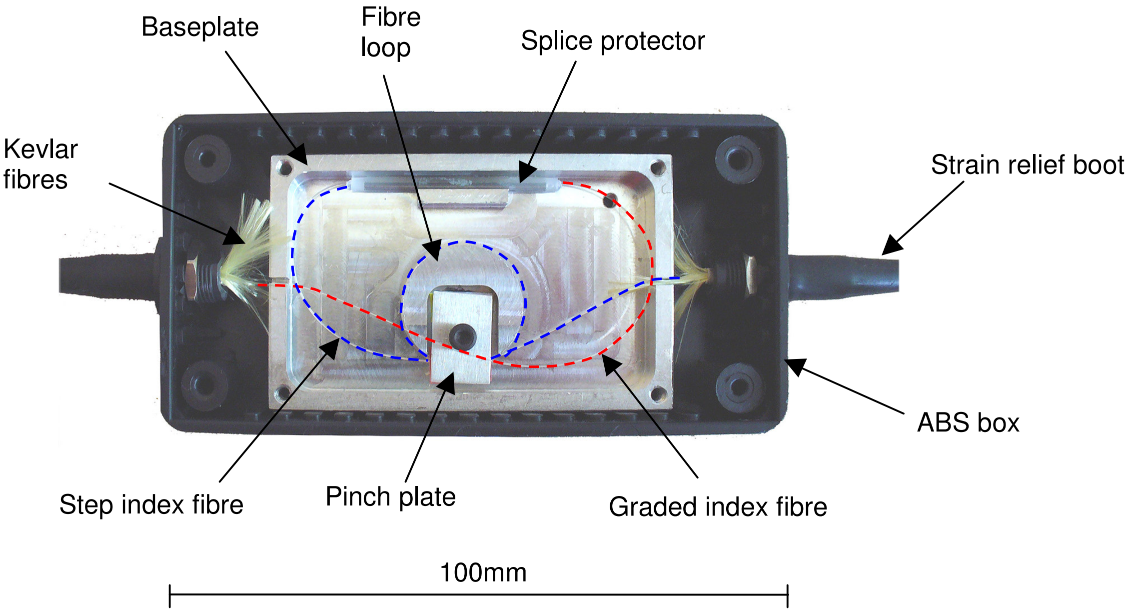

Figure 7.1. Photograph of inside of mode controller package, prior to potting.

It was found that a mechanically stable loop could be achieved by forming the fibre into a simple loop and then passing the fibre end back through the loop. The crossover point in the loop was then located under an aluminium pinch plate as shown schematically in Figure 7.2, and the applied load was controlled by a adjusting a centrally located screw. The fibres were sandwiched between two 400um polypropylene shims to provide the required elastic loading on the fibre, discussed in section 5.1.4. To prevent the pinch plate tilting, and jamming on the screwthread, it was kept square by attaching two 500um polypropylene shims, as shown in the figure, to the other end of the pinch plate. In this way, the degree of mode-scrambling could be controlled very precisely by careful adjustment of the screw.

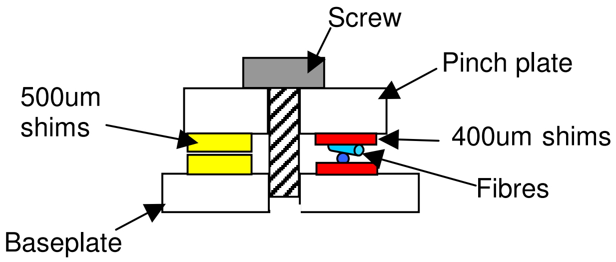

Figure 7.2. Schematic of the point loading mechanism in the mode control device.

The baseplate was fixed in position in the plastic box with a few drops of cyanoacrylate adhesive. The input and output fibre cables were loose-tube 3mm diameter PVC cables with integral kevlar strengthening fibres. The reason that a loose tube construction was used was that the step-index fibre was not available in cabled form and the fibre had to be manually threaded through the 900um inner tube. Also, in order to meet IEC requirements on core diameter, the graded-index fibres were specially selected for this application, and therefore had to be manually threaded as well.

The ends of the 3mm cables were located approximately at the inner end of the strain relief glands, mounted in each end of the box. The kevlar fibres, however, protruded inside the box by about 15mm, as shown in Figure 7.1. The reason for this was so that, once the box was filled with potting compound, the kevlar fibres would be anchored firmly in place, preventing the cables from being disturbed.

The assembly procedure was as follows:

a) Thread the fibres through the loose tube cables.
b) Form a loop in the step-index fibre.
c) Splice the step and graded fibres together.
d) Mount the fibres on the baseplate in the box.
e) Connect the input fibre to a light source and the output fibre to the measurement system.
f) Adjust the pinch plate screw, and fibre bend radius, until the MPD passes the IEC template for both singlemode and fully-filled launch conditions.

g) Fill the box with potting compound.
h) Fit connectors on the input and output cables. Re-test the MPD to ensure it has not changed during assembly.

The potting compound chosen was a flexible polyurethane encapsulant, with a hardness value of 75 on the Shore A scale, to allow for differential thermal expansion in the finished package. Figure 7.3 shows a completed device after potting, where the kevlar fibres have been totally covered to provide a good bond. The encapsulant is dark grey in colour and thus provides security against reverse engineering of the device. The final step is to attach the plastic lid to the box and apply the labelling. Labelling is important because, for IEC compliance, there are two sizes of the mode controller, 50um and 62.5um, and also the device is non-reciprocal, so clear marking of the input and output ports is essential.

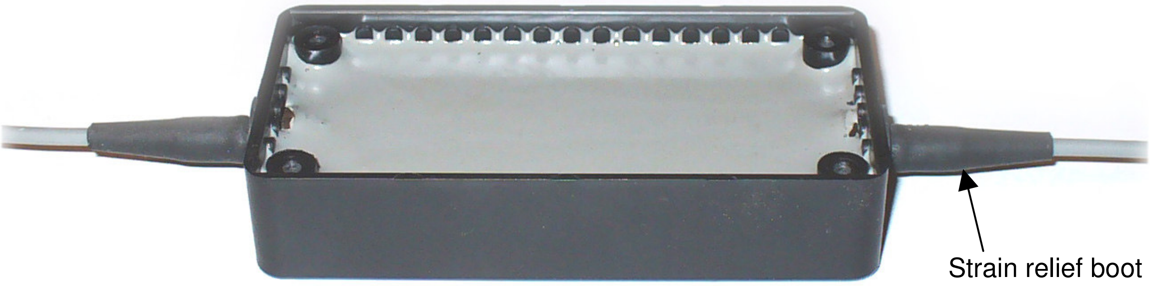

Figure 7.3. Photograph of mode controller after potting.

7.1.2 Reliability and Environmental testing

The construction of the mode controller is robust and offers protection against mis-handling, but two sources of failure have been identified. The degree of protection offered by the rubber strain relief boots, shown in Figure 7.3, is adequate for most purposes but some particularly rough handling resulted in a kink occurring in the fibre cable at the outer end of the boot such that the fibre inside was broken. An improvement to the design would be to use a more sophisticated, ribbed, boot of the type used in high quality fibre connectors.

A more significant failure has been observed in a small number of 62.5um devices, where the rising edge of the MPD curve, which is normally quite linear, as shown in Figure 6.8, becomes convex, particularly under singlemode launch conditions. This effect is known usually to occur between setting up the device and the potting process, but there is a possibility that it has once occurred several weeks after manufacture. The shape of the MPD indicated that it is likely to be due to a relaxation of the load applied by the pinch plate. It was thought to be unlikely that the pinch plate, or its securing screw, could have moved within the potting compound and so an experiment was carried to investigate possible degradation to the fibre coating caused by point-loading. It was found that, for the 60um step-index fibre, the inner coating appeared to de-laminate from the cladding for applied loads of only 6N, which is a normal loading used in the device. A typical result is shown in Figure 7.4, where the inner coating has become separated from the cladding over a length of about 1.2mm. The effect of this is to cause a relaxation in the elastic deformation of the fibre and a subsequent reduction in the curvature spectrum, and the degree of mode-scrambling achieved.

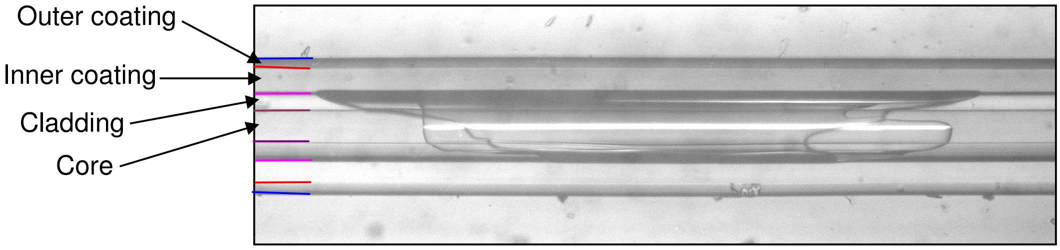

Figure 7.4. Photograph of 60um step-index fibre after loading to 6N in point-load mode-scrambler.

This sort of failure is catastrophic and cannot be repaired. There have been no known failures of this type in 50um devices, however, and similar experiments on the 50um step-index fibre have showed no de-lamination for loads of up to 10N. The 60um fibre is part of a suite of step-index fibres produced by OFS, Inc. and, according to its datasheet, has a *dual-acrylate* coating. The 50um fibre used in this work was supplied by Thorlabs Ltd, and has a much tougher coating, which is evident by the increased forced required to strip the coating prior to termination.

Unfortunately, Thorlabs do not manufacture a 60um version of this fibre. A possible improvement to the design of the mode controller may be to introduce a low-viscosity potting agent into the contact area under the pinch plate during alignment. In this way the fibres would be encapsulated more firmly and therefore prevented from moving if some de-lamination occurs. To ensure good contact with the potting agent, the use of a weak vacuum for degassing would be an advantage. An alternative approach would be to arrange for the pinch plate to be spring-loaded to maintain a constant loading on the fibres even if the coating relaxes.

7.1.2.1 Temperature Cycling

To test the thermal stability of the mode controller, two devices, 50um and 62.5um, were placed in a *Montford* environmental chamber and cycled over the temperature profile shown in Figure 7.5. An MPD measurement was taken at each of the data points shown in the figure.

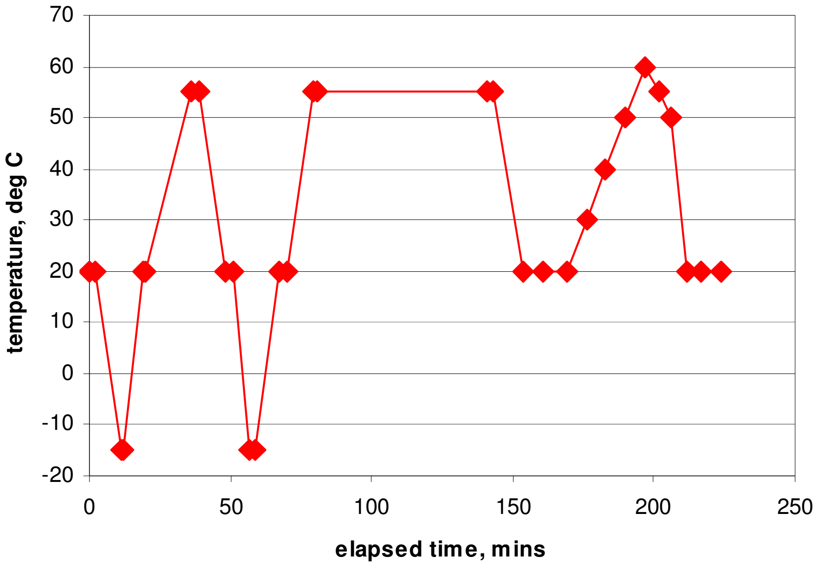

Figure 7.5. Temperature profile for thermal testing of mode control devices.

In this experiment, at least 1m of the 1.5m long output pigtails of the mode controllers were located outside the oven, in order to minimise thermal effects on the cable. It was found that the MPD was very stable for the 50um device up to the measurement at 20°C occurring at 150 mins, as shown in Figure 7.6(a). The corresponding data for a 62.5um device, shown in Figure 7.6(b), exhibited some variation but this did not appear to correlate with temperature. Encircled flux data for the two devices, showed very similar reproducibility, so it was concluded that neither device had suffered any degradation in modal performance over temperature cycling in the range -15°C to +55°C.

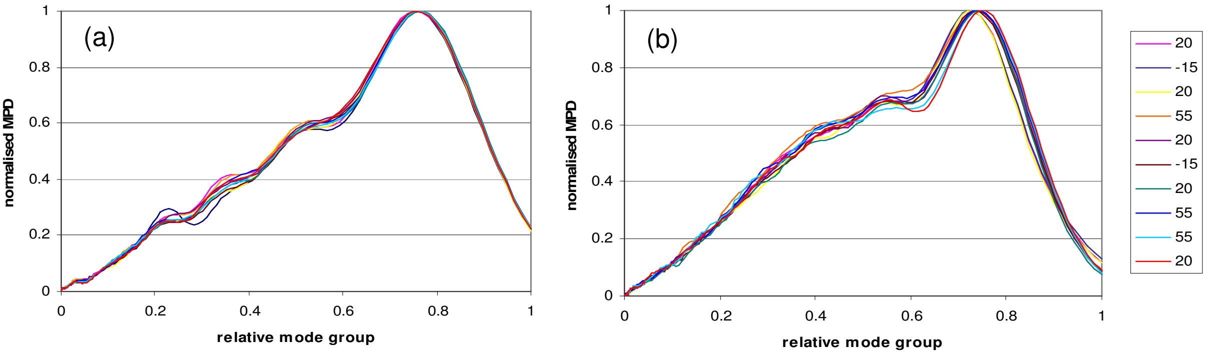

Figure 7.6. Measured MPDs for (a) 50um, and (b) 62.5um mode controllers during temperature cycling, up to 150mins.

The insertion loss of the devices was also measured during the experiment, where, in Figure 7.7, it can be seen that there is a slight inverse correspondence with temperature for both devices. The unshaded data points represent measurements at the start of the experiment and at 150mins. There is a slight net decrease in loss for the 62.5um device of approximately 0.2dB.

For the final part of the experiment, commencing at 150mins, the output pigtail of the 50um device was withdrawn into the oven, leaving only about 30cm outside the oven. The temperature was then increased to 60°C in 10°C steps. The MPD plots for the this device are shown in Figure 7.8, where it can be seen that the MPD is constant up to 50°C but then shifts markedly to the left at 60°C, and, as the temperature is reduced to 20°C, the MPD continues to move to the left. This is indicative of a strong attenuation of the higher order modes. The 62.5um device, however, showed no change during this part of the experiment.

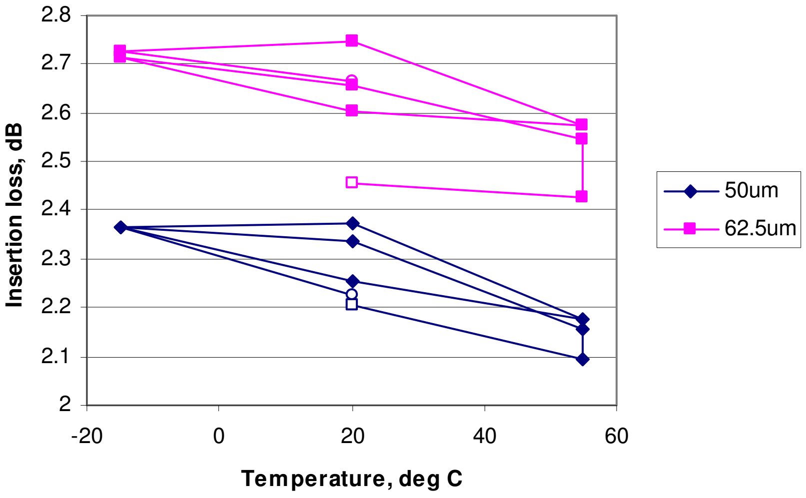

Figure 7.7. Measured insertion loss for 50um and 62.5um mode controllers during temperature cycling.

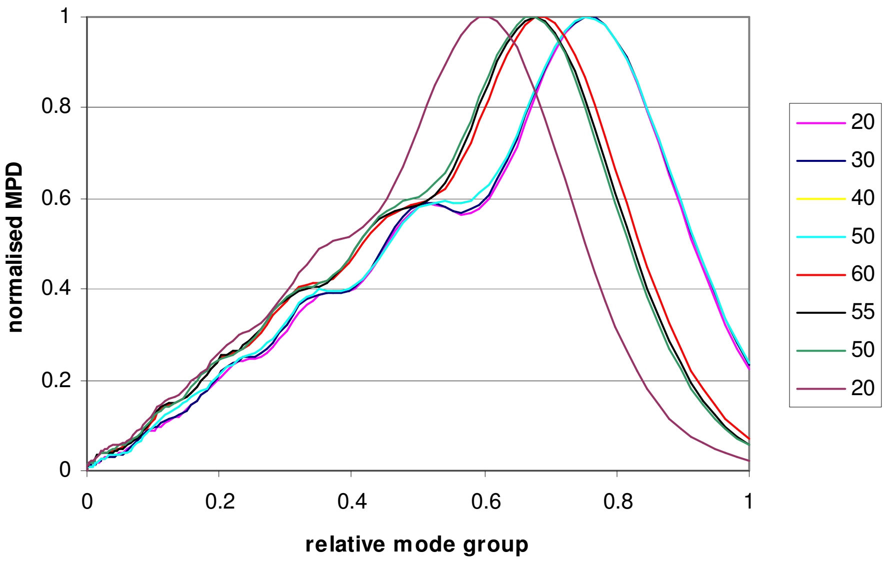

Figure 7.8. Measure MPDs of 50um mode controller as the temperature was elevated to 60°C and cooled to 20°C.

There appeared to be no sharp bends in the output pigtail of the 50um device, but it was noticed that the natural curve of the cable was no longer uniform along its entire length, with a tendency to twist back on itself. To investigate the cause of this catastrophic failure, a short, 20mm section of the outer cable, and the kevlar reinforcement fibres, was removed. The fibre inside the inner tube appeared to take the form of a helix with approximately 13mm period. One edge of the inner plastic tube was then cut and this caused the fibre to spring through the gap, as shown in Figure 7.9. The MPD was re-measured and was the same as for the final 20°C measurement in Figure 7.8.

Next, the remaining part of the inner tube was cut through, and the two cable sections sprung apart to reveal about 30mm of fibre, shown in Figure 7.10. The MPD was then re-measured and was found to have returned to its original value, prior to the first experiment.

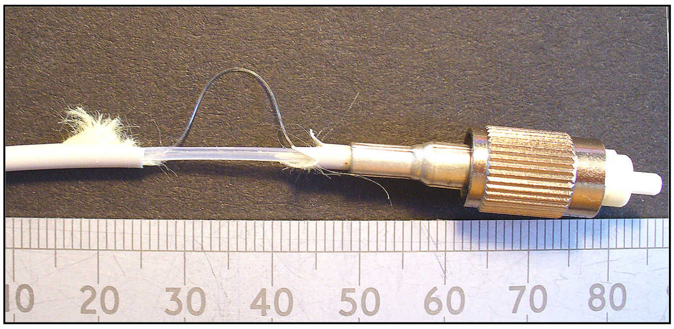

Figure 7.9. Removal of 20mm section of outer cable and kevlar of 50um mode controller and edge of inner tube, after temperature cycling.

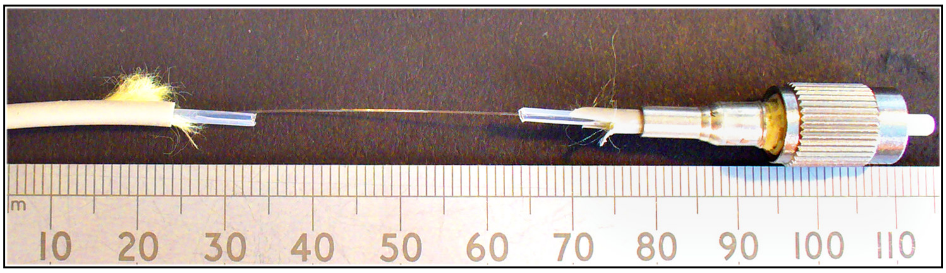

Figure 7.10. Inner tube cut through in sample shown in Figure 7.9.

It was clear from these observations that the inner tube, which was made from poly(butylene terephthalate) (PBS), had shrunk by about 30mm in the 60°C temperature test. This had caused the fibre to form into a helix to take up the excess length, resulting in bend-induced attenuation of the higher order modes. When the tube was cut the fibre relaxed, returning the MPD to its original shape.

This sort of shrinkage is, however, not uncommon in cable manufacture and is caused by residual stresses in the material resulting from hot extrusion and cold quenching during the manufacturing process. Further testing on other cable samples of the same type indicated shrinkage of 1.2% at 50°C and 1.9% at 60°C

The period λ of a helix inside a tube is given by

$$\lambda = \frac{R\pi 2a}{\sqrt{1-R^2}} \tag{7.1}$$

where: R is the ratio of the length of the shrunken tube to the fibre length, and
a is the tube bore radius.

In this case, the fibre length was 1460mm, the bore radius was 0.4mm, and, for a temperature of 60°C, gives a total shrinkage of 27.7mm with a helix period of 12.7mm, which agrees well with the observed value of about 13mm.

The curvature c of a helix is given by

$$c = \frac{a}{a^2 + (\lambda/2\pi)^2} \tag{7.2}$$

which, in this case, corresponds to a fibre bend radius of 10.6mm. The number of helix cycles of the fibre in the tube is 114. Thus, the fibre is effectively subjected to a mandrel-wrap mode-filter consisting of 114 turns around a 10.6mm radius mandrel. It is likely that the reason no effect on the MPD was seen in the first experiment at 55°C was that, for that experiment, a shorter section of the output pigtail was inside the oven. This is borne out by the fact that the 62.5um mode controller showed no effect at either temperature, where, for that device, the pigtail length inside the oven was short for both experiments.

In summary, shrinkage in the inner tube of the fibre cable caused catastrophic mode-filtering at 60°C. One possible solution may be to expose the cable to thermal preconditioning before assembling the mode controller, to allow shrinkage to take place. Another is to ensure that the tube is not captive at both the connector and mode controller ends.

7.2 Chapter Summary

This chapter has described the manufacture of a ruggedised mode control device for field use. The design requirements were that it would comply with international link testing standards, be robust and reliable, protect proprietary information, be relatively cheap and also easy to manufacture. The design described in this chapter satisfied these requirements well, apart from two reliability issues.

The first was due to coating delamination of the step-index fibre in the 62.5um device. This led to reduced elastic deformation of the fibre under the pinch plate and a subsequent reduction in the degree of mode-scrambling. While this was not found to occur very often, some means of preventing it is required, such as by filling up the area around the fibre, inside the pinch plate, with resin. Extended testing on a number of devices should also be carried out to establish the likelihood of failure occurring after the polyurethane potting compound has properly hardened. The coating of the 50um step-index fibre was much harder and showed no signs of delamination.

The other source of failure occurred during temperature cycling and was found to be due to shrinkage of the inner tube in the output pigtail of the device. At 60°C the shrinkage, which was measured to be 1.9%, caused the fibre inside the tube to buckle into a helix with a curvature radius of 10.6mm. The effect on the mode distribution was to strip out high-order modes resulting in non-compliance with the target MPD template. To eliminate this effect, some thermal pre-conditioning of the cable may be carried out, or the design could be changed so that the inner tube is not captive at both ends, and an excess length incorporated to allow for shrinkage.

CHAPTER 8

CONCLUSIONS AND FUTURE WORK

8.1 Conclusions

The motivation for this thesis primarily arose out of a need for new ways of providing control over the mode distribution in multimode fibres for testing high bandwidth Local Area Networks (LANs). A shift to multimode fibre as the medium of choice for Gigabit Ethernet systems has stimulated the development of several new fibre types has led to a raft of new international standards.

Whilst methods of mode-scrambling and mode-filtering have been employed by the industry for many years, their performance in terms of Mode Power Distribution and Encircled Flux distributions has not been thoroughly investigated. Furthermore, the use of such methods has often been subjective and somewhat idiosyncratic. For example, it has been widely accepted in the industry that the additional of a mandrel-wrap mode-filter serves to produce an Equilibrium Mode Distribution, even for underfilled sources, such as OTDR's. This is in fact, not the case, and has subsequently led to confusion when comparing measurements made on LED sources and OTDRs.

This thesis commenced with providing an overview of LANs and the requirements for tighter mode control. The sensitivity of both bandwidth and attenuation to the launched modal distribution has been described and comparative measurements of insertion loss for different sources highlighted to the need for tighter mode control.

The theory of multimode fibres was presented in Chapter 3, providing the background for the mode field computations used throughout this work. Chapter 4 described the experimental apparatus that was constructed to perform mode profile measurements. Its accuracy was discussed and its range of applicability was investigated. It was found that, using a novel near-field reconstruction method, the technique was sufficiently accurate for most mode power distributions, but could lead to errors for well-filled fibres. A new approach to computing the MPD was presented, consisting of referencing the measured intensity profile against modelled Laguerre-Gauss solutions.

In Chapter 5, a range of mode control devices was investigated. These were divided into two types, those that provided mode-scrambling and those that provided mode-filtering. It was found that Long Period Gratings provided an effective means of coupling power from low-order modes to high-order modes but they did not generally lead to a uniform mode distribution. This is because, in graded-index fibres, $\Delta\beta$ between all adjacent mode groups is equal, so that a particular period causes light to be progressively transferred across the entire mode spectrum, eventually being lost as radiation modes. This leads to a dearth of low-order modes and a rectangular-shaped near-field intensity profile. It is unlikely, therefore, that LPGs could be tailored to produce mode profiles to satisfy the new LAN standards, but they might have application in sensors, where a bias towards high-order modes could improve sensitivity. It was found that a refractive index LPG, which was written by UV exposure, gave a narrow, rectangular, near-field profile. This was due to the diameter of the writing spot being somewhat smaller than the fibre core diameter and so the grating did not extend out to the higher-order modes near to the core/cladding boundary. This profile may have application where a reasonably square launch is required on a smaller diameter fibre such as to approximate towards a Limited Phase Space (LPS) launch on a standard graded-index fibre. Another area for further work would be to experiment with LPGs in step-index fibre. Here, $\Delta\beta$ between adjacent modes is not uniform and so selective coupling between particular modes may be possible

Also, in Chapter 5, various mode filtering mechanisms were described. Experiments with an air-gap filter showed that the measured near-field distribution of a 50um fibre agreed well with the modelled distribution, when mode equalisation within each mode group was assumed in the model. It was therefore concluded that mode equalisation had taken place naturally over the one metre length of fibre used. In fact, it was proposed that the level of agreement with the model could be used as an indicator of the degree of mode coupling present. Later work with microbending, however, revealed that the fibre used in the air-gap experiment had an asymmetric feature in the refractive index profile near to the core centre, and failure to stimulate Hermite-Gauss (HG) modes by microbending with this fibre may have been due to strong mode-coupling caused by this feature. By contrast, it was possible to readily demonstrate HG modes with a 62.5um fibre, which had a symmetric index profile. It would be useful, therefore, to repeat the air-gap experiment with a fibre of known symmetry to see if the degree of mode equalisation required by the model was different.

It has been widely accepted by the industry that a long fibre length will automatically lead to an EMD and so an experiment was carried out to test this by launching a range of mode distributions into range of fibre types with lengths ranging from 100m to 2700m. It was found that, while there was some tendency towards an EMD, as the higher-order modes suffered greater attenuation, there was only limited evidence of coupling from the lowest-order modes to mid-order modes. Thus, it cannot be assumed that a long fibre leads to equalisation and thus it is preferable to launch an EMD directly, using the techniques described here.

Chapter 6 described some applications of the mode control techniques investigated in this thesis. By using combinations of mode-scramblers and mode-filters, it was possible to simulate an EMD launch and an LPS launch. Compliance with the ISO/IEC MPD template was easily achieved for under-filled and over-filled launches at both 850nm and 1300nm. A new IEC encircled flux template was found to be much tighter, requiring very careful adjustment of the point-load mode-scrambler and fibre bend radius. A paper detailing the design and performance of a mode control device to satisfy these requirements has been submitted to IET Optoelectronics Journal. A round robin, co-ordinated by this author, is currently being undertaken by the IEC in order to establish if present measurement technology is sufficiently accurate to justify the proposed encircled flux template.

The wavelength sensitivity of the MPD of a device compliant with the ISO/IEC standard was investigated and it was found, both theoretically and experimentally, that with a parabolic reference it was slightly more fully-filled at 850nm than at

1300nm. Re-computing the MPD with a modelled Laguerre reference indicated that, in fact, the reverse was true and that the device was more fully-filled at 1300nm. This observation served to emphasise the limitations of using a parabolic reference, which were discussed in Chapter 4.

The sensitivity to polarisation of the mode control techniques described has not been investigated. Most of the work in this thesis has, in fact, used LED sources, which are unpolarised, due to problems associated with near-field speckle. It would be interesting, however, in future work to study the effect of polarisation on the point-load mode-scrambler and the microbend grating, which are asymmetric structures.

A multimode sensor was also described in Chapter 6 that worked by combining a singlemode source with the high-order modes using fused biconic-tapered couplers. The MPD consisted of two clearly distinguishable peaks where the relative height of the peaks was sensitive to applied stimulus. In this manner, the device was insensitive to the launched light level. Sensitivity of the device to microbending and bend radius was demonstrated. The measurement was found to be non-linear, but the device might find application as a threshold detector in, for example, pressure or displacement. The configuration could also find application in monitoring the integrity of a secure communication channel, although this application was not investigated.

Results of an experiment to demonstrate Mode Group Diversity Multiplexing (MGDM) using a fused biconic-taper coupler were presented. It was shown that two multiplexed channels could be propagated over 985m of multimode fibre with minimal degradation from mode-coupling. Channel isolation was shown to be 8.6dB. it would be interesting to extend the principle of MGDM to a higher number of channels using, for example, a combination of evanescent coupling and offset-launch coupling

Finally, in Chapter 7, the design and construction of a ruggedised package for mode control devices was described. The assembly procedure consisted of tuning the mode profile to meet a certain requirement and then potting it, for protection and security. Two main sources of unreliability in the design were discovered. One concerned the coating of the 60um step-index fibre, which was found to occasionally delaminate, leading to a reduced amount of mode-scrambling. Some further work is required in this area to solve this problem, such as (a) to obtain a similar fibre type, but with a tougher coating, similar to the coating of the 50um step-index fibre which did not show any signs of delamination, or (b) introduce resin around the contact area of the fibres to ensure they cannot move. Further, prolonged testing of the current design is required to assess the failure rate and whether failures occur only during manufacture or at some time afterwards. The other failure mechanism was due to shrinkage in the inner tube of the fibre cable at elevated temperature. It was found that shrinkage was about 1.9% at 60°C, leading to an effective bend radius of 10.6mm on the fibre. A possible solution to this problem is to thermally condition the cable before attaching the fibre connectors.

8.2 Future Work

It has been shown in this thesis that various methods of mode-scrambling and mode-filtering can be employed to achieving compliance with emerging modal standards. As fibre LAN systems continue to become more widespread, the need for mode control devices will grow and efforts in improving the tunability and manufacturing of such devices will no doubt be rewarded.

The use of LPGs in graded-index fibres did not provide uniform mode-scrambling but they may find use in specific applications, such as for launching selective groups of modes. Investigation on the use of LPGs in multimode step-index fibre might be advantageous, where mode-coupling effects are somewhat different.

It was found that the degree of coupling between degenerate modes in a mode group depends on perturbations in the refractive index profile and this might be explored as a means of achieving a more uniform distribution in, for example, an offset launch for MGDM applications. Analysis of results of an air gap mode-filter showed that it appeared to be an effective means of assessing the degree of intra-group mode-coupling.

The feasibility of a two-channel MGDM was demonstrated and a productive area for further research would be to explore techniques for launching multiple channels.

Finally, some of the techniques for mode control described in this thesis could be tested for their suitability to Plastic Optical Fibre (POF), where new applications may arise.

CHAPTER 9

REFERENCES

1 F. P. Kapron et al., 'Radiation losses in glass optical waveguides', *Appl.Phys. Lett.,* vol. 17, no. 10, pp. 423-425, 1970.

2 IEEE 802.3-2002, ‘Information Technology - Telecommunication & Information Exchange Between Systems - Local and Metropolitan Area Networks - Specific Requirements, Part 3: Carrier Sense Multiple Access with Collision Detection (CSMA/CD) Access Method and Physical Layer Specifications 2002’.

3 TIA/EIA-455-203 (2001), FOTP-203 - Launched Power Distribution Measurement Procedure for Graded-Index Multimode Fiber Transmitters

4 TIA/EIA-455-54-B (2001), ‘FOTP-54 - Mode Scrambler Requirements for Overfilled Launching Conditions to Multimode Fibers’

5 TIA/EIA-455-204 (2000), ‘ FOTP-204 - Measurement of Bandwidth on Multimode Fiber.

6 J. B. Schlager et al., 'Measurements for Enhanced Bandwidth Performance Over 62.5 um Multimode Fiber in Short-Wavelength Local Area Networks', *IEEE J. Lightwave Technol.,* vol. 21, no. 5, pp. 1276-1285, 2003.

7 TIA-455-220-A (2003), ‘FOTP-220 - Differential Mode Delay Measurement of Multimode Fiber in the Time Domain’

8 TIA-492AAAC-A (2003), ‘Detail Specification for 850-nm Laser-Optimized, 50-um Core Diameter/125-um Cladding Diameter Class Ia Graded-Index Multimode Optical Fibers’

9 P. Pepeljugoski et al., 'Development of System Specification for Laser-Optimized 50 um Multimode Fiber for Multigigabit Short-Wavelength LANs', *IEEE J. Lightwave Technol.,* vol. 21, no. 5, pp. 1256-1275, 2003.

10 L. Raddatz et al., 'Influence of restricted mode excitation on bandwidth of multimode fiber links', *IEEE J. Photon. Technol. Lett.,* vol. 10, no. 4, pp. 534-536, 1998.

11 L. Raddatz et al., 'An experimental and theoretical study of the offset launch technique for the enhancement of the bandwidth of multimode fiber links', *IEEE J. Lightwave Technol.,* vol. 16, no. 3, pp. 324-331, 1998.

12 ISO/IEC14763-3 (2006), ‘Information technology — Implementation and operation of customer premises cabling — Part 3: Testing of optical fibre cabling’.

13 R. Olshansky and D. A. Nolan, 'Mode-dependent attenuation of optical fibres: excess loss', *Appl.Opt.,* vol. 15, no. 4, pp. 1045-1047, 1976.

14 M. Y. Loke and J.N McMullin, 'Simulation and measurement of radiation loss at multimode fiber macrobends', *IEEE J. Lightwave Technol.,* vol. 8, no. 8, pp. 1250-1256, 1990.

15 D. Gloge, 'Bending Loss in Multimode Fibers with Graded and Ungraded Core Index', *Appl.Opt.,* vol. 11, no. 11, pp. 2506-2513, 1979.

16 K. Kitayama et al., 'Impulse Response Prediction Based on Experimental Mode Coupling Coefficient in a 10-km Long Graded-Index Fiber', *IEEE J. Quantum Electron.,* vol. 16, no. 3, pp. 356-362, 1980.

17 J. M. Senior, “*Optical Fiber Communications*”, section 2.3, Prentice Hall, second edition, 1992.

18 D. Gloge, 'Weakly Guiding Fibers', *Appl.Opt.,* vol. 10, no. 10, pp. 2252-2258, 1971.

19 http://www.mathsoft.com

20 S. Berdague and P. Facq, 'Mode division multiplexing in optical fibers', *Appl.Opt.,* vol. 21, no. 11, pp. 1950-1955, 1982.

21 D. Gloge and E. A. J. Marcatili, 'Impulse response of fibers with ring-shaped parabolic index distribution', *Bell Syst. Tech. J.,* vol. 52, no. 7, pp. 1161-1168, 1973.

22 D. Gloge and E. A. J. Marcatili, 'Multimode theory of graded-core fibers', *Bell Syst. Tech. J.,* vol. 52, no. 9, pp. 1563-1579, 1973.

23 Y. Liu et al., 'Accurate mode characterization of the graded-index multimode fibers for the application of mode-noise analysis', *Appl.Opt.,* vol. 34, no. 9, pp. 1540-1543, 1995.

24 M. J. Adams et al., 'Leaky rays on optical fibres of arbitrary (circularly symmetric) index profiles', *Electron. Lett.,* vol. 11, no. 11, pp. 238-240, 1975.

25 R. Olshansky, 'Leaky modes in graded index optical fibers', *Appl.Opt.,* vol. 15, no. 11, pp. 2773-2777, 1976.

26 F. Sladen et al., 'Determination of optical fiber refractive index profiles by a near-field scanning technique', *Appl.Phys. Lett.,* vol. 28, no. 8, pp. 225-258, 1976.

27 Y. Daido et al., 'Determination of modal power distribution in graded-index optical waveguides from near-field patterns and its application to differential mode attenuation', *Appl.Opt.,* vol. 18, no. 13, pp. 2207-2213, 1979.

28 O. G. Leminger and G. K.Grau, 'Near-field intensity and modal power distribution in multimode graded-index fibres', *Electron. Lett.,* vol. 16, no. 17, pp. 678-679, 1980.

29 A. R. Mickelson and M. Eriksrud, 'Mode-continuum approximation in optical fibers', *Opt. Lett.,* vol. 7, no. 11, pp. 572-574, 1982.

30 '*The MPX Modal Explorer'*, http://www.ardenphotonics.com.

31 IEC 61300-3-31 (2003), 'Fibre optic interconnecting devices and passive components - Basic test and measurement procedures - Part 3-31: Examinations and measurements - Coupled power ratio measurement for fibre optic sources'.

32 W. H. Press et al.,'*Numerical Recipes in C'*, Cambridge University Press, chapter 14, 2nd Edition, 2002.

33 I. Fatadin et al., 'Accurate Magnified Near-Field Measurement of Optical Waveguides Using a Calibrated CCD Camera', *IEEE J. Lightwave Technol.,* vol. 24, no. 12, pp. 5067-5074, 2006.

34 IEC 61280-4-1 (Committee Draft 2007), 'Installed cable plant – Multimode attenuation measurement'.

35 J. G. N. Baines, A. G. Hallam et al., 'Fiber Diameter Measurements and Their Calibration', *IEEE J. Lightwave Technol.,* vol. 8, no. 9, pp. 1259-1268, 1990.

36 W. H. Press et al., 'Numerical Recipes in C: The Art of Scientific Computing', Cambridge University Press, Second Edition, ch.14, 1992.

37 IEC 60793-1-20 (2001), 'Optical fibres - Part 1-20: Measurement methods and test procedures - Fibre geometry'.

38 D. Rittich, 'Practicability of determining the modal power distribution by measured near and far-fields', *IEEE J. Lightwave Technol.,* vol. 3, no. 3, pp. 625-661, 1985.

39 M. Calzavara et al., 'Reliability of a new method for measurements of modal power distribution in optical fibres with application to mode scrambler testing', *Electron. Lett.,* vol. 17, no. 15, pp. 543-545, 1981.

40 A. M. Vengsarkar et al., 'Long-period gratings as band-rejection filters', *IEEE J. Lightwave Technol.,* vol. 14, no. 1, pp. 58-65, 1996.

41 V. Bhatia, 'Applications of long-period gratings to single and multi-parameter testing', *Optics Express,* vol. 4, no. 11, pp. 457-466, 1999.

42 S. W. James and R. P. Tatum, 'Optical fibre long-period grating sensors: characteristics and application', *Meas. Sci. Technol.,* vol. 14, no. , pp. R49-R61, 2003.

43 J. W. Berthold, 'Historical review of microbend fiber-optic sensors', *IEEE J. Lightwave Technol.,* vol. 13, no. 7, pp. 1193-1199, 1995.

44 L. Su et al., 'Microbend-induced mode coupling in a graded-index multimode fiber', *Appl.Opt.,* vol. 44, no. 34, pp. 7394-7402, 2005.

45 L. Su et al., 'CO_2-Laser-induced long-period gratings in graded-index multimode fibers for sencor applications', *IEEE J. Photon. Technol. Lett.,* vol. 18, no. 1, pp. 190-192, 2006.

46 Patent EP0840146, 'Method for making long-period gratings', Lucent Technologies Inc., 1998.

47 TIA/EIA-555-204 (2000), 'Measurement of Bandwidth on Multimode Fiber.'

48 '*Roark's Formulas for Stress and Strain'*, 7th edition, W. C. Young and R. G. Budynas, McGraw-Hill, 2002.

49 R. Olshansky, 'Distortion Losses in Cabled optical Fibers', *Appl.Opt.,* vol. 14, no. 1, pp. 20-21, 1975.

50 E. J. Borowski and J. M. Borwein, '*Collins Dictionary of Mathematics'*, Harper Collins, 1989.

51 D. Marcuse, 'Coupled mode theory of round optical fibers', *Bell Syst. Tech. J.,* vol. 52, no. 6, pp. 817-842, 1973.

52 Y. C. Yang et al., 'Elasto-optics in double-coated optical fibers induced by axial strain and hydrostatic pressure', *Appl.Opt.,* vol. 41, no. 10, pp. 1989-1994, 2002.

53 K. Yamashita et al., 'Launching condition dependence of bandwidth in graded-index multimode fibers fabricated by MCVD or VAD method', *IEEE J. Lightwave Technol.,* vol. 3, no. 3, pp. 601-607, 1985.

54 W. T. Welford, '*Optics*', Oxford University Press, 2nd edition, 1984.

55 IEC 61300-3-4 (2001), Fibre optic interconnecting devices and passive components – basic test and measurement procedures – Part 3-4: Examinations and measurements – Attenuation'

56 L. Raddatz et al., 'Influence of restricted mode excitation on bandwidth of multimode fiber links', *IEEE J. Photon. Technol. Lett.,* vol. 10, no. 4, pp. 534-536, 1998.

57 M. Hackert and G. Brown, 'System design methodology for power budgeting of 62.5um multimode fiber systems', *IEEE J. Lightwave Technol.,* vol. 11, no. 2, pp. 205-211, 1993.

58 IEC 61280-4-1 (Committee Draft 2007), 'Installed cable plant – Multimode attenuation measurement'.

59 J. Villatoro et al., 'High resolution refractive index sensing with cladded multimode tapered optical fibre', *Electron. Lett.,* vol. 40, no. 2, pp. 106-107, 2004.

60 D. Donlagic and B. Culshaw, 'Microbend Sensor Structure for Use in Distributed and Quasi-Distributed Sensor Systems Based on Selective Launching and Filtering of the Modes in Graded Index Multimode Fiber', *IEEE J. Lightwave Technol.,* vol. 17, no. 10, pp. 1856-1868, 1999.

61 M. Calzavara et al., 'A new approach to investigating mode coupling phenomena in graded-index optical fibres', *Opt. Quantum Electron.,* vol. 17, pp. 157-167, 1985.

62 Y. Shinmura et al., 'Obervation of mode in graded-index optical fibers with bending and cross-talk in MDM', *IEICE Trans. Electron.,* vol. E80-C, no. 6, pp. 828-830, 1997.

63 M. Yoshikawa and K. Kameda., 'Single-mode separation for mode-division multiplexing by holographic filter', *IEICE Trans. Electron.,* vol. E77-C, no. 9, pp. 1526-1528, 1994.

64 P. S. Szczepanek and J. W. Berthold III, 'Side launch excitation of selected modes in graded-index optical fibers', *Appl.Opt.,* vol. 17, no. 20, pp. 3245-3247, 1978.

65 C. P. Tsekrekos et al., 'Design considerations for transparent mode group diversity multiplexing link', *IEEE J. Photon. Technol. Lett.,* vol. 18, no. 20, pp. 2359-2361, 2006.

66 C. K. Asawa, 'Intrusion-alarmed fiber optic communication link using a planar waveguide bimodal launcher', *IEEE J. Lightwave Technol.,* vol. 20, no. 1, pp. 10-18, 2002.

67 L.G. Cohen and S.J Jang, 'Interrelationship between water absorption loss and dispersion in multimode fiber', *Appl.Opt.,* vol. 20, no. 9, pp. 1635-1639, 1981.

68 K. M. Patel et al., 'Spatially resolved detection and equalization of modal dispersion limited multimode fiber links', *IEEE J. Lightwave Technol.,* vol. 24, no. 7, pp. 2629-2636, 2006.

69 Patent WO2005/010562, 'Multimode fiber optic intrusion detection system', Network integrity Systems, Inc., 2005.

70 Patent GB2405488, ‘Device for controlling the mode distribution in multimode optical fibre’, Andrew G Hallam, 2005.

APPENDIX A - Patent search on mode control devices

The results of a patent search on mode control devices is presented, where, in each case, the patent number is given, followed in brackets by the original assignee and the year of filing, and a short description of the device.

The patents have categorised as to whether they are intended *as Mode Scramblers*, *Mode Conditioners* or *EMD generators*.

A.1 Mode Scramblers

JP11038255 (Furukawa, 1997): step-index mode scrambler with overlapping turns.

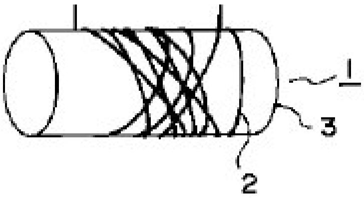

US4934787 (Mitsubishi Rayon, 1989): step-index fibre wrapped around twin cylinders in a figure of eight pattern.

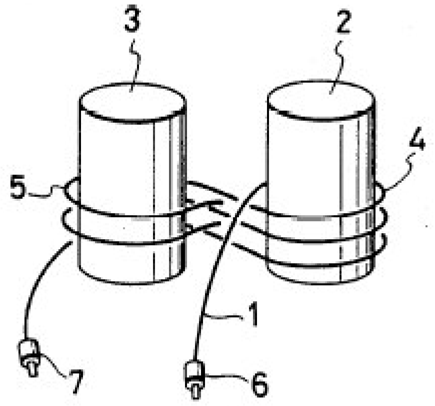

US4229067 (Corning, 1978): combination of step-index and graded-index fibres to make a mode-scrambler. ‘Step-graded’ to give smooth, uniform filling of test fibre. ‘Step-graded-step’ to give uniform overfill of fibre under test.

EP0367073 (Sumitomo, 1989): uses ‘step-graded-step’ and ‘graded-step-graded’ mode-scramblers for making coupler measurements. Also mentions use of side pressure to achieve mode scrambling.

US4974930 (AT&T, 1989): use of ultra-violet light to modify index of fibre cladding, such as periodically, to make a mode-scrambler.

US4676594 (AT&T, 1984): use of notch in side of fibre to make a mode-scrambler.

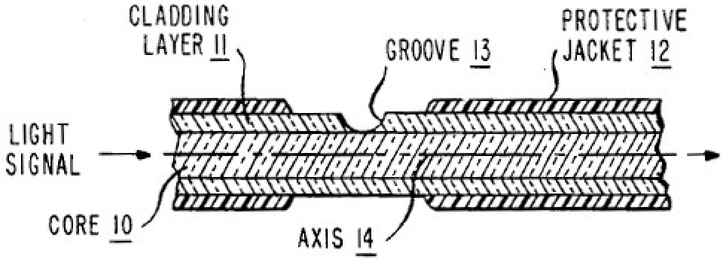

DE3411272 (Siemens, 1984): use of 'serpentine' fibre wrapping to achieve mode-scrambling. Adjust the separation of two sets of interlocking pins to give controlled bend radii.

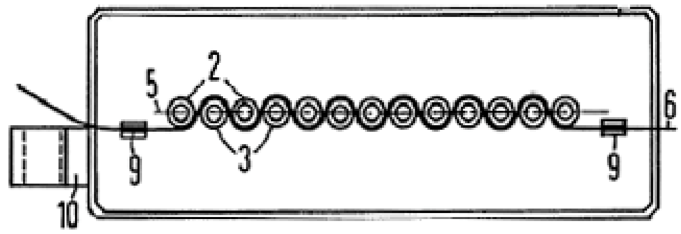

JP2163707 (Mitsubishi Rayon, 1988): wraps fibre around twin cylinders with displaced turns to give a range of bend radii.

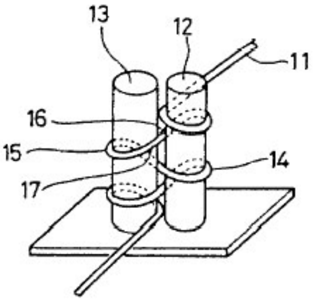

JP59062804 (Nippon, 1982): use of a diffuser between two fibre ends to give mode-scrambling. Also describes a version with a *reflective* film and diffuser so that fibres are connected to the same side of the device.

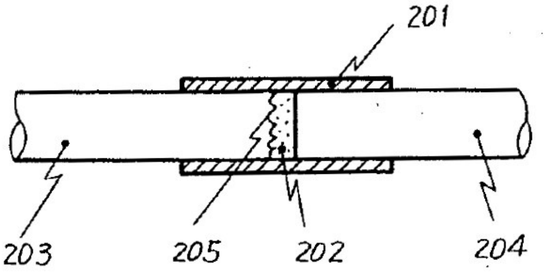

JP59037503 (Nippon, 1982): use of bi-conical tapers to make a mode-scrambler.

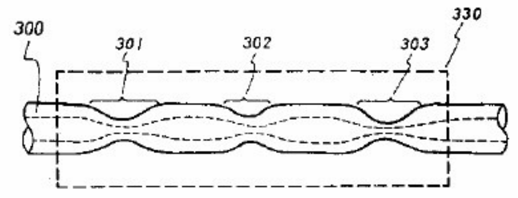

JP62299808 (Yokohama University, 1986): zig-zag planar waveguide for mode-scrambling. Used for mode-insensitive fibre couplers..

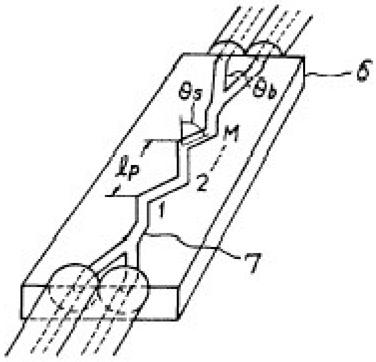

JP57027211 (Fujitsu, 1980): thermally form a lump or a kink in a fibre to make a mode-scrambler.

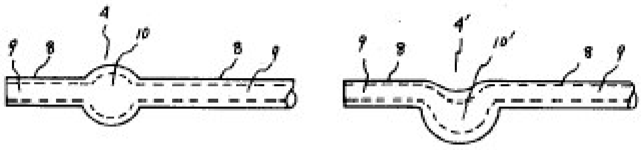

JP58202402 (Nippon, 1982): fill the gap between two fibre sections having angled ends with appropriate material to act as a mode-scrambler.

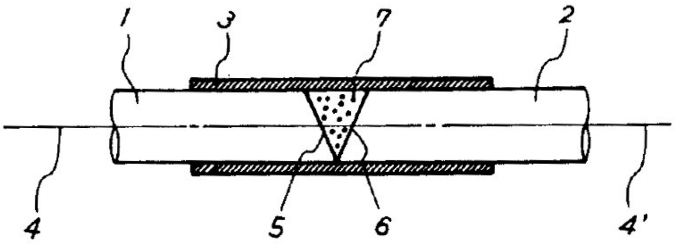

JP60178409 (Yokokawa, 1984): fibre bent between pins in orthogonal directions to impart a twist on the fibre to make a mode-scrambler.

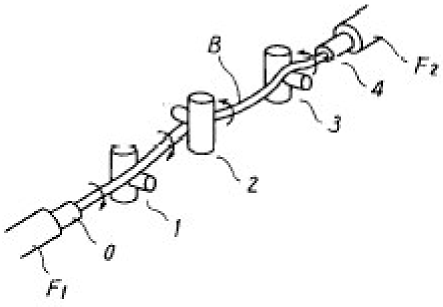

US6330382 (Corning, 2001): tapered fibre coupler for filling mode volume of multimode fibre from a single-mode fibre source.

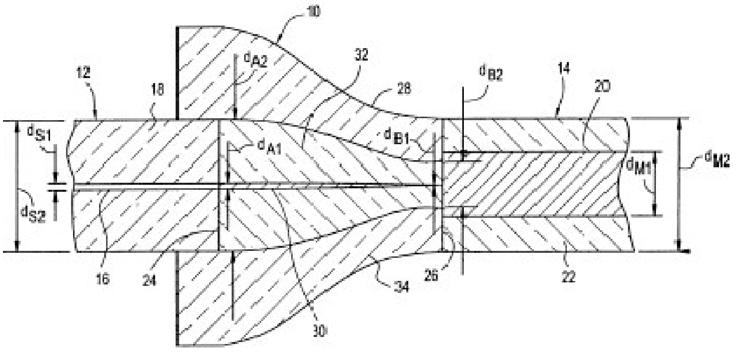

US4763976 (Corning, 1987): Similar to above.

US4877305 (US private, 1988): a fibre is passed through a length of tubing that has a variety of non-planar bends. The various radii encountered by the fibre causes mode scrambling. See also US4932748.

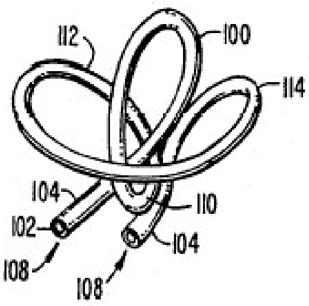

JP53011040 (Nippon, 1976): mode scrambler made by pressing a body 27 with an rough surface 26 onto a fibre 13 using heatshrink tubing 25.

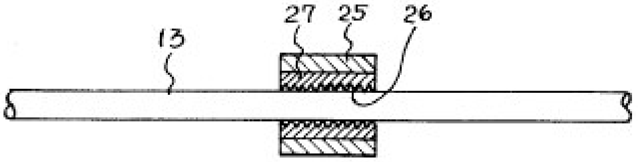

US3980391 (Plessey, 1975): device to interchange power between low-order and high-order modes for group delay equalisation. A compensator consisting of sections P,R of standard graded fibre and section Q, of inverse gradient fibre, are sandwiched between the input and output fibres f1 and f2.

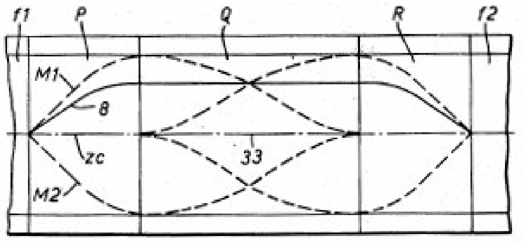

US6810175 (Terabeam Corp., 2002): a laser beam is offset from axis of graded-index fibre which is coupled to a step-index fibre. The mode-scrambler produces a 'substantially-filled' numerical aperture.

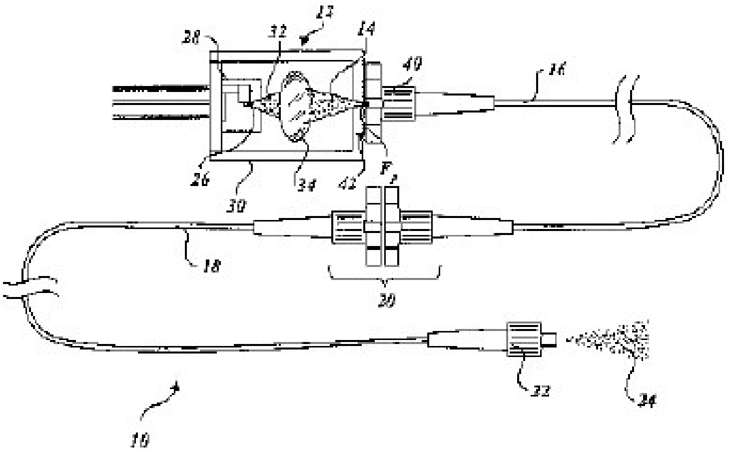

US6895146 (Terabeam Corp., 2001): a diffusing material is positioned between the end of a single-mode launch fibre and a multimode output fibre to excite higher-order modes

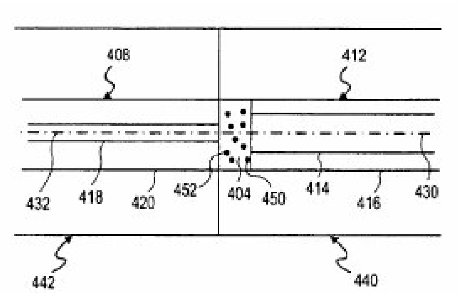

JP58207016 (Nippon Electric, 1983): Prism 25 has an angled front surface and an uneven back surface 26 so that light from laser source 21 is launched via lens 22 into a plurality of modes in multimode fibre 23 giving a uniform distribution.

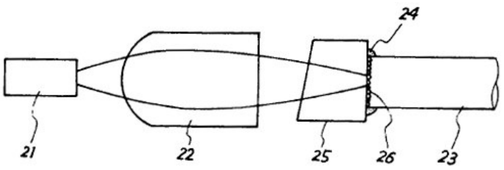

A.2 Mode Conditioners

US5416862 (AT&T, 1993): selective excitation of higher-order modes into multimode fibre 12 by introducing angle θ between the axis of single-mode launch fibre 16 and axis of the multimode fibre.

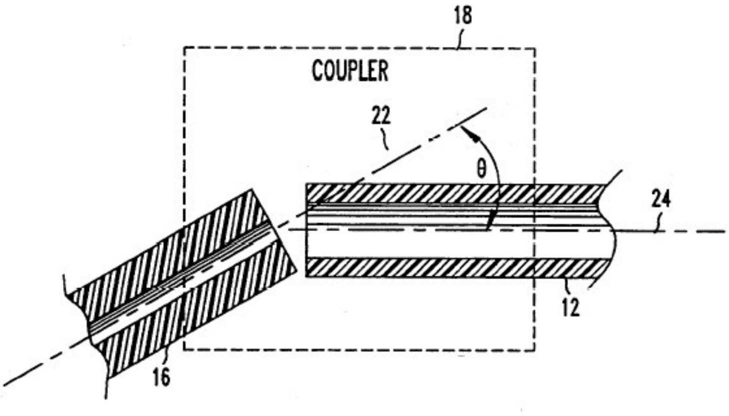

JP2000231027 (Hitachi, 1999): mode conditioner comprising an offset launch for coupling single-mode fibre to multimode fibre to excite mid-order modes. Utilises an eccentric ferrule.

JP2000147334 (Hitachi, 1998): mode conditioner comprising a stub of single-mode fibre between source and a multimode fibre, which employs an offset between the fibre cores to excite mid-order modes. The end of the single-mode fibre nearest to the source is angled.

US6064786 (Hewlett Packard, 1997): describes how coupling single-mode pigtailed laser sources to the nominal centre of a multimode fibre can result in a lower bandwidth than obtained with a fully-filled fibre. This is due to Differential Mode Delay (DMD) caused by index perturbations in the vacinity of the core centre. Optimum bandwidth can, however, be obtained by using an ‘offfset launch’ where a single-mode fibre 20 is coupled to multimode fibre 6 with an axial offset X between the fibre centres.

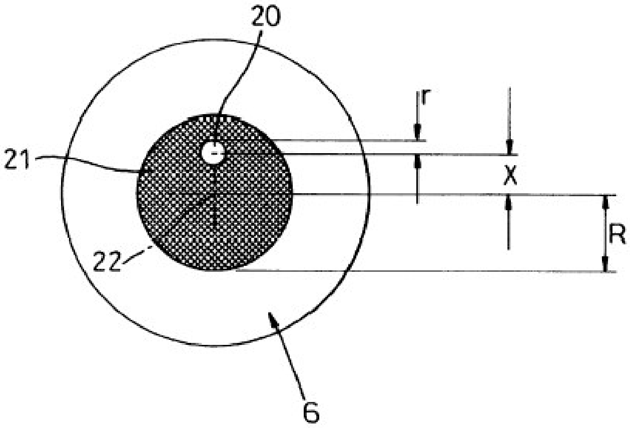

JP2000047065 (Hitachi, 1998): mode conditioner comprising an angled endface 25 on single-mode pigtail 11 to excite mid-order modes in multimode fibre 32.

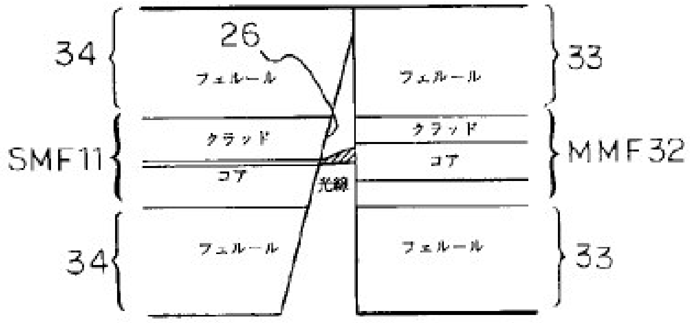

US4053764 (US Air Force, 1975): Fibre-optic tap consisting of an array of output fibres arranged in an arc around the input fibre. The output fibres selectively filter out particular mode groups depending on their angular orientation.

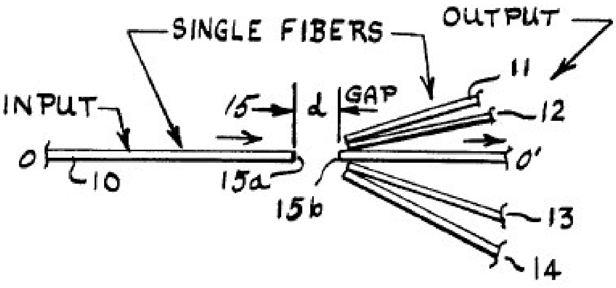

US4381137 (Hydroacoustic Inc., 1981): separates first and second order modes of a fibre using a reflector with a small aperture in it. Measures amount of mode-coupling as a sensing device.

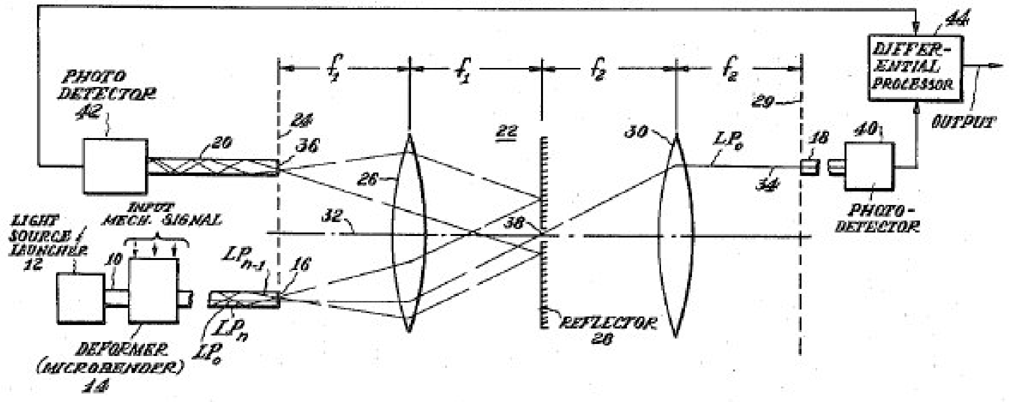

A.3 EMD Generators

JP54068254 (Fujitsu, 1977): alternating fibre sections laterally, or angularly, displaced to give an EMD.

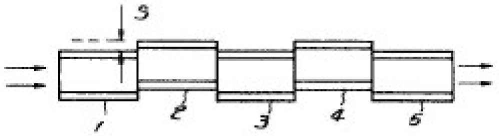

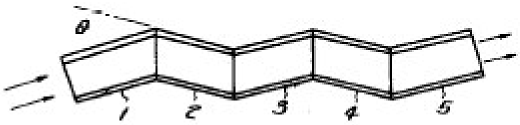

US4998792 (IBM, 1990): mode conditioner for creating equilibrium mode distribution. Consists of a gap 34 between two fibre ends followed by a mandrel wrap mode scrambler 36. The gap functions as a mode filter, stripping off all but the lowest modes, while the curved region acts as a mode scrambler redistributing the light energy into the intermediate modes. Typical gap is 1mm and typical mandrel diameter is 20mm.

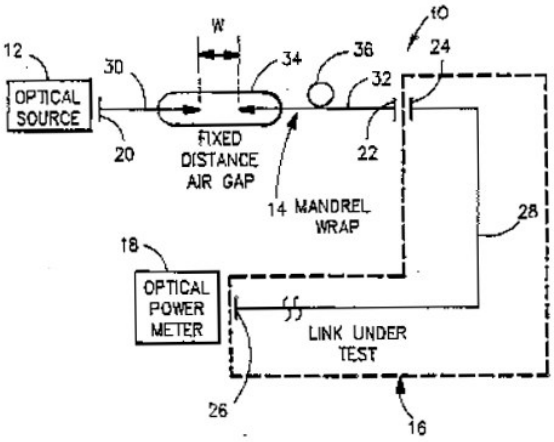

US5892866 (Honeywell, 1996): phase filter 37 to achieve EMD.

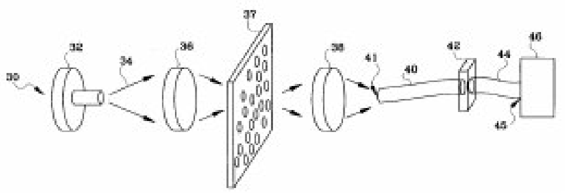

US6415076 (IBM, 2000): called a 'mode-conditioning patch' (MCP). Flared waveguide 20 for expanding output of singlemode fibre 21 to produce equilibrium mode distribution in multimode fibre 12.

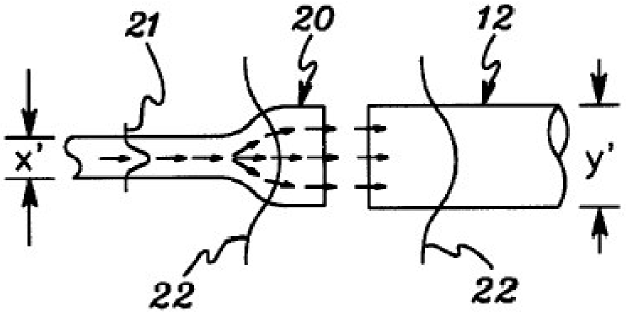

APPENDIX B - Market survey on mode control devices

The results of a market survey on commercially available mode control devices is presented below. The devices have been categorised as Mode Conditioning Patchcords, Mode Scramblers, Mode Filters and Deadzone Eliminators.

B.1 Mode Conditioning Patchcords

These are patchcords with an offset launch for Gigabit Ethernet. Designed to couple from singlemode pigtailed 1300nm laser into mid-order modes of multimode fibre so as to give a stable launch with minimal Differential Mode Delay.

An example of a mode-conditioning patchcord is shown below. They are typically designed for duplex operation where only the outward fibre contains an offset splice. The typical cost is around £100.

These devices are now made by many companies, including

Fiberdyne (www.fiberdyne.com)

Discount Cables USA (www.discountcablesusa.com)

Turnkey Fibre Solutions (www.turnkeyfibre.com)

Pro-link (www.connectworld.net)

Tech Optics (www.techoptics.com)

LeaderOPteC (www.leaderoptec.com)

Fibre Technologies Ltd (www.fibre.co.uk)

FibreFab Ltd (www.fibrefab.co.uk)

A novel launch scheme for coupling light into the skew rays of a graded index fiber has been described by **Digital Optics Corp.** (*J. Lightwave Technol.,* vol. 19, no. 5, pp. 753-758, 2001.).

This is accomplished by utilising a *diffractive* optical element between the single-mode launch fiber and the graded index system fibre. An example of a Vortex diffractive element on a 125um fibre stub is shown below:

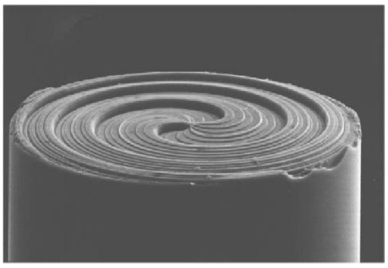

B.2 Mode Scramblers

Newport FM-1 (www.newport.com): Presses the fibre between two corrugated surfaces using a control knob. Price £376.

Control Optics FMS-305 (www.controloptics.com): Similar to the Newport FM-1. Price $250.

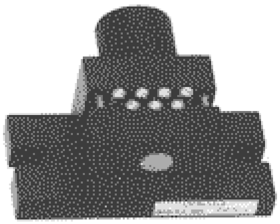

National Institute of Standards and Technology (*Electron. Lett.,* vol. 37, no. 17, pp. 9-10, 2001). A mode scrambler based on an annealed step-index fibre is shown to have reproducible performance and source-launch-alignment insensitivity. De-vitrification produces scattering centres in the fibre that distribute light uniformly over both angle and radius. An all-fibre mode scrambler with a 10 cm length and an insertion loss <3.5 dB is demonstrated.

B.3 Mode Filters

Precor Fiberoptics (www.auriganet.com). Consists of a simple patchcord with a few loops in it.

Noyes (www.afltele.com): Plastic mandrels with diameter and thread pitch to comply with TIA standards.

Fluke Networks (www.flukenetworks.com): Plastic mandrels with diameter and thread pitch to comply with TIA standards.

B.4 Deadzone Eliminators

These devices are used to temporally separate the deadzone that follows the front-end Fresnel reflection of an OTDR, from the fibre under test. They normally comprise nothing more complicated than a long length of fibre.

Noyes (www.afltele.com): *Fibre Rings*. Simple length of fibre with no apparent mode-conditioning. Length 150m.

Fluke Networks (www.flukenetworks.com): *Launch Cable*. Simple length of fibre with no apparent mode-conditioning. Length 100m.

EXFO (www.exfo.com): *Pulse Suppressor Box*. Simple length of fibre with no apparent mode-conditioning. Lengths 300 to 1500m.

Megger (www.megger.com): *Mode Conditioning Patchcord*. Features internal TIA and IEC mandrel-wrap mode filters. Length 50m.

Fiber Plus International (www.fiberplus.com): *Dead Zone Eliminator*. Simple length of fibre with no apparent mode-conditioning. Lengths 50m to 1500m.

APPENDIX C – Mode tabulation for 50um graded-index fibre at 850nm

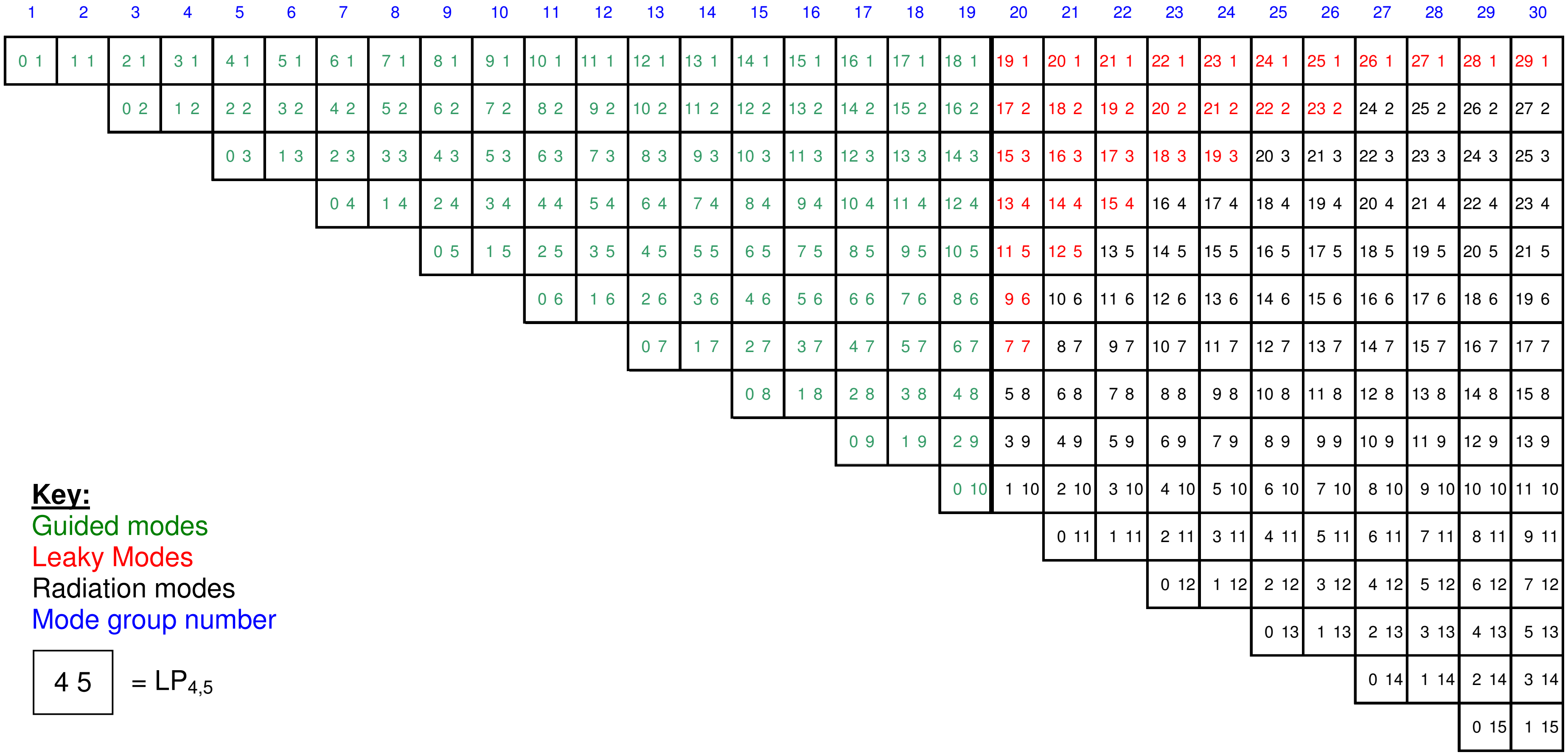

1	2	3	4	5	6	7	8	9	10	11	12	13	14	15	16	17	18	19	20	21	22	23	24	25	26	27	28	29	30
0 1	1 1	2 1	3 1	4 1	5 1	6 1	7 1	8 1	9 1	10 1	11 1	12 1	13 1	14 1	15 1	16 1	17 1	18 1	19 1	20 1	21 1	22 1	23 1	24 1	25 1	26 1	27 1	28 1	29 1
		0 2	1 2	2 2	3 2	4 2	5 2	6 2	7 2	8 2	9 2	10 2	11 2	12 2	13 2	14 2	15 2	16 2	17 2	18 2	19 2	20 2	21 2	22 2	23 2	24 2	25 2	26 2	27 2
				0 3	1 3	2 3	3 3	4 3	5 3	6 3	7 3	8 3	9 3	10 3	11 3	12 3	13 3	14 3	15 3	16 3	17 3	18 3	19 3	20 3	21 3	22 3	23 3	24 3	25 3
						0 4	1 4	2 4	3 4	4 4	5 4	6 4	7 4	8 4	9 4	10 4	11 4	12 4	13 4	14 4	15 4	16 4	17 4	18 4	19 4	20 4	21 4	22 4	23 4
								0 5	1 5	2 5	3 5	4 5	5 5	6 5	7 5	8 5	9 5	10 5	11 5	12 5	13 5	14 5	15 5	16 5	17 5	18 5	19 5	20 5	21 5
										0 6	1 6	2 6	3 6	4 6	5 6	6 6	7 6	8 6	9 6	10 6	11 6	12 6	13 6	14 6	15 6	16 6	17 6	18 6	19 6
												0 7	1 7	2 7	3 7	4 7	5 7	6 7	7 7	8 7	9 7	10 7	11 7	12 7	13 7	14 7	15 7	16 7	17 7
														0 8	1 8	2 8	3 8	4 8	5 8	6 8	7 8	8 8	9 8	10 8	11 8	12 8	13 8	14 8	15 8
																0 9	1 9	2 9	3 9	4 9	5 9	6 9	7 9	8 9	9 9	10 9	11 9	12 9	13 9
																		0 10	1 10	2 10	3 10	4 10	5 10	6 10	7 10	8 10	9 10	10 10	11 10
																				0 11	1 11	2 11	3 11	4 11	5 11	6 11	7 11	8 11	9 11
																						0 12	1 12	2 12	3 12	4 12	5 12	6 12	7 12
																								0 13	1 13	2 13	3 13	4 13	5 13
																										0 14	1 14	2 14	3 14
																												0 15	1 15

Key:

Guided modes

Leaky Modes

Radiation modes

Mode group number

4 5 = $LP_{4,5}$

APPENDIX D - Publications

Patent GB2405488, ‘*Device for controlling the mode distribution in multimode optical fibre’, Andrew G Hallam, 2005.*

IEC PAS 61300-3-43: '*Examinations and measurements - Mode transfer function measurement for fibre optic sources'*, First edition, Feb 2006.

A.G.Hallam et al., '*Mode Control for Emerging Link Performance Standards*', Optical Fibre Measurement Conference, Teddington, UK. Oct. 2007.

A.G.Hallam et al., '*Mode Control for Emerging Link Performance Standards*', Submitted to IET Optoelectronics Journal, Nov. 2007.

APPENDIX E - List of Programmes

During the course of this work the following computer programmes were developed, where *.MCD* and *.VBP* refer to MathCad and Visual Basic applications, respectively:

1. ***Laguerre.MCD***

   Computes the guided and leaky Laguerre-Gauss field solutions for a parabolic-index fibre. Required parameters are the fibre core diameter, the numerical aperture, the cladding index and the wavelength. Also computes the Mode Power Distribution and the far-field modal diffraction pattern.

2. ***Bessel.MCD***

   Computes the guided and leaky Bessel field solutions for a step-index fibre. Required parameters are the fibre core diameter, the numerical aperture, the cladding index and the wavelength. . Also computes the far-field modal diffraction pattern.

3. ***Bessel - Laguerre Overlap.MCD***

   Computes the field overlap of modes in a step-index fibre with both guided and leaky modes in a graded-index fibre. Required parameters are the mode-fields of the step and graded-index fibre, the number of mode groups in the graded fibre and the core diameter of the graded fibre. Also computes the Mode Power Distribution in the graded-index fibre.

4. ***Fresnel Diffraction.MCD***

   Computes the near-field diffraction of step-index Bessel modes. Required parameters are the mode-fields of the step-index fibre, the core diameter, the wavelength and the diffracting distance.

5. ***Mode Group Display.VBP* & *Mode Group Display.EXE***

   Displays near-field distribution and Mode Power Distribution of graded-index fibre, as the Mode Transfer Function is manually adjusted. The MTF is then calculated from the near-field for comparison. Also demonstrates mode-group field patterns and mode summation.

APPENDIX F - Glossary of Terms

Cladding mode
A *mode* that is confined to the cladding of an optical fibre which is of higher refractive index than the surrounding medium

Coupled Power Ratio
The ratio of the power carried in a multimode fibre to that coupled into a single-mode fibre positioned on the axis of the multimode fibre and butt-coupled to it.

Encircled Flux
A measure of the fraction of the total power, as a function of radius, radiating from the core of a multimode optical fibre.

Equilibrium Mode Distribution (EMD)
That condition in a multimode fibre where the relative distribution of power among the propagating modes is statistically constant with propagation length.

Fully-filled
A fibre that carries equal power in each of the guided modes is said to be fully-filled.

IEC
International Electrotechnical Commission

IEEE
Institute of Electrical and Electronics Engineers

Leaky Mode
One of a particular class of *modes* which decay monotonically for a finite distance in the cladding but become oscillatory beyond that distance. Such a *mode* gradually leaks out of the fibre as it travels along it, producing attenuation.

Limited Phase Space (LPS) Launch
Illuminating an optical fibre where the numerical aperture (NA) and/or the spatial extent of the illuminating field is less than that the respective NA and core size of the fibre.

Local Area Network (LAN)
A communication network for providing voice and/or data services to a network of computers and work stations, typically over distances of tens to hundreds of metres.

Long Period Grating (LPG)
A periodic perturbation to an optical fibre, with period typically in the range of hundreds of micrometres.

Macrobending Loss
Loss in a multimode fibre caused by the fibre being bent with a radius of less than a centimetre or so.

Modal Distribution
See *Mode Power Distribution.*

Mode
In an optical fibre, one of the possible field distributions of propagating electromagnetic radiation.

Mode-conditioning
Modifying the *mode power distribution* in an optical fibre.

Mode Controller
A device for modifying the *mode power distribution* in an optical fibre in a controlled fashion.

Mode Coupling
In an optical fibre, the exchange of power between propagating *modes*.

Mode Division Multiplexing (MDM)
The independent transfer of information in different *modes* of an optical fibre.

Mode Group Diversity Multiplexing (MGDM)
The independent transfer of information in different *mode groups* of an optical fibre.

Mode Filter
A device used to select, reject, or attenuate certain *modes* or *mode groups*.

Mode Group
A group of *modes* that all have the same propagation velocity. A typical graded-index multimode fibre with a core diameter of 50um and a numerical aperture of 0.21 will potentially support about 19 *mode groups* at an optical wavelength of 850nm.

Mode Mixer
See *Mode Scrambler.*

Mode Overlap Integral
A mathematical construct for determining the efficiency of energy coupling between *modes* in an optical fibre.

Mode Power Distribution (MPD)
The relative amounts of power propagating in the *mode groups* of an optical fibre. The MPD is equal to the *Mode Transfer Function* multiplied by *the relative mode group* number.

Mode Scrambler
A device for inducing *mode coupling* in an optical fibre**.** Mode scramblers are used to provide a *mode power distribution* that is independent of the optical source for purposes of laboratory or field measurements or tests.

Mode Stripper
A device for converting optical fibre cladding *modes* to radiation modes; as a result, the cladding modes are removed from the fibre. *Note:* Often a material such as the fibre coating or jacket having a refractive index equal to or greater than that of the fibre cladding will perform this function

Mode Transfer Function
The relative amounts of power propagating in the *modes* of an optical fibre.

Mode Volume
The number of bound *modes* that an optical fibre is capable of supporting.

Normalised Frequency
In an optical fibre, the dimensionless quantity, V, given by

$$V = ak_o NA$$

where: a is the fibre core radius,
NA is the numerical aperture of the fibre,
k_o is the free space wave number.

Power-Law Index Profile
In optical fibres, a class of index profiles n(r) characterised by

$$n(r) = n_{core}\left[1 - 2\Delta\left(\frac{r}{a}\right)^{\alpha}\right]^{0.5}$$

where: n_{core} is the refractive index at the core centre,
Δ is the relative index difference between the core and the cladding,
α is the profile shape factor,
a is the core radius,
r is a radial variable.

Principle Mode Number
A dimensionless quantity used to identify a particular *mode group* in a graded index fibre.

Profile Parameter
In the *power-law index profile* of an optical fibre, the parameter, α , that defines the shape of the refractive-index profile. *Note:* The optimum value of α for minimum dispersion is approximately 2.

Radiation Mode
An unbound *mode* that is not confined to the core or the cladding of an optical fibre.

Relative Mode Group
A dimensionless quantity given by dividing the *Principle Mode Number* by the maximum *Principle Mode Number.*

Steady State Distribution (SSD)
In an SSD, the output *mode power distribution* is the same as the input *mode power distribution*. There may be many different SSD distributions for a particular fibre or device.

TIA
Telecommunications Industry Association